SLAC-25 (Part One)
UC-28, Particle Accelerators
and High-Voltage Machines
UC-34, Physics
TID-4500

1963 SUMMER STUDY REPORT

PART ONE

Summer 1963

by

K. Berkelman, G. R. Bishop, C. de Vries, G. Feldman,
D. B. Isabelle, D. B. Lichtenberg, J. Mathews, J. Pine, R. Wilson

Technical Report
Prepared Under
Contracts AT(04-3)-400 and AT(04-3)-476
for the USAEC
San Francisco Operations Office

Printed in USA. Price $3.00. Available from the Office of Technical Services, Department of Commerce, Washington 25, D.C.

PREFACE

The papers in this report were written by members of a group assembled at the Stanford Linear Accelerator Center (SLAC) during the summer of 1963. Not all of the members of the group were present at the same time, and in some cases work done late in the summer may affect the conclusions of work done earlier.

These papers were written informally and were in general not intended for journal publication, since some of the work reported is preliminary and speculative. We suggest that anyone who wishes to cite one of these papers in the literature should obtain the author's permission to do so.

In most cases the authors, now widely dispersed, of these papers have not had the opportunity to proof-read the final draft copies of their work; we regret any typographical errors that may therefore result.

Some additional work done at SLAC during the summer is still being written up or is in the publishing process. This second (small) group of papers will probably appear separately as Part Two of this report.

Members of the SLAC 1963 summer study group whose papers appear in this report were as follows:

K. Berkelman	Cornell University Ithaca, New York
G. R. Bishop	Laboratoire de l'Accélérateur Linéaire Orsay, France
C. de Vries	Instituut voor Kernphysisch Onderzoek Ooster Ringdijk 18 Amsterdam, Netherlands
G. Feldman	Johns Hopkins University Baltimore, Maryland
D. B. Isabelle	High-Energy Radiation Section National Bureau of Standards Washington 25, D.C.
D. B. Lichtenberg	Indiana University Bloomington, Indiana

J. Mathews — California Institute of Technology
Pasadena, California

J. Pine — Sloan Laboratory of Physics
California Institute of Technology
Pasadena, California

R. Wilson — Cambridge Electron Accelerator
Harvard University
Cambridge, Massachusetts

TABLE OF CONTENTS

			Page
SLAC-25-A	D. B. Lichtenberg	Comparison of estimated pion fluxes at the AGS with pion fluxes expected at SLAC	1
SLAC-25-B	G. Feldman	A charge and isotopic spin analysis on the weak interactions	19
SLAC-25-C	D. B. Isabelle	Beam current monitors for a high energy linac	30
SLAC-25-D	J. Pine	Positron beam from the SLAC accelerator	63
SLAC-25-E	G. R. Bishop	Considerations of the use of monochromatic photon beams	88
SLAC-25-F	C. de Vries	Elastic e-p kinematics for SLAC	125
SLAC-25-G	C. de Vries	Statistical fits to electron-proton and electron-deuteron cross sections	134
SLAC-25-H	C. de Vries	Possibilities with a 2 BeV/c spectrometer for electron-proton scattering at SLAC energies	149
SLAC-25-I	C. de Vries	Electron-proton scattering at 180°	160
SLAC-25-J	K. Berkelman	Electron scattering at 20 GeV	167
SLAC-25-K	R. Wilson	Elastic electron-proton scattering choice of angles and energies	187
SLAC-25-L	R. Wilson	Photoproduction of μ pairs and e pairs at SLAC	195
SLAC-25-M	J. Mathews	Pair production of vector bosons in the Coulomb field of a nucleus	200

COMPARISON OF ESTIMATED PION FLUXES AT THE AGS WITH PION FLUXES EXPECTED AT SLAC

by

D. B. Lichtenberg

We present here a comparison of the pion fluxes expected at SLAC with tentative estimates of pion fluxes produced at the Brookhaven AGS.

I. PIONS AT THE AGS

Cocconi, Koester, and Perkins[1] have obtained an empirical formula for the energy and angular spectrum of pions produced at the AGS.

The formula in the lab system is

$$\frac{d^2N(E\theta)}{dEd\Omega} = \frac{nE^2}{2\pi p^2 T} e^{-E(1/T + \theta/p)} \tag{1}$$

where E is the pion energy, θ is the pion angle (in radians), n is the effective pion multiplicity, p is half the average transverse momentum of the pions, and T is a parameter depending on the initial proton energy. The quantity $d^2N/dEd\Omega$ is the number of pions produced per steradian per BeV for each proton interaction. In the formula, n is about equal to half the true multiplicity, as the formula applies only to the pions in the forward cone in the center-of-mass system. For 30 BeV protons

$$n = 3,\ T = 3.75 \text{ BeV},\ p = 0.18 \text{ BeV} \tag{2}$$

The formula was compared with measurements by Baker et al.[2] at angles greater than 4°. For this comparison, formula (1) should be multiplied by a factor of $1/3$ to compare with pions of a particular charge and by an additional factor of 0.4 to account for the fraction of protons which interact in the target. Putting in these numbers, (1) becomes

$$\frac{d^2N}{dEd\Omega} = \frac{0.4\ E^2}{2\pi p^2 T} = e^{-E(1/T + \theta/p)} \text{ ster}^{-1} \text{ BeV}^{-1} \text{ proton}^{-1} \tag{3}$$

The agreement between the formula and experiment is shown in Fig. 1, reproduced from Ref. 1. The formula does not hold for very low energy pions ($E < 1$ BeV) or for high energy pions $E > \frac{2}{3} E_{\text{proton}}$.

One difficulty with using the formula is that it is needed at $\theta = 0^\circ$, where it has not been tested. Previously, it was thought that the formula was too high by about a factor of 5 at 0°, but preliminary evidence from the AGS suggests that it might be even a factor of 2 too low.[3] We shall give tentative results using this formula, emphasizing that our results depend on the extrapolation of the formula to an untested region. Careful measurements of pion fluxes in the forward direction are presently underway at CERN, and results should be available soon.

II. PIONS FROM THE DRELL PROCESS

Thiebaux[4] has calculated expected fluxes of pions produced by a thin target bremmstrahlung spectrum from 20 BeV electrons. Thiebaux assumed that 10^{10} electrons are incident on a 0.1 radiation length target to produce photons, and the photons are incident on a 10 cm hydrogen target to produce pions via the Drell[5] process. Thiebaux assumed a constant pion-nucleon total cross section of 28 mb. A table of his numbers is appended to this report.

The numbers in Thiebaux's table can be fairly well fit for pions between 5 and 15 BeV by the following empirical formula, assuming 10^{10} electrons,

$$N(\text{Thiebaux}) = \frac{n_o E e^{-E/T_o}}{2\pi m T_o} \frac{\theta^2}{(m^2/E^2 + \theta^2)^2} \tag{4}$$

where m is the pion mass and n_o and T_o are parameters given by

$$n_o = 400, \; T_o = 2.5 \text{ BeV} \tag{5}$$

This formula applies for 20 BeV incident electrons. No attempt was made to get a fit for other incident electron energies.

In actual practice, a target will be used which is much thicker than

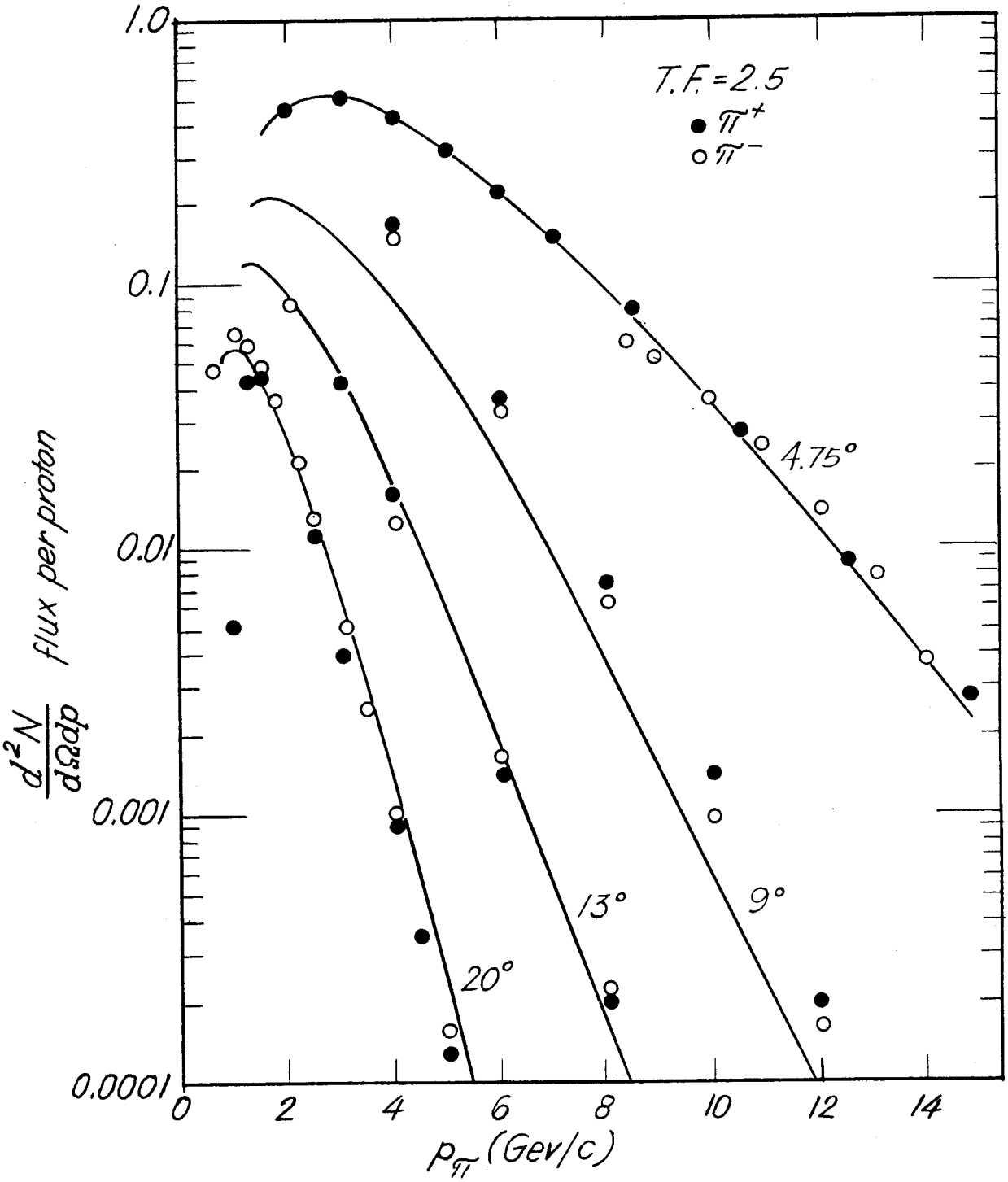

FIG. 1--Brookhaven π^+ and π^- spectra from targets of Al and Be bombarded with 29.5-GeV protons. Curves:
$n_\pi = 1.2 \times \text{T.F.} \approx 3.0$.
$K_\pi = 0.38$
$T = 3.75$ GeV; $p_o = 0.18$ GeV/c.

that assumed by Thiebaux. To get an estimate of the expected flux, assume a 1 radiation length beryllium target to produce photons.

We wish to modify Thiebaux's numbers to account for the difference between a 0.1 radiation length target assumed by Thiebaux and a 1 radiation length target. We shall do this in a particularly simple way, at the cost of losing some accuracy.

Let the number of photons N_γ a distance t within the target be given by

$$N_\gamma(t) = 10tN_\gamma(0.1), \quad t < 0.6$$
$$= 6N_\gamma(0.1), \quad 0.6 \leq t \leq 1$$

where t is given in radiation lengths and $N_\gamma(0.1)$ is the number of photons assumed by Thiebaux. This simple formula overestimates the number of high energy photons and underestimates the number of low energy ones.

We also wish to modify Thiebaux's numbers to take into account the difference between a 10 cm hydrogen target for producing pions assumed by Thiebaux and the 1 radiation length Be target which we assume.

The number of pions produced in the Be target is given by

$$N_\pi \text{ (produced)} = \int_0^1 N_\gamma(t)dt/\lambda(\text{Be})$$

where $\lambda(\text{Be})$ is the mean free path (in radiation lengths) for photons to produce pions in Be. The number of pions N_π emerging from the Be is less than this because of attenuation of the pion beam. This number is given by

$$N_\pi = \int_0^1 N_\gamma(t)e^{-(1-t)\lambda_\pi} \, dt/\lambda(\text{Be})$$

where $\lambda_\pi \approx 1.5$ is the pion mean free path in Be in radiation lengths.

Integrating, we obtain

$$N_\pi = 10 N_\gamma (0.1) Y(0.6)/\lambda(\mathrm{Be})$$

where

$$Y(a) = -\lambda_\pi^2 \, e^{-a/\lambda_\pi} + \lambda_\pi^2 \, e^{-1/\lambda_\pi} + a\lambda_\pi$$

On the other hand, according to Thiebaux's calculations, the number of pions produced N_π^T is

$$N_\pi^T = N_\gamma (0.1) F/\lambda(\mathrm{H})$$

where $\lambda(\mathrm{H})$ is the mean free path for photons to produce pions in hydrogen and where $F = \frac{10}{819} = 0.0122$ is the length of the pion target assumed by Thiebaux, both expressed in radiation lengths.

Then

$$\frac{N_\pi}{N_\pi^T} = \frac{10\lambda(\mathrm{H})Y(0.6)}{\lambda(\mathrm{Be})F} = 200$$

where we have made the estimate $\lambda(\mathrm{Be})/\lambda(\mathrm{H}) = 1.5$. Thus we simply scale up Thiebaux's numbers by a factor of 200 for 10^{10} incident electrons, or, for the flux per electron, we multiply by 2×10^{-8}. (This approximation somewhat overestimates the number of high energy pions and underestimates the number of low energy pions.) Then the number of pions produced per incident 20 BeV electron is given by

$$\frac{d^2N}{dE d\Omega} = \frac{8.0 \times 10^{-6} E_e^{-E/T_o}}{2\pi M T_o} \frac{\theta^2}{\left(m^2/E^2 + \theta^2\right)^2} \text{ ster}^{-1} \text{ BeV}^{-1} \text{ electron}^{-1} \quad (6)$$

In Fig. 2 we compare the predictions of this formula at $\theta = 1^o$ with the numbers found by Thiebaux (multiplied by 2×10^{-8}). This formula also fails at very low and very high energies.

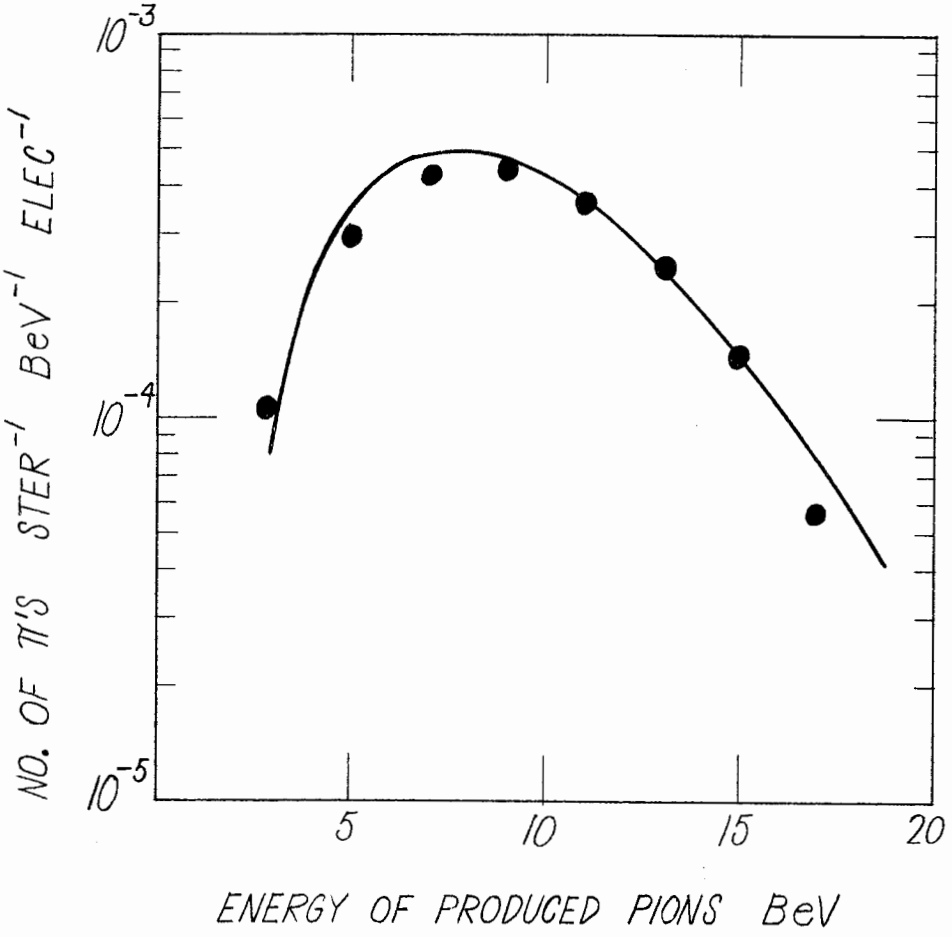

FIG. 2--Calculated number of π's of one charge produced at 1° per incident 20 BeV electron.
Points: Calculated by Thiebaux, (the numbers in Thiebaux's table multiplied by 2×10^{-8}).
Solid line: From empirical formula, Eq. (6) of text.

III. COMPARISON OF PION FLUXES INTEGRATED OVER ANGLES

Next consider the pion fluxes integrated out to some angle θ. Integrating formula (3), we obtain for the number of pions of given charge produced within an angle θ per proton (assuming 40 percent of the protons interact in the target)

$$\frac{dN}{dE} = \frac{0.4}{T} e^{-E/T} f\left(\frac{E\theta}{p}\right) \tag{7}$$

where

$$f(x) = 1 - e^{-x}(1 + x) \tag{8}$$

Integrating formula (6), we get for the number of pions of given charge produced within an angle θ per electron, assuming a 1 radiation length Be target

$$\frac{dN}{dE} = 8.0 \times 10^{-6} \frac{E}{mT_o} e^{-E/T_o} g\left(\frac{E\theta}{m}\right) \tag{9}$$

where

$$g(x) = \frac{1}{2}\left[\log (1 + x^2) - \frac{x^2}{1 + x^2}\right] \tag{10}$$

The functions f and g are plotted in Fig 3. The function g diverges logarithmically, but should be used only for small angles.

One should not compare $f(x)$ and $g(x)$ for the same value of x because the inherent width of the pion distribution is not the same for incident protons and electrons. Letting

$$\frac{E\theta}{m} = X ,$$

then

$$\frac{E\theta}{p} = \frac{m}{p} x = 0.775x \quad .$$

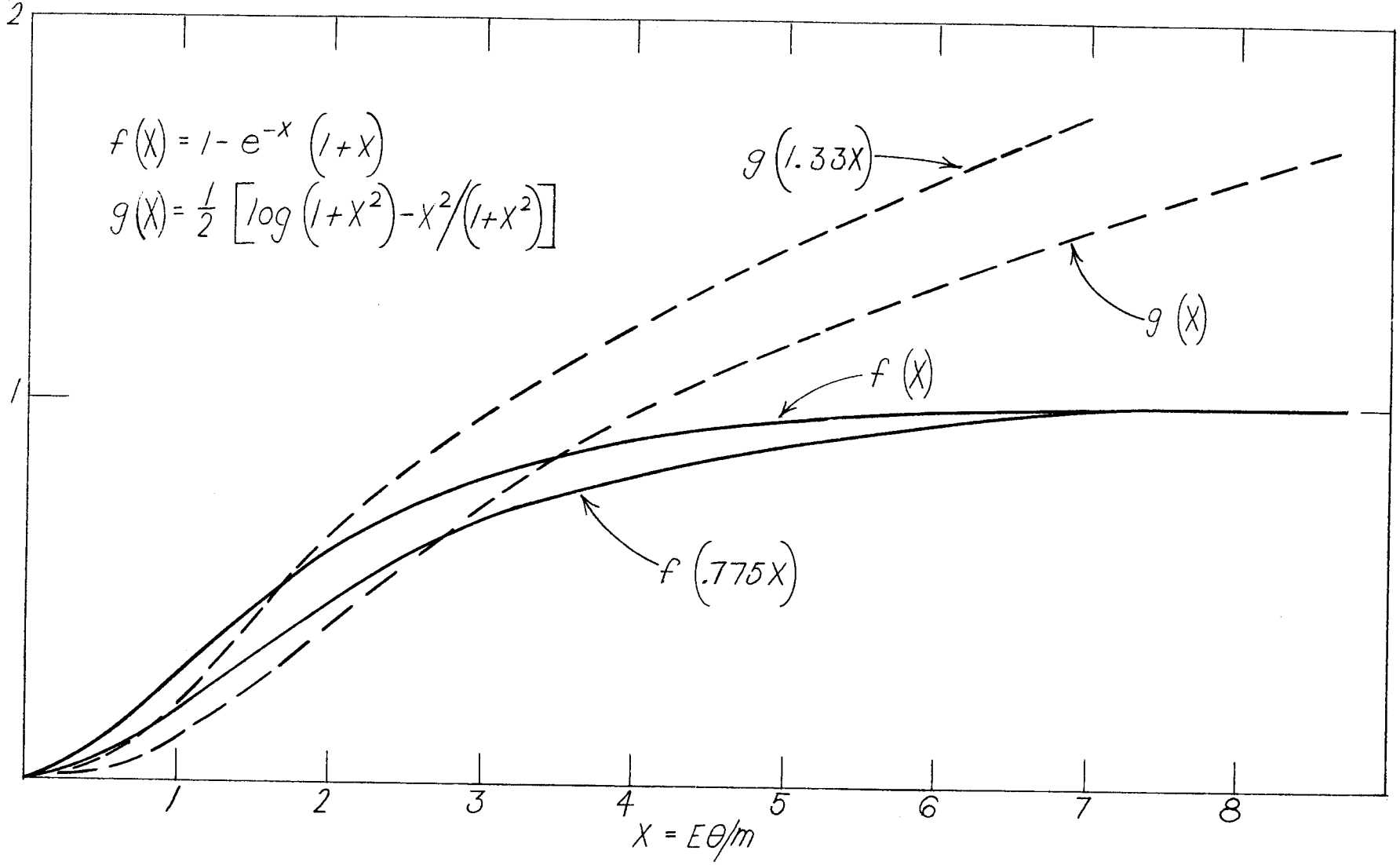

FIG. 3--Comparison of (unnormalized) pion fluxes of a given energy within an angle θ from protons [the function f (.775x)], and from electrons [the function g (x)], where $x = E\theta/m$.

Thus $f(0.775x)$ should be compared with $g(x)$. Also, if the pion angular distribution found in the CEA experiment applies at 20 BeV, the pion angular distribution will be somewhat narrower than that predicted by Drell.[6] The CEA experiment can be fit rather well,[7] except at the smallest angles, by an angular distribution which has the form of the Drell distribution, but with $E\theta/m$ replaced by $\frac{4E\theta}{3m}$. If this result is true at 20 BeV, then $g(x)$ should be replaced by $g(1.33x)$. The functions $f(0.775x)$ and $g(1.33x)$ are also shown in Fig. 3. By coincidence the functions $f(0.775x)$ and $g(1.33x)$ are equal just at the Drell angle $\theta_D = m/E$. The angular functions f and g in (7) and (9), are comparable for angles in the region $1/2\theta_D \lesssim \theta \lesssim 4\theta_D$ and, to a first approximation, can be neglected. Setting the angular functions equal to 1/2 in (7) and (9), we can obtain the approximate number of pions per incident particle within a cone of half angle $\theta \approx 2\theta_D$. The results are shown in Fig. 4. In Fig. 5 we show the approximate number of pions for 3×10^{14} electrons/sec and 2×10^{11} protons/sec.

In both Fig. 4 and Fig. 5, we also show the pion flux calculated by Fries[8] from photoproduction assuming a 1 radiation length Be target. Fries' curve multiplied by a factor of 2 to make it directly comparable to our calculation* and ours agree within a factor 2, which is all that can be expected in view of the approximations. We repeat that our appro

tions are such as to overestimate the number of pions at the high energy end of the spectrum, and to underestimate the number at the low energy end.

---

*The factor 2 arises from three corrections: (1) In Fries' calculation, the pions are attenuated in Cu by a factor 0.423 after leaving the Be. (2) Fries used a Drell cross section almost a factor 2 larger than the one used by Thiebaux. (3) Fries calculated the number of pions within an angle $1\frac{1}{2}\theta_D$ rather than within an angle $2\theta_D$. This correction can be made from the curve $g(x)$ in Fig. 3. We thus multiply Fries' numbers by the combined factor

$$\left(\frac{1}{0.423}\right)\left(\frac{1}{2}\right)(1.65) \approx 2$$

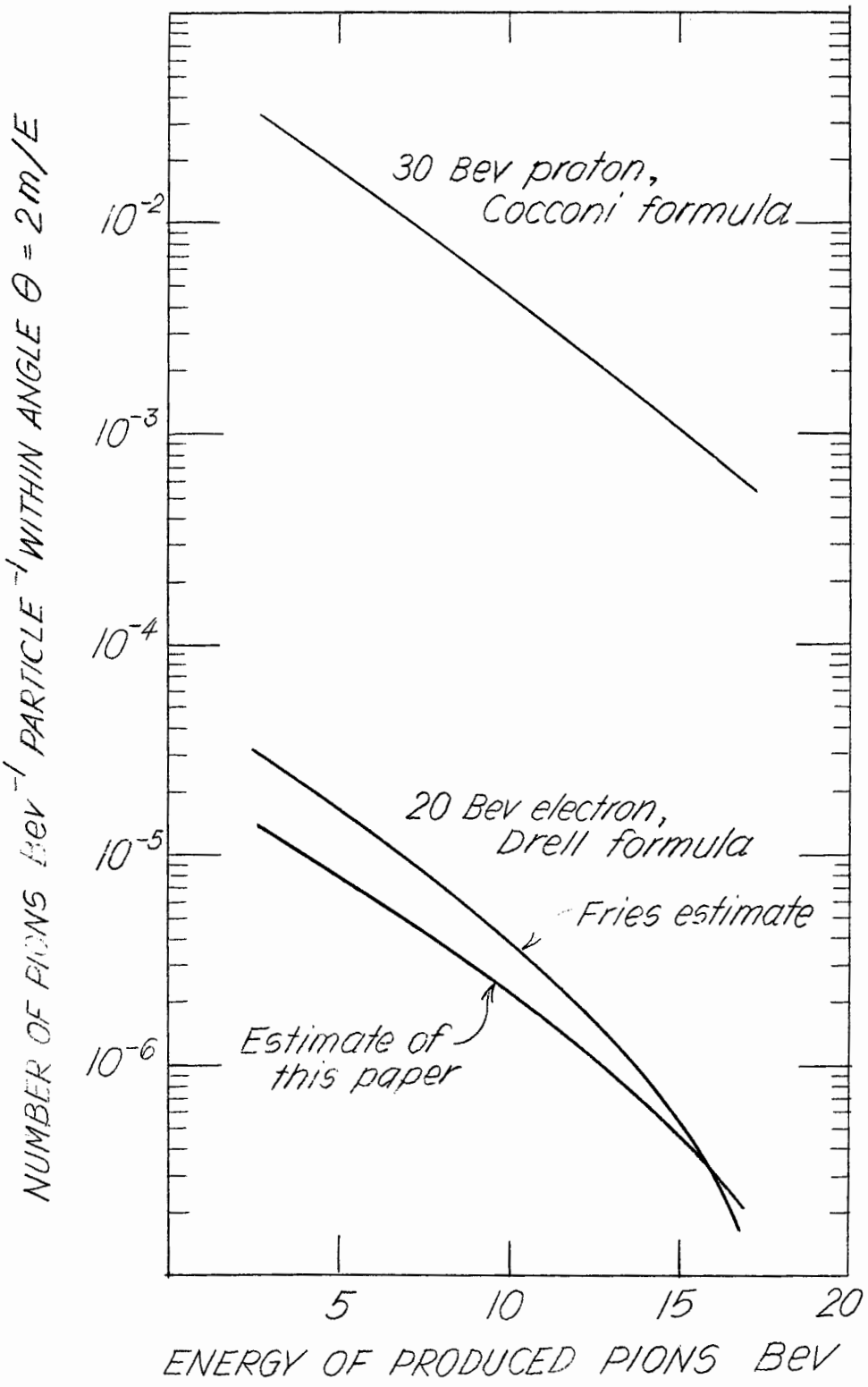

FIG. 4--Comparison of pion fluxes within twice the Drell angle per proton (target efficiency 0.4) and per electron (one radiation length beryllium target).

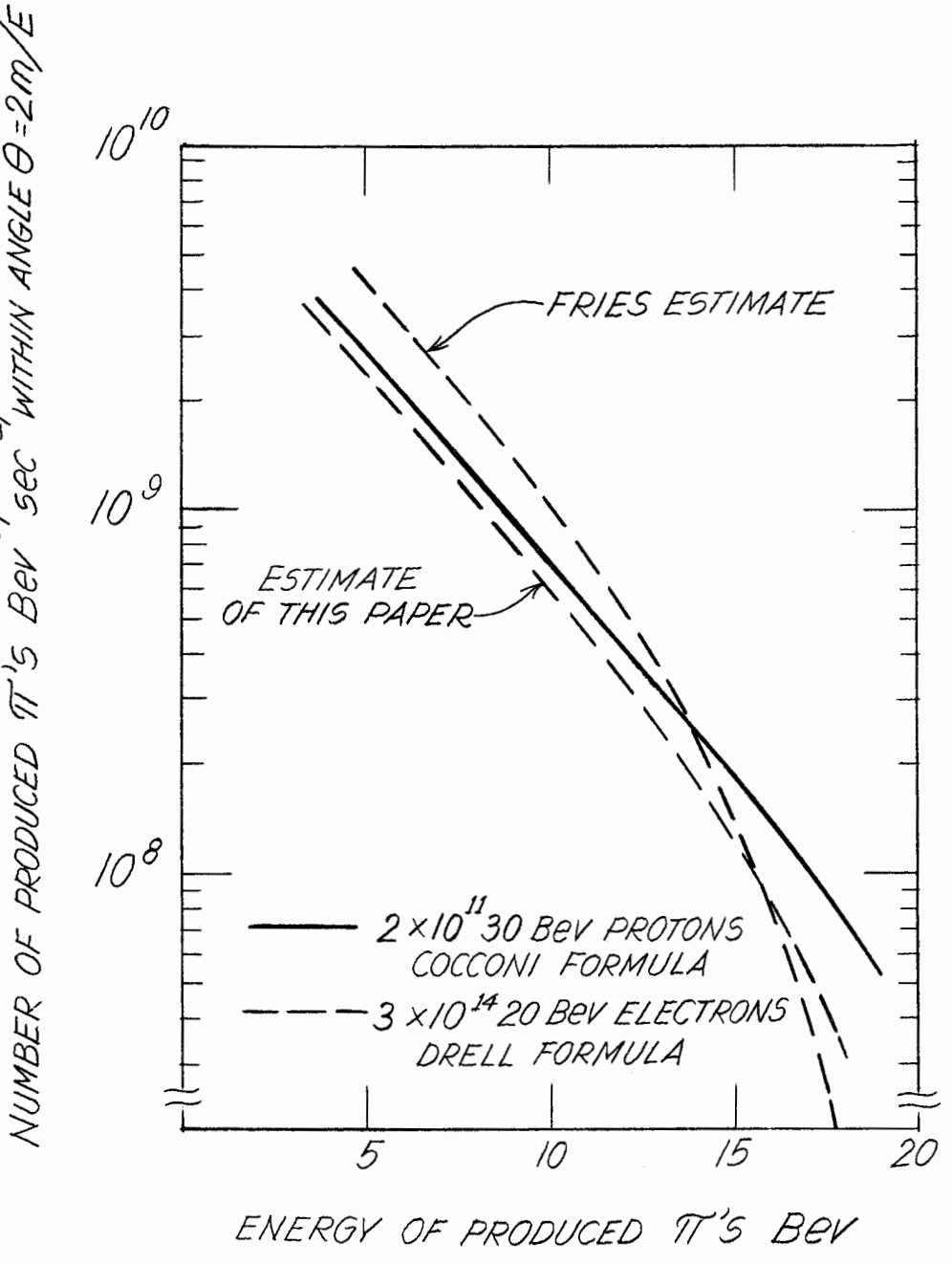

FIG. 5--Comparison of estimated pion fluxes at the AGS with pion fluxes expected at SLAC from the Drell process.

IV. CONCLUSIONS

According to Fig. 5, approximately the same number of high energy pions are produced at the AGS by 2×10^{11} 30 BeV protons as can be expected from 3×10^{14} 20 BeV electrons. This conclusion depends on the validity of the following assumptions:

1. The Cocconi-Koester-Perkins formula is correct at very small angles ($\theta < 1^{\circ}$). This assumption is being tested by experiments currently underway at CERN.

2. The Drell process is the dominant source of high energy pions from an electron machine. It is possible to think of other processes which may lead to copious pion production by photons, but such estimates are not necessarily reliable. There will almost certainly be many more low energy pions (say, $E < 5$ BeV) from other processes. For example, below a few BeV, ordinary photoproduction becomes more important than the Drell process.

3. A target thickness of 1 radiation length is the most that can be tolerated. The net effect of a thicker target will be to produce many more low energy pions but not to produce more high energy pions. For sufficiently thick targets, the number of high energy pions will be reduced.

There are two main reasons why our conclusions are more unfavorable for an electron machine than the conclusions reached by J. Ballam.[9]

1. We have used the Cocconi-Koester-Perkins formula to compute the number of pions produced per proton, rather than the statistical model used by Ballam. The Cocconi formula predicts many more pions at small angles than does the statistical model.

2. Ballam compared pions from 25 BeV electrons with pions from 25 BeV protons, whereas we have compared pions from 20 BeV electrons with pions from 30 BeV protons.

I should like to thank Professor H. P. Noyes and Dr. M. Thiebaux for very valuable discussions.

NO. OF ORELL-PRODUCED PIONS/SR/BEV/C

MACHINE ENERGY IN BEV 20.00

NO. ELECTRONS PER PULSE 0.10000E 11
RADIATION LENGTHS 0.10
HYDROGEN TARGET THICKNESS CM 10.00
NO. H ATOMS PER CC 0.42235E 23

ANGLE	OBSERVED PARTICLE MOMENTUM IN BEV/C						
	0.10	0.20	0.50	1.00	2.00	.00	
0.20	0.564E-01	0.298E-00	0.379E 01	0.278E 02	0.198E 03	0.001E	03
0.40	0.226E-00	0.119E 01	0.151E 02	0.111E 03	0.779E 03	0.233E	04
0.60	0.507E 00	0.268E 01	0.340E 02	0.247E 03	0.171E 04	0.496E	04
0.80	0.902E 00	0.476E 01	0.603E 02	0.436E 03	0.294E 04	0.819E	04
1.00	0.141E 01	0.744E 01	0.940E 02	0.674E 03	0.440E 04	0.117E	05
1.20	0.203E 01	0.107E 02	0.135E 03	0.957E 03	0.602E 04	0.151E	05
1.40	0.276E 01	0.146E 02	0.183E 03	0.128E 04	0.772E 04	0.183E	05
1.60	0.360E 01	0.190E 02	0.238E 03	0.164E 04	0.944E 04	0.210E	05
1.80	0.456E 01	0.240E 02	0.299E 03	0.204E 04	0.111E 05	0.232E	03
2.00	0.563E 01	0.296E 02	0.367E 03	0.246E 04	0.127E 05	0.249E	05
2.20	0.681E 01	0.358E 02	0.441E 03	0.290E 04	0.141E 05	0.260E	05
2.40	0.810E 01	0.426E 02	0.521E 03	0.336E 04	0.154E 05	0.267E	05
2.60	0.950E 01	0.499E 02	0.607E 03	0.384E 04	0.166E 05	0.270E	05
2.80	0.110E 02	0.577E 02	0.698E 03	0.432E 04	0.175E 05	0.269E	05
3.00	0.126E 02	0.662E 02	0.794E 03	0.480E 04	0.183E 05	0.266E	05
3.20	0.144E 02	0.752E 02	0.895E 03	0.528E 04	0.189E 05	0.261E	05
3.40	0.162E 02	0.847E 02	1.000E 03	0.575E 04	0.193E 05	0.254E	05
3.60	0.181E 02	0.947E 02	0.111E 04	0.621E 04	0.196E 05	0.247E	05
3.80	0.202E 02	0.105E 03	0.122E 04	0.666E 04	0.198E 05	0.238E	05
4.00	0.224E 02	0.116E 03	0.134E 04	0.709E 04	0.198E 05	0.230E	05
4.20	0.248E 02	0.128E 03	0.146E 04	0.750E 04	0.198E 05	0.221E	05
4.40	0.270E 02	0.140E 03	0.158E 04	0.790E 04	0.196E 05	0.212E	05
4.60	0.295E 02	0.153E 03	0.170E 04	0.827E 04	0.194E 05	0.203E	05
4.80	0.321E 02	0.166E 03	0.183E 04	0.862E 04	0.191E 05	0.194E	05
5.00	0.348E 02	0.180E 03	0.195E 04	0.894E 04	0.188E 05	0.186E	05
5.20	0.376E 02	0.194E 03	0.208E 04	0.924E 04	0.185E 05	0.178E	05
5.40	0.405E 02	0.208E 03	0.221E 04	0.951E 04	0.181E 05	0.170E	05
5.60	0.435E 02	0.223E 03	0.234E 04	0.976E 04	0.177E 05	0.162E	05
5.80	0.466E 02	0.239E 03	0.247E 04	0.998E 04	0.173E 05	0.155E	05
6.00	0.498E 02	0.254E 03	0.260E 04	0.102E 05	0.168E 05	0.148E	05
6.20	0.531E 02	0.271E 03	0.273E 04	0.104E 05	0.164E 05	0.142E	05
6.40	0.565E 02	0.287E 03	0.286E 04	0.105E 05	0.160E 05	0.136E	05
6.60	0.600E 02	0.305E 03	0.298E 04	0.106E 05	0.155E 05	0.130E	05
6.80	0.636E 02	0.322E 03	0.311E 04	0.107E 05	0.151E 05	0.124E	05
7.00	0.673E 02	0.340E 03	0.324E 04	0.108E 05	0.147E 05	0.119E	05
7.20	0.711E 02	0.358E 03	0.336E 04	0.109E 05	0.142E 05	0.114E	05
7.40	0.750E 02	0.377E 03	0.348E 04	0.110E 05	0.138E 05	0.109E	05
7.60	0.790E 02	0.396E 03	0.360E 04	0.110E 05	0.134E 05	0.105E	05
7.80	0.831E 02	0.415E 03	0.371E 04	0.110E 05	0.130E 05	0.101E	05
8.00	0.873E 02	0.434E 03	0.383E 04	0.110E 05	0.126E 05	0.968E	04

NO. OF DRELL-PRODUCED PIONS/SR/BEV/C

MACHINE ENERGY IN BEV 20.00

NO. ELECTRONS PER PULSE 0.10000E 11
RADIATION LENGTHS 0.10
HYDROGEN TARGET THICKNESS CM 10.00
NO. H ATOMS PER CC 0.42235E 23

ANGLE	OBSERVED PARTICLE MOMENTUM IN BEV/C					
	4.00	5.00	6.00	7.00	8.00	9.00
0.20	0.129E 04	0.227E 04	0.352E 04	0.498E 04	0.653E 04	0.806E 04
0.40	0.486E 04	0.830E 04	0.124E 05	0.168E 05	0.210E 05	0.246E 05
0.60	0.996E 04	0.162E 05	0.229E 05	0.292E 05	0.344E 05	0.378E 05
0.80	0.156E 05	0.240E 05	0.318E 05	0.381E 05	0.420E 05	0.434E 05
1.00	0.210E 05	0.303E 05	0.377E 05	0.424E 05	0.441E 05	0.433E 05
1.20	0.256E 05	0.345E 05	0.404E 05	0.430E 05	0.427E 05	0.402E 05
1.40	0.290E 05	0.368E 05	0.408E 05	0.414E 05	0.395E 05	0.360E 05
1.60	0.313E 05	0.375E 05	0.396E 05	0.386E 05	0.356E 05	0.316E 05
1.80	0.325E 05	0.369E 05	0.374E 05	0.353E 05	0.318E 05	0.277E 05
2.00	0.328E 05	0.356E 05	0.348E 05	0.320E 05	0.282E 05	0.242E 05
2.20	0.325E 05	0.339E 05	0.321E 05	0.288E 05	0.250E 05	0.212E 05
2.40	0.318E 05	0.319E 05	0.295E 05	0.260E 05	0.222E 05	0.186E 05
2.60	0.307E 05	0.298E 05	0.269E 05	0.234E 05	0.198E 05	0.164E 05
2.80	0.294E 05	0.278E 05	0.246E 05	0.211E 05	0.177E 05	0.146E 05
3.00	0.280E 05	0.258E 05	0.225E 05	0.191E 05	0.159E 05	0.130E 05
3.20	0.265E 05	0.240E 05	0.206E 05	0.173E 05	0.143E 05	0.117E 05
3.40	0.251E 05	0.222E 05	0.189E 05	0.157E 05	0.129E 05	0.105E 05
3.60	0.236E 05	0.206E 05	0.173E 05	0.143E 05	0.117E 05	0.950E 04
3.80	0.223E 05	0.191E 05	0.159E 05	0.131E 05	0.107E 05	0.863E 04
4.00	0.210E 05	0.178E 05	0.147E 05	0.120E 05	0.976E 04	0.787E 04
4.20	0.198E 05	0.166E 05	0.136E 05	0.111E 05	0.895E 04	0.720E 04
4.40	0.186E 05	0.154E 05	0.126E 05	0.102E 05	0.823E 04	0.661E 04
4.60	0.175E 05	0.144E 05	0.117E 05	0.943E 04	0.760E 04	0.609E 04
4.80	0.165E 05	0.135E 05	0.109E 05	0.874E 04	0.703E 04	0.562E 04
5.00	0.156E 05	0.126E 05	0.101E 05	0.812E 04	0.652E 04	0.521E 04
5.20	0.147E 05	0.118E 05	0.945E 04	0.757E 04	0.606E 04	0.484E 04
5.40	0.139E 05	0.111E 05	0.884E 04	0.706E 04	0.565E 04	0.450E 04
5.60	0.131E 05	0.104E 05	0.829E 04	0.661E 04	0.528E 04	0.420E 04
5.80	0.124E 05	0.982E 04	0.778E 04	0.619E 04	0.494E 04	0.393E 04
6.00	0.118E 05	0.926E 04	0.732E 04	0.581E 04	0.463E 04	0.368E 04
6.20	0.112E 05	0.875E 04	0.689E 04	0.547E 04	0.435E 04	0.346E 04
6.40	0.106E 05	0.827E 04	0.650E 04	0.515E 04	0.410E 04	0.325E 04
6.60	0.101E 05	0.783E 04	0.614E 04	0.486E 04	0.386E 04	0.307E 04
6.80	0.960E 04	0.743E 04	0.581E 04	0.459E 04	0.365E 04	0.289E 04
7.00	0.914E 04	0.705E 04	0.551E 04	0.435E 04	0.345E 04	0.274E 04
7.20	0.871E 04	0.670E 04	0.523E 04	0.412E 04	0.327E 04	0.259E 04
7.40	0.830E 04	0.637E 04	0.496E 04	0.391E 04	0.310E 04	0.246E 04
7.60	0.793E 04	0.607E 04	0.472E 04	0.372E 04	0.294E 04	0.233E 04
7.80	0.757E 04	0.578E 04	0.450E 04	0.354E 04	0.280E 04	0.222E 04
8.00	0.724E 04	0.552E 04	0.428E 04	0.337E 04	0.266E 04	0.211E 04

NO. OF DRELL-PRODUCED PIONS/SR/BEV/C

MACHINE ENERGY IN BEV 20.00

NO. ELECTRONS PER PULSE 0.10000E 11
RADIATION LENGTHS 0.10
HYDROGEN TARGET THICKNESS CM 10.00
NO. H ATOMS PER CC 0.42235E 23

ANGLE	OBSERVED PARTICLE MOMENTUM IN BEV/C					
	10.00	11.00	12.00	13.00	14.00	15.00
0.20	0.941E 04	0.104E 05	0.110E 05	0.109E 05	0.102E 05	0.891E 04
0.40	0.272E 05	0.285E 05	0.282E 05	0.264E 05	0.233E 05	0.190E 05
0.60	0.392E 05	0.385E 05	0.358E 05	0.316E 05	0.263E 05	0.203E 05
0.80	0.425E 05	0.395E 05	0.350E 05	0.296E 05	0.236E 05	0.176E 05
1.00	0.404E 05	0.361E 05	0.309E 05	0.252E 05	0.195E 05	0.142E 05
1.20	0.362E 05	0.313E 05	0.261E 05	0.209E 05	0.159E 05	0.113E 05
1.40	0.315E 05	0.267E 05	0.218E 05	0.172E 05	0.129E 05	0.912E 04
1.60	0.272E 05	0.226E 05	0.183E 05	0.142E 05	0.106E 05	0.741E 04
1.80	0.234E 05	0.192E 05	0.154E 05	0.119E 05	0.876E 04	0.611E 04
2.00	0.202E 05	0.164E 05	0.130E 05	0.999E 04	0.735E 04	0.511E 04
2.20	0.175E 05	0.142E 05	0.112E 05	0.851E 04	0.623E 04	0.432E 04
2.40	0.153E 05	0.123E 05	0.963E 04	0.732E 04	0.535E 04	0.369E 04
2.60	0.134E 05	0.107E 05	0.838E 04	0.635E 04	0.463E 04	0.319E 04
2.80	0.118E 05	0.944E 04	0.735E 04	0.556E 04	0.404E 04	0.278E 04
3.00	0.105E 05	0.836E 04	0.649E 04	0.490E 04	0.356E 04	0.245E 04
3.20	0.940E 04	0.744E 04	0.577E 04	0.435E 04	0.315E 04	0.217E 04
3.40	0.844E 04	0.667E 04	0.516E 04	0.388E 04	0.281E 04	0.193E 04
3.60	0.761E 04	0.600E 04	0.464E 04	0.349E 04	0.252E 04	0.173E 04
3.80	0.890E 04	0.543E 04	0.419E 04	0.315E 04	0.228E 04	0.156E 04
4.00	0.628E 04	0.494E 04	0.381E 04	0.285E 04	0.206E 04	0.141E 04
4.20	0.573E 04	0.450E 04	0.347E 04	0.260E 04	0.188E 04	0.129E 04
4.40	0.526E 04	0.412E 04	0.317E 04	0.238E 04	0.172E 04	0.117E 04
4.60	0.484E 04	0.379E 04	0.291E 04	0.218E 04	0.157E 04	0.108E 04
4.80	0.446E 04	0.349E 04	0.269E 04	0.201E 04	0.145E 04	0.991E 03
5.00	0.413E 04	0.323E 04	0.248E 04	0.186E 04	0.134E 04	0.915E 03
5.20	0.383E 04	0.300E 04	0.230E 04	0.172E 04	0.124E 04	0.847E 03
5.40	0.356E 04	0.279E 04	0.214E 04	0.160E 04	0.115E 04	0.787E 03
5.60	0.332E 04	0.260E 04	0.199E 04	0.149E 04	0.107E 04	0.733E 03
5.80	0.311E 04	0.243E 04	0.186E 04	0.139E 04	0.100E 04	0.684E 03
6.00	0.291E 04	0.227E 04	0.174E 04	0.130E 04	0.936E 03	0.640E 03
6.20	0.273E 04	0.213E 04	0.163E 04	0.122E 04	0.878E 03	0.599E 03
6.40	0.257E 04	0.200E 04	0.153E 04	0.115E 04	0.825E 03	0.563E 03
6.60	0.242E 04	0.189E 04	0.144E 04	0.108E 04	0.776E 03	0.530E 03
6.80	0.228E 04	0.178E 04	0.136E 04	0.102E 04	0.732E 03	0.499E 03
7.00	0.216E 04	0.168E 04	0.129E 04	0.960E 03	0.691E 03	0.472E 03
7.20	0.204E 04	0.159E 04	0.122E 04	0.908E 03	0.653E 03	0.446E 03
7.40	0.193E 04	0.151E 04	0.115E 04	0.860E 03	0.619E 03	0.422E 03
7.60	0.184E 04	0.143E 04	0.109E 04	0.816E 03	0.587E 03	0.401E 03
7.80	0.174E 04	0.136E 04	0.104E 04	0.775E 03	0.557E 03	0.380E 03
8.00	0.166E 04	0.129E 04	0.989E 03	0.737E 03	0.530E 03	0.362E 03

NO. OF DRELL-PRODUCED PIONS/SR/BEV/C

MACHINE ENERGY IN BEV 20.00

NO. ELECTRONS PER PULSE 0.10000E 11
RADIATION LENGTHS 0.10
HYDROGEN TARGET THICKNESS CM 10.00
NO. H ATOMS PER CC 0.42235E 23

ANGLE	OBSERVED PARTICLE MOMENTUM IN BEV/C					
	16.00	17.00	18.00	19.00	19.50	19.80
0.20	0.703E 04	0.480E 04	0.256E 04	0.758E 03	0.205E 03	0.343E 02
0.40	0.141E 05	0.902E 04	0.452E 04	0.126E 04	0.330E 03	0.543E 02
0.60	0.143E 05	0.874E 04	0.418E 04	0.112E 04	0.287E 03	0.466E 02
0.80	0.119E 05	0.707E 04	0.329E 04	0.857E 03	0.218E 03	0.351E 02
1.00	0.945E 04	0.550E 04	0.252E 04	0.645E 03	0.163E 03	0.262E 02
1.20	0.744E 04	0.428E 04	0.194E 04	0.492E 03	0.124E 03	0.198E 02
1.40	0.593E 04	0.338E 04	0.152E 04	0.384E 03	0.963E 02	0.154E 02
1.60	0.479E 04	0.271E 04	0.121E 04	0.305E 03	0.765E 02	0.122E 02
1.80	0.393E 04	0.222E 04	0.989E 03	0.248E 03	0.620E 02	0.991E 01
2.00	0.327E 04	0.184E 04	0.819E 03	0.205E 03	0.512E 02	0.817E 01
2.20	0.276E 04	0.155E 04	0.688E 03	0.172E 03	0.429E 02	0.685E 01
2.40	0.235E 04	0.132E 04	0.585E 03	0.146E 03	0.365E 02	0.581E 01
2.60	0.203E 04	0.114E 04	0.504E 03	0.126E 03	0.313E 02	0.499E 01
2.80	0.177E 04	0.989E 03	0.438E 03	0.109E 03	0.272E 02	0.433E 01
3.00	0.155E 04	0.868E 03	0.384E 03	0.955E 02	0.238E 02	0.380E 01
3.20	0.137E 04	0.767E 03	0.339E 03	0.843E 02	0.210E 02	0.335E 01
3.40	0.122E 04	0.683E 03	0.301E 03	0.750E 02	0.187E 02	0.298E 01
3.60	0.110E 04	0.611E 03	0.270E 03	0.671E 02	0.167E 02	0.266E 01
3.80	0.987E 03	0.551E 03	0.243E 03	0.604E 02	0.150E 02	0.240E 01
4.00	0.894E 03	0.498E 03	0.220E 03	0.546E 02	0.136E 02	0.217E 01
4.20	0.813E 03	0.453E 03	0.200E 03	0.496E 02	0.124E 02	0.197E 01
4.40	0.743E 03	0.414E 03	0.182E 03	0.453E 02	0.113E 02	0.180E 01
4.60	0.681E 03	0.379E 03	0.167E 03	0.415E 02	0.103E 02	0.165E 01
4.80	0.626E 03	0.349E 03	0.154E 03	0.382E 02	0.951E 01	0.151E 01
5.00	0.578E 03	0.322E 03	0.142E 03	0.352E 02	0.877E 01	0.140E 01
5.20	0.535E 03	0.298E 03	0.131E 03	0.326E 02	0.812E 01	0.129E 01
5.40	0.497E 03	0.277E 03	0.122E 03	0.302E 02	0.753E 01	0.120E 01
5.60	0.463E 03	0.257E 03	0.113E 03	0.281E 02	0.701E 01	0.112E 01
5.80	0.432E 03	0.240E 03	0.106E 03	0.263E 02	0.654E 01	0.104E 01
6.00	0.404E 03	0.225E 03	0.989E 02	0.245E 02	0.611E 01	0.973E 00
6.20	0.378E 03	0.210E 03	0.927E 02	0.230E 02	0.573E 01	0.912E 00
6.40	0.355E 03	0.198E 03	0.870E 02	0.216E 02	0.538E 01	0.856E 00
6.60	0.334E 03	0.186E 03	0.819E 02	0.203E 02	0.506E 01	0.805E 00
6.80	0.315E 03	0.175E 03	0.772E 02	0.191E 02	0.477E 01	0.759E 00
7.00	0.298E 03	0.165E 03	0.728E 02	0.181E 02	0.450E 01	0.716E 00
7.20	0.281E 03	0.156E 03	0.689E 02	0.171E 02	0.425E 01	0.677E 00
7.40	0.266E 03	0.148E 03	0.652E 02	0.162E 02	0.403E 01	0.641E 00
7.60	0.253E 03	0.140E 03	0.618E 02	0.153E 02	0.382E 01	0.608E 00
7.80	0.240E 03	0.133E 03	0.587E 02	0.146E 02	0.363E 01	0.577E 00
8.00	0.228E 03	0.127E 03	0.558E 02	0.138E 02	0.345E 01	0.549E 00

NO. OF DRELL-PRODUCED PIONS/SR/BEV/C

MACHINE ENERGY IN BEV 20.00

NO. ELECTRONS PER PULSE 0.10000E 11
RADIATION LENGTHS 0.10
HYDROGEN TARGET THICKNESS CM 10.00
NO. H ATOMS PER CC 0.42235E 23

ANGLE	OBSERVED PARTICLE MOMENTUM IN BEV/C
	19.90
0.20	0.867E 01
0.40	0.136E 02
0.60	0.117E 02
0.80	0.877E 01
1.00	0.652E 01
1.20	0.494E 01
1.40	0.383E 01
1.60	0.304E 01
1.80	0.246E 01
2.00	0.203E 01
2.20	0.170E 01
2.40	0.145E 01
2.60	0.124E 01
2.80	0.108E 01
3.00	0.943E 00
3.20	0.833E 00
3.40	0.740E 00
3.60	0.662E 00
3.80	0.596E 00
4.00	0.539E 00
4.20	0.490E-00
4.40	0.447E-00
4.60	0.409E-00
4.80	0.376E-00
5.00	0.347E-00
5.20	0.321E-00
5.40	0.298E-00
5.60	0.277E-00
5.80	0.259E-00
6.00	0.242E-00
6.20	0.227E-00
6.40	0.213E-00
6.60	0.200E-00
6.80	0.189E-00
7.00	0.178E-00
7.20	0.168E-00
7.40	0.159E-00
7.60	0.151E-00
7.80	0.143E-00
8.00	0.136E-00

LIST OF REFERENCES

1. G. Cocconi, L. J. Koester, and D. H. Perkins, Berkeley High Energy Physics Study, UCRL-10022; p. 167 (1961).
2. W. F. Baker, et al., Phys. Rev. Letters 7, 101 (1961).
3. J. Cronin, private communication.
4. M. Thiebaux, private communication. An improved calculation is given by Thiebaux in SLAC Report No. 21, "Pion photoproduction in hydrogen and beryllium," Stanford Linear Accelerator Center, Stanford University, Stanford, California (October 1963).
5. S. D. Drell, Report No. M-200-7a, Stanford Linear Accelerator Center, Stanford University, Stanford, California (1960).
6. A. Odian, private communication.
7. H. P. Noyes, private communication.
8. D. Fries, Internal Memorandum,Stanford Linear Accelerator Center, Stanford University, Stanford, California (1963).
9. J. Ballam, Report No. M-200-8, Stanford Linear Accelerator Center, Stanford University, Stanford, California (1960).

A CHARGE AND ISOTOPIC SPIN ANALYSIS ON THE WEAK INTERACTIONS

by

G. Feldman*

I. INTRODUCTION AND ASSUMPTIONS

This paper will attempt to analyze the weak interactions in terms of Yukawa interactions. Specifically, it is assumed that the Lagrangian for the weak interactions can be written

$$L = \sum_{ij\alpha} f_{ij\alpha}(\bar{F}_i F_j)\bar{W}_\alpha + \text{h.c.} \equiv \sum_{ij\alpha} f_{ij\alpha} J_{ij} \bar{W}_\alpha + \text{h.c.} \qquad (1)$$

where the F_i are fermion fields (F_i destroys the fermion F_i and creates an anti-F_i) and the W_α are vector bosons. The spatial characteristics are understood to be A-V; that is, $(\bar{F}_i F_j)$ stands for $\bar{F}_i \gamma_\mu (1 + \gamma_5) F_j$. The object of the analysis is to find the minimum number of W's which will fit the assumptions (to be stated below) and to find out what relations exist amongst the $f_{ij\alpha}$.

A direct coupling of bosons (K, π, etc.) to W is not assumed, since such an effective coupling will arise via the strong interactions once the J_{ij} is known. For example, if the J_{ij} contains the term $(\bar{\Lambda}p)$, then because this transforms like an $I = 1/2$, $I_3 = +1/2$, B (baryon number) = 0, S (strangeness) = 0 current, there must exist (via the strong interactions) a current of the form $(\sqrt{1/3}\pi^0 K^+ + \sqrt{2/3}\pi^+ K^0)$, also. Similarly, $(\bar{\Lambda}p)$ can be taken to represent $(\sqrt{1/3}\,\bar{\Sigma}_0 p + \sqrt{2/3}\,\bar{\Sigma}^- n)$.

From the Lagrangian (1) there follows an effective four-fermion Lagrangian L_{eff} given by

$$L_{eff} = \sum_{ijkl\alpha} G^{(\alpha)}_{ijkl} J_{ij} \bar{J}_{kl} + \text{h.c.} \qquad (2)$$

---

*Presently at The Johns Hopkins University, Baltimore, Maryland.

where

$$G^{(\alpha)}_{ijk\ell} = \frac{f_{ij\alpha} f_{k\ell\alpha}}{m^2_\alpha} \tag{3}$$

and we have assumed that the masses m_α of all of the W_α are such that $m^2_\alpha >> q^2$, the momentum transfer of interest, and that all of the f's are real.

We list below the assumptions made to determine the number of W's and the couplings.

A. Universal Fermi Interaction. Specifically, in L_{eff}, $G_\mu = G_\beta = G_{\mu\ cap}$, where these are the μ-decay, β-decay, and μ capture coupling constants respectively.

B. No Neutral Lepton Currents. That is, reactions such as

$$n \to p + e^- + \bar{\nu}_e$$

$$\mu^- + p \to n + \nu_\mu$$

$$\mu^+ \to e^+ + \nu_e + \bar{\nu}_\mu$$

$$\Lambda \to p + e^- + \bar{\nu}_e$$

etc., occur; but reactions such as

$$\mu^+ \to e^+ + e^- + e^+$$

do not occur to first order in G.

C. $|\Delta S| \neq 2$ Rule. In non-leptonic decays, $|\Delta S| = 2$ transitions can occur only to orders higher than order G ($\approx f^2/m_W^2$).

D.1. $\frac{\Delta Q}{\Delta S} = +1$ only, in strangeness changing leptonic decays.

D.2. $\frac{\Delta Q}{\Delta S} = \pm 1$ in strangeness changing leptonic decays.

E. $|\Delta I| = 1/2$ Rule. In non-leptonic decays of strange particles, the I-spin must change by one-half unit.

II. CONSEQUENCES OF THE ASSUMPTIONS

We will assume that the types of currents that exist are of the form J_S^Q and J_ℓ^Q where Q and S are the charge and strangeness, respectively, that the currents can destroy, and J_ℓ^Q is a lepton current. We will assume the possible currents are such that

$$Q = 0, \pm 1; \qquad S = 0, \pm 1 \tag{4}$$

(The current J_1^{-1} is simply the hermitian conjugate of a J_{-1}^1 current. We do not consider a current J_2^1, although one could, in principle, have these, and they have in fact been considered by d'Espagnat.[1]

A. As a consequence of Assumption A, the universal Fermi interaction, one would require that there exists a current J such that

$$J = J_o^1 + J_\ell^1 + \ldots \tag{5}$$

where

$$J_o^1 = \bar{n}p, \qquad J_\ell^1 = \bar{e}\nu_e + \bar{\mu}\nu_\mu \tag{6}$$

and thus

$$L = f(J\bar{W} + \bar{J}W) + \ldots \tag{7}$$

B. Assumption B implies that we include also currents of the type J_1^1 (and possibly J_{-1}^1) but no currents J_ℓ^o.

Possible currents of the type J_1^1 are $(\bar{\Lambda}p)$, $(\bar{\Sigma^-}n)$, $(\bar{\Sigma^o}p)$. A current of the type J_{-1}^1 is $(\bar{n}\Sigma^+)$. Thus one can include Assumptions A and B with the minimum number of terms by writing

$$J = J_o^1 + J_1^1 + J_{-1}^1 + J_\ell^1 + \ldots \tag{8}$$

$$K^+ \to \pi^+ + \pi^+ + \ell^- + \bar{\nu} : \quad -\sqrt{\frac{12}{5}}\, g_{23}$$

$$K^+ \to \pi^+ + \pi^- + \ell^+ + \nu : \quad -2\sqrt{\frac{1}{15}}\, g_{23} + \sqrt{\frac{1}{3}}\, g_{13} - \sqrt{\frac{1}{3}}\, g_{11} + \sqrt{\frac{8}{3}}\, g_{01}$$

$$K^+ \to \pi^0 + \pi^0 + \ell^+ + \nu : \quad 2\sqrt{\frac{1}{15}}\, g_{23} + \sqrt{\frac{2}{3}}\, g_{01}$$

$$K_0^2 \to \pi^+ + \pi^0 + \ell^- + \bar{\nu} : \quad \sqrt{\frac{4}{3}}\, g_{13} - \sqrt{\frac{1}{3}}\, g_{11}$$

$$K_1^0 \to \pi^+ + \pi^0 + \ell^- + \bar{\nu} : \quad 2\sqrt{\frac{3}{5}}\, g_{23} + \sqrt{\frac{1}{3}}\, g_{13} + \sqrt{\frac{1}{3}}\, g_{11}$$

where the $g_{\alpha\beta}$ are the amplitudes associated with the 2π's being in an I state of α, and where the $|\Delta I|$ from the K to this 2π state is $\beta/2$, and ℓ is an e or μ.

(2) In Σ and Ξ decays, we list the relative amplitudes

$$\Sigma^- \to n + \ell^- + \bar{\nu} \quad : \quad \sqrt{2}b_1 + b_3$$

$$\Sigma^0 \to p + \ell^- + \bar{\nu} \quad : \quad b_1 - \sqrt{2}b_3$$

$$\Sigma^+ \to n + \ell^+ + \nu \quad : \quad \sqrt{3}b_3$$

$$\Xi^- \to \Sigma^0 + \ell^- + \nu \quad : \quad c_1 + \sqrt{2}c_3$$

$$\Xi^0 \to \Sigma^+ + \ell^- + \nu \quad : \quad -\sqrt{2}c_0 + c_3$$

$$\Xi^0 \to \Sigma^- + \ell^+ + \nu \quad : \quad \sqrt{3}c_3$$

All of the consequences listed in this section follow from the assumption that the $|\Delta I| = 1/2$ rule is valid for non-leptonic decays and that the current $\bar{n}p$ always appears in the combination $(\bar{n}p + \bar{e}\nu_e + \bar{\mu}\nu_\mu)$ (which is the simplest way of insuring Assumption A). If we drop the latter assumption, we do not have the restrictions placed on the amplitudes as listed above.

LIST OF REFERENCES

1. B. d'Espagnat, Nuovo Cimento Series X, 18, 287 (1960).
2. T. D. Lee and C. N. Yang, Phys. Rev. 119, 1410 (1960).
3. T. D. Lee, Phys. Rev. Letters 9, 319 (1962).

Whether J' should contain a lepton current will be discussed later. In order to satisfy the first three assumptions one may put $f' = 0$. However, this puts a restriction on the type of leptonic decays of strange particles that can occur. This is now discussed below.

D.1. $\frac{\Delta Q}{\Delta S} = +1$ only; that is, in those currents which contain leptons the strangeness changing parts must be of the type J^1_1 and not J^1_{-1}.

Consequently, for D.1 to hold, L must be of the form of Eq. (13), provided either $f' = 0$, or J' as given by Eq. (15) contains no lepton currents.

D.2. $\frac{\Delta Q}{\Delta S} = \pm 1$. In contradiction to Assumption D.1, this says that $f' \neq 0$ and that J' must contain lepton currents. If it is assumed that in the $\frac{\Delta Q}{\Delta S} = -1$ component of strange particle decays one has both electron and muon decay, it is then important to make sure one does not contradict Assumption A, the universal Fermi interaction. The simplest way of assuring this is to write

$$J' = J^1_o + J^1_\ell + J^1_{-1} + \ldots \tag{16}$$

If the J^1_o were not included above, then the μ-decay effective Lagrangian would result from both the $J\overline{W}$ and $J'\overline{W}'$ part of the interaction, whereas β-decay and μ-capture would result from only the $J\overline{W}$ part.

Thus, choosing the Lagrangian to be Eq. (13) with J given by Eq. (14) and J' by Eq. (16), one has

$$G_\beta = G_\mu = G_{\mu cap} = \frac{f^2}{m_w^2} + \frac{f'^2}{m'^2_w} \tag{17}$$

The Fermi coupling for $\Lambda \rightarrow p + e^- + \overline{\nu}_e$, G_Λ, is

$$G_\Lambda = \alpha \frac{f^2}{m_w^2} \tag{18}$$

The Fermi coupling for $\Sigma^+ \to n + e^+ + \nu_e$, G_{Σ^+}, is

$$G_{\Sigma^+} = \gamma \frac{f'^2}{m_{W'}^2} \tag{19}$$

The conclusion of this section is that if Assumption D.2 holds rather than Assumption D.1, it is necessary to introduce four intermediate bosons – a W boson of charge +1 and its antiparticle $\overline{W}$ of charge -1, and a W' of charge +1 and its antiparticle $\overline{W'}$ of charge -1.

It is important that $W \neq W'$, because if they were the same one could write L as

$$L = (fJ + f'J')\overline{W} + (f\overline{J} + f'\overline{J'})W \tag{20}$$

and L_{eff} would contain a $J\overline{J'}$ which has an $S = 2$ component, in violation of Assumption C.

E. Assumption E, the $|\Delta I| = 1/2$ rule, can be formulated to state that the strangeness changing non-leptonic part of $L_{eff}(\mathcal{L}_s)$ must transform like a component of an $I = 1/2$ spinor. Specifically, in L_{eff} we have the terms

$$\mathcal{L}_s = G \sum_{\alpha} \overline{J}_o^{-\alpha} J_1^{\alpha} + h.c. \tag{21}$$

where α runs over the charge 0, ±1, and we must choose the J_S^Q such that $\sum_{\alpha} \overline{J}_o^{-\alpha} J_1^{\alpha}$ transforms like an $I = 1/2$, $I_3 = -1/2$ component. (It should be the $I_3 = -1/2$ component for this term ($S = +1$) in order that L_{eff} be neutral.)

The currents J_o^Q consist of a nucleon and an antinucleon and so can transform as an $I = 0$, or $I = 1$ multiplet.

The currents J_1^Q consist of a nucleon and an antihyperon (Σ or Λ) and can transform like an $I = 1/2$ or $I = 3/2$ multiplet. It is only necessary that the currents so obtained are combined such that $\sum_{\alpha} \overline{J}_o^{-\alpha} J_1^{\alpha}$ transforms like $I = 1/2$, $I_3 = -1/2$.

Consider now the following Lagrangian:

$$L = f(J^{+}\overline{W^{+}} + J^{o}\overline{W^{o}} + J^{-}\overline{W^{-}}) + h.c. \tag{22}$$

where (we shall neglect the lepton currents for the time being)

$$J^{+} = c^{+}(\overline{n}p) + \frac{1}{c^{+}}(\sqrt{2}\overline{\Lambda}p) + \frac{\delta}{c^{+}}(-j_{\frac{1}{2}}) \tag{23}$$

$$J^{o} = \frac{c^{o}}{\sqrt{2}}(\overline{p}p - \overline{n}n) + \frac{1}{c^{o}}(-\overline{\Lambda}n) + \frac{\delta}{c^{o}}(\sqrt{2}j_{-\frac{1}{2}}) \tag{24}$$

$$J^{-} = c^{-}(\overline{p}n) + \frac{\delta}{c^{-}}(\sqrt{3}j_{-\frac{3}{2}}) \tag{25}$$

with

$$j_{-\frac{3}{2}} = \overline{\Sigma^{+}}n \tag{26}$$

$$j_{-\frac{1}{2}} = \sqrt{\frac{1}{3}}\,\overline{\Sigma^{o}}p + \sqrt{\frac{2}{3}}\,\overline{\Sigma}_{o}n \tag{27}$$

$$j_{+\frac{1}{2}} = \sqrt{\frac{2}{3}}\,\overline{\Sigma}_{o}p - \sqrt{\frac{1}{3}}\,\overline{\Sigma^{-}}p \tag{28}$$

and for completeness

$$j_{\frac{3}{2}} = \overline{\Sigma^{-}}p \tag{29}$$

(Thus, the j_i are just the components of an $I = 3/2$ multiplet, and c^{+}, c^{o}, c^{-} and δ are constants.)

Assuming $m_{w^{+}} = m_{w^{o}} = m_{w^{-}} \equiv m_{w}$, one is led to the following relevant

(for the $|\Delta I| = 1/2$ rule) part of $L_{eff}(\mathcal{L}_s)$:

$$\mathcal{L}_s = \frac{f^2}{m_W^2}\left[\sqrt{2}\,(\bar{\Lambda}p)(\bar{p}n) - (\bar{\Lambda}n)\,\frac{(\bar{p}p - \bar{n}n)}{\sqrt{2}}\right]$$

$$+ \frac{f^2\delta}{m_W^2}\left[-\,j_{\frac{1}{2}}\bar{p}n + \sqrt{2}\,j_{-\frac{1}{2}}\,\frac{\bar{p}p - \bar{n}n}{\sqrt{2}} + \sqrt{3}\,j_{-\frac{3}{2}}\bar{n}p\right] + \text{h.c.} \tag{30}$$

The coefficients in the J^Q have been chosen so that the expressions in square brackets in Eq. (30) transform like $I = 1/2$, $I_3 = -1/2$; that is, they obey the $|\Delta I| = 1/2$ rule.

The parameter δ will or will not be zero depending on whether one assumes D.1 or D.2.

(If one had allowed currents of the type J^1_2, one could have built up a correct $\mathcal{L}_s$ without introducing neutral currents and thus neutral W's. See Ref. 1.)

If D.1 is assumed, one sets $\delta = 0$; there is no need for a J^- and thus no need for a W^-, and one can take

$$L = f(J^+\overline{W^+} + J^O\overline{W^O}) + \text{h.c.} \tag{31}$$

with J^+, J^O given by Eqs. (23) and (24) with δ set equal to zero.

We are therefore led to introduce four bosons, a W^+ and W^O and their antiparticles.[2] (As mentioned above, we cannot take $W^O = \overline{W^O}$ because a violation of Assumption C would follow.)

If we assume D.2, $\delta \neq 0$, the Lagrangian is given by Eq. (22), and we are led to introduce six intermediate bosons, W^+, W^O, W^- and their antiparticles, all different.

To complete the scheme we must add the lepton currents. This must be done in such a way that Assumption A is not volated. The simplest way of doing this is to make the replacement

$$(\bar{n}p) \rightarrow (\bar{n}p) + (\bar{e}\nu_e) + \bar{\mu}\nu_\mu) \tag{32}$$

Thus, in Eq. (23) the term $c^+[(\bar{e}\nu_e) + (\bar{\mu}\nu_\mu)]$ should be added, and to Eq. (25) the term $c^-[(\bar{\nu}_e e) + (\bar{\nu}_\mu \mu)]$ should be added.

Clearly, this is not the most general way of including the lepton currents without violating Assumption A. In fact, the replacement Eq. (32) will lead to certain consequences of leptonic decays of strange particles, which will be discussed later. The most general replacement is to add to J^+ in Eq. (23) the terms $\alpha^+(\bar{e}\nu_e) + \beta^+(\bar{\mu}\nu_\mu)$ and to add to J^- in Eq. (25) $\alpha^-(\bar{\nu}_e e) + \beta^-(\bar{\nu}_\mu \mu)$, subject only to the restrictions

$$c^+\alpha^+ + c^-\alpha^- = c^+\beta^+ + c^-\beta^- = \alpha^+\beta^+ + \alpha^-\beta^- \qquad (33)$$

III. SOME OTHER CONSEQUENCES AND ASSUMPTIONS

A. The case of $c_+ = c_o = c_- = 1$ with replacement Eq. (32) has been discussed by Lee.[3]

Here we have the J_o^Q parts of the current transforming like an $I = 1$ multiplet. Thus we can take the W-particles to have the following properties and selection rules in their interactions, namely that (W^+, W^o, W^-) form an $I = 1$ triplet with $S = +1$ and that $(\overline{W^-}, \overline{W^o}, \overline{W^+})$ form an $I = 1$ triplet with $S = -1$. The selection rules are then

$$W \rightarrow \text{non-strange particles } \Delta I = 0, \quad |\Delta S| = 1$$

and

$$W \rightarrow 1 \text{ strange} + \text{non-strange } |\Delta I| = \frac{1}{2}, \quad \Delta S = 0 \ .$$

B. The Lepton-Current Assumption. If we make the assumption given by Eq. (32), this is equivalent to the assumption that the lepton current transforms like an $I = 1$ multiplet whose neutral component is zero.

Thus, the $\Delta I = \frac{1}{2}$ rule for non-leptonic decays implies a "$|\Delta I| = \frac{1}{2}$ rule" for leptonic decays where we treat the lepton current as transforming like an $I = 1$ multiplet with 0 neutral component.

For example, let us consider the decays of $K \rightarrow \pi$ + leptons. The $|\Delta I| = \frac{1}{2}$ for non-leptonic decays plus replacement Eq. (32) implies that

the most general effective (Kπ-lepton) interaction is of the form

$$f_{\frac{1}{2}}[\sqrt{2}(\pi^{o}K^{+} + \sqrt{2}\pi^{+}K^{o})j_{\ell}^{-} - (\sqrt{2}\pi^{-}K^{+} - \pi^{o}K^{o})j_{\ell}^{o}]$$

$$+ F_{\frac{3}{2}}[3(\pi^{-}K^{o})j_{\ell}^{+} + \sqrt{2}(\pi^{-}K^{+} + \sqrt{2}\pi^{o}K^{o})j_{\ell}^{o} - (\sqrt{2}\pi^{o}K^{+} - \pi^{+}K^{o})j_{\ell}^{-}] + \text{h.c.} \tag{34}$$

where

$$\begin{aligned} j_{\ell}^{-} &= (\bar{\nu}_{e}e) + (\bar{\nu}_{\mu}\mu) \\ j_{\ell}^{o} &= 0 \\ j_{\ell}^{+} &= (\bar{e}\nu_{e}) + (\bar{\mu}\nu_{\mu}) \end{aligned} \tag{35}$$

from which it follows, for example, that the amplitudes a_{+} and a_{o} for

$$K^{+} \rightarrow \pi^{o} + e^{+} + \nu_{e}$$

and

$$K_{2}^{o} \rightarrow \pi^{-} + e^{+} + \nu_{e} \quad \left[K_{2}^{o} = \frac{1}{\sqrt{2}}(K_{o} - \bar{K}_{o})\right]$$

are

$$a_{+} = a_{o} = \sqrt{2}(f_{\frac{1}{2}} - f_{\frac{3}{2}}) \ . \tag{36}$$

The interaction (34) has been constructed such that the square brackets transform like an $I = 1/2$ component if we assume that $(j_{\ell}^{+}j_{\ell}^{o}j_{\ell}^{-})$ transform like an $I = 1$ multiplet.

There are other results which follow from these assumptions.

(1) In $K \rightarrow 2\pi$ + leptons, we list the relative amplitudes for the relevant decays.

where

$$J_1^1 = \alpha(\overline{\Lambda}p) + \ldots \tag{9}$$

and

$$J_{-1}^1 = \gamma(\overline{n}\Sigma^+) \tag{10}$$

Again

$$L = f(J\overline{W} + \overline{J}W) + \ldots \tag{11}$$

and still only two intermediate bosons are required.

C. The $|\Delta S| \neq 2$ rule implies that in L_{eff} (which is proportional to $J\overline{J}$) there is no $(L_{eff})^{Q=0}_{|S|=2}$.

If J is as given by Eq. (8), then there exists a term in $J\overline{J}$ which is

$$(L_{eff})^{Q=0}_{S=2} = \frac{f^2}{m_W^2} J^1_1 \overline{J}^{-1}_{-1} = \frac{f^2}{m_W^2} \alpha\gamma(\overline{\Lambda}p)(\overline{\Sigma^+}n) + \ldots \tag{12}$$

Thus, one must not allow a J^1_1 and a J^1_{-1} to couple to the same W-meson.

One must take

$$L = f(J\overline{W} + \overline{J}W) + f'(J'\overline{W'} + \overline{J'}W') + \ldots \tag{13}$$

where now

$$J = J^1_0 + J^1_1 + J^1_\ell + \ldots \tag{14}$$

and

$$J' = J^1_{-1} + \ldots \tag{15}$$

BEAM CURRENT MONITORS FOR A HIGH ENERGY LINAC

D. B. Isabelle

I. INTRODUCTION

The problem of beam monitoring for SLAC is far more complicated than for machines such as Mark III or the Orsay linac. This is due to the high energy of the electrons (20 GeV) and the relatively high intensity of the beam ($\sim$ 100 μA).

The purpose of this report is to study the different types of classical monitors used in conjunction with a linac and to discuss if they can be adapted to the SLAC case. The first type to be considered is the Faraday cup, a piece of material in which all the beam is stopped; this is the only absolute monitor at our disposal. Then we shall consider the monitors which give only a relative indication and therefore must be calibrated. Among these the most commonly used is the Secondary Electron Monitor, which presents the advantage of being useful over a very large range of current. Because this type of monitor places some material in the beam path, heat problems will have to be considered. A second type of relative monitor is the Induction Monitor (or ferrite core monitor); it works as a pulse transformer and presents the great advantage of introducing no perturbation of the beam. At the end of this study we will consider some other types of monitors which also present the advantage of leaving the beam undisturbed but whose accuracy is more doubtful.

Before starting this study it will be worthwhile to summarize the requirements of the SLAC machine. First of all, the dynamic range of currents to be detected is very wide; some experiments will be done with a very good energy resolution of the beam at a reduced current, while other experiments such as the production of neutrinos will require the use of the full beam. So we can say that we must have at our disposal current monitors which can provide measurement of intensity from 30×10^{-9} A up to 150×10^{-6} A. On the other hand, there is a need for a monitor giving a non-destructive indication of the beam intensity; such monitors will be used as safety devices to turn off the machine if,

due to bad steering or failure of a component, the beam has disappeared between two such safety monitors. For this purpose an accuracy of 10-20% might be good enough, while the experimentalist will ask for a few tenths of a percent at least. In the conclusion we will summarize the quality of the different types we are going to study and show in which range and for which purpose each can be used.

II. FARADAY CUP

The design of a Faraday cup to be used with an electron beam of very high intensity and very high energy is not trivial not only because a few megawatts of power must be dealt with, but also because at the shower maximum the electron multiplicity is very large (> 100). The designs proposed up to now have all proved to be impractical. We shall consider the possibility of modifying one of the beam dumps now under design for use as a Faraday cup possessing a relatively good efficiency.

A. Size of the Faraday Cup

The scheme presently considered for a beam dump consists of water tanks with a length of 15 X_o (H_2O) (where X_o (A) is the radiation length for material A), in which the water moves with a speed of 25 ft/sec. The tank is followed by a stack of water cooled copper plates with an overall length of 15 X_o (Cu). Such a device is supposed to stop more than 95% of the primary beam power.

It has been shown[1] that for a 500 MeV primary beam a thickness of 42 X_o is sufficient to collect all the electron charges with an accuracy of better than 0.1%. To reduce the energy from 20 BeV to 500 MeV we need only 4 X_o additional thickness, because the beam energy is mainly lost through radiation. This implies that a 20 BeV Faraday cup must have an overall length of 46 X_o, which means that 16 X_o of some material must be added behind the beam dump to transform it into a conservative Faraday cup (that is, if one is concerned with the longitudinal development of the shower). It has also been shown that it is important to have a low Z material as the external skin of the cup in

order to decrease the photoeffect production of electrons by low energy photons. Lead poured in an aluminum jacket can be used for this purpose.

However, a shower cascade also has a radial development about which very little is known, at least experimentally. Up to now Faraday cup designers have been using the experimental results of Kantz and Hofstadter[2] to determine the radius to be given to the cup, but those measurements have been done only for an incident energy of 183 MeV. R. Mozley of SLAC is repeating the same type of measurements at higher energy. His results will also provide a check to the calculations done by Zerby and Moran[3] using the Monte Carlo method. Unfortunately, the latter calculations of the longitudinal and radial shower extension have only been done for an overall thickness of 10 radiation lengths; they give no definitive information about the low energy part of the shower, which is the part that will have the larger diameter. From their calculations, it can be derived that at a depth of 10 radiation lengths about 10% of the energy is outside a cylinder of one radiation length diameter. Because the water part in the beam dump will have a length of 15 X_o (H_2O), a jacket consisting of a few radiation lengths of a heavy material must be put around the core of the beam dump. Again, we must remember in the final design that the external surface must be made of a low Z material.

It has been shown[1] that for high energy primary electrons the number of back-scattered electrons on the entrance face of the cup is very small, but the number of secondary electrons can be of the order of a few percent. However, these electrons have a very low energy (a few electron volts) so that a permanent magnet which provides a field of a few hundred Gauss will be strong enough to recapture them.

B. Insulation Problems

This will surely be the more complicated problem to solve. The beam dump will be cooled through a heat exchanger. If deionized water is used in the secondary circuit and if insulating leads are provided between the heat exchanger and the external water circuit, it would seem reasonable that insulation would not be too complicated a problem. Unfortunately, the results obtained with the present Mark IV Faraday cup seem to contradict this statement. This cup, which is water cooled

in a way similar to the method described above, is operating as a battery even without any beam on it. It will therefore be worthwhile to examine the causes of this phenomenon to gain helpful information for the SLAC final design.

As we want to collect all the charge deposited in the cup, it will be necessary that all the electric components are connected together. It is also necessary to collect the charge contained in the water itself. As pure water is an insulator, there will be little chance for the charged particles to reach a metallic surface, but as the water will be subjected to irradiation, we can hope that its conductivity will be good enough. If it is not, a very important source of charge leak will result. If a relatively large number of low-energy electrons can be produced on the surface of the copper plates by photoeffect and then stopped in the water, they must be re-collected to avoid completely upsetting the charge balances. It must also be hoped that the efficiency of re-collection will be the same for both the electrons and the ions produced in the water. We do not need to take into account the charge losses due to the escaping mu-mesons, as the difference between μ^- and μ^+ will be small as compared to the total number (less than 10^{-3} of the number of incident electrons).

In order to have a good Faraday cup, it will also be necessary to install a vacuum tank so that no charge leakage can be produced by the air. Because many ionizing particles will go out of the beam dump it is likely that the air around it will be ionized; however, due to the size of the beam dump, the cost of a vacuum tank will be prohibitive.

There are two ways to check the problem of insulation. The first one, which will provide information about the leakage through the cooling system, is to run the cup with and without cooling (for a very short time) and to compare the efficiency using a secondary electron monitor as a reference device. The second way consists of sending a γ-ray beam into the cup and looking for any charge collected.

C. Conclusion

It seems to us that the problem of insulation will be a major one to solve. It would be easy to modify the beam dump so that it is capable of

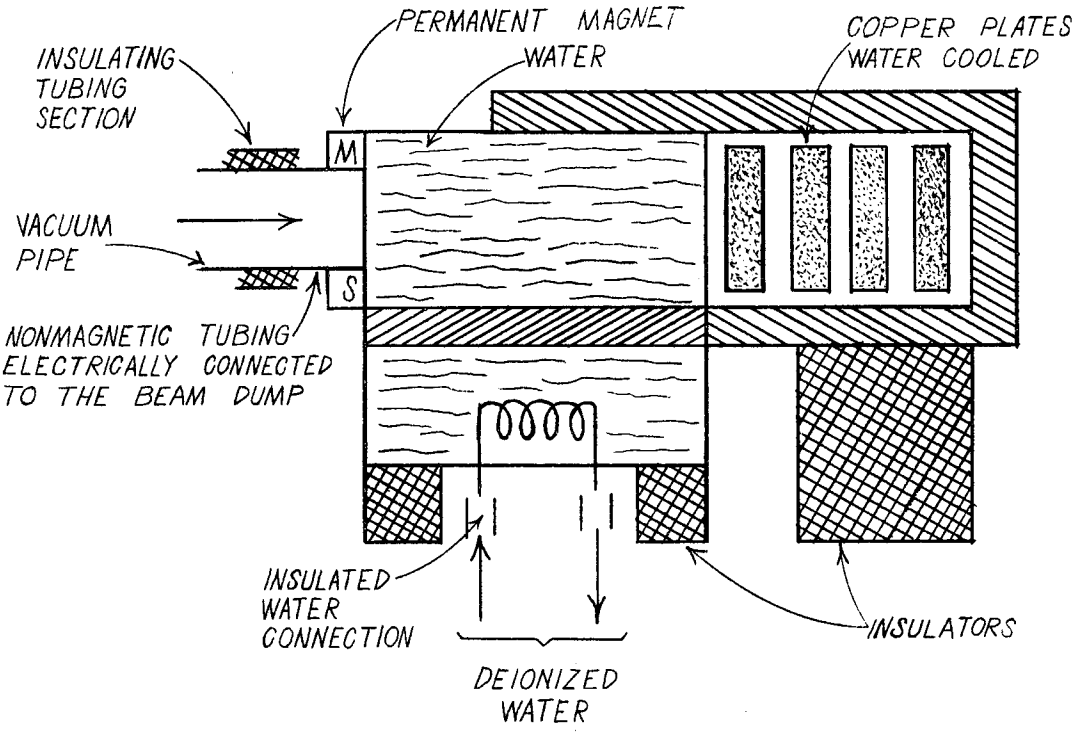
PERMANENT MAGNET
WATER
COPPER PLATES
WATER COOLED
INSULATING
TUBING
SECTION
M
VACUUM
PIPE
S
NONMAGNETIC TUBING
ELECTRICALLY CONNECTED
TO THE BEAM DUMP
INSULATED
WATER
CONNECTION
INSULATORS
DEIONIZED
WATER

FIG. 1

stopping more than 99% of the charge, but it is impossible to make any guess about the importance of the leaks. Therefore, the Faraday cup solution will be considered only if no other accurate and absolute monitor can be provided (see Fig. 1).

III. THE SECONDARY ELECTRON MONITOR

During the past ten years secondary electron monitors (referred to hereafter as SEM) have been used in connection with electron linacs[4] to measure beam intensity. An SEM is made by using a stack of very thin foils in an evacuated tank which has thin windows to allow the beam to get in and out. All the odd foils are electrically connected together and are maintained at a potential difference with respect to the even foils.

The principal characteristic of interest is that an SEM may be used to monitor the beam current without intercepting an appreciable fraction of the beam. One problem is that the efficiency of an SEM has been shown to be relatively unstable when aluminum foils were used. An experiment done in Orsay,[5] about a year ago, demonstrated that it was possible to stabilize the efficiency by using a clean metallic surface – gold, for example. If this result is verified for other metals, it will demonstrate that these monitors can be used for long periods without need of recalibration. Under such conditions we believe that an accuracy of 10^{-3} can be achieved.

The main problem which has to be solved for an SEM to be used with a high-intensity beam is dissipation of the heat produced by the electron energy losses in the foils. We shall first consider this problem and show how it can be solved. Then we shall discuss the general design of such a monitor. Finally, we shall discuss some of the calibration problems and the accuracy which can be achieved.

A. Heat Problem

We start by assuming that the beam is a cylinder of radius r_o and that our foil is a disk of external radius r_1 and thickness ℓ. Also, we assume that by one means or another the temperature T_1 of the edge

of the disk is kept constant (we discuss later how this can be done).

The amount of heat g which is transferred from the center of the foil to its edge per unit of time is given by Fourier's law, which for our case can be written[6]

$$g = \frac{2\pi k \ell (T - T_1)}{\ell n(r_1/r_o)} \tag{1}$$

where T is the temperature at the center of the disk, and k is the heat conductivity which is assumed to be independent of the temperature.

The equilibrium temperature at the center of the disk will be reached when the amount of heat Q deposited by the beam per second is equal to the amount of heat dissipated by conductivity:

$$g = Q \tag{2}$$

We use N for the number of electrons in the beam per second, and ΔE for the energy loss in cal $g^{-1}cm^{-2}$. So we have

$$Q = N\Delta E \rho \ell \tag{3}$$

where ρ is the density in g cm^{-3}.

Using (1) and (3) in (2) we have

$$T - T_1 = \frac{N\Delta E}{2\pi} \ell n(r_1/r_o)\frac{\rho}{k} \tag{4}$$

From Eq. (4) we see that in order to have the smallest $(T - T_o)$ we should choose a material for which ρ/k is small. In Table I we show this ratio for different metals at room temperature (300^oK). This seems to favor the choice of aluminum or beryllium as the metal to be used, but as we shall see later the secondary electron emission characteristics of these two elements are less favorable than for the others.

TABLE I

Metal	Be	Al	Ti	V	Fe	Cu	Ag	Au
ρ	1.84	2.7	4.5	5.69	7.8	8.9	10.5	19.3
k	0.40	0.55	0.05	0.08	0.18	0.95	1.0	0.85
ρ/k	5.26	4.91	9.0	71.1	43.3	9.37	10.5	22.7

We now consider the way in which the temperature of the edge of the disk can be kept constant. One way of doing this is to mount all of the disks in a cylinder made of a material which has very good emissivity and thus to transfer the heat to the walls of the vacuum chamber which can be easily cooled. We use the Stefan-Boltzmann law:

$$g' = \sigma AF(T_1^4 - T_o^4)$$

where F is a factor that takes into account the geometrical configuration and the fact that the emissivity is smaller than 1. A conservative figure for F seems to be 0.5. Here σ is the Stefan-Boltzmann constant, which is 5.68×10^{-5} erg $cm^{-2}d^{-4}s^{-1}$.

At equilibrium we have

$$g' = Q$$

so

$$A(T_1^4 - T_o^4) = \frac{N\Delta E\rho\ell}{\sigma F} \qquad (5)$$

To minimize the difference in temperature it is necessary to choose a large value for A. But this is more or less incompatible with Eq. (4), according to which we would like to have the ratio r_1/r_o as small as possible.

Numerical applications. We assume the following parameters:

$N = 2 \times 10^{14}$ electrons per second

$\Delta E = 2$ MeV $cm^2 g^{-1}$ (the actual value will doubtless be smaller)

$\ell = 1$ mil $= 2.5 \times 10^{-3}$ cm

$A = 600\ cm^2$

$r_o = 0.1$ cm

$r_1 = 10$ cm

We have summarized the results for these conditions in Table II, in which it can be seen that even in the worst case, that of gold, the temperature in the center is below the melting point of the material. Our principal concern, then, will be with the variation of secondary electron emission versus temperature (see below). We have also indicated in Table II the temperature rise per pulse, which shows that there will be no problem of overheating during the beam pulse.*

TABLE II

	Be	Al	Cu	Ag	Au
$\rho(g/cm^3)$	1.84	2.7	8.9	10.5	19.3
c(cal/g)	0.45	0.23	0.103	0.60	0.032
Q (erg/sec)	3×10^6	4.3×10^6	1.42×10^7	1.68×10^7	3.1×10^7
$(T - T_1)\ ^oC$	59	55	105	117	254
$T_1\ ^oK$ $(T_o = 300^oK)$	302	302	307	309	316
$T_1\ ^oK$ $(T_o = 240^oK)$	244	244	254	256	268
T^oC $(T_o = 300^oK)$	88	74	139	153	297
T^oC $(T_o = 240^oK$	30	26	66	80	249
ΔT^oC per pulse	0.62	0.31	0.14	0.81	0.043

*As the foils we are using are very thin (1 mil) and their number small (11-21), the overall thickness of the SEM expressed in radiation length will be very small (~ 1/100 of a radiation length) we do not need to take into account any shower effect.

Note: We derived Eq. (4) assuming that the foil has a uniform thickness along a radius. In the case of a low-energy electron beam it would be necessary to have a large surface of thin foil because the beam can have a large diameter due to multiple scattering through the target and various windows. This is not the case for a very high energy machine, where the beam will always have a very small diameter; under these conditions we can reduce the radius of the thin foil. Then we have to consider two cases:

1. We can first calculate the variation of temperature in the center when the radius of the overall system decreases. The results of such a calculation are shown in Fig. 2. It can be seen that as long as the radius does not become too small the temperature remains constant within a few ^{o}C.

2. We can also mount the thin foil in the center of a disk of greater thickness, ℓ_1, so the heat dissipation by conductivity will become larger. Assuming that the thin foil has a radius r_2, and that r_1 is the radius of the large ring, the heat conductivity for the two materials being respectively k and k_1, we can rewrite Eq. (4) in the following way:

$$T - T_1 = \frac{N\Delta E}{2\pi} \frac{\rho}{k} \left[\ell n(r_2/r_o) + \frac{\ell k}{\ell_1 k_1} \ell n(r_1/r_2) \right]$$

For example, if $r_2 = 1.5$ cm, $\ell/\ell_1 = 1/10$, and $k = k_1$, we find that the temperature difference between the center and the edge will be 1.6 times smaller with the composite mounting than with the simple foil.

B. Choice of the Foil

To decide which type of foil we want to use in the SEM two factors must be taken into consideration: first, the heat behavior of the material as it has been discussed in the previous section; second, its secondary electron emission efficiency.

From the values of the ratio ρ/k tabulated in Table I we see that the two best metals from the heat point of view seem to be beryllium and aluminum. We do not have any information about the secondary electron

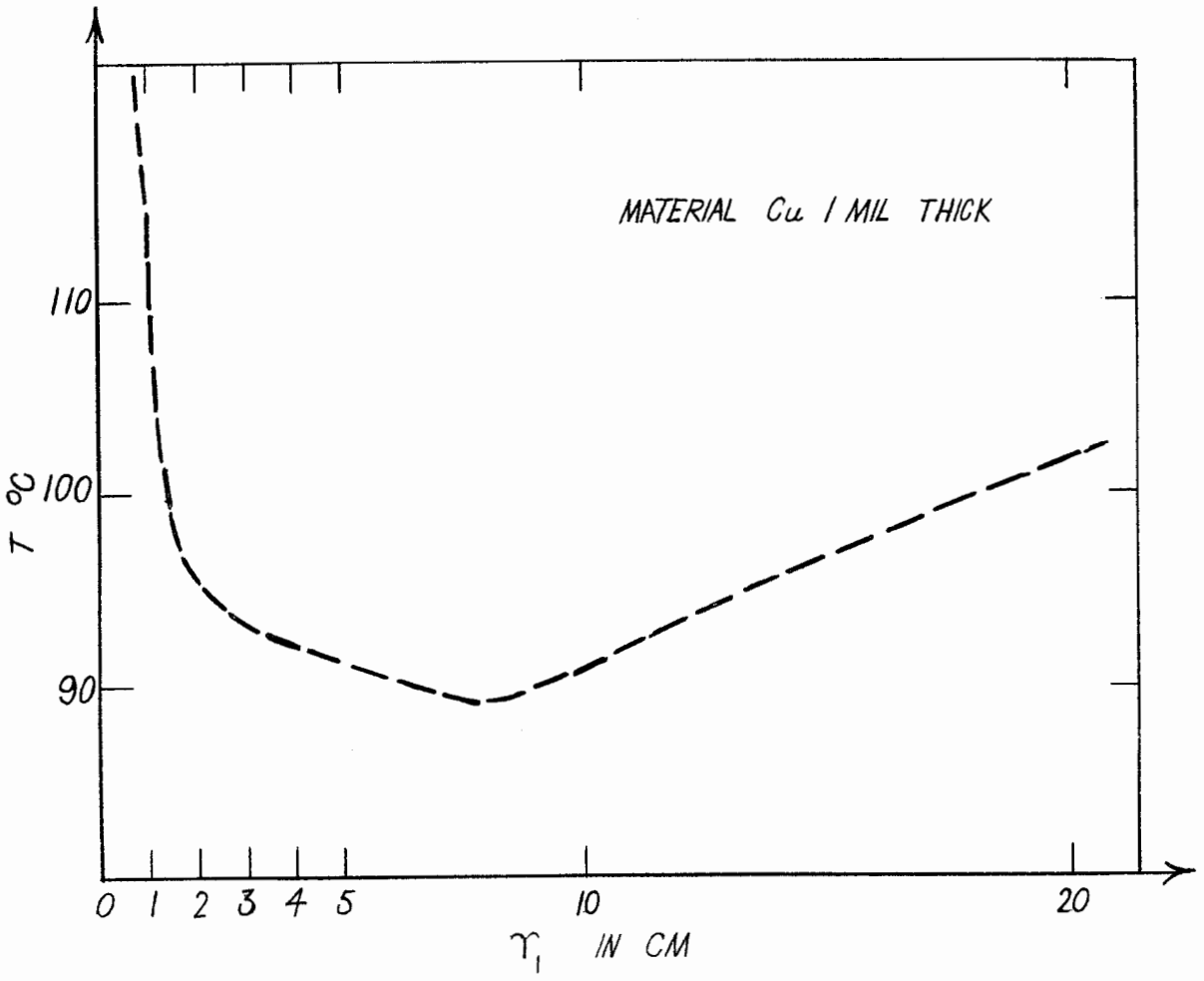

FIG. 2

emission properties of beryllium, but aluminum has been extensively used in many laboratories, and it has been shown that its efficiency is a strong function of the surface state. It is well known that secondary electrons are produced in the molecular layers lying close to the surface, so in the case of aluminum foil they are produced in the aluminum oxide layer whose behavior depends on the radiation damage caused by the primary electrons. Beryllium metal is also covered with a layer of oxide, so it is likely that it will behave similarly to aluminum.

A way of removing these instabilities consists of making a gold deposit (~ 1 micron thick) on the aluminum foil. This has been done successfully at Orsay,[5] and it has been shown that the efficiency is much more stable and also that it is possible to open the SEM to air and then pump it down again without seeing any variation in efficiency. This could be a solution as long as the heating and fatigue of the foil do not produce a separation between the gold layer and the aluminum foil.

Another solution would be to use copper foil. But as we increase the Z of the material the thickness of the SEM expressed in radiation lengths will also increase, so as the aluminum radiation length is 6.2 times the copper one it will be necessary to use thinner foils as well as a smaller number of foils if we want to keep the background production at the same level. Another possibility is to put the SEM further downstream; as the multiple scattering for the high energy is very small this will not imply an increase of the useful diameter of the SEM.

C. General Design of the SEM

A general design of an SEM which takes into account the conclusions we have reached in our study is shown in Fig. 3. No emphasis has been put on mechanical detail, but we want to point out a few important facts which must be kept in mind for the final design.

a. The insulator must be quartz or ceramic, for obvious reasons of radiation damage, the second type being more convenient since it can be easily machined.

b. The internal surface of the vacuum chamber and the external surfaces of the fixed shells in which the foil is mounted must be covered with a black enamel. If iron is used it must be oxidized.

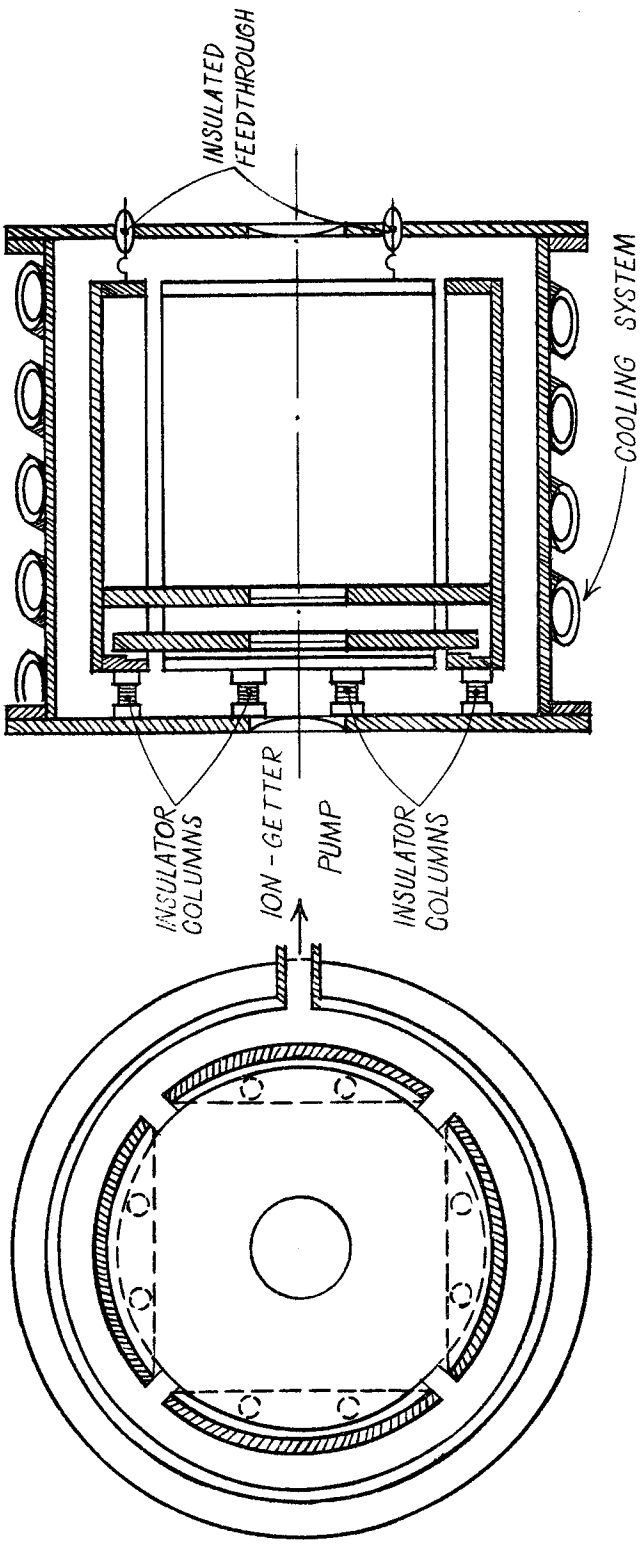
INSULATED FEEDTHROUGH
COOLING SYSTEM
INSULATOR COLUMNS
ION - GETTER PUMP
INSULATOR COLUMNS

FIG. 3

c. The vacuum should be provided by an ion-getter pump, and metal gaskets should be used. A magnetic shield must be provided between the pump permanent magnet and the SEM body so that no magnetic field can disturb the electron path between foils.

d. It may also be important to cool the two flanges in such a way that no damage will be produced if, due to a bad steering, the beam hits them. The system which is used to cool the wall can also be used for the flanges.

e. The windows used to let the beam in and out will have to be cooled. These can be of the same type as those used at the end of the machine.

D. Calibration and Accuracy of the SEM

The only way to have an absolute and accurate calibration of the SEM is to compare its response to that of a Faraday cup. In the case of SLAC it seems very difficult to design a cup with a 99.9% efficiency because of the large power carried in the beam ($\approx$ 2 megawatts). Another possibility would be to use an induction monitor, but no integrating circuit has been developed up to now which will provide an accuracy of the order of 0.5% or better.

We suggest here two other ways of calibrating which could give good accuracy:

1. Measurements done up to now either at Stanford or at Orsay seem to demonstrate that the efficiency of an SEM is more or less independent of the number of electrons per beam pulse.* This has been verified for average current up to 1 μa only, and it will be interesting to see if it remains true for larger currents. Such experiments will be performed next year with the NBS linac. If this constancy is verified, it would be possible to build a Faraday cup for an average current 10 to 100 times smaller than the maximum and to calibrate the SEM against it.

2. It has been observed both at Stanford and Orsay that the efficiency seems to increase proportional to $\ln p/mc^2$, where p is the incident electron momentum. This law has been verified between 100 and

*(An increase of 1% has been seen for a number of electrons per pulse varying from 10^7 to 10^{11}.)

600 MeV. As an external electron beam is now available on the CEA machine, it would be interesting to build an SEM which could be calibrated on Mark III up to 1 BeV and at CEA from 1 to 6 BeV. Measurements for one or two values of the primary energy would be done at both places to normalize the Faraday cup efficiencies. If the law according to which the efficiency increases were verified up to 6 BeV there would be no reason not to believe an extrapolation up to 20 BeV.

To determine the accuracy to which this calibration could be done we first have to consider the accuracy with which we can measure the efficiency of an SEM by comparing the current produced to the one measured in a Faraday cup at the same time. At Orsay, with the gilded-foil SEM, and for currents between 10^{-3} and 10^{-7} amp, we have been able to obtain measurements which can be repeated within 2×10^{-3}. The main error in this measurement was caused by small instabilities in the current integrators and leakage in the integrating capacity. We think that a reproducibility of 10^{-3} can be obtained with a minimum of effort.

If we now consider the error made on the determination of the SEM efficiency using the two methods of calibration previously discussed, we see that Method 2 should give the best overall accuracy since we should be able to determine the efficiency up to 6 GeV with an accuracy of 2×10^{-3}; since this varies as $\ell n\ p/mc^2$, the extrapolation would permit us to know the efficiency at 20 BeV with an accuracy better than 5×10^{-3}. For the case of Method 1 we would have to reduce the current by a factor of 100 at least, and even then it would not be possible to achieve an accuracy better than 10^{-2}.

E. Conclusions

The preceding discussion has shown the possibility of building an SEM for high-intensity electron current, in which the temperature of the foil could be kept to a reasonable value without the use of water cooling. However, as we have already noted, a few points need to be investigated in more detail before deciding on the final design; we summarize these below:

1. Study of the stability of secondary electron emission efficiency for various types of materials. This work is expected to be done by

J. Muray using a small SEM on the Mark IV accelerator.

2. Study of foil fatigue. A project using a powerful electron gun from an old klystron is under study at SLAC; another source of information will be the measurements done at the NBS.

3. Study of efficiency variation as a function of primary intensity. This is more or less related to the preceding point; experiments planned at NBS will give valuable information.

4. Study of the efficiency as a function of the primary electron energy (see Section D.2). This method seems to be the one which will give us the best knowledge of SEM efficiency.

IV. INDUCTION CURRENT MONITOR

The induction current monitor has been widely used for a long time in industry to monitor very high intensity current. These monitors have also been used to measure the currents produced by klystron tubes. More recently, due to the necessity to measure current inside particle accelerators in a nondestructive way, studies have been done in different laboratories about the possibility of using such a monitor even with relatively low intensity beams and very sharp pulses.

The principle of such a monitor is obvious even if its realization is not elementary. The basic idea is to have a magnetic core on which are wound a few turns of wire and through which the beam to be detected is traveling. This is a pulse transformer whose primary circuit is the beam itself. One of the important points in the design of such a monitor is to be able to find a material having a large μ even for the frequency we have to consider, as the rise time of the system must be short compared to the width of the pulse. This width can be as small as 1/10 μsec, so we really need to have a rise time of the order of nanoseconds if we do not want to lose any information about the shape of the pulse.

Many other practical problems occur in the realization of such a monitor, but they will be discussed in a later section. We would like first to discuss the two ways in which the signal produced can be used; that is to say, the fast integrator and the resonant circuit. Then we will outline the advantages and inconveniences of such a monitor as well

as the range of current over which it can be used. Let us summarize some of the equations on which the behavior of such a monitor is based. It is possible to show by a long but tedious calculation that the voltage induced through one turn on a coil of magnetic permeability μ is given by the following expression[7] if the beam axis and the coil axis are parallel (see Fig. 4).

$$\mathcal{V} = \frac{\mu_o a}{2\pi} \frac{di}{dt} \left\{ - k \ln \frac{\rho_2}{\rho_1} + \sum_1^n \frac{1}{n} r_o^n \left[\frac{2k(k-1)\left(\rho_2^n - \rho_1^n\right) - 2k(k+1)\rho^{-2n}\left(\rho_2^{-n} - \rho_1^{-n}\right)}{(k+1)^2\rho_2^{2n} - (k-1)^2\rho_1^{2n}} \right] \cos\theta \right\}_{emu} \quad (1)$$

where

$k = \mu/\mu_o$

ρ_2 and ρ_1 are respectively the outside and inside diameter of the core

r_o defines the position of the beam axis relative to the coil axis

θ = angular position of the loop.

From that equation we see immediately that if the beam and coil axis are at the same position ($r_o = 0$) then we have the classical equation

$$\mathcal{V} = - \frac{k\mu_o a}{2\pi} \ln \frac{\rho_2}{\rho} \times \frac{di}{dt}$$

and if we have N turns wound on the core the induced voltage V will be N times larger than the one induced in one turn

$$V = N\mathcal{V} = - \frac{k\mu_o Na}{2\pi} \ln \frac{\rho_2}{\rho_1} \times \frac{di}{dt} \quad (2)$$

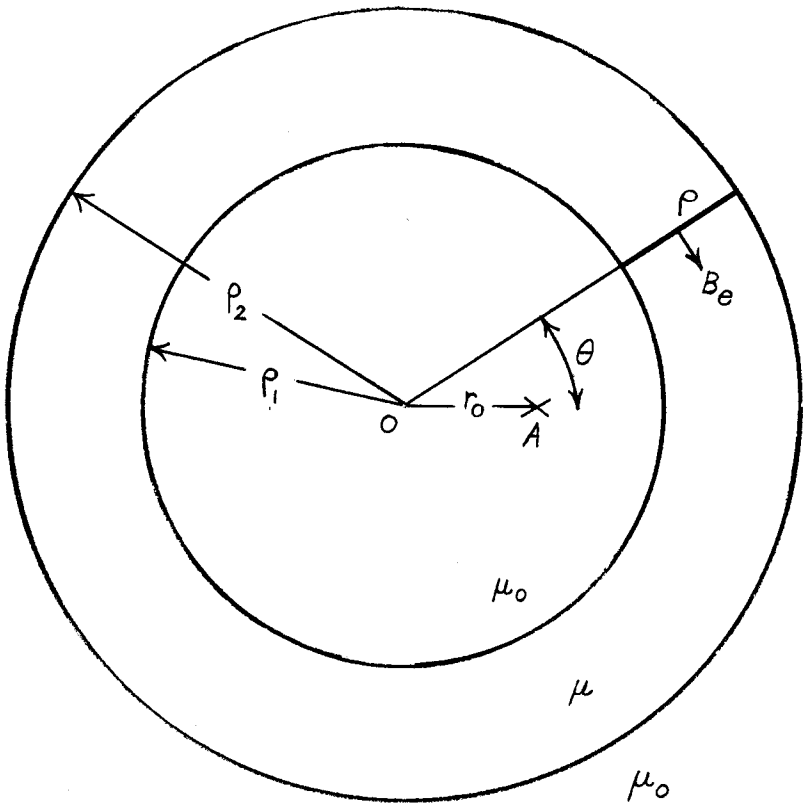

FIG. 4

It is also clear that as long as the beam axis is the same as the core axis, no symmetry is required in the wiring of the coil. However, if the beam is no longer axial, it is absolutely necessary to have a symmetric wiring if we do not want to detect any effect due to the beam position. If a perfectly symmetric coil is used, the induced voltage is again given by Eq. (2) if the beam axis and the coil axis are parallel. If the beam axis forms an angle Φ with the coil axis then it has no influence as long as the beam is going through the center of the coil, but the beam position can give a very small effect if the beam is out-centered. This component will be very difficult to estimate, but it must be at least of the order Φ^3/r^2; this is negligible compared to the main beam (Φ will be equal to only a few milliradians).

We must remember that we are dealing with ultra-relativistic electrons while the equations used have been derived using classical electrodynamics. But it can be shown very easily that the Laplace law is still valid due to the fact that the expansion of the transverse electromagnetic field is compensated by the contraction of lengths. This fact has also been verified experimentally by Bergère et al.[8]

A. The "Fast-Integrator" Type of Circuit

This type of circuit is most commonly used in conjunction with an induction monitor. Many authors[9,10,11,12] have described and analyzed it and we would like only to emphasize the main conclusions which can be derived from them.

First, the value of the coil parameter must be determined. The following factors should be considered:

1. The geometrical dimensions, at least the inside diameter of the coil, which will be imposed by the experimental conditions under which the monitor is to operate. Another limitation will come from the type of core that is available on the market. An OD/ID ratio of the order of 1.5 is a good value.

2. The self-inductance L of the coil must be chosen as a compromise between the fact that L must be as large as possible in order to have a large output signal, but the wiring capacitance and resistance must be kept small if the rising time of the output is to be short

compared to the beam pulse width. If the latter quantity is supposed to vary over a large range, it will surely be wise to have a different type of coil to match properly each experimental condition.

3. It is also important to have a slow decaying time of the output signal so that it will reproduce as well as possible the shape of the beam pulse.

4. We do not want to have any oscillation in the circuit; therefore, the value of the resistance must be chosen in such a way that we are below the critical damping condition.

As an example, at Orsay a core of ferrite material with the following characteristics has been used:

Inside diameter	200 mm
Outside diameter	350 mm
Thickness	50 mm
Magnetic permeability	40 at 10 Mc/sec

The coil was made of 100 regularly spaced turns of enamel-insulated copper wire (1 mm in diameter) and the self-inductance of the coil was 0.7 mHenry. This gave a very good reproducibility of the shape of the pulse. It is not obvious that ferrite is the best material to be used for the core; one of the main objections is its behavior under radiation. Cores made of wrapped sheets of permalloy metal have been used successfully. More information is necessary in this field.

The signal appearing at the ends of the coil is relatively weak (few tens of millivolt) and it will be necessary to amplify it so that it can be carried from the monitor location to the control panel. A high gain ($\approx$ 1000) and wide-band amplifier has to be used (Fig. 5). This can be achieved with a strong feedback network which can be of two types, depending on whether we include the magnetic circuit in the feedback loop[13] (Fig. 6) or not. The latter type has been widely used and gives reasonable results. The overall feedback design must theoretically give a better result due to the fact that it will eliminate completely the effect of the secondary winding resistance, but the complete analysis of this system has never been done taking into account the

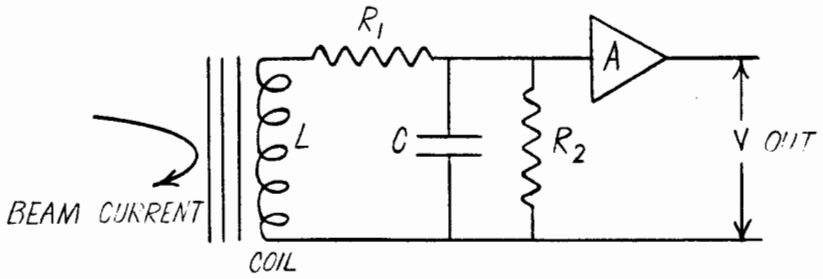

L = COIL SELF INDUCTANCE
R_1 = COIL INTERNAL RESISTANCE
R_2 = DAMPING RESISTANCE
C = STRAY CAPACITANCE
A = AMPLIFIER

FIG. 5

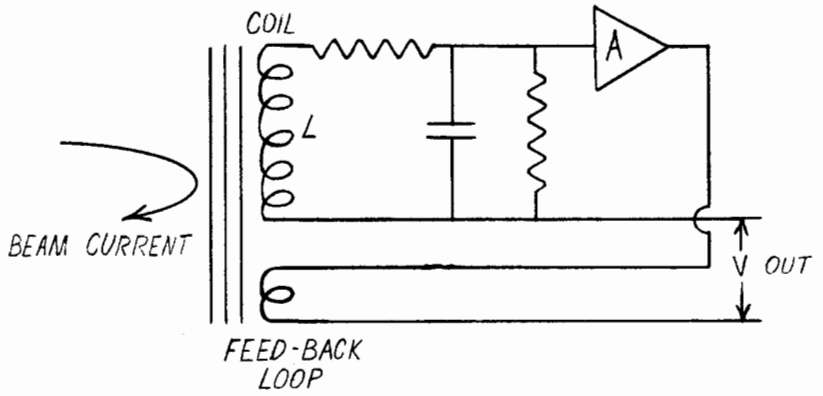

FIG. 6

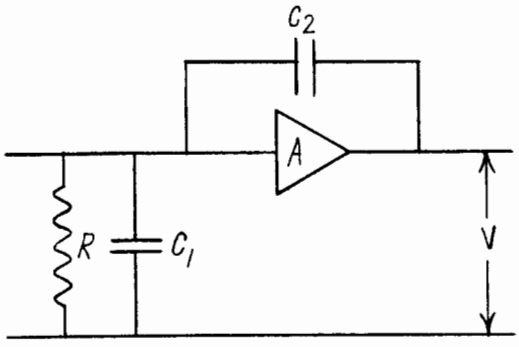

V = INTEGRATED VOLTAGE
R_1, C_1 = LEAKAGE RESISTANCE AND CAPACITANCE
C_2 = INTEGRATING CAPACITANCE
A = HIGH GAIN AMPLIFIER

FIG. 7

influence of leakage and stray capacitances as well as phase shift in the amplifier. It will be worthwhile to investigate this more deeply both theoretically and experimentally.

In integrating the signal, it must be remembered that in a pulse transformer the output signal has an undershoot whose area is equal to the signal itself, and it will be necessary to include a diode in the circuit to eliminate the unwanted part of the signal. Some consideration must be given to this part of the network as we need to have a very stable zero volt bias. Such a discriminator will be followed by a current integrator, but because the impedance of the current source will be relatively small, a classical current integrator such as the vibrating capacitor type cannot be used. It is possible to design a low input impedance current integrator having a good accuracy by using a design of the type given on Fig. 7. With such an integrator J. E. Leiss[14] has been able to measure current of 10^{-7} amp on a 10,000 ohm impedance with an accuracy of a few tenths of a percent.

B. The "Resonant Circuit" Type of Monitor

In the fast-integrator the damping resistance must prevent the circuit from resonating, but we can also build the circuit as an oscillator. Such a circuit has been tried with some success by J. Haissinsky and B. Richter[15] on the Mark III accelerator at Stanford. The resonant circuit was made by the self-inductance of the coil associated with the capacitance of the connecting cable.

The principle of the electronic system is presented on Fig. 8. The idea is to select with an appropriate delay-gate circuit the first negative spike of the resonating signal, which is sent to the amplitude-to-time converter. This provides a signal whose duration is proportional to the amplitude of the spike. During this time a gate is open through which pulses produced by a frequency stabilized oscillator are counted.

Such a device works as a ballistic galvanometer, and the amplitude of the spike is directly proportional to the charge q that went through the monitor, independent of the time distribution of the electrons in the beam pulse. This can be shown in the following: if we integrate two times over the length Δt of the beam pulse the equation of the

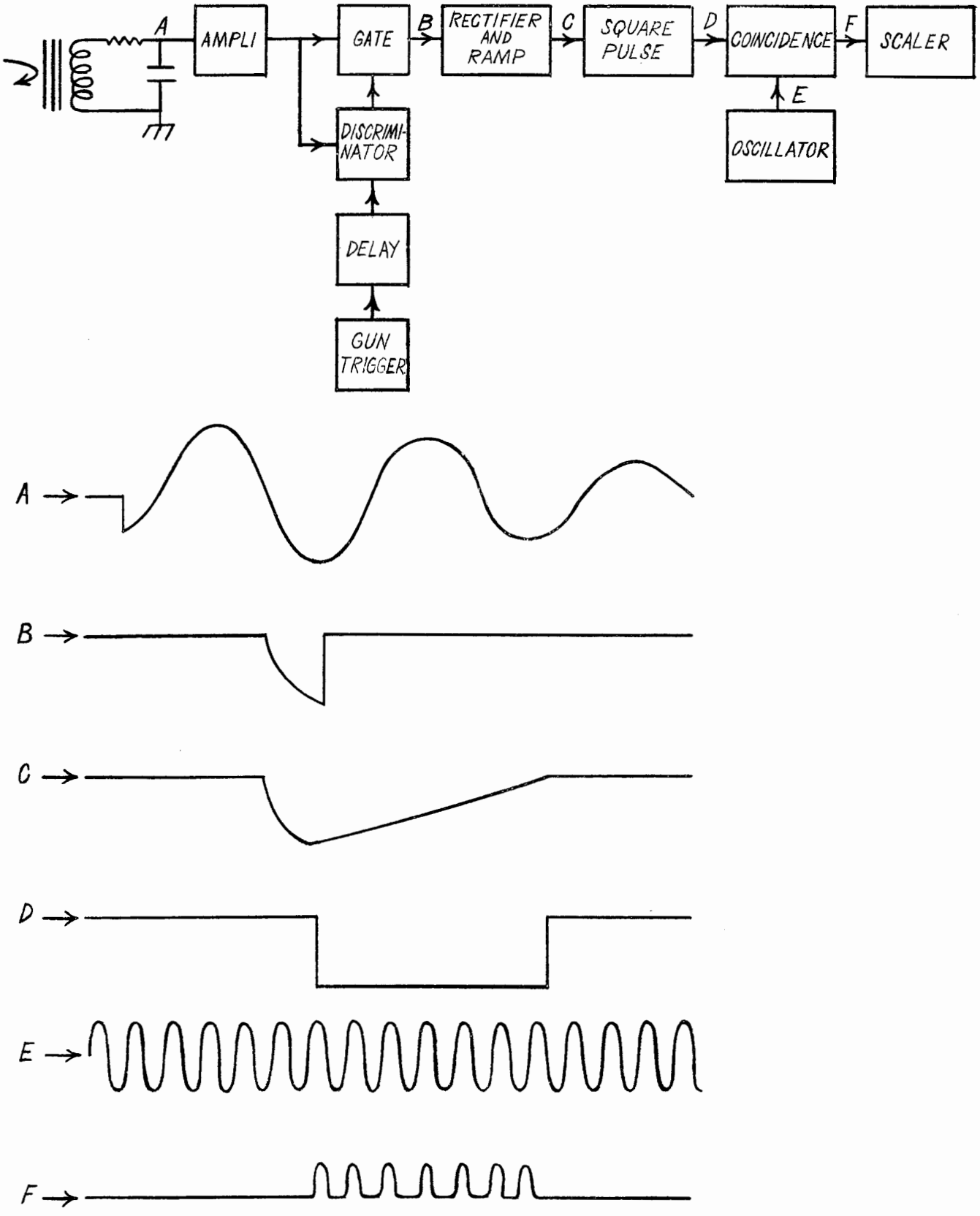
A
AMPLI
GATE
B
RECTIFIER AND RAMP
C
SQUARE PULSE
D
COINCIDENCE
F
SCALER
E
OSCILLATOR
DISCRIMI-NATOR
DELAY
GUN TRIGGER
A
B
C
D
E
F

FIG. 8

equivalent network (Fig. 8)

$$\lambda \frac{di}{dt} = LC \frac{d^2V}{dt^2} + CR \frac{dV}{dt} + V$$

we obtain

$$\lambda q = LCV + \int_0^{\Delta t}\int Vdtd\tau + RC \int_0^{\Delta t}\int V\, dt$$

where L, C and R are the characteristics of the oscillating circuit, V is the signal appearing across the capacitor C, and di/dt is the rate of change of the beam current pulse. In the last equation it is clear that if the last two terms on the right side are small, then V is proportional to q. In the Stanford case the parameters have been chosen such that the contribution of those two terms was about two-thousandths that of the principal terms.

With this type of monitor Haissinsky and Richter have been able to achieve a reproducibility of the order of 1%. It is surely possible that this figure can be improved by using a more elaborate circuit design, but there is a main objection to that monitor. The electronics involved is so complicated that it increases the possibility of instabilities, and it will be necessary to check the efficiency of such a monitor relatively often.

C. Other Problems Related to the Construction of an Induction Monitor

We have already mentioned factors governing the choice of the magnetic material to be used for the core, as well as the fact that it is very important to have a perfectly axially symmetric winding of the coil. The noise pick-up problem must now be considered. The first source of noise will be due to electrons striking the core; they will induce in the coil a signal much larger than the induction signal. This can be avoided by using a core with a large enough inside diameter.

The second source of noise will be due to the rf pick-up; this can be avoided by providing an electrostatic shield around the coil. But it must be remembered that the shield is not closed[16] (Fig. 9); the only Eddy currents which can be induced will therefore produce a magnetic field parallel to the coil axis. A good precaution is to insulate this shield electrically from the accelerator vacuum tubing. From the experience at Orsay with this rf shielding problem it seems possible to solve it, particularly if the monitor is far from any rf source, as will be be the case in the SLAC switchyard or experimental rooms. The same problem of rf pick-up can also appear on the cable, so it will be wise to put the amplifier as close as possible to the monitor. The noise problems with the "resonant circuit" monitor seems to be more easily resolved than with the "fast integrator" type.

The advantage of the induction monitor is that its results are independent of the electron energy, and it can therefore be calibrated at low energy against a Faraday cup. Then an additional loop through which a standard pulse can be sent will provide a convenient way to check both the electronic stability and any other efficiency shift caused, for example, by a variation of the magnetic susceptibility of the core under radiation.

D. Conclusion

It seems difficult at the present time to determine which of the two types of electronic circuits will provide the best accuracy. We suggest that the overall feedback system as well as the "resonant circuit" type be studied in more detail. In either case it will be difficult to obtain an accuracy of the order of 0.1% for current smaller than 10 μamp, because noise problems become too difficult to solve below this current.

V. OTHER TYPES OF MONITORS

We will now discuss other monitors which can eventually be used with an electron linac but which will not provide a good accuracy. Although they are of no value in performing an accurate experiment, they can be used as indicators of current variation for the tuning of the machine.

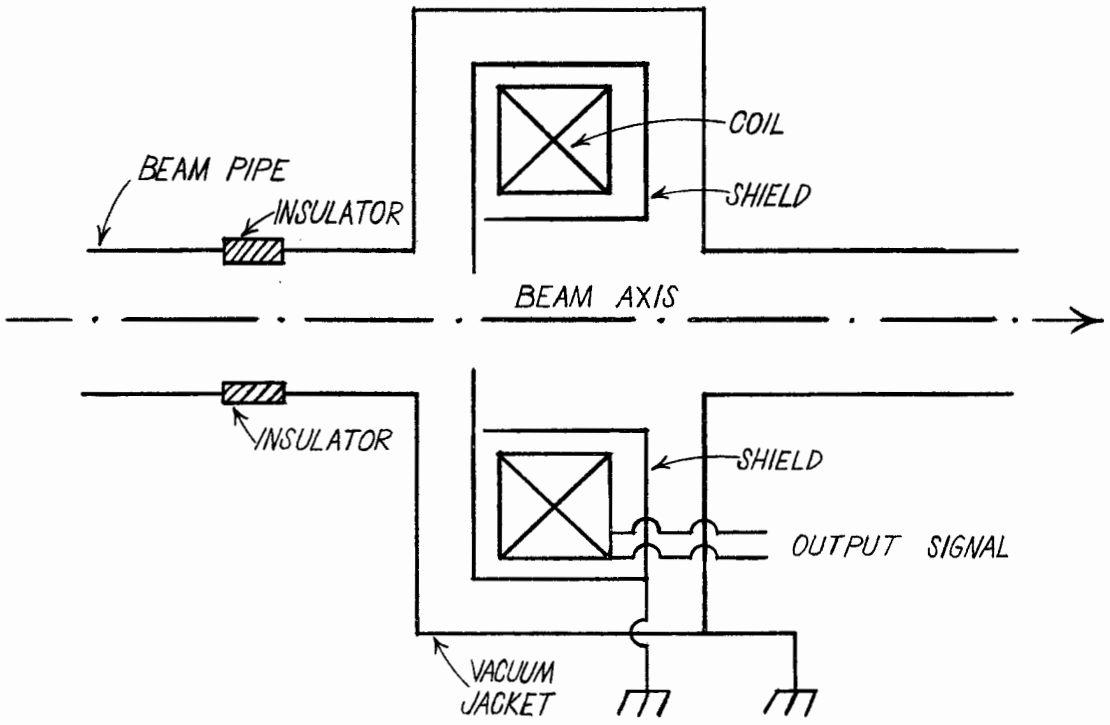
COIL
SHIELD
BEAM PIPE
INSULATOR
BEAM AXIS
INSULATOR
SHIELD
OUTPUT SIGNAL
VACUUM
JACKET

FIG. 9

We have presently in mind two types of monitors: the rf cavity monitor and the synchrotron radiation light monitor. We will discuss each of these to see what sort of accuracy can be achieved and in which range they can be useful.

A. The RF Cavity Monitor

When an electron beam goes through a cavity it produces an electric field proportional to the beam current intensity. It is well known that the current function $i(t)$ can be analyzed using a Fourier expansion. Then the spectra have a main frequency $f = \omega/2\pi$. If one of the spectrum frequencies corresponds to one of the resonant frequencies of the cavity, the latter will oscillate at this frequency. In general the cavity is designed so that its resonant frequency is the main frequency f of the Fourier expansion.

The rf power produced in the cavity is coupled out with an appropriate coupling device such as a loop, and the detection of the signal can be achieved using an rf diode like the one used to measure the klystron power. The signal can be displayed on an oscilloscope; the size of the signal is proportional to the current, but depends also on the shape of the beam pulse.

It has been shown by Callède[17] that if the detector response is linear the beam pulse shape does not have any influence, while if the detector response is not linear the response of the cavity depends on the beam pulse shape. For example, the difference between a square and a trapezoidal pulse response can be more than 30 percent. As the commonly available detector has a quadratic response, this type of monitor can be used to give an indication of the tuning of the machine, but surely not to monitor the beam for an accurate experiment.

RF cavity monitors have been used with the Orsay linac[17] as well as with the Saclay machine,[18] and details about those measurements can be found in the literature. But in all the cases considered the size of the cavity was relatively small (the diameter through which the beam can go is of the order of 2 cm), and it seems very difficult to design an rf cavity having the needed electrical characteristics with a large inside diameter. This will forbid the use of this type of monitor in any area

where the beam can have relatively large dimensions, which will be the case practically all along the SLAC switchyard. There, even if the beam is confined in a small space, its position can change by a relatively large amount and it can hit the cavity rather than going through it.

B. The "Synchrotron Radiation Light" Monitor

The basic principle of this monitor is to detect the light produced by the synchrotron radiation as the electrons are deflected by a magnet (Fig. 10). The frequency spectrum emitted by such radiation has a width proportional to the electron energy; it is characterized by the critical frequency ω_c beyond which there is negligible radiation at any angle and this critical frequency is given by

$$\omega_c = 3\gamma^3 \left(\frac{C}{R}\right) = 3 \left(\frac{E}{mc^2}\right)^3 \left(\frac{C}{R}\right)$$

where E is the electron energy, R the radius of curvature and mc^2 the electron rest mass. For a 20 BeV electron deflected with a radius of curvature of about 350 meters (SLAC pulsed magnet) we found that $\omega_c = 1.68 \times 10^{20}\ s^{-1}$, which corresponds to a critical wavelength $\lambda c = 1.78$ Å. If the emitted light is detected with a photomultiplier that responds to wavelengths between 3500 and 6000 Å, we will be very far from the critical wavelength. Under those conditions synchrotron radiation theory tells us that the intensity of the emitted light is independent of the electron energy. If the amount of produced light is detectable we will have an intensity monitor whose response is energy independent.

Under those conditions the energy radiated per unit solid angle per unit frequency interval and which is detected in the direction of the velocity vector is given by[19]

$$\left.\frac{dI(\omega)}{d\Omega}\right|_{\theta=0} \approx \frac{e^2}{c} \left[\frac{\Gamma\left(\frac{3}{2}\right)}{\pi}\right]^2 \left(\frac{3}{4}\right)^{1/3} \left(\frac{\omega P}{c}\right)^{2/3} \quad (\text{for } \omega \ll \omega_c)$$

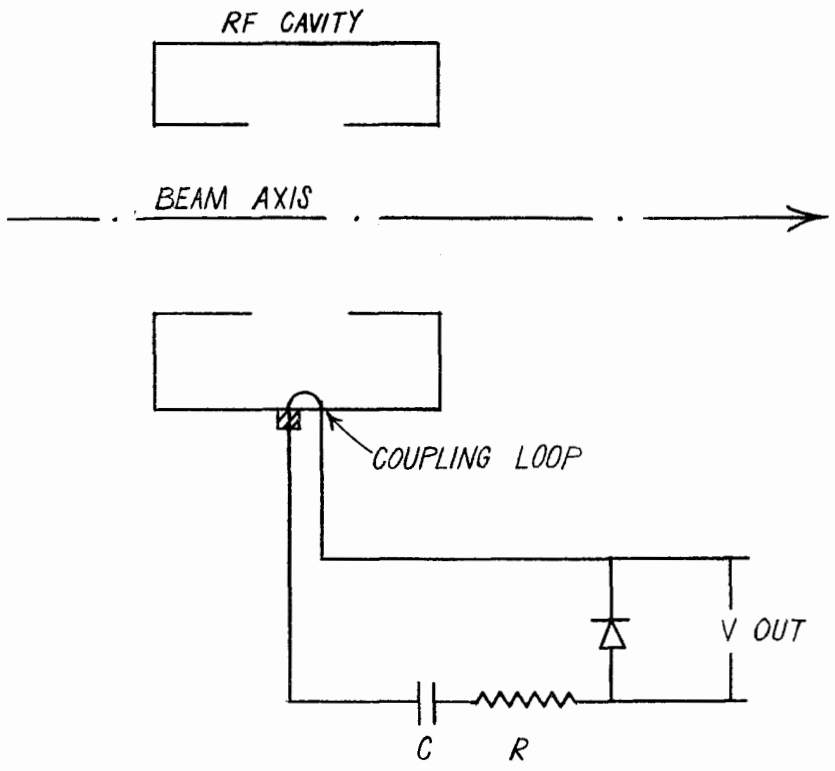

FIG. 10

while the angle in which most of the energy is radiated is given by

$$\theta_c \approx \frac{1}{\gamma}\left(\frac{\omega_c}{\omega}\right)^{1/3} \quad (\text{for} \quad \omega \ll \omega_c)$$

Assuming the same parameters as the ones we used to estimate ω_c we find that

$$\theta_c = \frac{1}{4.10^4}\left(\frac{4000}{1.8}\right)^{1/3} = 3.26 \times 10^{-4} \text{ rad}$$

This angle is small enough that we can assume that all the emitted light will reach the detector (photomultiplier for example); the intensity is then given by

$$\delta I(\omega) = 3.25 \frac{e^2}{c} \frac{\omega R}{c}^{1/3}$$

Now we can assume that the photocathode of the detector has a uniform sensitivity between 3500 and 6000 Å; under such conditions the intensity of the emitted light will be

$$\delta I = 7.5 \times 10^{-28} \text{ watts per electron}$$

The light can be seen along the direction of its velocity for the period

$$\Delta t \approx \frac{1}{\gamma^3}\frac{R}{c} \approx 10^{-20} \text{ second}$$

whereas the detector will be able to see the particle for a time of about 10^{-8} second. Therefore, the intensity really detected will be $\approx 10^{12}$ times larger than δI.

A phototube with a photocathode sensitivity of 50 mA/watt and a gain of 10^8 will be able to detect power as low as about 10^{-9} watts, which will correspond to 10^7 electrons per pulse. If the current is too large saturation of the photomultiplier will appear, but then a neutral density filter can be used as well as a frequency selective filter. The calibration of the device will have to be done with each type of filter.

If such a monitor is designed, it will be very important to keep the photomultiplier far enough from the beam so that no electron will strike the glass in front of the photocathode, in which case it would produce a large amount of light by Cerenkov radiation. This problem can be solved by using a small metallic mirror to deflect the light by 90°, for example.

In addition, there are other sources of light while the electron travels along its trajectory (due to the residual gas in the vacuum pipe) – ionization as well as Cerenkov light. The intensity of the latter will be very weak compared to the synchrotron radiation (the ratio is of the order of γ^3), and the ionization light may now appear to be negligible. However, this light is radiated in all directions; as long as the residual gas pressure is constant it will not change the calibration because its intensity is also proportional to the beam current. In fact, it could also be used as a monitor.

The synchrotron radiation light monitor is used with a storage ring to monitor the number of particles stored.

VI. CONCLUSIONS

The main conclusion of this study is that at the present time we have no monitor which will provide an accurate beam monitoring over the required range of beam intensity (30×10^{-9} A to 150×10^{-6} A). The main problem remains the absolute calibration of any relative monitor, as the discussion has shown that the construction of a Faraday cup will be very complicated and expensive for the high energy and current considered. Among the relative monitors, the induction current monitor is easiest to calibrate because its efficiency is independent of the electron energy, but it presents two disadvantages: (1) its sensitivity is not

good enough to allow measurement of currents smaller than ~ 10 μamp, and (2) its accuracy is only of the order of 1 percent at the present time. It seems reasonable that its accuracy can surely be increased by one order of magnitude, thus making this monitor useful for the experimentalist. The secondary electron monitor will be able to cover the full range of currents involved, but it needs to be calibrated, if possible, for the energy at which it will be used. The other types of monitors discussed in this paper can only be used when a low accuracy is required.

We summarize the characteristics of those monitors in Table III.

TABLE III

TABLE SUMMARIZING THE PROPERTIES OF MONITORS WHICH CAN BE USED AT SLAC

Monitor	Range of Average Current (Ampere)	Accuracy	Accuracy Limitation	Calibration
Faraday cup	$10^{-11} - 10^{-6}$	< 0.1%	Integrator calibration	None
SEM	$10^{-11} - 10^{-4}$	~ 0.1%	Stability of secondary emission	Must be done for each used energy
Induction Monitor	$10^{-5} - 1$	~ 0.5%	Electronic stability	Energy independent
RF Cavity	$10^{-7} - 1$	~ 5%	Sensible to beam pulse shape	Energy independent
Light Detector		~ 5%		

ACKNOWLEDGMENT

We wish to thank H. DeStaebler, E. Garwin, J. Muray, D. Neet, B. Richter and R. Taylor for fruitful comments and suggestions on the problem.

LIST OF REFERENCES

1. D. B. Isabelle, L'Onde Electrique 421, 66 (1962).
2. A. Kantz and R. Hofstadter, Nucleonics 12, 3.37 (1954).
3. C. D. Zerby and H. S. Moran, Report ORNL-3329, Oak Ridge National Laboratory, Oak Ridge, Tennessee (1962).
4. G. W. Tautfest and H. R. Fechter, Rev. Sci. Instr. 26, 229 (1955).
5. D. B. Isabelle and Ph. Roy, Nucl. Instr. and Methods 20, 17 (1963).
6. M. Jakob and G. A. Hawkins, Elements of Heat Transfer (John Wiley and Sons, Inc., New York, 1957); 3rd Ed. p. 30.
7. J. C. Bergstrom, Internal Report, University of Saskatoon, Saskatchewan, Canada (1963).
8. R. Bergère, E. Delezenne and A. Veyssiere, Nucl. Instr. and Methods 15, 327 (1962).
9. W. E. Shoemaker, LRL Report No. 105, Livermore Research Laboratory (now Lawrence Radiation Laboratory), Livermore, California (1954).
10. L. E. Bess, J. Ovadia and J. Valassis, Rev. Sci. Instr. 30, 985 (1959).
11. R. Yamada, Report INSJ-37, Institute of Nuclear Studies, University of Tokyo, Japan (1961).
12. J. T. Hyman, Report NIRL/R/30, Rutherford High Energy Laboratory, Great Britain (1963).
13. R. Yamada, Japan J. Appl. Phys. 1, 92 (1962).
14. J. E. Leiss, private communication.
15. J. Haissinsky and B. Richter, private communication.
16. I. A. Grishaev, N. I. Mocheshuikov and V. F. Ivanov, Instruments and Experimental Techniques (USSR) 4, 537 (1960).
17. G. Callède, Internal Report LAL 21, Laboratoire de l'Accélérateur Lineaire, Orsay, France (1962).
18. R. Bergère, E. Delezenne and A. Veyniere, Nucl. Instru. and Methods 15, 327 (1962).
19. See for example J. D. Jackson, Classical Electrodynamics (John Wiley and Sons, Inc., New York, 1962); Chapter 14.

POSITRON BEAM FROM THE SLAC ACCELERATOR

by

J. Pine

I. INTRODUCTION

Figure 1 shows schematically the proposed method of positron beam production. Electrons of energy E^- ($\approx$ 5 GeV in Stage I) are incident on a radiator $\approx$ 5 radiation lengths thick. Positrons emerging from the radiator, mainly with low energies, are accelerated by the remainder of the

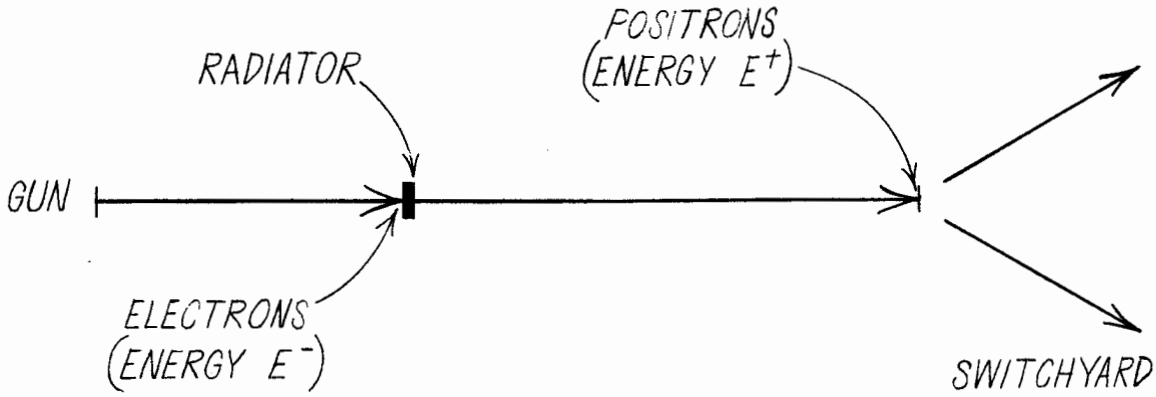

FIG. 1

accelerator (suitably back-phased with a master phase shifter) to energy E^+ ($\approx$ 10 GeV in Stage I). The positron intensity is approximately proportional to the electron beam power, so that the radiator location represents a compromise between high positron intensity and high positron energy. This technique has previously been used with the Stanford Mark III accelerator.[1]

This report mainly discusses the energy, angle, and spatial distributions of positrons emerging from the radiator, and the beam transport problem from radiator to beam switchyard. The thermal and mechanical problems associated with the radiator are briefly considered. None of these subjects is treated in great detail or with the care which will

ultimately be necessary. The main conclusion is that it appears feasible to obtain a positron beam of intensity $\gtrsim 1\%$ of the electron beam incident on the radiator.[2]

II. POSITRONS EMERGING FROM THE RADIATOR

A. Energy Spectrum

From Approximation A of shower theory,[3] the energy distribution of positrons emerging from a radiator of optimum thickness (maximum total positron yield) is given by

$$n(E)dE = \frac{0.069\ E^-}{\left[\ell n\left(\frac{E^-}{E}\right)\right]^{\frac{1}{2}}\ E^2}\ dE \qquad (1)$$

where $n(E)dE$ is the number of positrons in dE at E per incident electron of energy E^-. This expression should be a good approximation for $E_c \ll E \ll E^-$, where E_c, the critical energy, is that energy at which the rate of energy loss by ionization equals the rate of energy loss by bremsstrahlung. To a good approximation,

$$E_c \approx \frac{630}{Z}\ \text{MeV} \qquad (2)$$

where Z is the atomic number of the radiator material.

In the neighborhood of E_c, and below, the ionization loss becomes important and the yield decreases progressively below Eq. (1). As a convenient approximation, we take

$$n(E)dE \approx (0.032)\ \frac{E^-}{(E + E_c)^2}\ dE \qquad (3)$$

which gives 1/4 of the yield of Eq. (1) at $E = E_c$ and $\ell n\ E^-/E_c = 6$

(a typical value). Then

$$N(>E) \equiv \int_{E}^{E^-} n(E)dE \approx (0.032)\,\frac{E^-}{E_c}\,\frac{1}{1+(E/E_c)} \qquad (4)$$

The logarithmic energy dependence of Eq. (1) has been eliminated, since in the region of interest to us it produces only a minor effect The form of Eqs. (3) and (4), and the numerical constant, produce good agreement with the Monte Carlo calculations of Zerby and Moran[4] for $6 \leq E \leq 300$ MeV, with $E^- = 5$ GeV and a gold radiator ($E_c = 8$ MeV) five radiation lengths thick. For $E/E_c \gg 1$, $E \ll E^-$, Eq. (3) is in agreement with Eq. (1) to $\approx 30\%$. We will assume Eq. (3) to be valid down to $E \approx E_c/2$, which is a mild extrapolation from the region where it can be checked against the Monte Carlo calculations.

Note that the integral positron yield varies, at least approximately, as $1/E_c$, and that a high Z radiator material is therefore desirable. Figure 2 is a graph of $1/(1 + E/E_c)$ vs. E/E_c, from which it may be seen that the energy band $E_c/2 \leq E \leq 2E_c$ contains about 1/3 of the total positron yield, i.e., about 7 positrons per incident electron for $E^- = 5$ GeV, $E_c = 8$ MeV.

B. Angular and Radial Distributions

Zerby and Moran[5] have done a three-dimensional Monte Carlo calculation for $E^- = 1$ GeV and three radiation lengths of lead. For positron energies $\approx E_c$ we expect these results to change only slightly at $E^- = 5$ GeV and five radiation lengths of lead. The calculation for lead of course applies to any material with $Z \approx 80$ and density ≈ 10 g/cm^3. For different densities and high Z we expect the angular distribution to be unchanged and the radial distribution to scale linearly in the density (the results of analytic shower theory are universal when distances are measured in radiation lengths).

A good fit to the Monte Carlo calculation (to $\approx 25\%$ or better) can

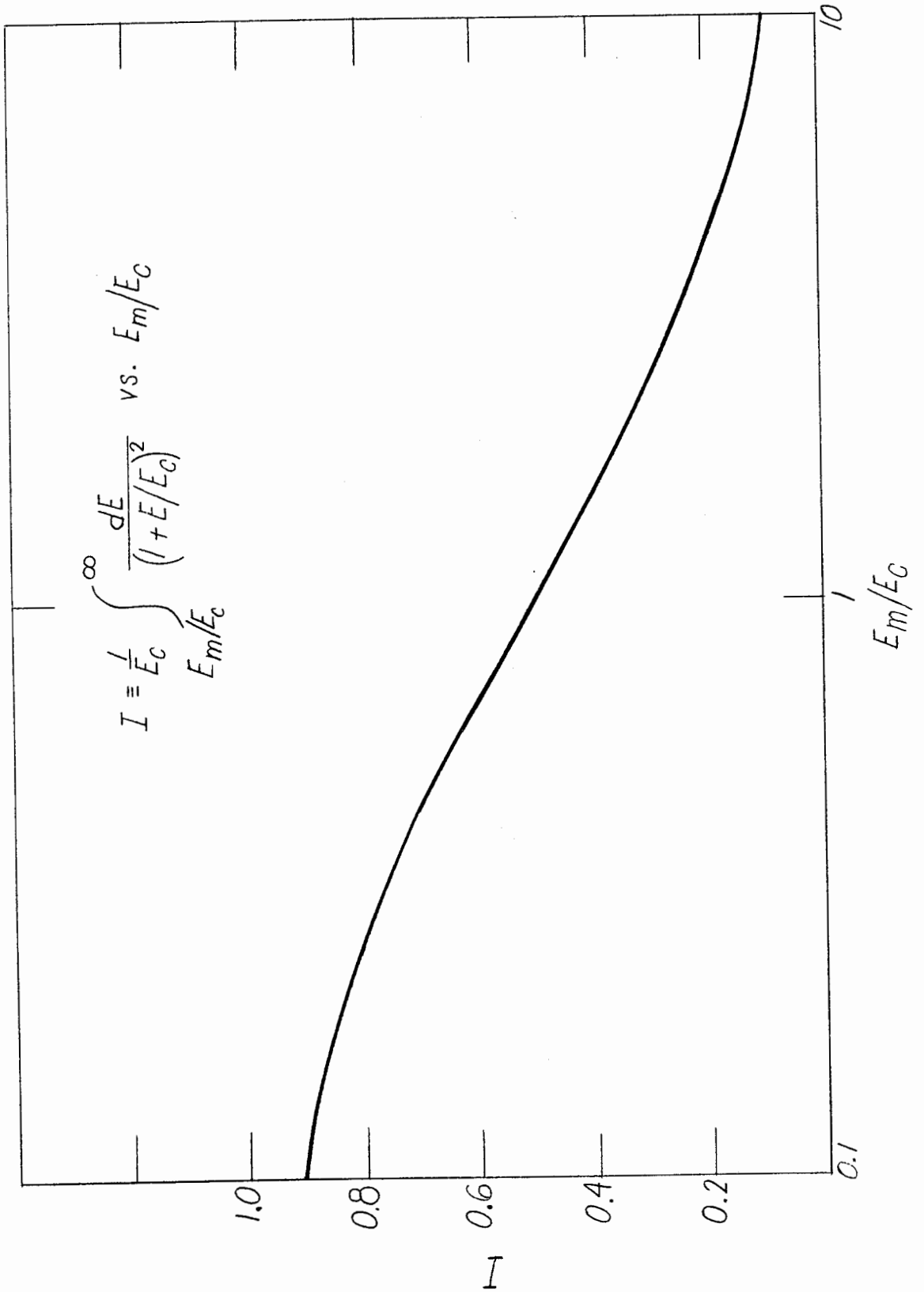
$I \equiv \frac{1}{E_c} \int_{E_m/E_c}^{\infty} \frac{dE}{(1+E/E_c)^2}$ vs. E_m/E_c
1.0
0.8
0.6
0.4
0.2
I
0.1
1
10
E_m/E_c

FIG. 2

be obtained with the integral radial and angular distributions:

$$N(< R) = \frac{(R/R_o)^2}{\left[1 + (R/R_o)^2\right]} \tag{5}$$

$$N(< \theta) = \frac{(\theta/\theta_o)^2}{\left[1 + (\theta/\theta_o)^2\right]} \tag{6}$$

where R is the radial distance from the shower axis and θ is the angle with respect to the shower axis. $N(< R)$ is the fraction of positrons at radii $\leq R$, integrated over all θ; while $N(< \theta)$ is the fraction with angles $\leq \theta$, integrated over all R. Any $R - \theta$ correlations are assumed to be unimportant, a conservative assumption from the standpoint of the phase space occupied by the source. The parameters R_o and θ_o, expected to depend upon the positron energy, correspond to the values of R and θ for which $N = 1/2$.

The integral distributions, Eqs. (5) and (6), correspond to differential intensities (per cm^2 or per steradian) of the form $(1 + x^2)^{-2}$, a function with longer tails than a Gaussian This is expected, since we are essentially looking at a sum of Gaussians with different variances. However, for $R \ll R_o$ or $\theta \ll \theta_o$, the distinction between Gaussians or Eqs. (5) and (6) is hardly relevant.

From the Monte Carlo results, the energy dependences of R_o and θ_o, for $E_c/2 \lesssim E \lesssim 2E_c$, may be well approximated, for example, by:

$$R_o = \frac{0.15}{E^{\frac{1}{4}}_{\text{MeV}}} \text{ cm} \tag{7}$$

$$\theta_o = \frac{1.73}{E^{\frac{1}{2}}_{\text{MeV}}} \text{ radians} \tag{8}$$

However, in order to form a physical picture which can give rise to energy

dependences similar to those of Eqs. (7) and (8), and perhaps to find the Z dependence by some logical introduction of E_c, we proceed in a different way. First we assume that R_o and θ_o are related via a characteristic length L_o such that $R_o = (1/2)L_o\theta_o$ where all three quantities are functions of E. We are assuming that the R and θ distributions are dominated by the scattering of the emergent positron and that L_o is some typical depth in the radiator at which the emergent positrons of energy E are produced.

Since we expect $L_o \approx 1$ radiation length for $E \gg E_c$, and that L_o decreases for $E \lesssim E_c$, we assume $L_o = (1 + E_c/E)^{-n}$. By using the Monte Carlo results to evaluate n in this formula, we find

$$L_o = \left(\frac{1}{1 + E_c/E}\right)^{\frac{1}{2}} \text{ (r.l./rad)} \tag{9}$$

accurate to within 5% for $E/E_c = 0.5$, 1.8, and 4.5. Next, we assume $\theta_o = (K'/E)L_o^m$, with K' and m to be chosen for a good fit to the Monte Carlo data at the three values of E/E_c just mentioned. The result is

$$\theta_o = \frac{10}{E_{MeV}} L_o^2 = \frac{10}{E_{MeV}} \left(\frac{1}{1 + E_c/E}\right) \text{ (rad)} \tag{10}$$

and this then determines the relation

$$R_o = \frac{5}{E_{MeV}} \left(\frac{1}{1 + E_c/E}\right)^{3/2} \text{ radiation length}$$

or (11)

$$R_o = \frac{2.5}{E_{MeV}} \left(\frac{1}{1 + E_c/E}\right)^{3/2} \text{ cm, for lead}$$

As yet, we have made no comparison with data for different radiator materials to determine whether the E_c dependences we have found are even vaguely correct. However, Eqs. (10) and (11) fit the Zerby and

Moran results for lead to within 10% for $E_c/2 \lesssim E \lesssim 3E_c$. For $E \gg E_c$ analytic shower theory (Approximation A) is independent of material when distances are measured in radiation lengths and energies in units of the critical energy. But this kind of reasoning is not so compelling at the low energies of interest here. The fact that θ_o comes out proportional to L_o^2 is certainly surprising, since from the usual multiple scattering situation we expect proportionality to $(L_o)^{\frac{1}{2}}$. However, a rather complicated combination of circumstances is acting to narrow the angular distribution at low energies, and the L_o^2 dependence happens to fit the net result, at least in lead.

Now we introduce the quantity Ψ_o, a measure of the square root of the phase space volume occupied by the positrons emerging from the radiator. Utilizing Eqs. (10) and (11):

$$\Psi_o \equiv E\theta_o R_o = p_{t_o} R_o = \frac{50}{E_{MeV}} \left(\frac{1}{1 + E_c/E}\right)^{5/2} \text{mc-cm} \qquad (12)$$

where p_{t_o} characterizes the distribution in transverse momentum, and the units anticipate those that will be used in discussing the acceptance of the beam transport system. For $E_c/2 \lesssim E \lesssim 3E_c$, Eq. (12) agrees with Ψ_o calculated directly from the Monte Carlo results to within about 20%. Since the positron intensity will ultimately depend upon $(\Psi_o)^{-2}$, we tabulate below the values of R_o, θ_o, and Ψ_o from the Monte Carlo results:

E (Mev)	R_o (cm)	θ_o (radians)	p_{t_o} (mc)	Ψ_o (mc-cm)
4	0.11	0.77	6.2	0.68
14	0.090	0.45	12.8	1.15
36	0.060	0.26	19.2	1.15

We have always assumed tacitly that θ_o is a small angle (i.e., $\sin\theta_o = \tan\theta_o = \theta_o$). Although we find $\theta_o \approx 0.8$ radians at 4 MeV, the small angle approximation introduces an error which is not serious by the crude standards of the discussion.

From Eqs. (3), (10), and (11) it is possible to find the overall useful positron yield for a given beam transport system acceptance, and, in particular, to see the overall dependence on Z and ρ, where ρ is the density. The result is that, for energies in a range characterized by maximum and minimum values of E/E_c, and for beam transport acceptance $\Psi \ll \Psi_o$, the useful yield goes as $Z(\rho)^2$. From the standpoint of radiator design, it will be important to verify the supposed dependences of Eqs. (10) and (11), or find correct ones, and then reexamine the dependence of the overall yield on Z and ρ. Furthermore, we have taken the very small values of R_o at face value, while if the minimum diameter of the incident beam is about 0.1 cm then R_o for lead is increased by about $\sqrt{2}$ and there is not much gain in increasing ρ beyond that of lead.

III. BEAM TRANSPORT

A. Introduction

The beam switchyard acceptance Ψ is approximately 0.6 mc-cm at 10 GeV. We reiterate the definition of Ψ:

$$\Psi \equiv (p_t)_{max} (r)_{max}, \text{ in mc-cm} \tag{13}$$

so that the phase space admittance is $\approx \pi\Psi^2$ (mc-cm)^2. This follows the practice instituted by Helm whose work[6,7,8,9,10] forms the basis for this section of this report. For the switchyard, the maximum transverse momentum is determined by a maximum angular divergence, so that Ψ is proportional to E^+, and will be less than 0.6 mc-cm at energies below 10 GeV.

An energy spread of 1% at 10 GeV corresponds to 100 MeV at the radiator, so that, from the energy and spatial distributions discussed in the previous section, the beam switchyard is capable of transmitting a sizeable fraction of the positrons from a radiator of high Z and ρ. The acceptance of the beam transport system along the machine from radiator to switchyard will be found to determine the positron intensity.

In order to maintain a high admittance for an appreciable range of energies, two beam transport optical systems have been investigated:

solenoidal focusing, in which positrons spiral around magnetic field lines along their direction of motion; and periodic focusing, in which a sufficiently closely spaced sequence of lenses produces an effect roughly like a continuous radial restoring force.

B. Periodic Focusing

Independent of positron beam requirements, a periodic strong focusing system is planned, in the form of quadrupole multiplets at the end of each sector. Helm[9,10] has discussed such systems in detail. Assuming a spacing of 330 feet and a useful accelerator radius of 0.85 cm (this radius is assumed throughout this section), we find, from Helm's work:

$$E_{min} = 7.0\Psi \text{ GeV} \tag{14}$$

where Ψ is in mc-cm (as it will always be, unless otherwise noted) and E_{min} is the lowest energy at which the acceptance is equal to Ψ. At $E = E_{min}/\sqrt{2}$, $\Psi = 0$.

A special system is clearly needed to focus the positrons from the time they leave the radiator until they reach an energy E_{min} given by Eq. (14). Helm has discussed two periodic focusing systems appropriate to this purpose:[6,8] the "40-foot" system, with single quadrupoles at the small gaps between 40-foot lengths of accelerator, and a "tapered" system, with quadrupoles whose spacing increases proportional to the positron energy, so as to minimize the total number of quadrupoles. We have provisionally chosen the latter system to go from an energy E_s to the energy E_{min}. The lower limit E_s corresponds to a quadrupole spacing so small that a continuous solenoid is preferable on the basis of cost and simplicity. The "40-foot" system would work in the upper end of this energy range, and it utilizes very small quadrupoles. However, it seems uneconomic in comparison with the tapered system when installation, alignment, and overall complexity are considered.

For the tapered system, from Helm's work:

$$|Q| = 9600\ \Psi \text{ (gauss/cm)(cm)} \tag{15}$$

and

$$L = \frac{0.22\gamma}{\Psi} \text{ cm} \tag{16}$$

where $|Q|$ is the quadrupole strength, L is the quadrupole spacing, and γ is the positron energy in units of mc^2. The expression for L assumes $(\Delta E/E) \ll 1$ in a distance L, which will be true for the values of Ψ of interest. The numerical constants also presuppose an accelerator gradient of 1.5 MeV/ft. In order to roughly estimate E_s we have assumed a cost per quadrupole of \$2500. The quadrupoles are sufficiently small so that the unit cost is only weakly Ψ-dependent. The solenoid cost has been estimated at 3,000 Ψ dollars/foot, or about 100 Ψ dollars/cm. From these estimates and Eq. (16),

$$\begin{aligned} E_s &\approx 60 \text{ MeV} \\ \gamma_s &\equiv \frac{E_s}{mc^2} \approx 120 \end{aligned} \tag{17}$$

This is a convenient result, since it corresponds to the use of one 40-foot section for radiator and solenoidally focused accelerator. The remaining focusing is with quadrupoles.

The dependence of the total number of quadrupoles on Ψ is obtained from Helm's formula:

$$L_n = \gamma_s \frac{0.22}{\Psi} e^{(n-\frac{1}{2})(\alpha)(0.22/\Psi)} \tag{18}$$

where L_n is the separation between the n-th and (n - 1)-th quadrupoles and α is the accelerator gradient in mc^2/cm (taken equal to 0.1 here). For matching with the sector multiplet system, L = 3,000 cm, independent of Ψ. Thus, assuming $\gamma_s = 120$, Eq. (18) can be solved for the total number of quadrupoles in the system as a function of Ψ. Figure 3 shows the result, and also indicates the number of 330-foot sectors involved in the tapered quadrupole system. Figure 4 shows L_n vs. n for $\gamma_s = 120$ and various values of Ψ.

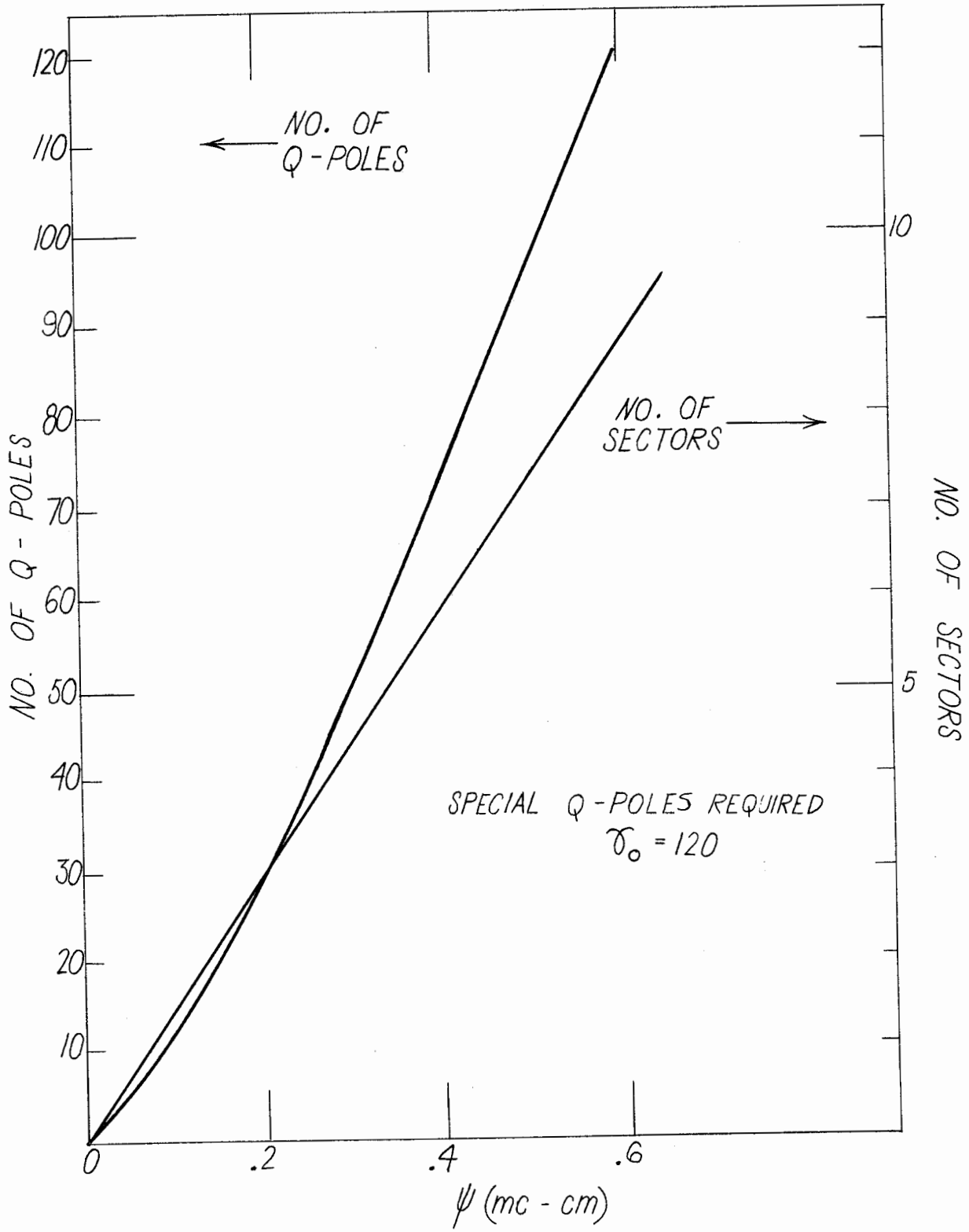
120
110
100
90
80
70
60
50
40
30
20
10
NO. OF Q-POLES
NO. OF Q-POLES
NO. OF SECTORS
10
5
NO. OF SECTORS
SPECIAL Q-POLES REQUIRED
$\gamma_0 = 120$
0
.2
.4
.6
ψ (mc - cm)

FIG. 3

The system discussed has phase space admittance and emittance which are asymmetric with respect to horizontal and vertical motions. Helm has pointed out that one extra quadrupole at the beginning and one at the end result in an axially symmetric system.

There are a number of aspects of this part of the system that have not been fully evaluated. Are single quadrupoles better than doublets or short solenoids? What are the alignment tolerances and energy tolerances (effect of one or more non-functioning klystrons)? These two questions are possibly related. Provisionally, we believe that a system with about 30 quadrupoles is probably manageable, in the sense that it can be tuned up to design performance with a reasonable amount of effort and special instrumentation. We propose combined beam position, shape, and intensity monitors of a crude sort located at approximately each fourth quadrupole. A small, simple, secondary emission monitor system for doing this has been thought through to some extent but not really designed.

Depending upon experience with the initial system, and upon pressure for more positron beam, the acceptance can be increased by adding quadrupoles. Also, doubling the gradient (Stage II operation) doubles the acceptance for given quadrupole spacings, assuming sufficient quadrupole strength $|Q|$ is available.

C. Solenoids

Here we mainly refer to the results of Ref. 7. For a uniform solenoid,

$$B = 5.8\ \Psi \text{ kilogauss} \tag{19}$$

which leads to reasonable fields for the values of Ψ of interest. The "wavelength" of the helical trajectory is given by

$$\lambda = \frac{2\pi\gamma}{B} \text{ cm} \tag{20}$$

where B is in "Helm units" of 1.7 kilogauss, i.e., $B_{\text{kilogauss}} = 1.7(B)$. These units of B will be used throughout, unless otherwise stated, and are "natural" in the sense that $p = Br$, for r in cm, p in mc, and B in Helm units.

In a tapered solenoid B varies as a function of axial coordinate, i.e., the B field lines expand or contract symmetrically about the axis. For an adiabatically tapered solenoid the charged particles spiral around the field lines such that each particle maintains the same field line (or a very close neighbor in a less-than-ideal case) as the center of its helix. The magnetic moment arising from the spiraling of the particle can be shown to be invariant. The wavelength of the spiral changes with radius in such a way that the product of the radius and the transverse momentum is invariant. (Trapped particles in the earth's radiation belts spiral in this way.) The condition for the validity of the adiabatic approximation is that the fractional change in B be small per $\lambda/2\pi$, i.e.,

$$\frac{dB}{dZ}\frac{\gamma}{B^2} \ll 1 \tag{21}$$

Then, the phase-space matching properties of the device can be summarized by:

$$\left(\frac{r_1}{r_o}\right)^2 = \left(\frac{p_{t_o}}{p_{t_1}}\right)^2 = \frac{B_o}{B_1} \tag{22}$$

where subscripts 0 and 1 refer to two locations along the axis of the solenoid.

Equation (22) is independent of positron energy, except through the requirement that the adiabatic condition, Eq. (21), is satisfied. Thus, with the aid of such a solenoid the positron source phase space, characterized by small r and large transverse momentum, can be matched to the accelerator-plus-quadrupole phase space characterized by larger r and smaller transverse momentum. For a source radius of 0.1 cm and an accelerator radius of 0.85 cm, we find $B_o = 72\ B_1$, where B_o and B_1 are the fields at radiator and accelerator, respectively. If B_o is limited to a maximum value of 20 kilogauss, then we find $B_1 = 280$ gauss, which corresponds, via Eq. (19), to an acceptance of only about 0.05 mc-cm. If we think it more realistic to take a source radius of 0.2 cm, then we can match up to an acceptance of 0.2 mc-cm.

When the solenoidal matching fails as a result of excessive initial field requirements then it still appears feasible to complete the matching with a simple lens system at the high energy end of the solenoid. At this point the initially interesting range of positron energies has been converted (by $\approx$ 60 MeV of accelerator) into an energy range with a spread of about $\pm$ 10%. Even if complete matching is possible within the solenoid it may be more convenient to run the solenoid at a field somewhat higher than optimum and complete the match with lenses. In this way the solenoid alignment requirements become less critical, since less than the full accelerator aperture is being used.

To conclude this subsection we estimate the length of tapered solenoid which appears to be required. From the adiabatic condition, Eq. (21), and under the assumption that the final field is much less than the initial field,

$$L_s \gg \frac{\gamma'}{B_{min}} \tag{23}$$

where L_s is the length of tapered solenoid, γ' is the maximum energy for which the adiabatic condition is to be fulfilled, and B_{min} is the final field. For $\gamma' = 32$ and $B_{min} = 0.68$, corresponding to $E \lesssim 2E_c$ for lead and $\Psi = 0.2$, we find $L_s \gg 47$ cm. If the matching is done while the positrons are being accelerated, then the length gets somewhat longer. It appears likely that the tapered solenoid can be contained in a drift space about one meter long between radiator and accelerator, or that at least the higher field part of the solenoid can be in this region. This has various virtues from the standpoint of simplicity and economy.

D. Phase Slip

We consider the effect of positron motion at an angle θ to the accelerator axis, assuming, as always, v = c. Then,

$$\frac{d\varphi}{dz} = \frac{\pi\theta^2}{\lambda_{rf}} \text{ radians/cm} \tag{24}$$

where $d\varphi/dz$ is the rate of change of phase relative to the traveling

rf wave of wavelength λ_{rf} and phase velocity c. We also assume $\cos\theta = (1 - \theta^2/2)$, which is sufficiently accurate for $\theta \lesssim 1/2$ radian. For a drift space of length d, the accumulated phase slip $\Delta\varphi$ is

$$\Delta\varphi = \frac{d}{\lambda_{rf}}\pi\theta^2 \tag{25}$$

since θ is a constant for this case. This equation is also valid inside a uniform solenoid.

For a drift space with a tapered solenoid, we find, from Eqs. (21) and (22),

$$\left(\frac{\theta}{\theta_o}\right)^2 = \frac{B}{B_o} = \frac{1}{\delta B_o z + 1} \tag{26}$$

where $\delta \ll 1/\gamma'$, with γ' the design maximum γ of the solenoid. Since $(\theta/\theta_o)^2 = (B/B_o)$, we integrate Eq. (24) with the aid of Eq. (26) to find $\Delta\varphi$ for a drift space of length d with a tapered solenoid. The result is

$$\Delta\varphi = \frac{\pi\theta_o^2}{\lambda_{rf}}\frac{1}{B_o\delta}\left[\ell n(1 + B_o\delta d)\right] \tag{27}$$

For a 30 cm drift space, with $\delta = 1/60$, and $B_o = 20$ kilogauss, $\Delta\varphi$ given by Eq. (27) is 0.3 that from Eq. (25). This choice of δ may give too steep a taper, but only detailed orbit tracing can tell. For a gentler taper $\Delta\varphi$ will of course be larger.

Finally, we consider the phase slip with uniform acceleration and constant transverse momentum (applicable to no focusing, uniform solenoidal focusing, and, approximately, to periodic strong focusing). In this case,

$$\frac{\theta}{\theta_1} = \frac{E_1}{E} = \frac{E_1}{E_1 + \alpha z} \tag{28}$$

where θ_1 and E_1 are the angle and energy at injection. For this

case, integrating Eq. (24) leads to

$$\Delta\varphi = \frac{\pi\theta_1^2}{\lambda_{rf}} \frac{E_1}{\alpha} \left(1 - \frac{E_1}{E_f}\right) \tag{29}$$

where E_f is the final energy and α is the gradient. The distance E_1/α, in which the injection energy is doubled, plays a role analogous to the drift space length, neglecting the factor in parentheses which will generally be close to 1. We omit the complicated calculation for the tapered solenoid with uniform acceleration, remembering that some reduction in $\Delta\varphi$ will result.

Almost all the phase slip will have occurred before the positrons receive much of their final energy, so that we can evaluate the maximum tolerable phase slip by knowing how the energy gain varies with phase. We limit the energy spread due to phase spread to 1%, corresponding perhaps to the natural energy width of the beam. It is easy to show that

$$\frac{\Delta E}{E} = \frac{1}{8} (\Delta\varphi)^2 \tag{30}$$

so that, for $\Delta E/E \leq 0.01$, $\Delta\varphi$ must be ≤ 0.28 radians.

First we will assume no adiabatic solenoid and obtain numerical results from Eqs. (25) and (29) for $\Psi = 0.2$ and positrons leaving the radiator at 4 MeV. We note that $\Delta\varphi$ is proportional to $(\Psi)^2$. We assume the radial shower size R_o to be 0.1 cm, so that the maximum value of θ, which will be used to calculate $\Delta\varphi$, is 0.25 radian. From Eq. (25), for d = 30 cm, $\Delta\varphi = 0.59$ radian, while from Eq. (29), with $\alpha = 0.1$ mc^2/cm and $E_1/E_f \ll 1$, $\Delta\varphi = 1.57$ radian.

In the above calculations the small value of R_o has maximized $\Delta\varphi$, and the value of α could be doubled for the first 10 feet of accelerator, but the results are not comforting. The tapered solenoid is a big help, however. With such a solenoid, the 30 cm drift space introduces about 0.2 radian phase slip, and the rapid taper which we have (perhaps hopefully) assumed reduces θ_1^2 in Eq. (29) by a factor of about seven. This leads to a phase slip in the accelerator of 0.22 radian, which will be

reduced by the continuing taper of the solenoid and yet further reduced by the fact that it is likely that α will be increased by a factor 1.4 in the first 10 feet of accelerator, just in the normal course of events. (The rf power which would have gone into 10 feet removed for the radiator will go into this section.)

Thus we find that the phase slip introduces problems which cannot be ignored, but that for $\Psi \leq 0.2$ things look tolerable. Above this acceptance, some of the lowest energy positrons which would otherwise be useful will be lost.

The 30 cm drift space length was originally chosen as a guess at a minimum convenient length. With the tapered solenoid it costs little or nothing in phase slip to increase the drift space length to about a meter. This will make the layout considerably more convenient.

IV. RADIATOR

The discussion here will be brief. Inasmuch as the radiator interacts with the accelerator structure less than does the beam transport optics, studies of the optical system have been emphasized until now.

In designing the radiator we assume an input beam of 60 microamperes average current at 5 GeV (0.3 megawatts average power). Since the width of the electron energy spectrum matters little, a current greater than 60 microamps will probably be available eventually. (More properly, the input power might ultimately go up to $\approx$ 1 megawatt, still assuming a Stage I accelerator.) Thus, our design input power represents less than the ultimate power and perhaps a reasonable guess for the beam power during the early phase of accelerator operation. The design of a radiator for an average beam power of order one megawatt appears to be very difficult, and may best be deferred until the pressure for positron beam current is better defined.

We assume (conservatively, from the point of view of radiator heating) that the shower size is characterized by $R_o = 0.1$ cm. [If we assume that the shower radial distribution is uniform out to R_o and 0 for $R > R_o$, the power density equals the maximum for the distribution which leads to Eq. (5).] From Eq. (4), we take $2N(> 0) = 40$, where the factor 2 takes

account of electrons as well as positrons. Using Eqs. (4) and (5) to estimate the heating (with an assumed energy loss of $4(Z/A)$ MeV/gm/cm^2 for the electrons and positrons), we find a maximum power input:

$$\begin{array}{c} 330 \text{ joules/gm-pulse, or} \\ 78 \text{ calories/gm-pulse} \end{array} \qquad (31)$$

assuming a high Z radiator. This technique for estimating the heating leaves something to be desired, and these numbers may be low by as much as a factor 2. Monte Carlo calculations designed to give the thermal input distribution are available and will ultimately be used.

Although shower maximum occurs at about 5 radiation lengths at 5 GeV, decreasing the radiator thickness to 4 radiation lengths only decreases the positron yield by about 10% while decreasing the average power dissipation by about 30%. We thus think in terms of 4 radiation lengths thickness and an average power dissipation of about 1/3 the beam power, or 100 kilowatts. This average power is high enough so that a small fixed radiator is out of the question. However, a moderate sized rotating wheel, or some similar technique for averaging the power over a large volume, allows the 100 kilowatts to be handled reasonably easily. At about 1/2 cm radiator motion per pulse, 360 pulses per second, the required radiator velocity is about 2 meters per second, a modest speed. In order to average over a larger volume during the 2 microsecond beam pulse a velocity $\gtrsim$ 1000 meters per second is needed. While such a speed may not quite be out of the question, we do not find the idea attractive enough to pursue further here.

The major radiator problem is the absorption of the one-pulse energy density given in Eq. (31). We restrict ourselves, perhaps provisionally, to materials with high values of Z and density, and for such materials the specific heat is in all cases approximately 1/30 cal/gm-C$^\circ$. Thus, a temperature rise of about 2000 C$^\circ$ is expected. We can classify radiator materials as solid-solid, solid-liquid, solid-vapor, liquid-liquid, and liquid-vapor according to the radiator status before and after heating by one pulse. The simplest to think about are the solid-solid and liquid-

liquid cases, although the liquid-vapor case may indeed be tractable. (The "vapor" final state is meant to imply that some, but not all, of the material is vaporized.)

Tungsten appears to be the best choice for a solid-solid radiator. The major problem appears to be mechanical failure from thermal stresses. In cylindrical symmetry, the maximum thermal stresses for a thin circular plate normal to the beam line are:[11]

$$f_{\theta_{max}} = - f_{r_{max}} = \frac{Y\alpha(\Delta T)}{2} \tag{32}$$

where it is assumed that the area of the plate is much larger than the beam cross section, in which case the plate need not really be circular. Y is Young's modulus, α is the thermal expansion coefficient, and (ΔT) is the temperature rise above an assumed constant temperature before the beam pulse. The stresses f_θ and f_r are the circumferential and radial stresses, respectively; and there is no shear stress. If the thermal stress exceeds the fatigue limit, then the radiator will ultimately fail mechanically. The fatigue limit can be roughly estimated as about 1/2 the tensile strength of the material, if detailed fatigue data are not available.

The table below summarizes the thermal stress situation for a variety of more or less promising materials. It is important to note that (ΔT) corresponds to the input energy at shower maximum given in Eq. (31). Variation with Z/A has been neglected, so that ΔT is about 25% low for the lowest Z materials. A thermal stress $\frac{1}{2}Y\alpha(\Delta T)$ has been evaluated for each material and called S_{th}. The tensile strength S_t is also given (as found from quick surveys of various handbooks), and the fatigue limit S_f is obtained from $\frac{1}{2}S_t$ unless direct data for S_f happen to have been found. The number of stress cycles before failure is a steep function of the stress, and S_f is the stress below which fatigue failure is essentially undetectable. The ratio S_f/S_{th} is a figure of merit, which, however, must be treated with great caution, mainly because room temperature values of S_f have been estimated. The ratio of melting point (M.P.) to temperature change has also been given.

From the table, we would guess that a radiator built up of layers of tungsten sheet might be useful at about 1/4 the design energy input, or less. The data for other materials are useful for assessing their usefulness as "windows" through which the beam is to pass. For energy densities like the design values at shower maximum, titanium appears most promising. Aluminum and steel compete at lower energy densities, and aluminum is attractive because of its high thermal conductivity. For aluminum, edge-cooled windows at moderate energy densities and total input energies are promising. The very low thermal conductivity of titanium requires that a titanium window be in contact with a coolant over one surface in high power applications. At 78 calories per gram, water, and some oils, may be traversed by the beam without boiling.

Material	Z	C_p (cal/gm-C°)	(ΔT) (C°)	M.P./(ΔT)	Y psi $\div 10^6$	(α) $\times 10^6$ $(C^o)^{-1}$	S_{th} psi $\div 10^3$	S_t psi $\div 10^3$	S_f/S_{th}
Beryllium	4	0.42	185	7	40	15	55	75	0.7
Magnesium	12	0.25	310	2.1	10	28	43	50	0.6
Aluminum	13	0.23	340	1.9	10	27	46	70	0.8
Titanium	22	0.12	650	2.8	15	9	44	90*	2.0
								60**	1.4
Steel	26	0.12	650	2.4	30	12	117	250/	1.0
Molybdenum	42	0.065	1200	2.2	43	5.5	142	250//	0.9
Tantalum	73	0.035	2200	1.3	27	6.7	200	130//	0.3
Tungsten	74	0.035	2200	1.5	51	4.5	250	600//	1.2

*Fatigue limit, high strength alloys

**Fatigue limit, pure titanium

/Aircraft alloy, measured fatigue limit 120,000 psi

//Tensile strength upper limits, attainable only with optimum cold working

The thermal stress problem may be avoided if the radiator consists of particles small compared with the beam diameter. If such particles are canned, then the canning material and the overall heat transfer present serious problems. If the particles are made to flow through the beam line like a liquid stream, then there may not need to be any material other than the particles in the beam at shower maximum. However, the "pumping" and heat transfer problems look formidable, and maintaining a high average density may not be easy either.

An application of the "small particle" principle is the "wire brush" radiator (brought to my attention by Al Odian). We envision closely packed tungsten wire "bristles" projecting radially from the periphery of a rotating wheel. The wheel does the "pumping," and it is probably not difficult to handle the heat transfer by conduction from bristles to wheel-rim and from wheel-rim to water, oil, etc. An average density $\gtrsim 1/2$ that of solid tungsten should be attainable; and the strength of tungsten is maximal for cold drawn wire. While the thermal stresses are not zero for a wire whose diameter is small compared with the beam diameter, the stresses decrease with wire diameter, and such a radiator may remain practical even for $\approx 2000\ C^{\circ}$ temperature rise. A more detailed study of this type of radiator is being made.

Another way to handle thermal stresses is to use a liquid radiator. Liquid lead, bismuth, or lead-bismuth alloy may be practical. The low boiling point of mercury, and its relatively low heat of vaporization, combine to produce a situation where a large fraction of the mercury is expected to vaporize at shower maximum. We have little feeling for the dynamics of this extremely rapid vaporization, but it seems tricky and hard to study in such a way that results can be scaled up to a full-sized radiator. The other metals mentioned allow temperature rises $\approx 1000\ C^{\circ}$ before any boiling occurs, and above the boiling point the higher heats of vaporization lead to boiling for only a small fraction of the material at "design shower maximum." We believe the heat transfer and pumping problems for the heavy liquid metal radiator are soluble. If further studies of the "wire-brush" radiator destroy some of our optimism, the liquid metal scheme will be looked into in more detail.

Returning to the "window" problem, we would like the radiator to be separated from the accelerator vacuum system. From the table which summarizes the thermal stress situation, the window problem appears reasonable at energy densities a factor 10 or more below that at shower maximum, and the electron beam fulfills this condition for a radius of 0.1 cm, or even somewhat less. The angular spread of the shower is such that a few centimeters downstream of the radiator the energy density is also low enough. The scattering introduced by a thin aluminum or titanium window at such a location is also tolerable (for the positron beam). However, the electron beam occupies a phase space volume small in comparison with the acceptance of the sector quadrupole system, and it would be undesirable to worsen this situation by leaving windows permanently in the beam line at the radiator location. Thus, the radiator-plus-windows are to be shifted into the beam line when positrons are to be made.

V. CONCLUSION

For conservatism, let the positron source radius R_o be 0.2 cm, to take account of possible thermal problems, phase space matching problems, possible errors in the Monte Carlo calculations or our interpretation of them, or a combination of these things. Then, assuming a beam transport system acceptance of 0.2 mc-cm for positrons produced at 4 to 16 MeV in a lead radiator, the positron yield per incident electron, n^+, is approximately

$$\begin{aligned} n^+ &= [N(>4, <16)][N(R<0.2)][N(\theta<1/16)] \\ &\approx (7)(1/2)(1/100) = 3.5\times10^{-2} \end{aligned} \tag{33}$$

where phase space matching problems are already to some extent accounted for by a factor 1/2 arising from a large range of R and small range of θ. This value of n^+ corresponds to an average positron beam current of about 2 microamps.

For comparison, we consider positron production by having the full energy electron beam strike a relatively thin radiator at the end of the accelerator. As a crude, and probably optimistic, estimate, we consider

the positrons to result from bremsstrahlung in one radiation length and pair production in one radiation length. Using the simplest thin target bremsstrahlung and pair production formulas,

$$n(E)dE = \frac{7}{9}\left(1 - \frac{E}{E_{max}}\right)\frac{dE}{E} \qquad (34)$$

where $n(E)dE$ is the number of positrons in dE at E, per incident electron. For $dE/E = 0.01$, and $E/E_{max} = 1/2$ (somewhat lower energy than the proposed "reaccelerated" positron beam), we have 4×10^{-3} positrons/electron. The beam switchyard acceptance is about $(0.6)(E_{GeV}/10)$ mc-cm, and we will assume these positrons have a source radius 0.1 cm. The "typical" transverse momentum, estimated from multiple scattering in 1/2 radiation length, will be about 20 mc, so the source requires about 2 mc-cm for complete transmission by the energy-analyzing system. The use of the beam switchyard thus reduces the intensity by about a factor 16 to 2.5×10^{-4} positrons/electron at 7.5 GeV.

We thus expect, for a positron beam with 1% energy spread, that the reacceleration system gains a factor greater than 100 in beam intensity. The intensities might be comparable for a special energy-analyzing system with large acceptance and for a beam energy spread of about 10%.

NOTES AND REFERENCES

1. D. Yount and J. Pine, "Production of positrons with the Stanford Mark III Accelerator," Nucl. Instr. and Methods 15, 45 (1962).
2. We wish, apologetically, to caution the reader that the superficial spirit of this note also implies less than the customary care in checking to eliminate both numerical and conceptual errors. Caveat emptor.
3. See B. Rossi, High Energy Particles (Prentice-Hall, 1952), Chapter 5, for detailed discussion of electromagnetic showers.
4. C. D. Zerby and H. S. Moran, ORNL-3360, Oak Ridge National Laboratory, Oak Ridge, Tennessee; p. 261.
5. C. D. Zerby and H. S. Moran, private communication June 25, 1963.
6. R. H. Helm, "Discussion of focusing requirements for the Stanford two-mile accelerator," SLAC Report No. 2, Stanford Linear Accelerator Center, Stanford University, Stanford, California (1962).
7. R. H. Helm, "Adiabatic approximation for dynamics of a particle in the field of a tapered solenoid," SLAC Report No. 4, Stanford Linear Accelerator Center, Stanford University, Stanford, California (1962).
8. R. H. Helm, "Misalignment and quadrupole error effects in a focusing system for the two-mile accelerator," SLAC Report No. 11, Stanford Linear Accelerator Center, Stanford University, Stanford, California (1963).
9. R. H. Helm, "Optical properties of quadrupole multiplets for sector focusing in the two-mile accelerator," SLAC Report No. 14, Stanford Linear Accelerator Center, Stanford University, Stanford, California (1963).
10. R. H. Helm, "Misalignment and quadrupole error problems affecting the choice of multiplet type for sector focusing of the two-mile accelerator," SLAC Report No. 15, Stanford Linear Accelerator Center, Stanford University, Stanford, California (1963).
11. Gatewood, Thermal Stresses (McGraw-Hill, New York, 1957); p. 101.

CONSIDERATIONS OF THE USE OF MONOCHROMATIC PHOTON BEAMS

by

G. R. Bishop

I. INTRODUCTION

Three methods of obtaining beams of monochromatic photons have been discussed; i.e., annihilation in flight of positrons,[1] coherent bremsstrahlung from crystals,[2] and interaction of the electron beam with the photons of a laser beam.[3] The first two methods give monochromatic beams accompanied by normal bremsstrahlung spectra, while the third, with suitable collimation, could give a very small contamination of lower photon energies. The choice of a method will depend on the experiment envisaged, the required photon energy, and the origin and intensity of the background. In this report, two experimental situations, illustrating two advantages of using a monochromatic beam, are examined. The first advantage is the extra constraint imposed by the fixed incident energy on many-body final states. The second advantage concerns two-body final states, which can be singled out by the extra kinematical constraint without the need for energy measurements in coincidence on the products that are necessitated by a normal bremsstrahlung beam. Coincidence measurements are rendered difficult by the duty cycle of the accelerator unless very low intensities are used. Under conditions where the accelerator is used at maximum beam current for production of secondary particle beams, which is likely to be most of the time, the methods mentioned above are capable of producing between 10^5 and 10^6 monochromatic photons per pulse. It is therefore useful to consider experimental situations capable of dealing with such intensities.

II. INELASTIC PHOTON SCATTERING OR NUCLEON RAMAN EFFECT

Because the existence of several nucleon isobars is proved or suspected, a nucleon level scheme can be drawn up. Of the excited levels, the first and second can be reached by M1,E2 or E1,M2 photon transitions, respectively; the third is reached by E2,M3 and the fourth by

M3,E4. The laboratory photon energies incident on a proton at rest that are necessary to excite these states are 348 MeV (1238), 750 MeV (1512), 1050 MeV (1688), and 1495 MeV (1688), so that with existing machines only the first three have been studied in photopion reactions.[4] The number of decay channels available to the excited states increases with the excitation energy, and it is clear that not all of them have been investigated. In particular, the possibility of a γ-ray emitted between the states in competition with other decay modes has not been investigated at all. This is due to the fact that experiments are usually carried out with a bremsstrahlung beam, so that many possibilities exist for observing a photon of lower energy than that responsible for producing a given resonance. For example, excitation of the 1512 MeV state with photon decay to the 1238 MeV state would give a photon of energy 274 MeV (less the recoil energy of the N^* system of 25 MeV) in the c.m. system. For $\theta_{c.m.} = \pi/2$, the photon would appear at $\theta_{Lab} = 63^\circ 36'$ with an energy of 278 MeV. With a bremsstrahlung beam it would be easy to find such a photon through Compton scattering or π^o decay. With a monochromatic beam produced by the laser technique it should be possible to observe the inelastic photon, and this is considered in detail for the 1512 MeV state in the following.

The interest of the experiment lies in determining another radiative matrix element of the pion-nuclear system. Those matrix elements that connect the ground state with the excited states are determined from photoproduction of pions or from elastic scattering of photons. For the latter process, our interpretation in terms of the isobar model has been given by Minami,[5] which is consistent with recent results.[6] Inelastic scattering total cross sections would give the square of the matrix element for the leading transition (E1 in the case of a 1512 to 1238 transition), and the angular distribution would give the amount of the next higher multipole order transition strength mixed in with the leading transition. This would be much too ambitious a program, because the inelastic photons are not monochromatic owing to the large level widths. However, for dipole transitions the E_γ^3 dependence of the transition probability and the resonance shape will tend to concentrate the strength somewhere near the difference in level energies.

Let us now consider in more detail the excitation and decay of the 1512 MeV level to see what characteristics we must give to the apparatus in order to look for inelastic photon emission. First of all, the choice of beam falls clearly on the laser technique. Using photons from a ruby laser (1.79 electron volts) and an electron beam energy of 5.61 BeV, we obtain photons of the desired energy (0.75 BeV) in the direction of the electron beam. This beam is later deflected for use in another experimental area.

In addition to the process under study, excitation of the 1512 level leads to the following final states from the initial state of photon plus proton.

	Statistical Weights
$\gamma + p \rightarrow p^{**} \rightarrow \pi^+ + n$	2/3
$\pi^o + p$	1/3
$\pi^+ + \pi^- + p$	1/2
$\pi^o + \pi^+ + n$	1/3
$\pi^o + \pi^o + p$	1/6
$\pi^+ + p^*$	1/6
$\pi^o + p^*$	1/3
$\pi^- + p^*$	1/2

(1)

The statistical weights are just those corresponding to conservation of isotopic spin, while production cross sections will be governed also by available phase space and the reaction mechanisms. The threshold for 3-pion production is 0.507 BeV, so that some three-pion final states will exist. The 2-pion production is known to be small at its threshold of 0.321 BeV and to rise to a shallow peak at about 300 MeV higher. If the same behavior is followed by the 3-pion production, the energy of 750 MeV presently considered may be low enough to avoid a lot of 3-pion production. To the above processes we now want to add

$$\gamma + p \rightarrow p^* + \gamma' \qquad (2)$$

and ask what experimental quantities we need to determine. The p^* will decay into $\pi^o + p$ or $\pi^+ + n$ in a time of the order of 10^{-23} sec, so that this particular final state will consist of $\gamma' + \pi^+ + n$ or $\gamma' + \pi^o + p$. The π^o's from all of the final states listed in Eq. (1) will decay into two photons with energy distributions that easily overlap the energy of the inelastic photon γ'. Thus we cannot rely on detection of γ' alone to define the reaction, even if its energy is measured at a given laboratory angle. What is needed is a signature for Eq. (2), which is the π^+ emitted in coincidence with γ' following decay of p^*. A partial cross section is measured, but the total one is easily obtained from the known branching ratio of p^* decay. Thus we measure the γ' angles and the π^+ momentum and energy. The system is completely determined if monochromatic incident photons are used and if a measurement of γ' energy overdetermines the system and helps to discriminate against background. There are three particle momenta to determine, i.e., nine parameters. For monochromatic incident photons we have energy conservation as one constraint, leaving eight parameters; momentum conservation as three constraints leaves five parameters to be determined. If the π^+ energy is identified and measured, we have three more constraints, leaving the two γ' photon polar and azimuth angles parameters.

The second feature which characterizes the particular state that we want to determine is the photon multiplicity. The background reactions listed in Eq. (1) and those due to 3-pion production will all contain an even number of photons from π^o decay (except for the influence of Dalitz pairs produced in 0.012 of π^o decays). The reaction in which we are interested contains one or three photons, depending on the p^* decay mode. To use this discriminatory feature will demand a high detection efficiency ϵ for photons. If $\epsilon < 1$, although both even and odd numbers of photon events will be reduced in the same ratio, the redistribution of even number events that become odd number ones through failure to detect one photon completely falsifies the number of odd events, as the latter are only a small initial fraction of all events. We can estimate the number of inelastic events by considering the ratio

$\Gamma'_\gamma/\Gamma_{total}$. The width for inelastic emission will supposedly be given by the expression

$$\Gamma_\gamma = \frac{\left[(\lambda\!\!\!^{-}/\mu c)/\lambda\!\!\!^{-}\right]^2}{1 + (a/\lambda\!\!\!^{-})^2} c_\gamma$$

which gives the radiative width used in the Breit-Wigner resonance formula fit to photopion production data.[7] Here $a = 1.4(\lambda\!\!\!^{-}/\mu c)$ and $c_\gamma = 2$ MeV, so that we expect $\Gamma'_\gamma \approx 1$ MeV. This is for an M1 transition, and it might be expected that the E1 transition would be faster. For a radius of 1f the width for emission of 270 MeV photons is 2.9 MeV. Compared with the total level width of 100 MeV, between 1 and 3 percent of inelastic photon events can be expected, with odd multiplicity.

The even multiplicity events can be estimated from Eq. (1) and the fact that 80 percent of p^{**} decays lead to a pion-nucleon system in a relative d-state. The remaining 20 percent will include the inelastic scattering and the multipion events, with the two-pion events of Eq. (1) dominating. The numbers of two-pion events with one or two π^o's will depend on whether p^* is formed or not. If p^* is not formed, then we have 1/3 with one pion and 1/6 with two pions. If p^* is formed, we have

1/6	$\pi^+ + p^* \rightarrow \pi^+ + \pi^- + p$	A
	or $\pi^+ + \pi^o + n$	
1/3	$\pi^o + p^* \rightarrow \pi^o + \pi^+ + n$	B
	$\pi^o + \pi^o + p$	
1/2	$\pi^- + p^* \rightarrow \pi^- + \pi^+ + p$	C

Case C gives no π^o's and occurs in 1/2 of these events. Case A gives one π^o and occurs in $1/16 \times 2/3 = 1/9$ of events, using the Clebsch-Gordon coefficients and the orientation of p^* in isospin space. Case B gives $1/3 \times 2/3 = 2/9$ of events with one π^o and $1/3 \times 1/3 = 1/9$ of events with two π^o's. From this the initial spectrum of photon

multiplicity can be constructed, indicating the number of events with n-photon multiplicity by A_n,

$$\begin{array}{cccccc} A_0 & A_1 & A_2 & A_3 & A_4 \\ \{0.634 - (x+y)\} & x & 0.334 & y & 0.033 \end{array}$$

which applies to the case of no p^* formation.

If the probability of detecting a photon is ϵ and the probability of not detecting it $1-\epsilon$, the initial spectrum will be changed to the form

$$A_0' = A_0 + A_1(1-\epsilon) + A_2(1-\epsilon)^2 + A_3(1-\epsilon)^4$$
$$A_1' = A_1\epsilon + A_2\epsilon(1-\epsilon) + A_3\epsilon(1-\epsilon)^2 + A_4\epsilon(1-\epsilon)^3$$
$$A_2' = A_2\epsilon^2 + A_3\epsilon^2(1-\epsilon) + A_4\epsilon^2(1-\epsilon)^2$$

and so on. Here the possibility of charge-exchange scattering of π^- on protons to give π^0's has not been taken into account. Now to obtain $\epsilon = 0.98$ we shall need $5 \times 7/9 = 3.9$ pair production lengths of radiation, or 5 radiation lengths in all in the detector. A detection efficiency of $\epsilon = 0.95$ will be obtained with 3.9 radiation lengths. However, $\epsilon = 0.95$ gives serious distortion of the multiplicity spectrum because with $x = 0.02$, $y = 0$, we find

$$A_0' = 0.616 \quad A_1' = 0.0348 \quad A_2' = 0.302 \quad A_3' = 1.41 \times 10^{-3} \quad A_4' = 0.027$$

A possible detector for these events would be a large spark chamber with a magnetic field. Using the expressions of Trilling,[8] one finds a resolution for the γ' energy of

$$\frac{\Delta p}{p} = 7.7 \times 10^{-2} \times 0.3^{1/3} \times \left(\frac{5}{D}\right)^{2/3} \times 4^{1/3} = \frac{2.4 \times 10^{-1}}{D^{2/3}}$$

where it has been supposed that the spark is determined in position to 0.2 mm. This gives 15 percent resolution for D = 2 meters, which will help to discriminate against background events. The thickness of the plates is 0.32 L_R or equivalent to 4.5 mm in thickness, and their separation is about 6.5 cm, so that about 30 plates are needed.

The kinetics of the signature events $\gamma' + \pi^+$ have not been worked out entirely. An upper value of the π^+ laboratory energy is 510 MeV. At 90° in the c.m. system, the energy of the π^+ in the laboratory when it is emitted in the direction of recoil of p^* is 364 MeV and $\theta_{Lab} = 10^\circ 18'$. If it is emitted in the same direction as the γ', its laboratory energy is 260 MeV and $\theta_{Lab} = 58^\circ 4'$. In the last case the π^+ will be stopped in the chamber (range 45 gm/cm of Cu, total normal thickness of chamber 64 gm/cm^2 of Cu). In any case, a good measurement of the $\pi^\pm$ momentum should be possible.

III. COMPARISON OF MUON AND ELECTRON INELASTIC SCATTERING

The probable availability of muon beams of a sufficient intensity to perform nucleon and nuclear scattering experiments prompts a comparison of the information that may be gained with the well known experiments on electron scattering. If the interaction of a muon with a nucleon system is purely electromagnetic, which can be expected for momentum transfers ≈ 1 BeV/c, then the cross section predicted by the first Born approximation may be safely used in a large variety of experimental conditions. The interaction energy is given by

$$< f|H|i > = \int A^\mu_\mu(x)\, J^\mu_N(x)\, dx$$

where $A^\mu_\mu(x)$ is the Moller potential generated by the scattered charges and $J^\mu_N(x)$ is the nuclear four-current. The interaction is gauge invariant if the nuclear current is conserved, i.e., $\partial J^\mu_N(x)/\partial x_\mu = 0$. In the Lorentz gauge $\partial A_\mu/\partial x_\mu = 0$ and $A^\mu_\mu = 4\pi J^\mu_\mu$, from which the Moller potential is easily obtained because the muon transition current has

the form

$$J_N^\mu = e\bar{\psi}_f \gamma_\mu \psi_i = e\bar{u}_f \gamma_\mu u_i \exp(-iqx)$$

where q is the four momentum transferred to the nucleus. The interaction becomes

$$< f|H|i > = -\frac{4\pi e}{q_\mu^2} (\bar{u}_f \gamma_\mu u_i) \int \exp(-iqx)\, J_N^\mu(x)\, d^4x$$

$$\equiv -\frac{4\pi e}{q_\mu^2} (\bar{u}_f \gamma_\mu u_i)\, J_N^\mu(q)$$

where $J_N^\mu(q)$ is the Fourier transform of $J_N^\mu(x)$. The Lorentz gauge condition gives

$$(\bar{u}_f q^\mu \gamma_\mu u_i) = 0$$

and conservation of current gives

$$q_\mu J_N^\mu(q) = 0$$

Now $\gamma_\mu = (\gamma_o, \vec{\gamma})$ and $q_\mu = (q_o, \vec{q})$, so that if we consider $\vec{\gamma}$ as decomposed into components parallel and transverse to the momentum transfer, we can write

$$\vec{\gamma} = \vec{\gamma}_t + \vec{q}\,\frac{\vec{\gamma} \cdot \vec{q}}{q^2} \equiv \vec{\gamma}_t + \vec{q}\,\frac{\gamma_o q_o}{q^2}$$

after applying

$$\gamma_\mu q_\mu = \gamma_o q_o - \vec{\gamma} \cdot \vec{q} = 0$$

Similarly, for J we obtain

$$\vec{J} = \vec{J}_t + \vec{q}\,\frac{q_o J_o}{q^2}$$

The product

$$\gamma^\mu J^\mu = \gamma_o J_o - \vec{\gamma}\cdot\vec{J} = \gamma_o J_o - \vec{\gamma}_t\cdot\vec{J}_t - \gamma_o J_o\,\frac{q_o^2}{q^2}$$

so that

$$\frac{\gamma^\mu J^\mu}{q_\mu^2} = -\frac{\gamma_o J_o}{q^2} - \frac{\vec{\gamma}_t\cdot\vec{J}_t}{q_\mu^2}$$

and we have absorbed the longitudinal and time-like photons into one term, and in addition have a transverse term. When this is substituted in the matrix element, the time integral can be performed, giving the energy delta function. Expressions such as $\gamma_o \exp(i\vec{q}\cdot\vec{r})$ and $\vec{\gamma}\exp(i\vec{q}\cdot\vec{r})$ are expanded in multipoles in the way indicated in Ref. 9, and the integrals over the muon variables can be made. The result is a cross section of the form

$$d\sigma = \left(\frac{e}{\hbar c}\right)^2 \frac{4\pi(\lambda+1)}{\lambda[(2\lambda+1)!!]^2}\,\frac{q^{2\lambda}}{K_i^2}\left[\sum_{\lambda=0}^{\infty}\frac{\lambda}{\lambda+1}\,B(C\lambda,q)\,V_L(\theta)\right.$$

$$\left.+\left\{\sum_{\lambda=1}^{\infty}B(M\lambda_1 q)+B(E\lambda_1 q)\right\}V_T(\theta)\right]$$

where the B's are nuclear matrix elements and $V_L(\theta)$, $V_T(\theta)$ are the densities of longitudinal and transverse virtual photons, respectively.

These are given by the relations

$$V_L(\theta) = \frac{\dfrac{4m^2c^2}{\hbar^2 k_i k_f} + \dfrac{k_i}{k_f} + \dfrac{k_f}{k_i} - \dfrac{K^2}{k_i k_f} + 2\cos\theta}{\left(\dfrac{k_i}{k_f} + \dfrac{k_f}{k_i} - 2\cos\theta\right)^2}$$

and

$$V_T(\theta) = \frac{\left(\dfrac{k_i}{k_f}\right)^2 + \left(\dfrac{k_f}{k_i}\right)^2 + 4 - \dfrac{K^2}{k_i k_f}\left(\dfrac{k_i}{k_f} + \dfrac{k_f}{k_i}\right) - 2\left(2\dfrac{k_i}{k_f} + 2\dfrac{k_f}{k_i} - \dfrac{K^2}{k_i k_f}\right)\cos\theta + 2\cos^2\theta}{\left(\dfrac{k_i}{k_f} + \dfrac{k_f}{k_i} - 2\cos\theta\right)\left[\dfrac{k_i}{k_f} + \dfrac{k_f}{k_i} - \dfrac{K^2}{k_i k_f} - 2\cos\theta\right]^2}$$

when $mc \ll k_i$, k_f and $K_1' \ll k_i$, k_f (K_1' is the energy transfer). These expressions reduce to

$$V_L(\theta) = (\cos^2\theta/2)/4\sin^4\theta/2$$

$$V_T(\theta) = (1 + \sin^2\theta/2)/8\sin^4\theta/2$$

and the cross section may be cast into the form

$$\frac{d\sigma}{d\Omega} = \sigma_{Mott}\left[F_L^2(q^2) + \left(\frac{1}{2} + \tan^2\theta/2\right)F_T^2(q^2)\right]$$

where F_T and F_L have multipole decompositions easily derived from the above.

Although $V_T(\theta)$ will be practically the same for both electrons and muons of, for example, an incident momentum of 400 MeV/c, $V_L(\theta)$ will be different because of the term $4m^2c^2/\hbar^2 k_i k_f$. Thus a comparison

of electron and muon scattering cross sections can tell us whether the scattering is mainly longitudinal or not. Putting in figures for $k_i = 400$ MeV/c, $\theta = 90^\circ$, and $K_1' = 150$ MeV, we find the virtual photon density for muons to be 23 percent greater than for electrons. Of course, this effect will be less important for higher energy incident muons.

Fixing attention on the Coulomb scattering case for the moment, we can write the scattering cross section at 0° as

$$\frac{d\sigma(c\lambda)}{d\Omega}(\theta = 0^\circ) = \left(\frac{e^2}{\hbar c}\right)^2 \frac{4\pi}{[(2\lambda + 1)!!]^2} 4k^2\Delta^{2(\lambda-2)} B(C\lambda, q \to 0)$$

where $\Delta = E_x/\hbar c$ is now the momentum transfer corresponding to real photon absorption. The reduced matrix element is related to the width of a state by

$$\hbar\tau^{-1} = \frac{8\pi(\lambda + 1)}{\lambda[(2\lambda + 1)]^2}\left(\frac{E_x}{\hbar c}\right)^{2\lambda+1} B(\lambda, J_f, J_i)$$

Now in nuclei some dipole levels with a width of 10 KeV are known in the giant resonance region at $E_x \approx \alpha_o$ MeV. This leads to a cross section of

$$\frac{d\sigma}{d\Omega} = 1.5 \times 10^{-27} \text{ cm}^2/\text{steradian}$$

At 0° to the incident beam the processes responsible for degrading the energy are electron scattering and bremsstrahlung. If an incident beam of electrons is used, these cross sections have orders of magnitude for a 20 MeV energy loss of 10 to 100 mbarns. Thus for electrons the final energy spectrum is dominated by the $1/E$ dependence of the bremsstrahlung process, and the nuclear absorption cross section is swamped out.

At Orsay an attempt was made to detect this excitation on a target of carbon by Bishop and Isabelle, but without definite success. However,

carbon is known to have rather broad dipole levels so that the cross section is smeared out over an energy band, making its detection difficult.

With a muon beam at least the background due to bremsstrahlung would be reduced by a factor of $(m_e/m_\mu)^2$ or 2.5×10^{-5}. If a muon beam of narrow dimensions was fired into a small aperture magnet, even some of the muons degraded in energy by a collision with a target electron would be deflected away sufficiently. The scattering cross section is

$$\Phi_{coll}(E, E')dE' = \frac{2C\, m_e c^2}{\beta^2} \frac{dE'}{(E')^2}$$

$$C = \frac{\pi NZ}{A} r_e^2$$

$$= 0.150 \frac{Z}{A} g^{-1}\ cm^2$$

when the energy transfer E' is much less than the maximum one (E_μ).

Ignoring angular distribution effects for the degrading processes, we calculate the following probabilities for scattering by a target of carbon of thickness 1 gm/cm^2 into a 1 MeV interval at 20 MeV energy loss:

Scattering by electrons	1.91×10^{-4}	
Nuclear absorption	7.41×10^{-5}	
Bremsstrahlung	1.12×10^{-3}	for electrons
	2.8×10^{-8}	for muons

Thus for muons the nuclear excitation would be detectable as a 30 percent effect at least. The usual sort of double focusing spectrometer or broad range spectrograph will be capable of doing this experiment. The effect is not limited to dipole transitions; quadrupole transitions could easily be measured as well.

The argument can be extended to the case of inelastic muon scattering with production of π-mesons. Thus for $E_{\mu i}$ = 1 BeV, E_f = 0.7 BeV, that

is, at the peak of the 3-3 resonance, the cross section at 0° cm hydrogen is calculated from the formula

$$\frac{d^2\sigma}{d\Omega_f dE_f} = \frac{\alpha}{4\pi^2} \frac{E_i - E_f}{E_i^2(1 - \beta_1\beta_2 \cos\theta)} \sigma_\gamma(E_i - E_f) F^2(q)$$

to be 9.1×10^{-31} cm^2/steradian. For 1 gm/cm^2 of target this leads to a scattering probability of 1.7×10^{-6} and to a production probability per muon of 5.5×10^{-7}, so that the inelastic scattering of muons at 0° with production of π-mesons is about 32 percent of the background effect.

IV. TWO-BODY FINAL STATES WITH MONOCHROMATIC PHOTONS*

A. Introduction

The use of monochromatic photon beams may simplify the detection of two-body final states in photoproduction experiments at high energies. If the reaction $\gamma + p \rightarrow x + y$ is studied with a well-determined energy for the photon, it suffices to measure the angle of emission of one of the outgoing particles (if the masses are known) in order to determine the kinematics of the process. If we measure the momentum of x at a fixed angle, the kinematics is overdetermined. This leads to an interesting situation, because by varying θ_x for fixed P_x or by varying P_x for fixed θ_x, the production of y will show up as a peak in the production cross section of x. If the experiment is made in a similar fashion with a bremsstrahlung spectrum, at the same kinematic conditions a step would be obtained superimposed on a continuous distribution due to final states of other masses. The occurrence of a step is more difficult to put in evidence as a statistically significant quantity, because in the bremsstrahlung case the continuum is given by an integration over events leading to fixed P_x and θ_x for any possible energy of the absorbed photon.

---

*This section was written with the invaluable collaboration of J. Perez y Jorba of Orsay, France.

Let us consider the production process

$$\gamma + p \rightarrow p + x_o$$

where x_o indicates a neutral system of any mass, and we measure the angle and momentum of the recoil proton. The spectrum at a fixed laboratory angle will be continuous due to the formation of multipion systems having no particular correlation between their energies and angles; superimposed on the spectrum will be peaks due to the formation of particular neutral particles such as the η, ω and φ mesons. The magnitudes of the cross sections for background and a particular neutral particle are governed by considerations of available phase space and interaction mechanisms, and the background may easily be of similar or greater order of magnitude than the resonances we want to study; therefore, it seems interesting to find a way of increasing the ratio of the two-body process counting rate over that due to phase space controlled background events.

B. Maximum Angle Technique

In Fig. 1 we plot the momentum angle relationship for recoil protons from the reactions $\gamma + p \rightarrow \eta^o + p$ and $\gamma + p \rightarrow \omega^o + p$ for incident photons of 5 BeV energy. If we choose θ and P corresponding to the particle we want to study, the phase space for multiparticle production will be proportional to the product of the bands $\Delta\theta$ and ΔP accepted by the system. The cross section for the two-body process will be proportional to ΔP or to $\Delta\theta$, so that it would appear useful to reduce ΔP or $\Delta\theta$; however, this effect is counterbalanced by determination of statistics, and a compromise must be found. From Fig. 1 we note, as is often the case with this kind of kinematics, that θ_{Lab} has a maximum value less than $\pi/2$.[10] If we choose to work at this maximum angle point we can reduce $\Delta\theta$ and correspondingly reduce the phase-space background at the expense of only a slight loss of counting rate for the two-body process.

Let us consider under what conditions a maximum angle is obtained in the general reaction $\gamma + p \rightarrow x + y$. If $M_x > M_p$, we always have a maximum angle θ_x (center-of-mass quantities will be distinguished from

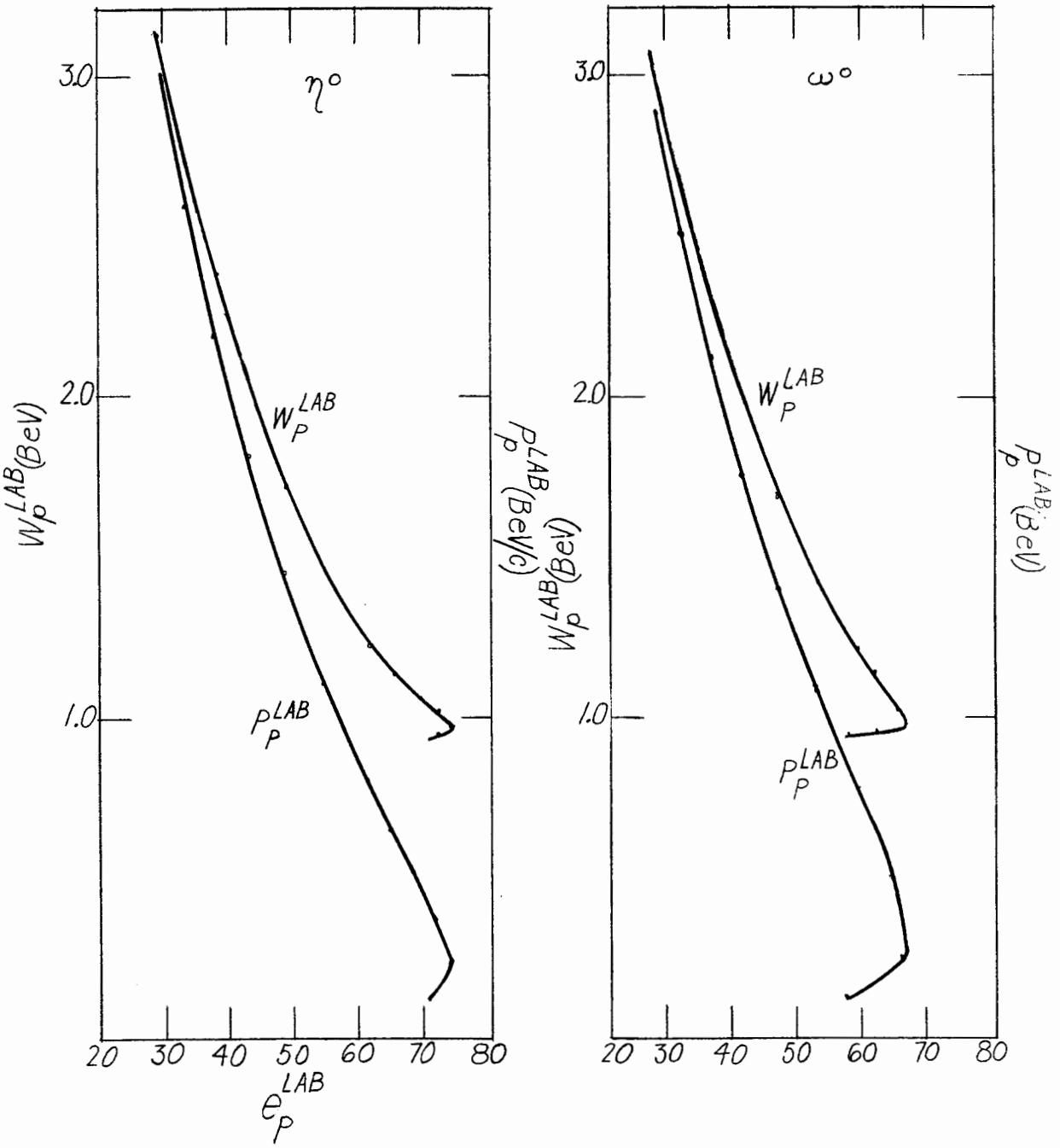
η°
ω°
3.0
2.0
1.0
W_P^{LAB}
P_P^{LAB}
W_p^{LAB}(BeV)
P_p^{LAB}(BeV/c)
P_p^{LAB}(BeV)
20 30 40 50 60 70 80
θ_P^{LAB}

FIG. 1

laboratory quantities by a star in the following).

If $M_x < M_p$, there is a region of energy just above threshold where there is a θ_x maximum. It is given by

$$\frac{\left(M_x + M_y\right)^2 - M_p^2}{2\,M_p} \leq E \leq \frac{M_y^2 - \left(M_x - M_p\right)^2}{2\left(M_p - M_x\right)}$$

Above this region, θ_x can go to π.

If now we specify $\gamma + p \rightarrow p + x_o$, we find the well known result that there is always a θ_p (max), whatever the value of the mass x_o.

If $M_{x_o} > M_p \equiv M$, we always have a θ_{x_o}(maximum).

If $M_{x_o} < M$, we have a θ_{x_o}(maximum) for

$$\frac{M_{x_o}\left(M_{x_o} + 2M\right)}{2M} \leq E \leq \frac{M_{x_o}\left(2M - M_{x_o}\right)}{2\left(M - M_{x_o}\right)}$$

Above this limit θ_{x_o} extends to π.

Returning to the case of $\gamma + p \rightarrow p + x_o$, we will always in principle be able to use the maximum angle technique. The value of the maximum angle for the proton in the laboratory is given by

$$\sin \theta_p = \frac{\eta_p^*}{\eta} = \frac{P_p^*}{M\eta} \tag{1}$$

Here P_p^* is the center-of-mass momentum, $\eta = \frac{E}{\mu}$ where E is the photon energy, and μ is the invariant mass of the system, $\mu^2 = M(2E + M)$. The relation

$$P_p^* = P_{x_o}^* \equiv P^*$$

is given by the equation

$$P^{*2} = \frac{(2EM - m^2)^2 - 4m^2M^2}{4\mu^2} \tag{2}$$

where $m \equiv M_{x_o}$.

This relation can be written in the center-of-mass system as

$$\cos \theta_p^* = - \frac{\gamma}{\eta} \frac{P^*}{E_p^*} = - \frac{\beta^*}{\beta}$$

where $\gamma = \frac{E + M}{\mu}$, $\eta = \beta\gamma$, $\beta^* = (P^*/E_p^*)$, and E_p^* is the total energy of the proton in the center-of-mass system.

If we now fix our attention on a given energy E, for each mass value m of a particle whose production is possible at this energy, we will have a well determined point in the $\theta_p - P_p$ plane for the condition of maximum angle.

The locus of these points when one varies the mass m is given by the relation

$$P_p = \frac{\eta M \cos \theta}{\sqrt{1 + \eta^2 \sin^2\theta}} \equiv \frac{\eta M \cos \theta}{\sqrt{\cos^2\theta + \gamma^2 \sin^2\theta}} \qquad (3)$$

Curves of this relation are plotted on Fig. 2 for E = 1.25, 2.5, 5 and 10 BeV. They all have a maximum at $\theta = 0^\circ$, $P_p = \eta M$, and then they decrease uniformly to 0 at $\theta = 90^\circ$. The slope at $\theta = 90^\circ$ is

$$\left(\frac{dP_p}{d\theta}\right)_{\theta=90^\circ} = \frac{\eta M}{\gamma}$$

They also have a point of inflection at $\sin^2\theta = \frac{1}{2\eta^2}$ when $\eta > 2^{-\frac{1}{2}}$.

The envelope of the curves is the curve $P_p = M \cot \theta$, which is the value of Eq. (3) when $E \to \infty$, so that at a fixed angle P_p does not exceed $M \cot \theta$ whatever the energy E.

If we discard the maximum angle condition and consider the general case, we find the following expression

$$P_p = \frac{\eta E_p^* \cos \theta \pm \gamma \sqrt{P^{*2} - \eta^2 M^2 \sin^2\theta}}{\cos^2\theta + \gamma^2 \sin^2\theta} \qquad (4)$$

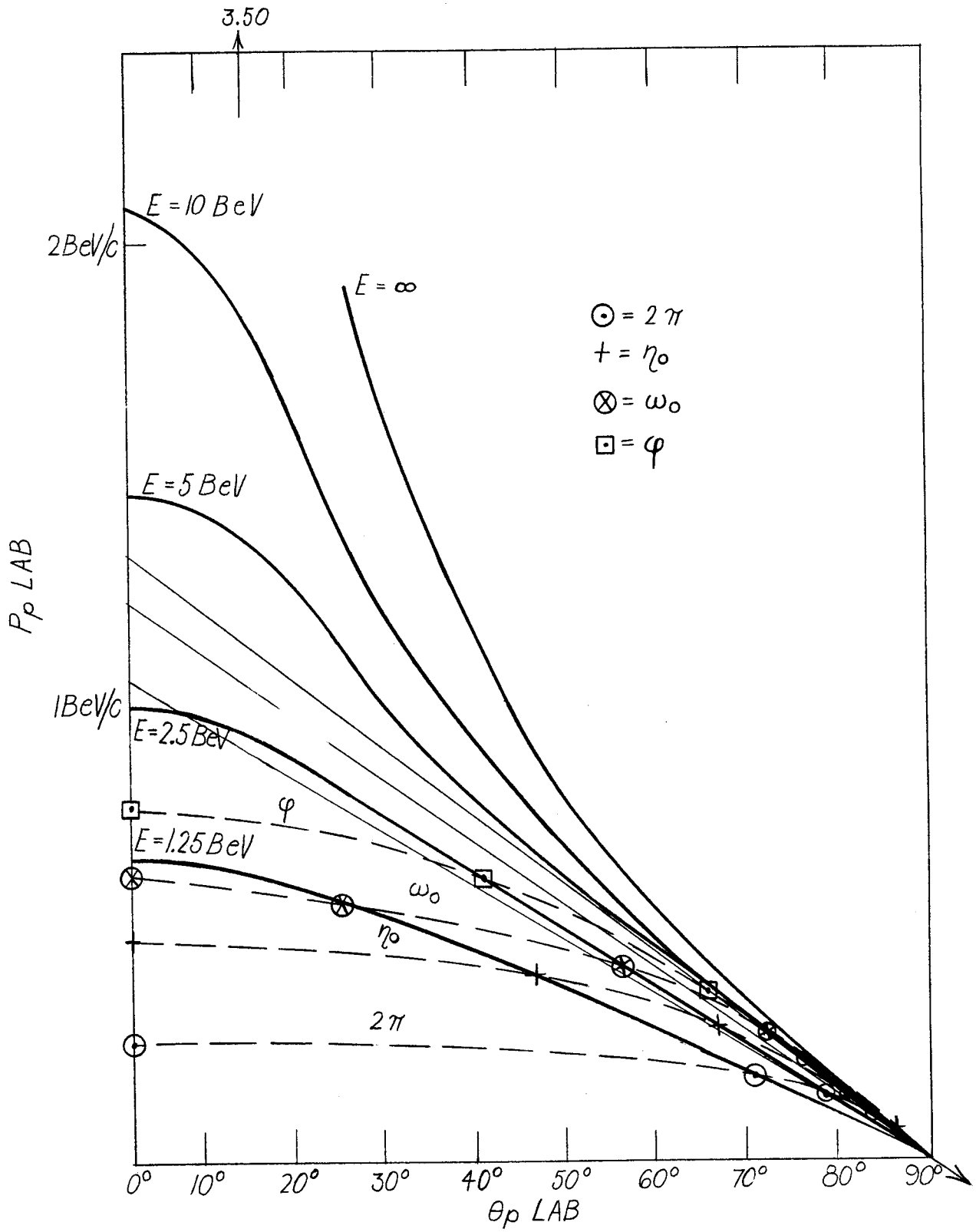
3.50
E = 10 BeV
2BeV/c
E = ∞
⊙ = 2π
+ = η₀
⊗ = ω₀
⊡ = φ
E = 5 BeV
P₀ LAB
1BeV/c
E = 2.5 BeV
φ
E = 1.25 BeV
ω₀
η₀
2π
0°
10°
20°
30°
40°
50°
60°
70°
80°
90°
θp LAB

FIG. 2

Returning to the maximum angle condition, we now calculate the locus of points of fixed mass when one varies the energy E. The corresponding angles are calculated through the expression

$$\cos^2\theta = \frac{m^2(4M^2 - m^2) + 4EMm^2}{4E^2M^2} \qquad (5)$$

and then the momentum P is determined from Eq. (3).

The points are calculated for the masses m = 0.276, 0.548, 0.782, and 1.020 BeV, corresponding to the systems $2\pi^o$, η_o, ω_o, and φ_o. The angles we find are

m(BeV)	E(BeV)			
	1.25	2.5	5	10
0.276	$70^o5'$	$77^o56'$	$82^o7'$	$84^o39'$
0.548	$49^o3'$	$65^o44'$	$74^o7'$	$79^o22'$
0.782	24^o	$54^o37'$	$67^o26'$	$74^o48'$
1.020		$42^o6'$	$60^o18'$	$70^o5'$

These points are indicated on Fig. 2 and are joined by curves that decrease continuously from a maximum at $\theta_p = 0^o$, given by the threshold condition

$$P = (m^2 + 2mM)/2(m + M)$$

to 0 for $\theta_p = 90^o$.

C. Calculation of Enhancement of Cross Section

The maximum angle, examples of which are given in Fig. 1, is chosen and it is supposed that $d\sigma/d\Omega^*$ is known at the energy E. The counting rate in the band $\Delta\theta$ needs to be computed about this angle (Fig. 3).

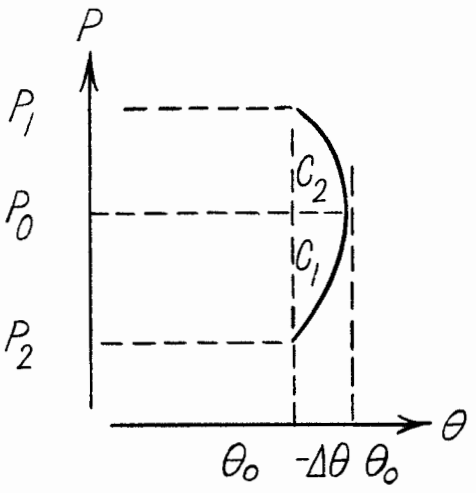

FIG. 3

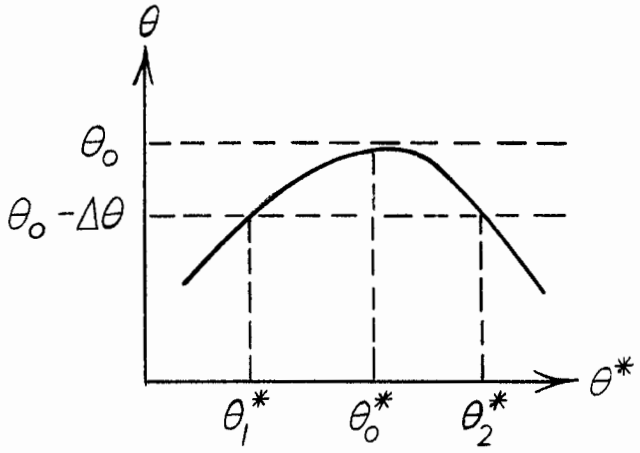

FIG. 4

The counting rate will be given by

$$\Delta\sigma = \int_{\theta_o - \Delta\theta(C_1)}^{\theta_o} \left(\frac{d\sigma}{d\Omega^*}\right)\left(\frac{d\Omega^*}{d\Omega}\right) d\Omega + \int_{\theta_o(C_2)}^{\theta_o - \Delta\theta} \frac{d\sigma}{d\Omega^*}\left(\frac{d\Omega^*}{d\Omega}\right) d\Omega \qquad (6)$$

Now consider the relation giving θ as a function of θ^* (Fig. 4). We can write

$$\Delta\sigma = \int_{\theta_1^*}^{\theta_2^*} \frac{d\sigma}{d\Omega^*}\, d\Omega^* \approx \left(\frac{d\sigma}{d\Omega^*}\right)_{\theta_o^*} \Delta\Omega^*$$

where

$$\Delta\Omega^* = \int\int_{\theta_1^*}^{\theta_2^*} \sin\theta^*\, d\theta^*\, d\varphi^* \approx \Delta\varphi^* \sin\theta_o^* \,(\theta_2^* - \theta_1^*)$$

Here $\Delta\theta$ is given and $\theta_2^* - \theta_1^*$ must be calculated as a function of $\Delta\theta$. We can write

$$-\Delta\theta = \frac{\left(\Delta\theta_o^*\right)^2}{2}\left(\frac{d^2\theta}{d\theta^{*2}}\right)_{\theta_o^*}$$

where $2\Delta\theta_o^* = \theta_2^* - \theta_1^*$. Thus

$$-\Delta\theta = \frac{\left(\theta_2^* - \theta_1^*\right)^2}{8}\left(\frac{d^2\theta}{d\theta^{*2}}\right)_{\theta_o^*}$$

and we have

$$\Delta\Omega^* = 2\Delta\varphi\sqrt{\Delta\theta}\sqrt{\frac{2\eta M^2 \sin\theta_o^*}{P^* E_p^*}} \qquad (7)$$

The quantity $\left(\frac{d^2\theta}{d\theta^{*2}}\right)_{\theta_o^*}$ is most easily obtained by differentiation of the relation

$$\tan\theta = \frac{P^* \sin\theta^*}{\gamma P^* \cos\theta^* + \eta E^*}$$

and application of the maximum angle condition

$$\cos\theta^* = -\frac{\gamma}{\eta}\frac{P^*}{E_p^*}$$

Equation 7 gives the solid angle corresponding to the maximum angle case. A typical value of $E = 5$ BeV, $m = 0.548$ BeV is $\Delta\Omega^* = 0.832\ \Delta\varphi\sqrt{\Delta\theta}$.

This can now be compared with two other sets of experimental conditions.

(1) We remain interested in the two-body kinematics but at an angle other than the maximum angle. Then $\Delta\Omega'^{*} = k\Delta\Omega$ where k is a kinematical factor of order unity. Considering the same $\Delta\theta$, $\Delta\Phi$ and ΔP as in the previous case,

$$\Delta\Omega'^{*} = k \sin\theta\, \Delta\theta\Delta\Phi = k'\Delta\theta\Delta\Phi$$

Thus the ratio to the maximum angle case is

$$\frac{\Delta\Omega'^{*}}{\Delta\Omega^{*}} = k'' \sqrt{\Delta\theta} \tag{8}$$

This shows that the choice of the maximum angle leads to an enhancement for the two-body kinematics over other angles of $\sqrt{\Delta\theta}$, so that if $\Delta\theta = 0.01$ the enhancement is by a factor of ten.

(2) The next concern is the ratio to the background, i.e., multibody kinematics. The cross section now involves an integration over the whole phase space; thus,

$$\Delta\sigma'' = \iiint \frac{d^2\sigma}{d\Omega^{*}dP}\, d\Omega^{*}dP \approx \frac{d^2\sigma}{d\Omega^{*}dP}\, \Delta\Omega''^{*}\Delta P \tag{9}$$

Because we want a comparison with the maximum angle case, we do not specify the cross section but rather write the ratio

$$\frac{\Delta\sigma''}{\Delta\sigma} \propto \frac{\Delta\Omega''^{*}}{\Delta\Omega}\, \Delta P \tag{10}$$

Here $\Delta\Omega''^{*}$ is of the same order of magnitude as $\Delta\Omega'^{*}$, but ΔP is the same as the maximum angle case, that is, $P_1 - P_2$, so that $\Delta P \approx \sqrt{\Delta\theta}$. Then the

ratio of Eq. (10) is $\Delta\theta$, and for $\Delta\theta = 0.01$ the enhancement factor is about 100 times.

D. Resolution

An interesting question now is to know what resolution in mass m can be obtained by variation of one of the parameters of the particular kinematical situation under consideration. Suppose that for fixed momentum the angle is increased by $\Delta\theta$, leaving the maximum angle condition (see Fig. 5).

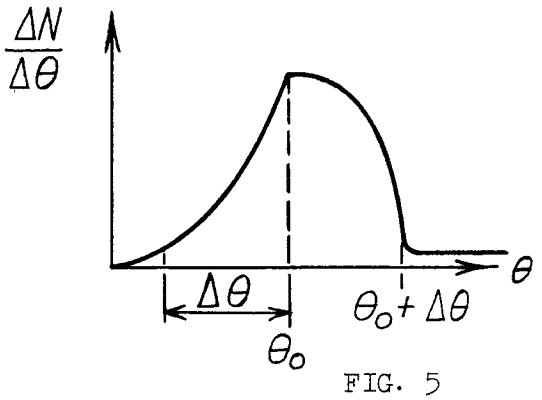

FIG. 5

It should be determined what mass Δm can be resolved with a certain angular resolution $\Delta\theta$. By calculating $dm/d\theta$ along the curve of Eq. (3) which gives the points of maximum angle for fixed E, it is found that

$$\frac{dm}{d\theta} = \frac{E^2M^2 \sin 2\theta}{m(m^2 - 2EM - 2M^2)} \tag{11}$$

(This is easily done by eliminating P^* from Eqs. (1) and (2) and differentiating.) As an example, for $E = 5$ BeV, $m = 0.548$ BeV, and $\Delta\theta = 0.01$ radians, it is seen that $\Delta m = 19.3$ MeV. This is evident again in Table I, which gives for $E = 5$ BeV the maximum proton recoil angles when multipion systems are formed (the mass difference $\pi^{\pm}$, π^{o} has been ignored), from which there exists a dispersion of about 4^{o} per pion mass.

TABLE I

Number of Pions	Mass (BeV)	Threshold (BeV)	Maximum Angle (θ_p^*)
1	0.135	0.145	$85^\circ 54'$
2	0.280	0.321	$81^\circ 54'$
3	0.415	0.507	$77^\circ 25'$
4	0.560	0.727	$73^\circ 44'$
5	0.695	0.954	$69^\circ 33'$

Another possible arrangement is to fix the angle θ and sweep E and P in such a way that the maximum angle condition is always fulfilled, thus exploring the mass spectrum as a function of energy. The momentum is given as a function of E by

$$P = \frac{EM \cos\theta}{\sqrt{(M+E)^2 - E^2\cos^2\theta}} \tag{12}$$

P starts from 0 at $E = 0$ (Fig. 6) with the slope $(dP/dE)_{E=0} = \cos\theta$, and increases continuously to reach the asymptotic value $M \cot\theta$. One then inquires what Δm can be separated with a spread ΔE of the incoming photon beam. Along the curve,

$$\frac{dm}{dE} = \frac{M}{m}\,\frac{2ME\cos^2\theta - m^2}{2M^2 + 2ME - m^2} \tag{13}$$

Using the previous example of $E = 5$ BeV, $m = 0.548$ BeV, and $\Delta E = 100$ MeV, it is found that $\Delta m = 6.1$ MeV.

In general, working at the maximum angle and accepting a large spread ΔE, there will be contributions of other masses m' formed by other energies E' in the band considered, but these masses will no longer fulfill the maximum angle condition (see Fig. 7).

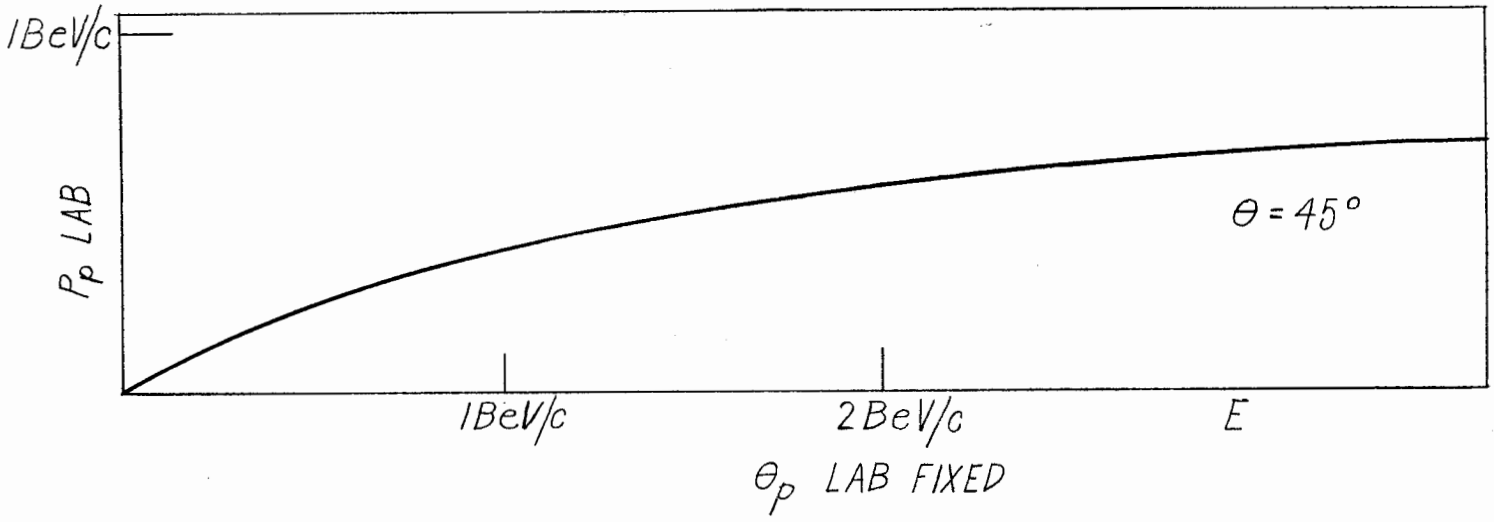

FIG. 6

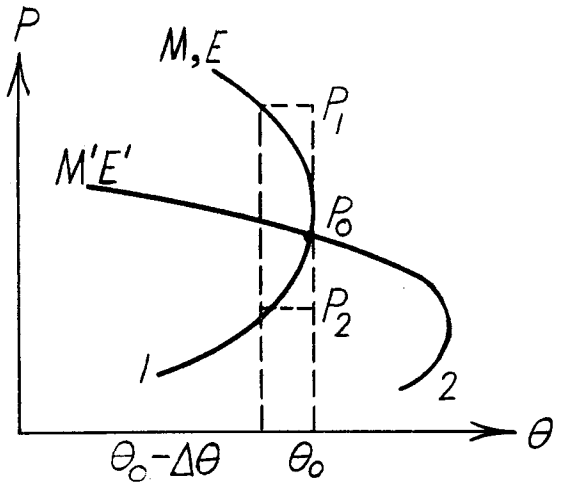

FIG. 7

This is not serious because of the enhancement ratio $\frac{\Delta\sigma'}{\Delta\sigma}$ discussed above. If θ, E and ΔE are fixed and P is varied, then the cross section as a function of P will have the different shapes of Fig. 8, where one notices that

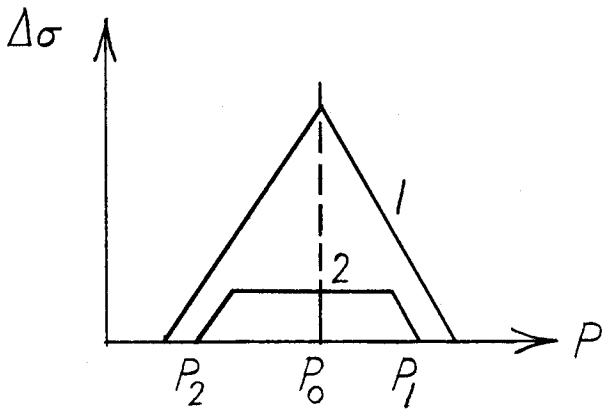

FIG. 8

for the second case (marked 2 in Figs. 7 and 8) we are working in "flat top" conditions unlike the maximum angle case one.

Finally, one asks what the variation of detected mass is when P and θ are fixed and E is varied. However, for the central mass

there is again an enhancement factor, while other masses will be of the second case considered.

$$\frac{dm}{dE} = \frac{4E_p^* \frac{M^2}{\mu^2}\left(\eta M^2+\eta P_p^2 \sin^2\theta - P_p E_p^* \cos\theta\right) - \left(\eta P_p \cos\theta - E_p^*\right) M\left[1-\left(\frac{M^2-m^2}{\mu^2}\right)^2\right]}{2m\left(1+\frac{M^2-m^2}{\mu^2}\right)\left(\eta P_p \cos\theta - E_p^*\right)}$$

E. Cross Sections and Backgrounds

As yet there is not much information on which to draw to make a useful extrapolation to the situation envisaged above. The most acute problem is that of the production of multipion final states. From comparison of Table I and Fig. 1, it is clear that for the η_o two-body final state the > 4 pion mass states can be discriminated against by the maximum angle effect alone. Phase space calculations and the statistical model may clarify the situation further. One experimental effect concerns the inelasticity, K, which is the ratio

$$\frac{\text{CMS energy used to produce new particles}}{\text{Original CMS kinetic energy}}$$

and which has values between $0.2 < K < 0.5$ generally for strong interactions. For a 5 BeV photon incident on a proton, $\mu = 3.2$ BeV; specifying to the particular state of one proton plus pions, $Q = 2.26$ BeV. With $K = 0.2$ there are then approximately 3.2 pions produced, and against these we do not entirely discriminate. However, a condition on P_p^* is also imposed by the use of the kinematics, and this may alter the phase space conditions.

First evaluate the case of production of $N = n + s$ final particles with n pions and s nucleons. The relative probability of this state can be calculated from the formulas of Milburn,[11] at least to orient

our ideas. The relative probability of this state is

$$S(n,s) = \frac{\Omega^{N-1}}{(2\pi\hbar)^{3(N-1)}} \sum \frac{d}{dW} \int_W \sum_{i=1}^{N} d^3p_i$$

where the integral is the volume of the $3(N-1)$ dimensional momentum space. The sum is taken over spin and isospin states, but that complication is ignored for these simple considerations. In the approximation where the nucleons are considered non-relativistic and the pions extremely relativistic, the phase space integral can be evaluated and yields

$$\left(\frac{dV}{dW}\right)_{approx} = \left[\frac{M^{3s/2}\ (2\pi)^{3/2(s-1)}}{(sM)^{3/2}}\right] \left[2^{3n}\ F^n\right] \times \frac{\left[W - sM - n\mu\right]^{3s/2+3n-5/2}}{\Gamma\left[3/2(s-1) + 3n\right]}$$

The statistical model of Fermi adds the extra condition that this phase volume for the final state be matched to that of the particles in statistical equilibrium inside a volume

$$\Omega = \left(\frac{2M}{W}\right)\frac{4}{3}\pi R^3$$

where $R = \hbar/\mu c = 1.4 \times 10^{-13}$ cm, i.e., is the volume of the pion cloud of a nucleon contracted by the Lorentz factor $\left(\frac{2M}{W}\right)$.

These expressions have been evaluated for 5 GeV photons incident on protons both with and without the statistical model factor, with the condition of one proton in the final state.

To come a little closer to the envisaged experimental conditions, the same problem is evaluated by Lepore and Stuart's method,[12] but with the extra condition that the center of mass momentum of the proton be that which it has for η^o production at $E = 5$ BeV. The phase space

factor is then

$$\frac{dV(E_t^*,p_t^*)}{dE_t^*} = \frac{\pi^{N-1}}{2^{N-2}} \times \frac{(E_t^{*2}-p_t^{*2})^{N-2}}{p_t^*} \times \sum_{i=1}^{N} C_i^N \frac{(E_t^*-p_t^*)^i (E_t^*+p_t^*)^{N-i}}{(N+i-2)!(2N-i-2)!} \left[\frac{E_t^*+p_t^*}{2N-i-1} - \frac{E_t^*-p_t^*}{N+i-1}\right]$$

The results thus obtained are given in Fig. 9. They indicate that the extra condition on the phase space integral imposed by two-body kinetics tends to push the contribution to the background from multipion systems to systems of higher orders.

The Fermi statistical model enhances this effect even more, but it is known to give poor comparison with other high energy data. However, it encourages us to believe that the maximum angle technique will be viable. The cross section for producing this background is not known, but one can guess at something of the order of α times the total π-p cross section, i.e., $30 \times \frac{1}{137}$ mbarns or 220 μbarns.

The total two-body cross sections can only be guessed at. It is known that at $\approx$ 1 BeV energies the ratio of photoproduction of π^o to η^o is about 8, while a ratio of 11 is found for the ratio of elastic $\pi^- + p$ cross sections to the η^o production cross section. Thus, if this ratio persists, η events might be expected to turn up 1/10 as often as π two-body events. This is the ratio expected from unitary symmetry models. Unitary symmetry also suggests[13] a way to calculate one partial cross section for η^o production, inasmuch as the ratio

$$\frac{\Gamma(\eta^o \to 2\gamma)}{\Gamma(\pi^o \to 2\gamma)} = \frac{1}{3}\left[\frac{M_\eta}{M_\pi}\right]^3$$

This leads to a lifetime for this decay of $\tau = 4.7 \times 10^{-18}$ sec. The branching ratios of η decay are

$$(3\pi^o) + (\pi^o\gamma\gamma) \approx (40 \pm 14)\%$$

$$(\gamma\gamma) \approx (31 \pm 11)\%$$

$$(\pi^+\pi^-\pi^o) \approx (23 \pm 4)\%$$

$$(\pi^+\pi^-\gamma) \approx (6 \pm 2)\%$$

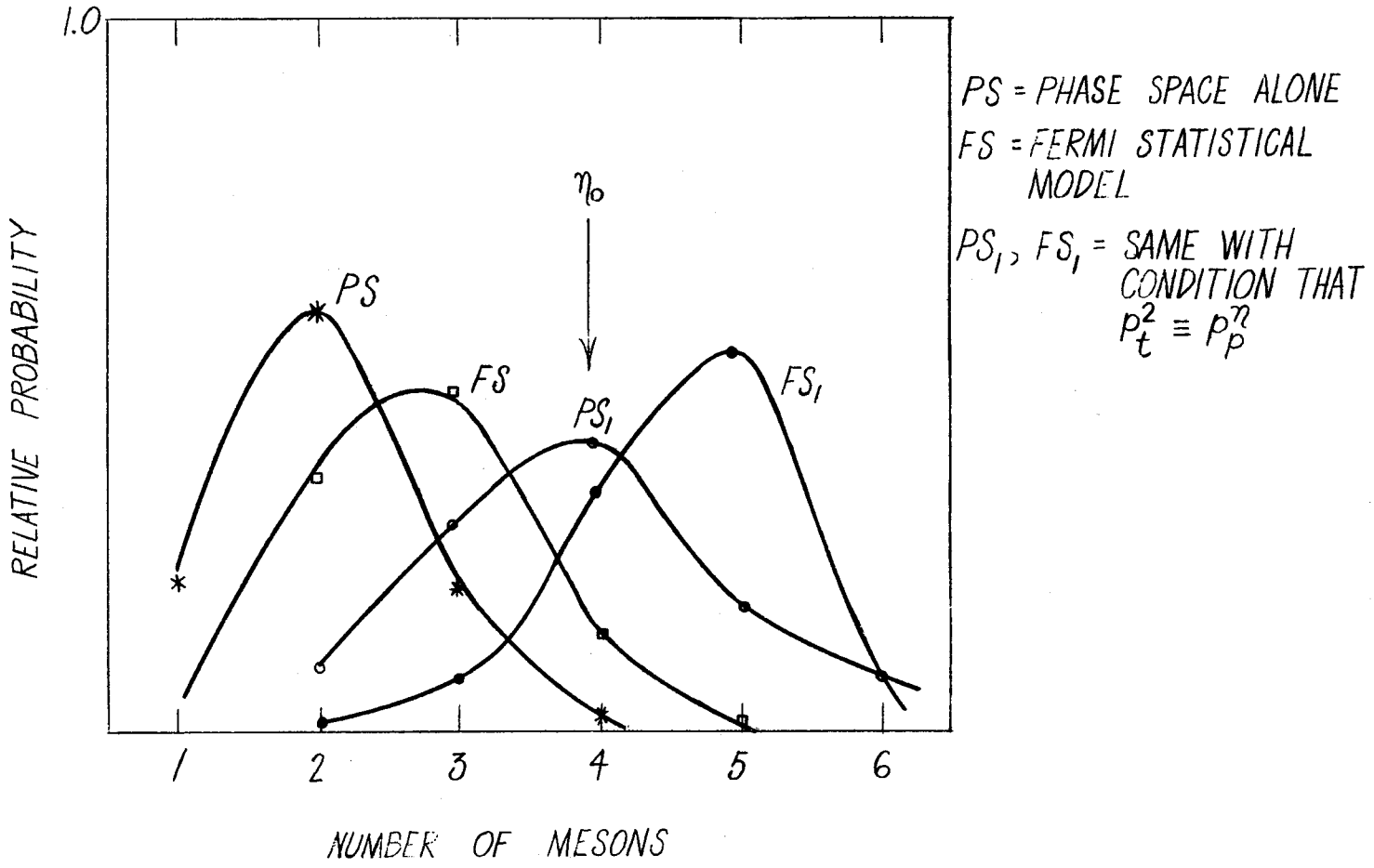

FIG. 9

SLAC-25-E
Bishop

The partial cross section for producing the η^o by the Primakoff diagram

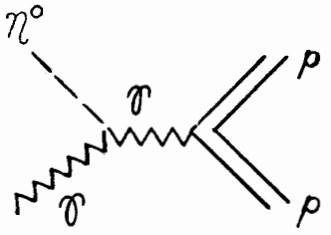

is

$$\frac{d\sigma}{d\Omega} = \frac{8Z^2e^2}{M_\eta^3 \tau} \frac{\beta^3 F^2(q^2) \sin^2 \theta}{(1 + \beta^2 - 2\beta \cos \theta)^2}$$

For 5 BeV photons incident on protons, this leads to a sharply peaked (at $\approx 1^o$) cross section of $Z^2F^2(q^2) \times 3.84 \times 10^{-32}$ cm^2/ster with a momentum transfer of $q \approx 100$ MeV/c. Thus on a proton a maximum cross section of about 3.5×10^{-32} cm^2/ster can be expected, but only for conditions under which the recoil proton will have very little energy. (From Fig. 1 the maximum laboratory angle for the proton corresponds to $\theta^* = 10^o$.) The measured cross section at $\theta^* = 106^o$ and 1 BeV is 24×10^{-32} cm^2/ster.

For ω^o production the cross section is finite at 0^o because the spin mismatch responsible for the $\sin^2 \theta$ term in the η case is absent. An estimation by Berman of this cross section for the one pion exchange

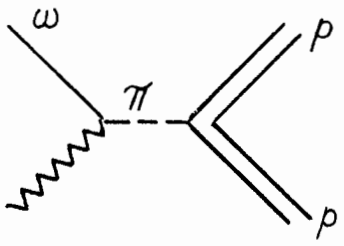

is $\frac{d\sigma}{d\Omega}(0^\circ) = 15$ μbarns. Now the pole at 5 BeV incident energy is at $\cos\theta^* = 1.032$, while $\cos\theta^* = 0.966$ for the maximum angle condition of Fig. 1, so that as long as the cross section does not perform any weird oscillations, this order of magnitude can be expected for the partial two-body cross section. Other partial cross sections should be present as well, but this one-pion exchange cross section should exist because there is evidence now from $\gamma + p = p + \pi^0$ that the ω exchange diagram is dominating the situation.

F. Apparatus

A liquid hydrogen target of radius determined by the half-aperture of the photon beam and the supportable multiple scattering of the outgoing protons would be used. A collimation of the beam to mc^2/E should allow good monochromation of the beam. Even for $E = 1.25$ BeV this is 4×10^{-4} radians, so if a collimation distance of 25 meters is chosen, the radius of the target is 1 cm. In order to detect the recoil proton for η^0 production, it may be necessary to descend to $p = 220$ MeV/c for $E = 5$ BeV. The multiple scattering angle is then $\Delta\theta = 1.5 \times 10^{-2}$ radians. The protons will be analyzed with a spectrometer; much useful work might be done with a maximum momentum of 1 BeV/c, for which a radius of 220 cm at 15 kG would be adequate, with a pole gap of 3 to 4 cm. This is a very compact magnet and in fact much higher fields would be obtainable. A Buechner type magnet with radial focusing over a 30 percent momentum band and a ladder counter detector would constitute a good apparatus for the experiment, and the small gap means that the magnet offers a good shield by itself. Of course it would be advantageous to keep the cylindrical symmetry of the experiment, which may be possible one day with an arrangement of superconducting current sheets (suggested by K. Brown). Using a 4-cm-long target with $\Delta\theta = 0.01$, $\Delta\varphi = 0.05$, $E = 5$ BeV and the maximum angle conditions for ω^0 production, we have

$$\Delta\Omega^* \approx 5 \times 10^{-3}$$

This, combined with Berman's estimate of the OPE cross section, gives a counting rate of $N = 1.3 \times 10^{-8} N_o$, where for $N_o = 10^7$ photons/second

we obtain $N = 0.1$ counts/second.

Each momentum interval is defined by two counters, a dE/dx and a total energy proton counter, in coincidence to give directionality. For 300 MeV/c protons the differential ionization density is seven times the minimum value. By biasing the counters good discrimination should be possible against a background of minimum ionizing particles. Suppose that 10^3 of such particles accompany each proton, and the accelerator pulse is 2 μsec while the detector resolving time is 2 nanoseconds the probability of simulating a proton pulse then is, from Poisson statistics, 7.3×10^{-5} at the 7-particle level, 5.1×10^{-4} at the 6-particle level, and 3.1×10^{-3} at the 5-particle level. The situation is better for the E-counter if this is arranged just to stop the protons; as a proton with 45 MeV kinetic energy is stopped by 2 gm/cm^2 of carbon (in which minimum ionizing particles lose 3.9 MeV), a pile-up of 11 pulses is needed to simulate the proton. Of course, the coincidence gives only directionality; it does not help the pile-up problem because the same particles traverse both counters.

The number of recoil protons produced by scattering of pair-produced electrons turns out to be a factor of at least 10^4 times less than the above estimate of the expected counting rate.

As choice of method for producing the photon beam, the crystal coherent bremsstrahlung process has some advantages at least for a spectrometer momentum of 300 MeV/c. This can be estimated in the general way discussed by DeWire.[2] He considers the case of background of electromagnetic origin for a spectrometer experiment, using first generation pairs with a spectrum proportional to k^{-1}. Other types of background may be produced with powers of k different from -1; thus, his formulas for secondary spectra produced with energy dependences k^n have been re-evaluated with $n = +1, 0, -1, -2, -3$. For 6 BeV photons produced by 20 BeV electrons incident on a diamond, this gives the expressions of Table II. Here C_B and C_R are the background and real counting rates if normal bremsstrahlung spectrum is used with maximum energy near the desired photon energy, and C_B', C_R' refer to the same quantities for the coherent bremsstrahlung case.

TABLE II

Power of k	Process	C_B/C_R	C_B'/C_R'
k		$B/R\left[1 - X_{min}\right]$	$B/R\left[0.069 - \frac{1}{2} X_{min}^2\right]$
k^0	π production	$B/R \log\left(\frac{1}{X_{min}}\right)$	$B/R\left[\left(0.3 - X_{min}\right) + 0.055\right]$
k^{-1}	Pair production	$B/R\left(1/X_{min}^{-1}\right)$	$B/R\left[\log_e \frac{0.3}{X_{min}} + 0.13\right]$
k^{-2}	Showers	$B/R\ \frac{1}{2}\left(1/X_{min}^2 - 1\right)$	$B/R\left[1/X_{min} - 3\right]$
k^{-3}	Pair followed by nucleon scattering	$B/R \times \frac{1}{3}\left[\frac{1}{X_{min}^3} - 1\right]$	$B/R\left[\frac{1}{2}\left(\frac{1}{X_{min}^2} - 11.1\right) + 0.89\right]$

This uses DeWire's notation in which $X_{min} = q/6$ (where q is the selected momentum in BeV/c) for normal bremsstrahlung, and $q/20$ for coherent bremsstrahlung.

We then evaluate these expressions with $q = 0.3$ and $q = 1$, with the following results.

TABLE III

Power of k	q = 0.3 BeV/c		q = 1 BeV/c	
	Normal Brem.	Coherent Brem.	Normal Brem.	Coherent Brem.
k	0.95	0.069	0.833	0.068
k^0	3.0	0.34	1.792	0.304
k^{-1}	19.0	3.13	5.0	1.92
k^{-2}	200.	64.	17.5	17.0
k^{-3}	2667.	2216.	72.	195.

We see that the coherent case presents some advantage at $q = 0.3$, decreasing as the energy dependence is more concentrated at lower photon energies.

G. Other Two-body Final States

Neutron emission with two-body kinetics is also present from reactions such as

$$\gamma + p \rightarrow \rho^+ + n$$

but as the ρ-width is about 100 MeV, the neutrons will be emitted over an angular range of about 4°. For incident photons of 8 GeV, the maximum angle is 73° and the neutron has a laboratory momentum of 250 MeV/c. This corresponds to a time-of-flight of 130 nanoseconds over a 10-meter path, so that reasonable resolution could be obtained with a modulated photon beam. The time-of-flight technique could produce a considerable reduction in background counts due to neutrons, but a sweep magnet would be needed to eliminate charged secondaries.

For the reaction

$$\gamma + p \rightarrow \Lambda^\circ + K^+$$

at 10 GeV, the maximum laboratory angle for the Λ° is $53^\circ 36'$ when it has a momentum of 0.72 BeV/c and travels about 5 cm on the average before decaying. The decay protons from the Λ° are concentrated in a cone of half angle $9^\circ 48'$ due to the recoil motion, and with momenta distributed from 0.735 to 0.489 BeV/c. The distance of 5 cm unfortunately does not seem enough to allow a reasonable collimation followed by detection of the decay proton with a spectrometer.

If any success at all is met with the maximum angle technique, it might be applied also to the coherent production of neutral particles from deuterium in reactions such as

$$\gamma + d \rightarrow \eta^\circ + d$$

In the impulse approximation the cross section would be

$$\frac{d\sigma_d}{d\Omega} = \left\{ \frac{2}{3}\left(K_n + K_p\right)^2 + \left(L_n + L_p\right)^2 \right\} F^2(q^2)$$

when the amplitudes of photoproduction on neutron and proton are

$$\vec{K}_n \cdot \vec{\sigma} + L_n \qquad \text{and} \qquad \vec{K}_p \cdot \vec{\sigma} + L_p$$

with separation into spin dependent and spin independent parts. The form factor of the deuteron

$$F(q) = \int \exp\left(\frac{i}{2}\vec{q} \cdot \Gamma\right) \psi^2(D)\, d\tau = \frac{2\alpha}{1 - \alpha P_t}\left[\frac{1}{q}\tan^{-1}\frac{q}{2\alpha} - \frac{1}{2}\rho_t\right]$$

where ρ_t = triplet effective range and $\alpha = \sqrt{M\epsilon}$.

By the maximum angle technique the coherent cross section can be measured for small angles $\theta_{\eta o}$ for which q is small and the deuteron form factor well known. The non-spin dependent part has an angular dependence proportional to $\sin^2 \theta_{\eta o}$, so it will be small for $\theta_{\eta o} \approx 0^o$. It is then seen that

$$\frac{d\sigma_d}{d\Omega} = \frac{2}{3}\left(K_n + K_p\right)^2 F^2(q^2)$$

or if

$$K_n = K_p \equiv K$$

then

$$\frac{d\sigma_d}{d\Omega} = \frac{8}{3} K^2 F^2(q^2)$$

The cross section for production from hydrogen is $\frac{d\sigma_P}{d\Omega} = K^2 + L^2$; thus, the ratio is

$$\frac{d\sigma_d}{d\Omega} \Bigg/ \frac{d\sigma_P}{d\Omega} = \frac{8}{3} F^2(q^2)$$

If this ratio is not observed, then $K_n \neq K_p$.

LIST OF REFERENCES

1. J. Cassels, Report No. M-200-4, Stanford Linear Accelerator Center, Stanford University, Stanford, California (1960).
2. J. W. DeWire, "Some aspects of the prospective experimental use of the Stanford two-mile accelerator," SLAC Report No. 5, Stanford Linear Accelerator Center, Stanford University, Stanford, California (Summer 1962).
3. R. F. Mozley, Internal Memorandum, Stanford Linear Accelerator Center, Stanford University, Stanford, California (1963).
4. R. Diebold, Phys. Rev. 130, 2096 (1963).
5. S. Minami, Nuovo Cimento 21, 401 (1961).
6. R. F. Stiening, E. Loh and M. Deutsch, Phys. Rev. Letters 10, 536 (1963).
7. M. Gell-Mann and K. Watson, Ann. Rev. Nucl. Sci. 4 (1954).
8. G. Trilling, "Some aspects of the prospective experimental use of the Stanford two-mile accelerator," SLAC Report No. 5, Stanford Linear Accelerator Center, Stanford University, Stanford, California (Summer 1962).
9. K. Alder, A. Bohr, T. Huus, B. Mottelson and A. Winther, Rev. Mod. Phys. 28, 432 (1956).
10. R. M. Sternheimer, Phys. Rev. 93, 642 (1954).
11. R. H. Milburn, Rev. Mod. Phys. 27, 1 (1955).
12. C. V. Lepore and R. N. Stuart, Phys. Rev. 94, 1724 (1954).
13. S. Okubo, Phys. Letters 4, 14 (1963).

ELASTIC e-p KINEMATICS FOR SLAC

by

C. de Vries

To facilitate considerations for electron-proton scattering experiments at SLAC energies, a simple IBM 7090 program has been written, which computes as a function of q^2 and θ (the four momentum transfer and angle of scattering in the lab) the following quantities:[1]

MOP = momentum of recoiling proton in lab system
KEP = kinetic energy of recoiling proton in lab system
EO = primary energy of the electron
EEL = scattered electron energy in the lab
EECM = scattered electron energy in the center-of-mass system
EPCM = total energy of the recoil proton in c.m. system
AECM = angle scattered electron in c.m. system (θ^*)
APL = angle recoiling proton in lab system (Φ)

The energies and momenta are given in BeV units.

In order to obtain estimates on counting rates, a model for the nucleon form factors has been used that gives a good fit to the presently known cross sections material from Stanford (see Section G of this report):

$$G_E^S = 0.5\left\{\frac{4.21}{1 + q^2/15.6} - \frac{4.32}{1 + q^2/26.6} + 1.11\right\}$$

$$G_E^V = 0.5\left\{\frac{1.29}{1 + q^2/8.6} - 0.29\right\}$$

$$G_M^S = 0.44\left\{\frac{5.86}{1 + q^2/15.6} - \frac{5.68}{1 + q^2/26.6} + 0.82\right\}$$

$$G_M^V = 2.353\left\{\frac{1.11}{1 + q^2/8.6} - 0.11\right\}$$

This model gives a χ^2 of 134 for 123 degrees of freedom.

[1]See for kinematic formulae: R. Herman and R. Hofstadter, High Energy Electron Scattering Tables (Stanford University Press, 1960).

From the model the following quantities have been calculated as a function of q^2 (QSQ in the notation of the program):

PCH = G_{ep} = charge form factor of the proton

PMAG = G_{mp} = magnetic form factor of the proton

whereas the computer output contains also the following quantities as a function of q^2 and θ (THETA):

SINS = Mott cross section = $\sigma_{NS} \times 10^{26}$ cm^2

$$GP = \frac{\left(\frac{d\sigma}{d\Omega}\right)_p}{\sigma_{NS}} = (1 + t)^{-1} G_{ep}^2 + t(1 + t)^{-1} G_{mp}^2 + 2t \tan^2\theta/2 \, G_{mp}^2$$

with $t = q^2/4M^2$

ROSE = $\left(\frac{d\sigma}{d\Omega}\right)_p \times 10^{26}$ cm^2 when detecting electrons

ROSP = $\left(\frac{d\sigma}{d\Omega}\right)_p \times 10^{26}$ cm^2 when detecting protons

RATIO = ROSE/ROSP

IRAT = 1/RATIO

RRATIO = RATIO per sin θ/sin Φ = $d\Phi/d\theta$

ERATE = counting rate electrons/sec per mster per g/cm^2 per 10 μA

PRATE = counting rate protons/sec per mster per g/cm^2 per 10 μA

All those quantities have been calculated for q^2 ranging from 25 to 1000 f^{-2} in steps of 25 and for θ ranging from 5 degrees to 175 degrees. Refinements can be made by changing the appropriate stepping cards in the program.

Some of the computed material has been plotted (see Figs. 1-7).*

*The numerical values in the tables agree with the form factor formula given above. The graphs are obtained using slightly different numbers of the parameters in an earlier stage of the work. Being a summer visitor, the author did not find time to remove this discrepancy. Moreover, the numbers are significant in a qualitative sense.

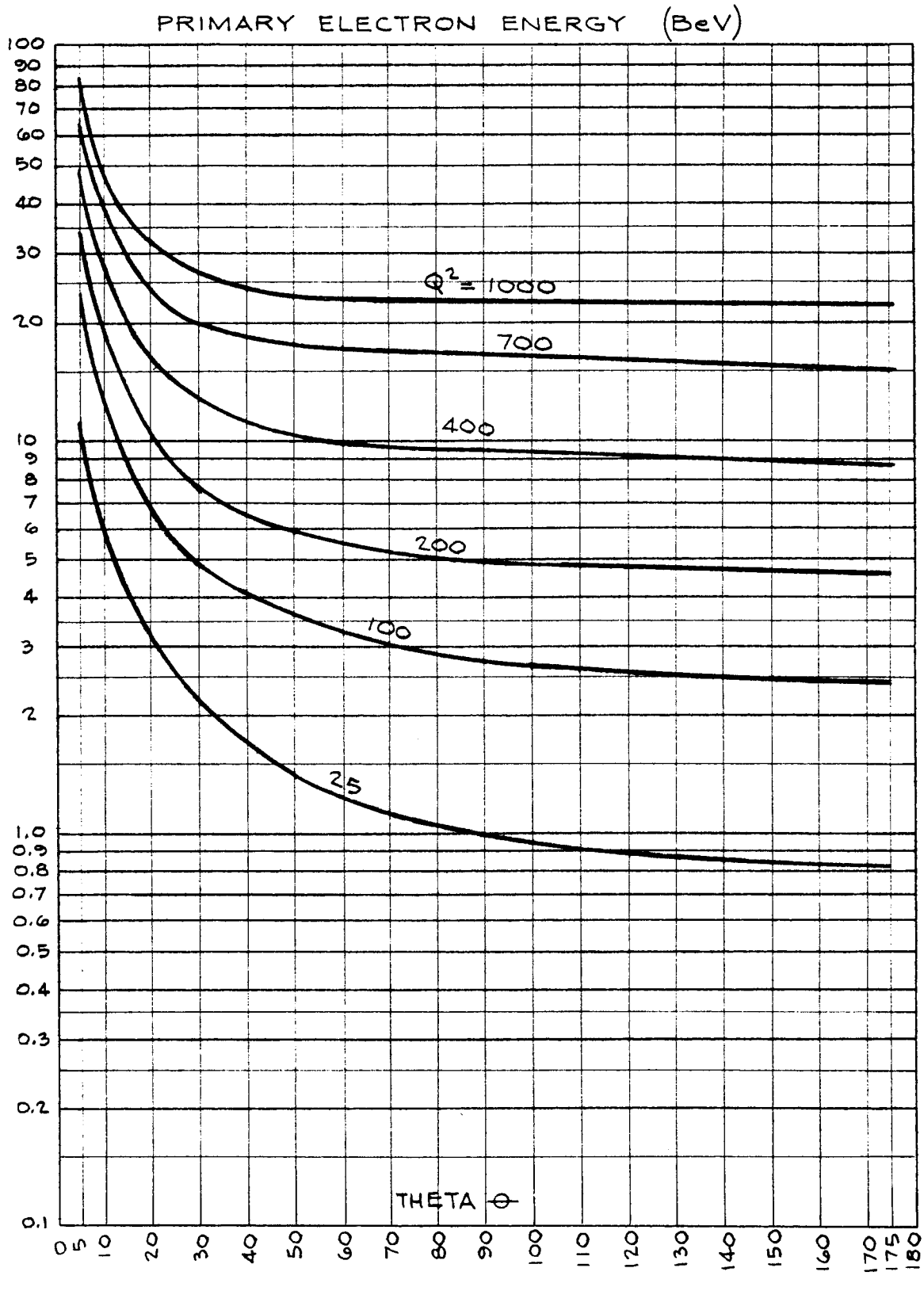
PRIMARY ELECTRON ENERGY (BeV)
100
90
80
70
60
50
40
30
20
10
9
8
7
6
5
4
3
2
1.0
0.9
0.8
0.7
0.6
0.5
0.4
0.3
0.2
0.1
Q^2 = 1000
700
400
200
100
25
THETA θ
0 5 10 20 30 40 50 60 70 80 90 100 110 120 130 140 150 160 170 175 180
Lab

FIG. 1

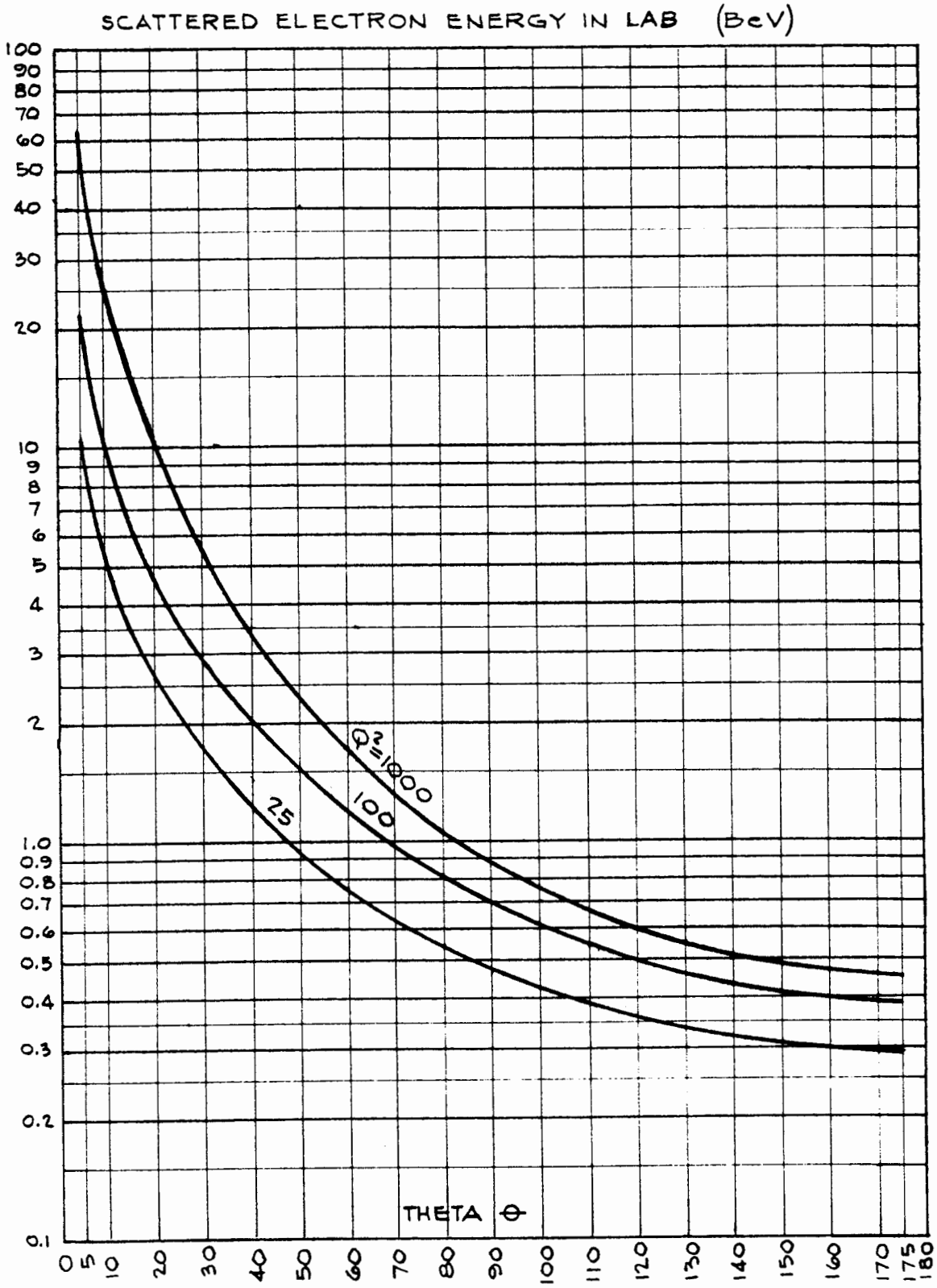
SCATTERED ELECTRON ENERGY IN LAB (BeV)
100
90
80
70
60
50
40
30
20
10
9
8
7
6
5
4
3
2
1.0
0.9
0.8
0.7
0.6
0.5
0.4
0.3
0.2
0.1
Q²=1000
100
25
THETA θ
0 5 10 20 30 40 50 60 70 80 90 100 110 120 130 140 150 160 170 175 180

FIG. 2

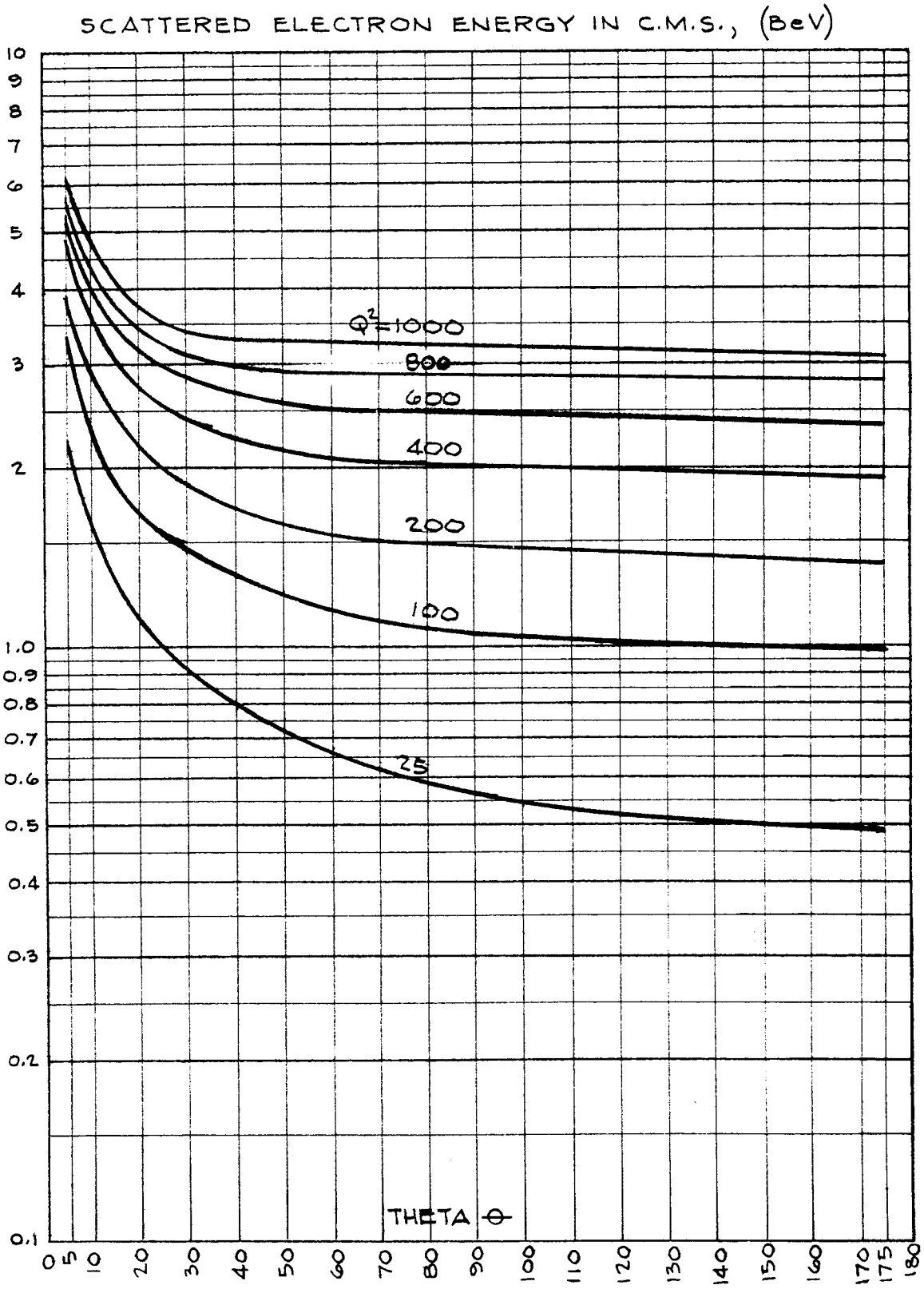
SCATTERED ELECTRON ENERGY IN C.M.S., (BeV)
10
9
8
7
6
5
4
3
2
1.0
0.9
0.8
0.7
0.6
0.5
0.4
0.3
0.2
0.1
Q^2=1000
800
600
400
200
100
25
THETA θ
0
5
10
20
30
40
50
60
70
80
90
100
110
120
130
140
150
160
170
175
180

FIG. 3

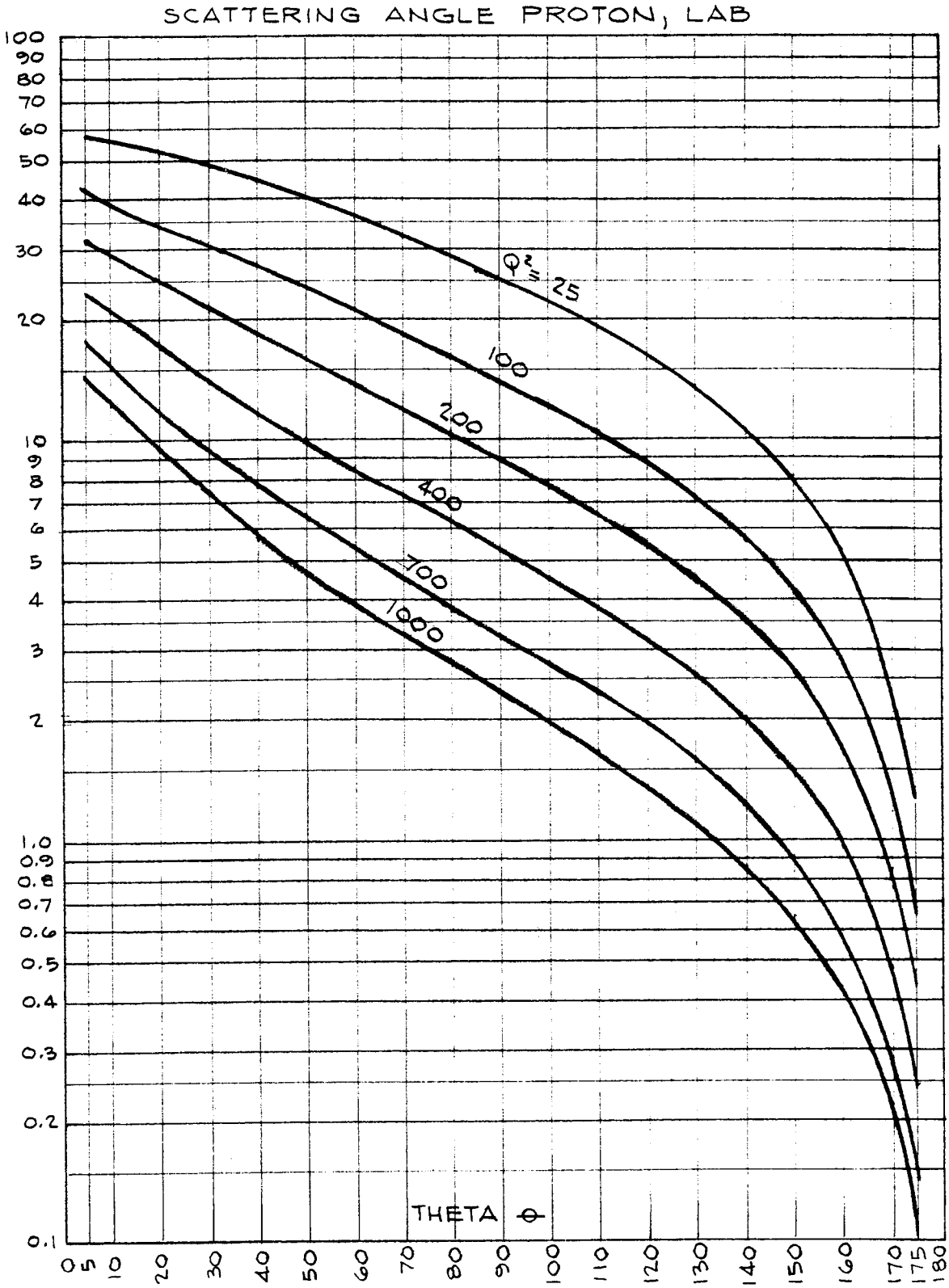
SCATTERING ANGLE PROTON, LAB
100
90
80
70
60
50
40
30
20
10
9
8
7
6
5
4
3
2
1.0
0.9
0.8
0.7
0.6
0.5
0.4
0.3
0.2
0.1
Q^2 = 25
100
200
400
700
1000
THETA ϕ
0
5
10
20
30
40
50
60
70
80
90
100
110
120
130
140
150
160
170
175
180

FIG. 4

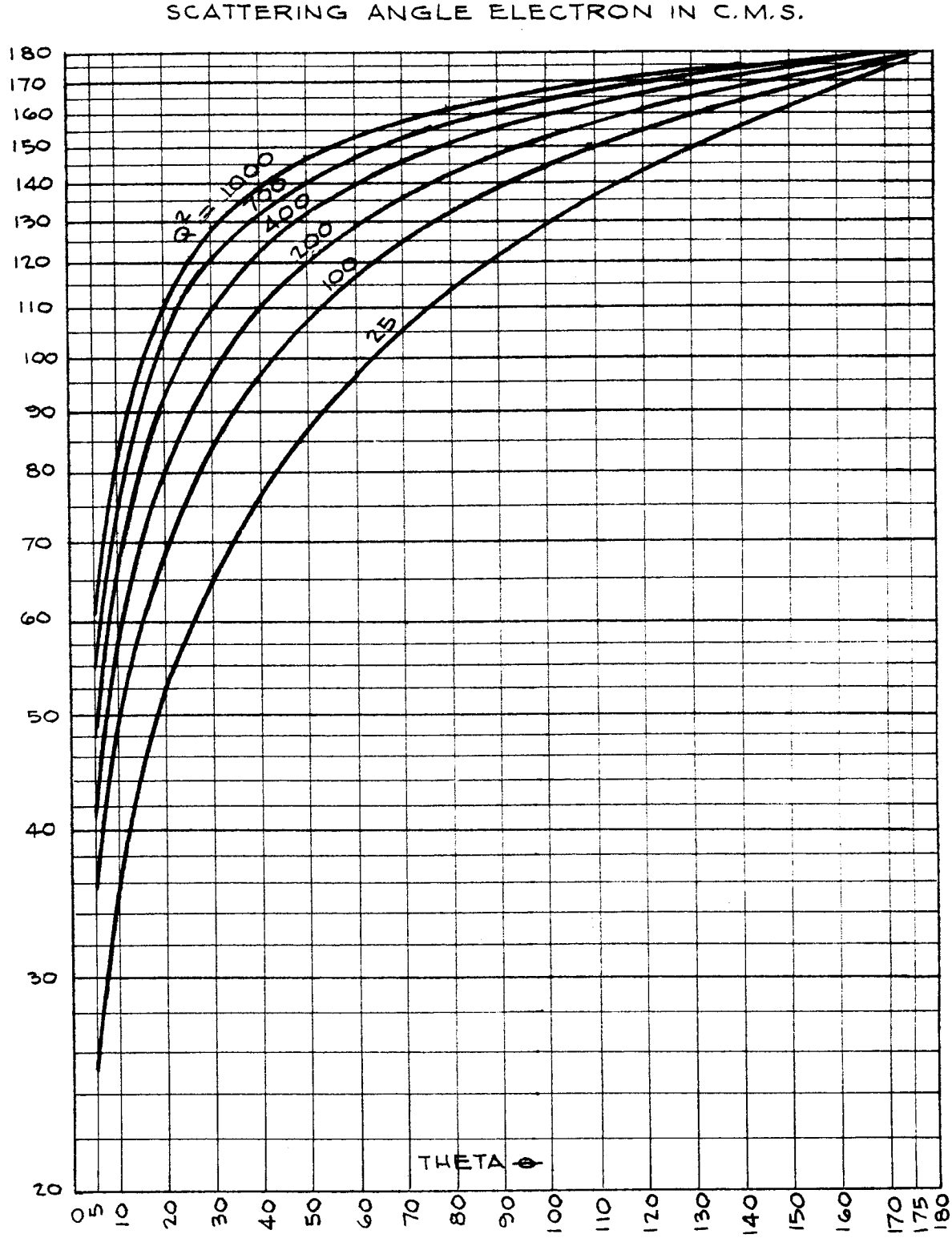
SCATTERING ANGLE ELECTRON IN C.M.S.
180
170
160
150
140
130
120
110
100
90
80
70
60
50
40
30
20
Q² = 1000
700
400
200
100
25
THETA
05
10
20
30
40
50
60
70
80
90
100
110
120
130
140
150
160
170
175
180

FIG. 5

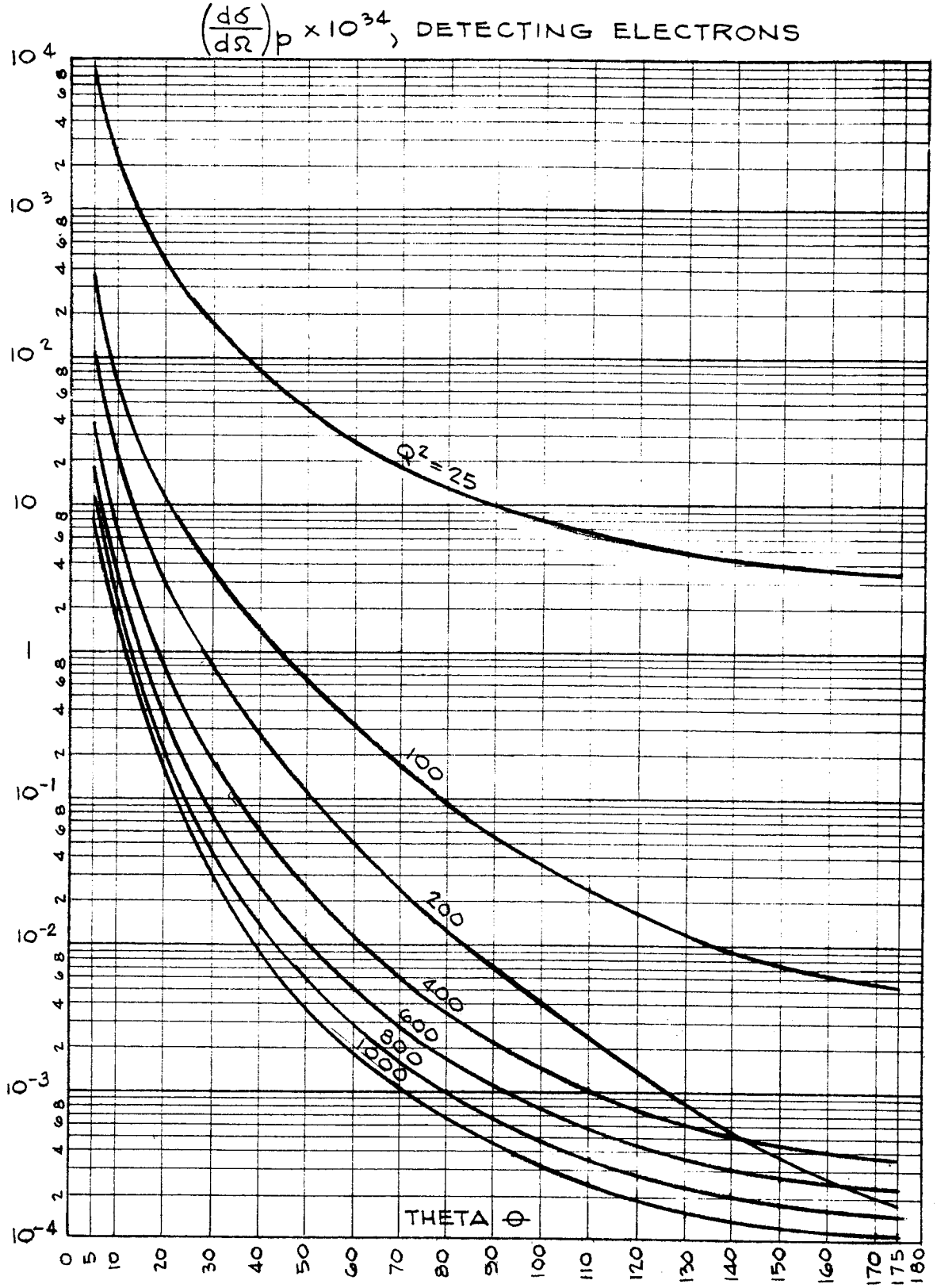
$\left(\frac{d\sigma}{d\Omega}\right)_p \times 10^{34}$, DETECTING ELECTRONS
10^4
10^3
10^2
10
1
10^{-1}
10^{-2}
10^{-3}
10^{-4}
$Q^2 = 25$
100
200
400
600
800
1000
THETA ϕ
0 5 10 20 30 40 50 60 70 80 90 100 110 120 130 140 150 160 170 175 180

FIG. 6

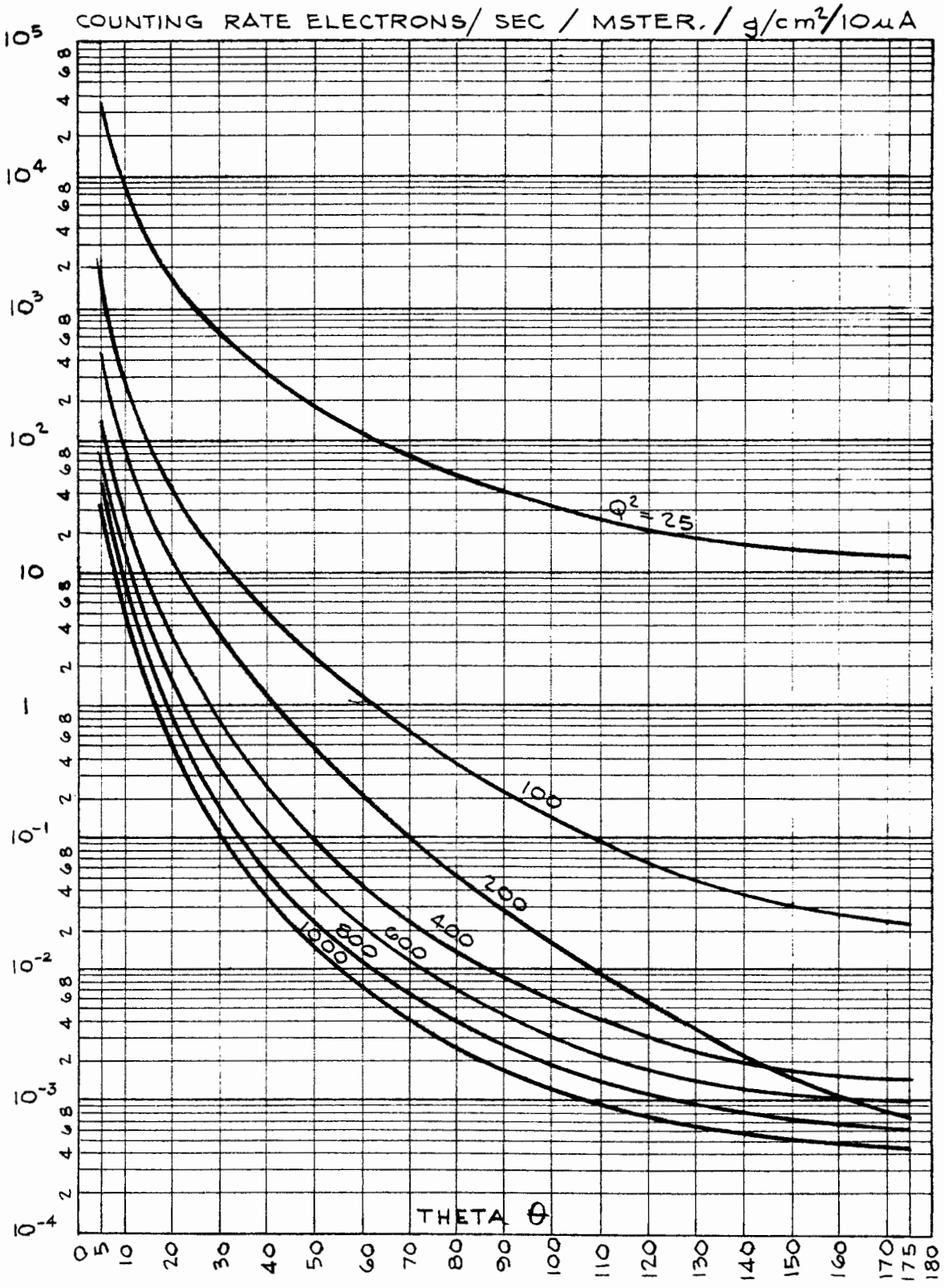
COUNTING RATE ELECTRONS/ SEC / MSTER. / g/cm²/10μA
10^5
10^4
10^3
10^2
10
1
10^{-1}
10^{-2}
10^{-3}
10^{-4}
2 4 6 8
$Q^2 = 25$
100
200
400
600
800
1500
THETA θ
0 5 10 20 30 40 50 60 70 80 90 100 110 120 130 140 150 160 170 175 180

FIG. 7

STATISTICAL FITS TO ELECTRON-PROTON AND ELECTRON-DEUTERON CROSS SECTIONS

by

C. de Vries

I. INTRODUCTION

At present several hundred cross sections for electron-proton and electron-deuteron scattering are known, which have been measured in laboratories at Stanford, Cornell, Orsay, and Harvard. It seems worthwhile to apply statistical methods to analyze these cross sections. Such methods have been employed by several authors to obtain fits to the electromagnetic form factor material derived from these cross sections. Fitting the raw cross section data, however, is to be preferred, because (a) the number of experimental points is much larger, and (b) smoothing procedures to obtain form factors are avoided.

The idea of the present paper is therefore to adopt a certain theoretical model for the isotopic form factors in order to derive theoretical cross sections (through the Rosenbluth and Durand formulae for electron-proton and electron-deuteron scattering, respectively). Those cross sections can then be compared point by point with the experimental data. The free parameters appearing in the model are adjusted by statistical methods. Obviously the final numerical values of those parameters will depend on which sets of data have been used in the process. in fact, as will be seen below, on the basis of our particular model bias, the results of the analyses can be used to discriminate against certain blocks of information. The bulk of the experimental data under consideration has been taken in the region of the four momentum transfer up to 25 f^{-2}. Some of the data covers the region from 25 to 45 f^{-2}. It is probably not meaningful to extrapolate the results of this analysis, but it is certainly useful to do so. One thus obtains "reasonable" estimates on cross sections in the region of very high q^2, which region will be covered by SLAC. At the end of the paper we will show the extrapolated results in terms of form factor behavior.

II. THEORETICAL MODEL

The following theoretical model for the isotopic form factors has been used:

$$\left.\begin{aligned} G_e^S &= \frac{s_{e1}}{1 + q^2/15.6} + \frac{s_{e2}}{1 + q^2/26.6} + (1 - s_{e1} - s_{e2}) \\ G_e^V &= \frac{v_{e1}}{1 + q^2/M_\rho^2} + (1 - v_{e1}) \\ G_m^S &= \frac{s_{m1}}{1 + q^2/15.6} + \frac{s_{m2}}{1 + q^2/26.6} + (1 - s_{m1} - s_{m2}) \\ G_m^V &= \frac{v_{m1}}{1 + q^2/M_\rho^2} + (1 - v_{m1}) \end{aligned}\right\} \qquad (1)$$

This model is based on dispersion theoretical ideas and strong pion-pion interactions (2-pion and 3-pion resonances). The resonances used here are the ($T = 0$, $J = 1$) three-pion states, $\omega(15.6f^{-2})$ and $\varphi(26.6f^{-2})$; and the ($T = 1$, $J = 1$) two-pion state, $\rho(M_\rho^2)$. The first two resonances will manifest themselves in the isoscalar form factors, G_e^S and G_m^S, whereas the third particle should contribute to the isovector form factors, G_e^V and G_m^V.

The formulae (1) are only approximate in the sense that the resonances are considered to be delta functions in the integrand of the more accurate form factor expressions:

$$G_{e,m}^{S,V} = \frac{1}{\pi} \int_0^\infty \frac{g(t')}{t' - t}\, dt' \qquad (2)$$

This approximation is very good for the scalar resonances ω and ρ, (780 ± 10) MeV and (1019 ± 2) MeV, respectively; but the ρ particle appears as a broad peak, (750 ± 100) MeV, in the spectral function $g(t)$ versus $t(=-q^2)$ plot. As has been shown by Kirson,[1] this peak can be

substituted to good approximation by a sharp resonance at a somewhat lower position than 750 MeV. Another important point should be mentioned: According to Scotti and Wong[2] in their analysis of nucleon-nucleon interaction, the effective position of the ρ-mass appeared to be about 600 MeV. These considerations have led us to adopt the mass of this particle as a free parameter in our analyses. Hence we have seven free parameters in the model, which number is reduced to six because of the constraint given by the results of the neutron-electron interaction determination:[3]

$$\left(\frac{dG_{en}}{dq^2}\right)_{q^2=0} = \left(\frac{dG_e^S}{dq^2}\right)_{q^2=0} - \left(\frac{dG_e^V}{dq^2}\right)_{q^2=0} = 0.021 \qquad (3)$$

The constant terms in the formulae (1) stand for either hard cores in the structure of the nucleons or for higher mass states, the q^2 dependent influence of which are not noticeable in the region of four momentum transfer under consideration.

Before discussing the results obtained with this model we wish to make the following remarks.

We have refrained from inserting into the model any speculative idea. For instance, no resonances have been employed other than those known at present. Moreover, we thought it better to refrain from constraints such as those given by the ideas of Sachs[4] on the high energy behavior of the form factors. Our philosophy is that either the formulae (1) represent a rather complete picture of the structure of the nucleons, in which case the adjustment of the parameters should validate these ideas; or (more likely) the formulae are not complete in the sense, for instance, that other resonances, not yet known, play a role. In this case it seems completely worthless to apply constraints obtained from theoretical ideas about the high energy behavior of the form factors in an analysis of rather low q^2 points.

However, one could attempt the same kind of analysis by employing another theoretical model. This fact has caused several physicists to attempt fits with models containing speculations about other resonances with either hard core or soft core terms. We will add to the confusion

by presenting the results of the present paper, which are based on a model without any speculation other than the theoretical ideas behind the model itself.

III. DATA SETS

The following data sets have been used in the analysis:

TABLE 1

Data Set	Method	Number of Points	Region of q^2	Reference
I	e-p: detecting electrons	58	3-25 f^{-2}	(5)
II	e-p: detecting electrons	114	3-30	(6)
III	e-p: detecting protons	7	6-18	(7)
IV	e-p: electron-proton coincidences	21	25-45	(8)
V	e-d: detecting electrons	71	3-22	(9)

There are several additional data sets[10-15] which at the date of this report have not been processed. However, the cross sections used here represent most of the total material available and it does not seem likely that the conclusions of this paper will have to be changed when a more complete analysis has been made. For instance, the results of the present analysis are in very good agreement with the results for proton form factors obtained at Orsay[10] and Stanford,[11] which data cover the very low region of q^2 (up to $3f^{-2}$).

IV. DISCUSSION ANALYSES

The IBM 7090 computer at Stanford was used to minimize the value of χ^2 by varying the initial set of parameters chosen.*

As it was known already that several systematic differences existed between the various data sets, separate analyses on the following combinations were performed.

Combination (a) Data sets I and V

(b) Data sets II and V

(c) Data sets I, II and V

(d) Data sets I, II, III, IV, and V

(e) Data sets IV and V

In the course of the work it has proved more convenient to keep the initial value for the ρ-mass (M_ρ^2) fixed. The minimum (five parameter) χ^2 value was then obtained as a function of the parameter M_ρ^2, as illustrated in Fig. 1. Each point represents a completely independent search on the five coefficients, s_{e1}, s_{e2}, s_{m1}, s_{m2}, and v_{m1}. The sixth coefficient, v_{e1}, follows from those parameters through the constraint given by formula (3). The numerical values of M_ρ^2 are given in units of f^{-2}, whereas the obtained minimum values of χ^2 are normalized to unity by dividing the actual values by the number of degrees of freedom.

The different curves correspond to the various combinations involved. As can be seen, the best fit is obtained when combining data II and V. Other good fits were obtained for the combinations I, V and IV, V, although in the latter case this does not mean very much because only 21 proton points were combined with 71 deuteron points, and the individual fit to those 21 points is poor (see also Table II). The minimum χ^2 for the three cases mentioned do not coincide, meaning that there are systematic differences between the corresponding blocks of information on proton cross sections. These discrepancies are reflected in the poor fits

*The search logic to do so has been kindly supplied to the author by H. P. Noyes and has been refined by A. Johansson. I am indebted to both as their contributions were essential for the ability to carry out the present analysis.

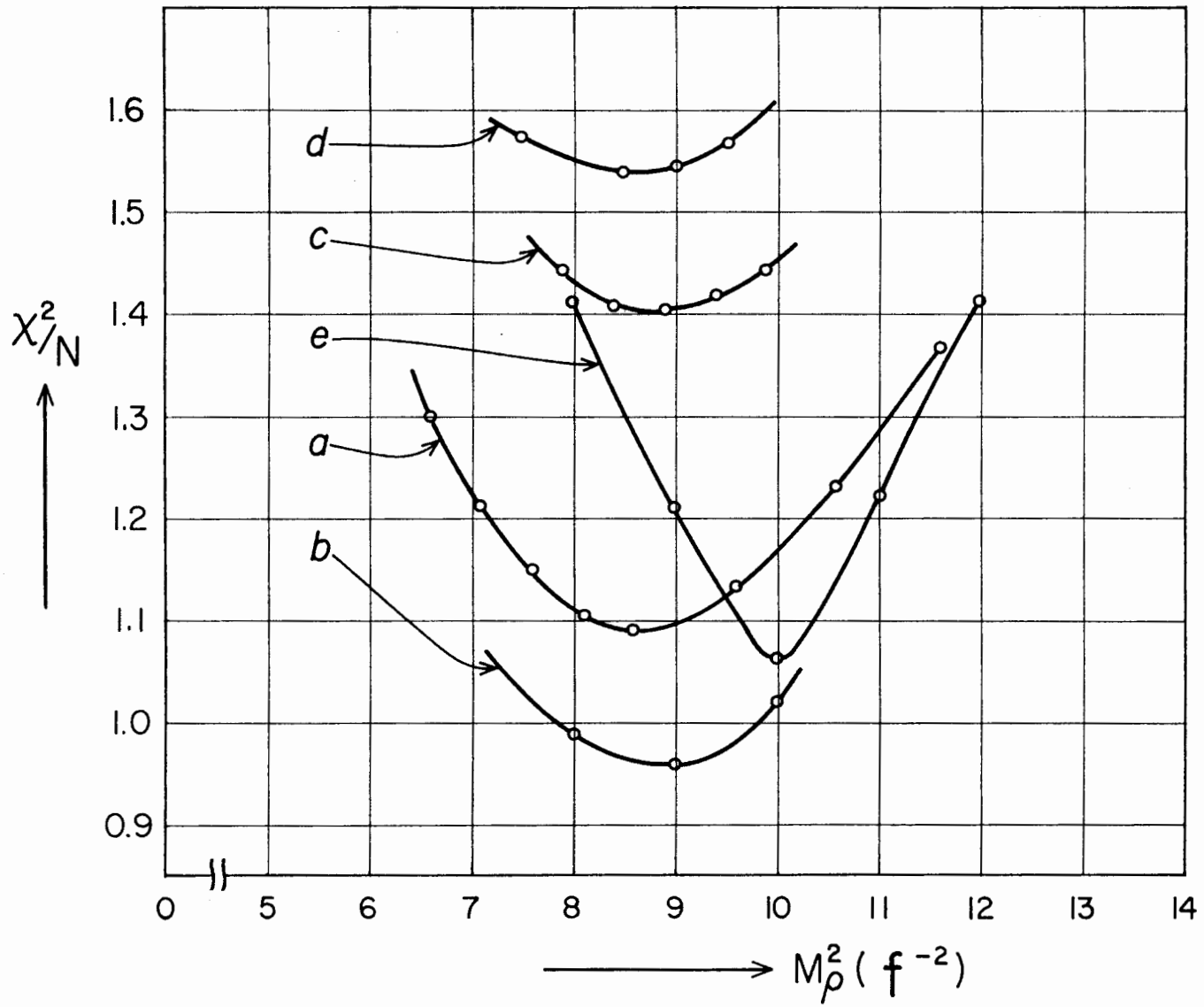

FIG. 1

TABLE II

PARAMETERS AND χ^2 VALUES FOR:

	Combination of Data Sets				
	a (129 points)	b (185 points)	c (243 points)	d (271 points)	e (92 points)
s_{e1}	4.21	2.89	3.12	3.58	3.41
s_{e2}	- 4.32	- 2.30	- 2.63	- 3.30	- 3.45
s_{m1}	5.86	5.13	4.65	3.74	5.07
s_{m2}	- 5.68	- 4.72	- 4.07	- 2.83	- 4.62
v_{e1}	1.29	1.26	1.27	1.25	1.31
v_{m1}	1.11	1.09	1.09	1.07	1.14
M_ρ^2	8.6	9.0	8.9	8.5	10.0
χ^2_I(58 points)	84.5	--	145.0	133.2	--
χ^2_{II}(114 points)	--	120.8	134.4	144.6	--
χ^2_{III}(7 points)	--	--	--	13.6	--
χ^2_{IV}(21 points)	--	--	--	57.2	37.4
χ^2_V(71 points)	50.0	50.8	52.9	60.2	54.1
χ^2total	134.5	171.6	332.3	408.8	91.5
χ^2/N	1.09	0.96	1.40	1.54	1.06

obtained when combining the different data sets. For example, the combination I, II, V delivers a χ^2 minimum of 1.40, which is probably totally due to the discrepancies between I and II. Study of the two sets of proton data directly reveals that, especially at the large angle points, the experimental values disagree. Also, the results from combination I, II, III, IV, V show that the different blocks of proton data involved are mutually inconsistent.

The numerical material presented in Table II will be helpful in studying the seriousness of the discrepancies. The table gives the numerical values of the parameters in the minimum of each of the curves shown. In addition, it quotes the individual χ^2 values to the separate data sets for those values of the parameters.

Figures 2a and 2b present the form factors of the nucleons in the region q^2 below $25f^{-2}$ as obtained from the results of this paper for the combination of data sets I, V (solid lines) and II, V (dashed lines).

It is gratifying to note that the proton form factor G_{ep}, shown in Fig. 3, is in very good agreement with the precise results of Orsay and Stanford in the low q^2 region. On the other hand, the results on the neutron form factor, G_{en}, disagree with those obtained from elastic scattering from the deuteron[11] ($G_{en} \equiv 0$) and those obtained from inelastic deuteron scattering by measuring the electron and neutron in coincidence[16] (Fig. 4).

V. EXTRAPOLATION INTO THE SLAC REGION OF q^2

To determine counting rate estimates for SLAC energies, we have applied the model for the isotopic form factors (formulae 1) in the region up to 1000 f^{-2}. The results are given in Fig. 5 and represent the different extrapolations as obtained from some of the results given above. The numbers with which the curves are labeled refer to the different combinations used in the χ^2 analyses (see Section IV above).

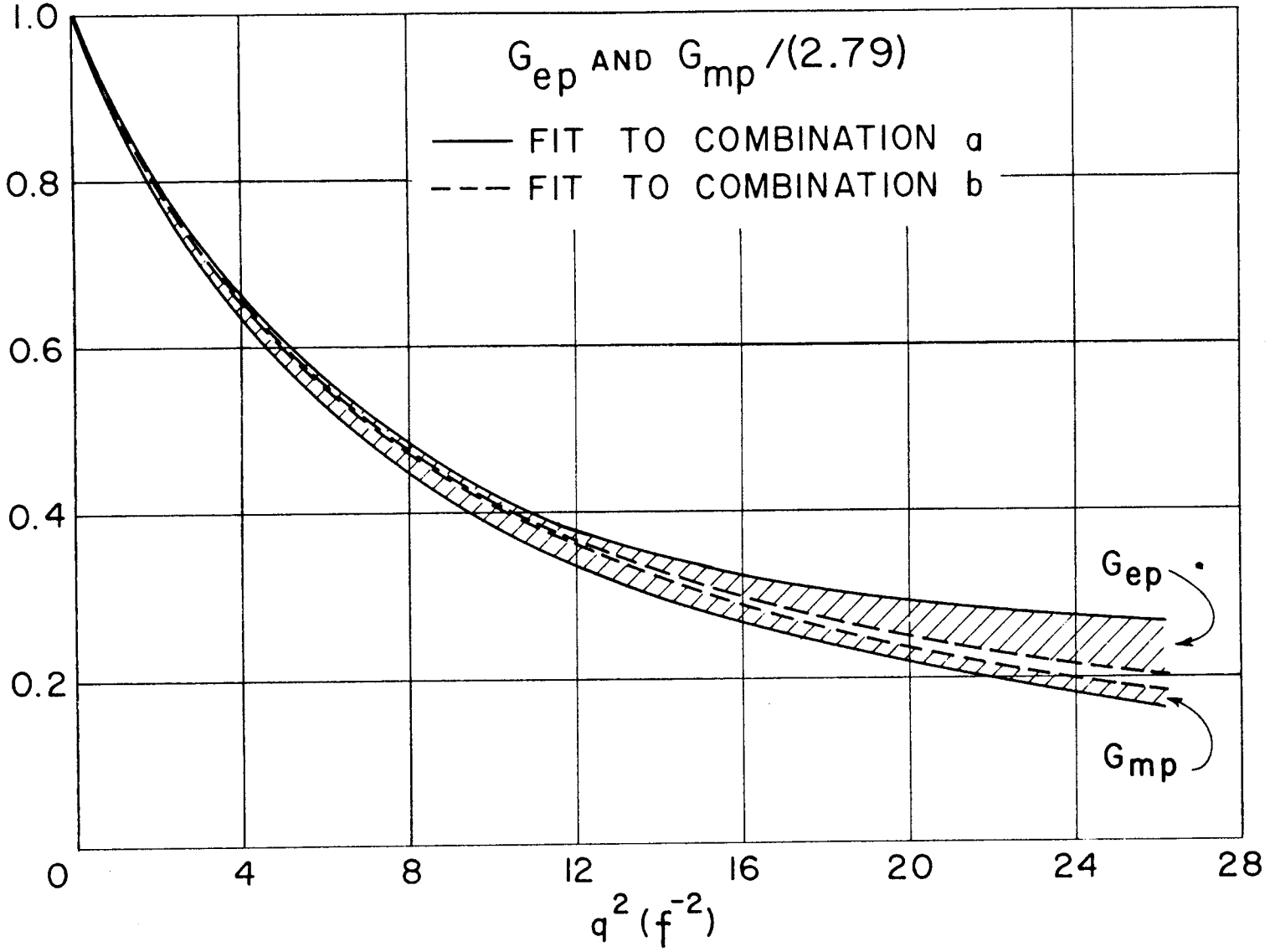
G_{ep} AND G_{mp} /(2.79)
FIT TO COMBINATION a
FIT TO COMBINATION b
G_{ep}
G_{mp}
1.0
0.8
0.6
0.4
0.2
0
4
8
12
16
20
24
28
q^2 (f^{-2})

FIG. 2a

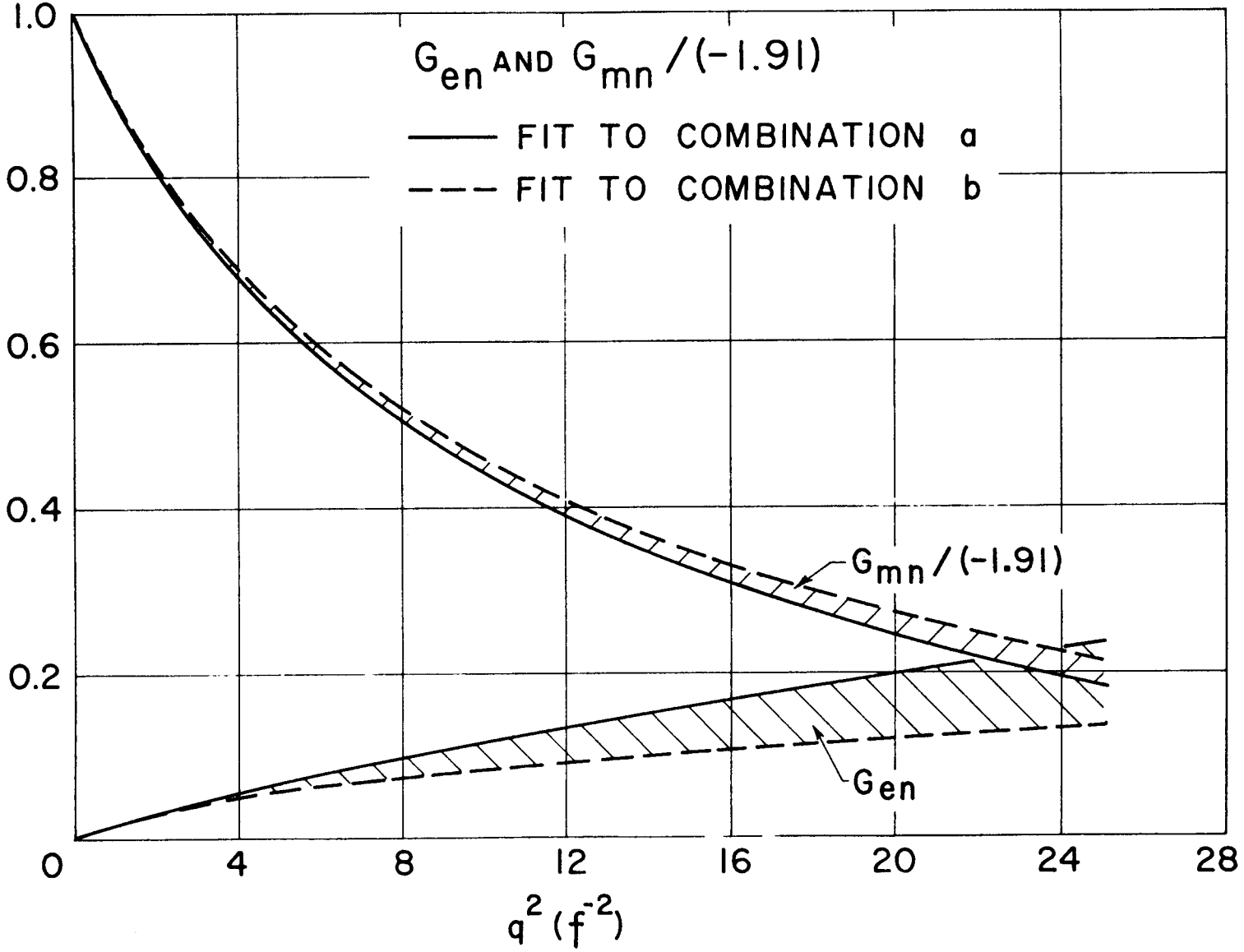
G_{en} AND G_{mn} /(-1.91)
FIT TO COMBINATION a
FIT TO COMBINATION b
G_{mn} /(-1.91)
G_{en}
1.0
0.8
0.6
0.4
0.2
0
4
8
12
16
20
24
28
q^2 (f^{-2})

FIG. 2b

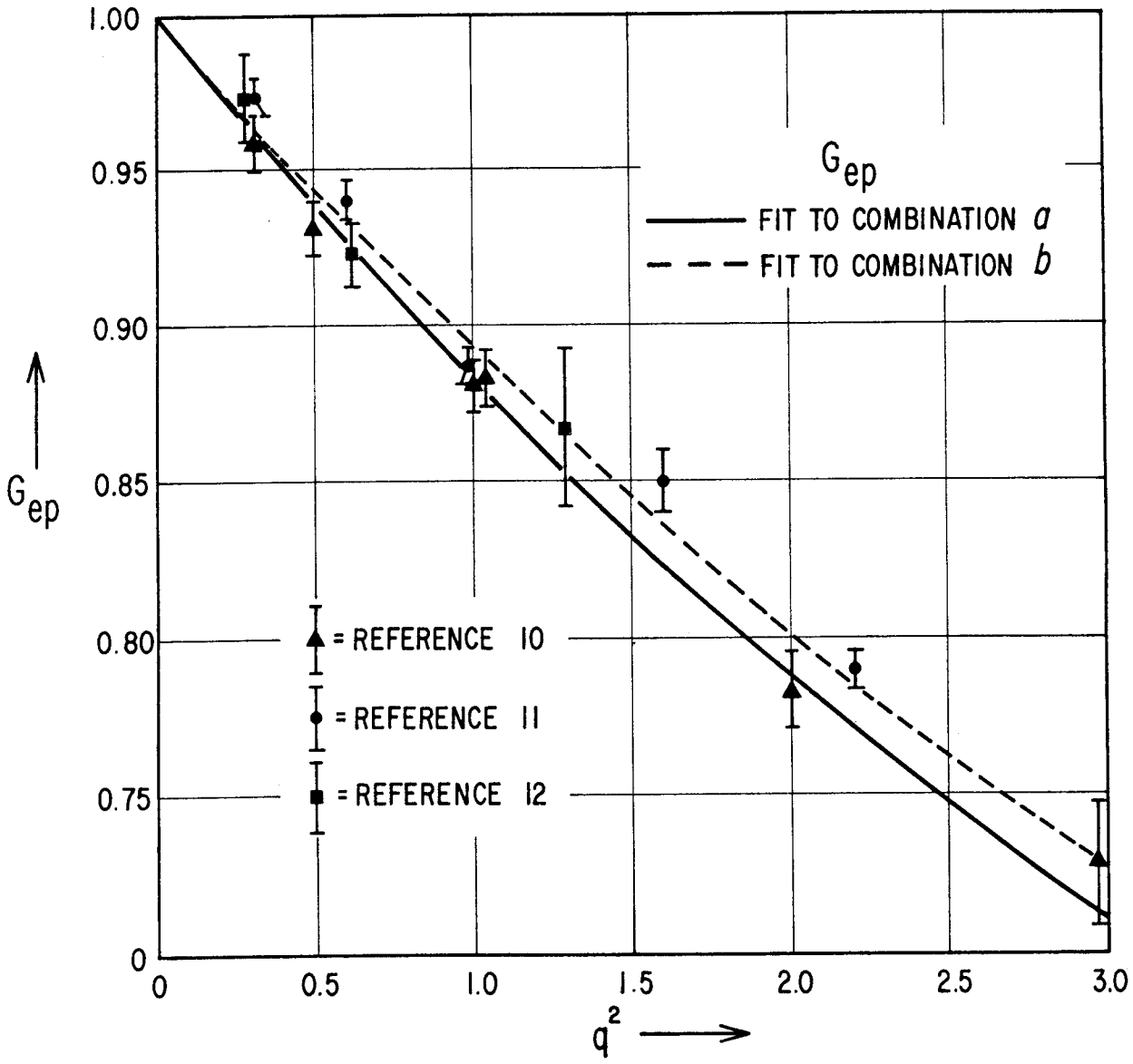
1.00
0.95
0.90
0.85
0.80
0.75
0
0
0.5
1.0
1.5
2.0
2.5
3.0
G_{ep}
G_{ep}
q^2
G_{ep}
FIT TO COMBINATION *a*
FIT TO COMBINATION *b*
= REFERENCE 10
= REFERENCE 11
= REFERENCE 12

FIG. 3

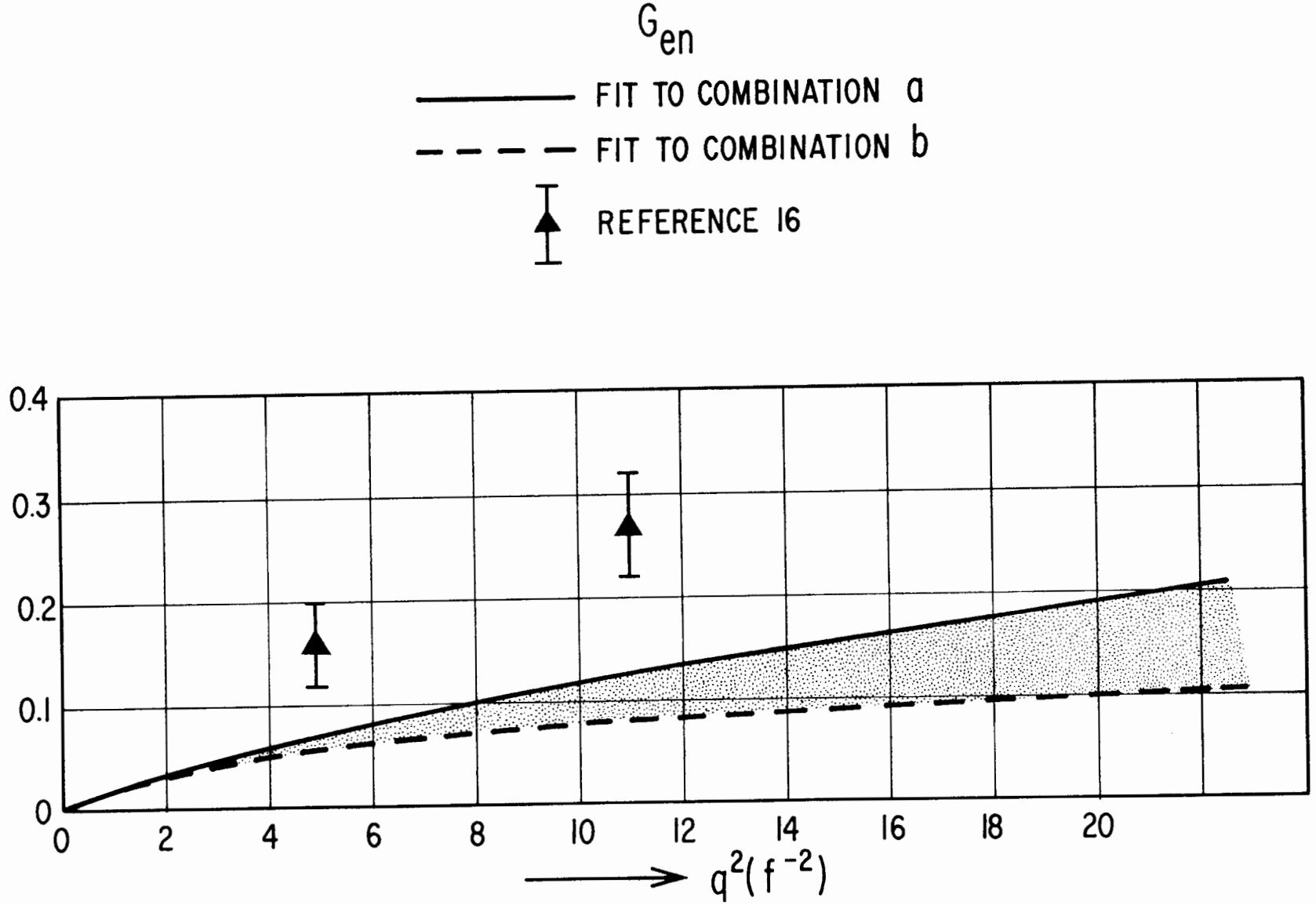
G_{en}
FIT TO COMBINATION a
FIT TO COMBINATION b
REFERENCE 16
0.4
0.3
0.2
0.1
0
0
2
4
6
8
10
12
14
16
18
20
$q^2(f^{-2})$

FIG. 4

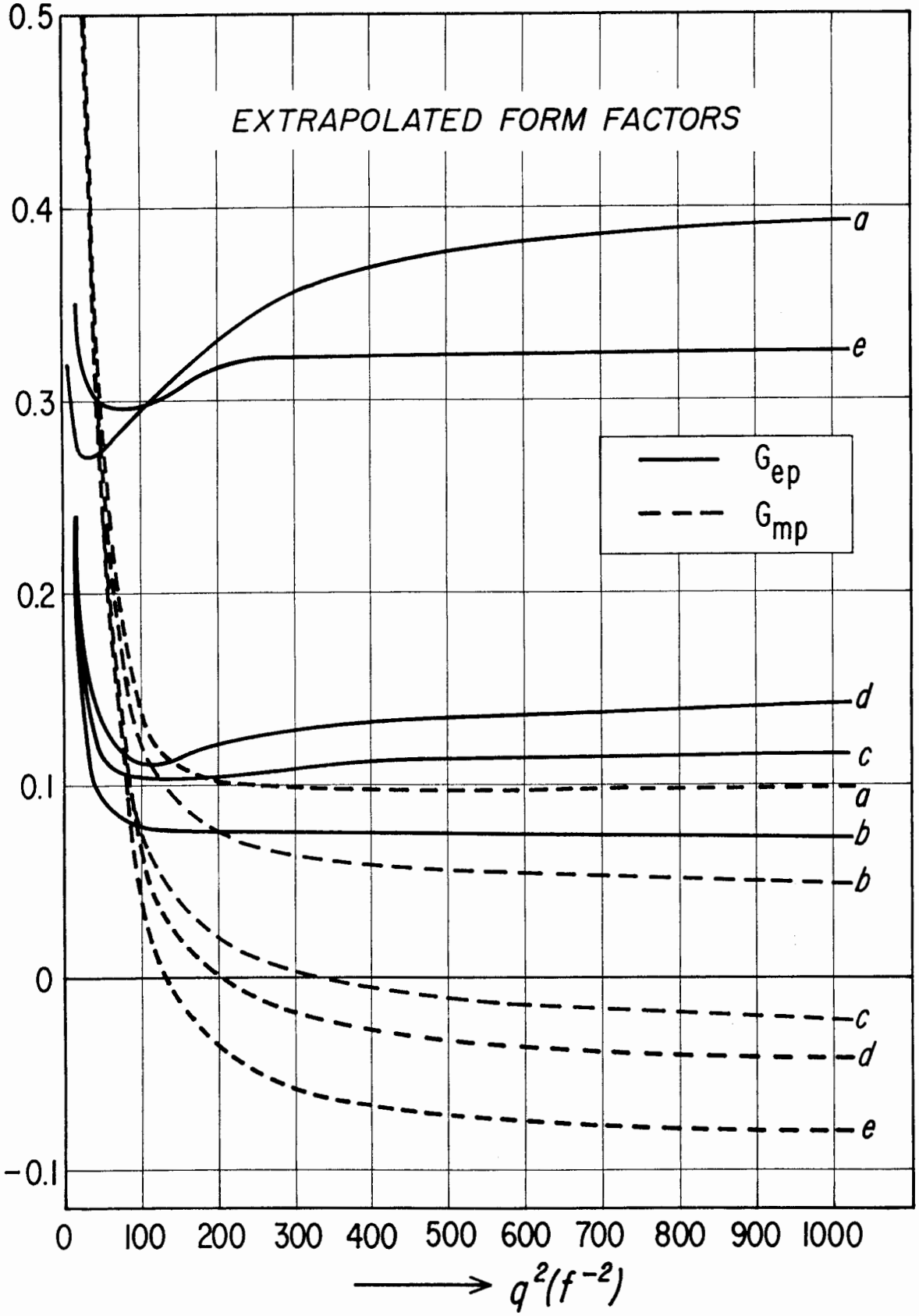
EXTRAPOLATED FORM FACTORS
0.5
0.4
0.3
0.2
0.1
0
-0.1
0
100
200
300
400
500
600
700
800
900
1000
$q^2(f^{-2})$
G_{ep}
G_{mp}
a
e
d
c
a
b
b
c
d
e

FIG. 5

The figure shows roughly

$$\left|\frac{G_{ep}}{G_{mp}}\right| > 1.4$$

for the high energy behavior of the extrapolated proton form factors.

As is pointed out in Section H, the true value for this ratio as well as the absolute magnitude of each of these form factors will be of the utmost importance for the future of electron-proton scattering experiments. If the ratio is low, no hope exists for separating the individual values at high momentum transfers, and if the absolute values (hard cores) are small, the cross sections are going to drop beyond reach. Further knowledge about either case will be very interesting.

A full and more complete account of the present results will be given in a forthcoming article.[17]

LIST OF REFERENCES

1. M. W. Kirson, Phys. Rev. (to be published).
2. A. Scotti and D. Wong, International Conference on Nucleon Structure, Stanford University, Stanford, California (1963).
3. D. J. Hughes, Phys. Rev. 90, 497 (1953).
4. R. G. Sachs, Phys. Rev. 126, 2256 (1962).
5. F. Bumiller et al., Phys. Rev. 124, 1623 (1961).
6. P. Janssens, private communication, preliminary data.
7. J. Dunning et al., Phys. Rev. Letters 10, 500 (1963).
8. K. Berkelman et al., Phys. Rev. 130, 2061 (1963), and K. Berkelman, private communication: $\frac{d\sigma}{d\Omega}/\sigma_{NS}$ at $q^2 = 45$ and $\theta = 120^{\circ}$ should be read as 0.180 instead of 0.108.
9. C. de Vries et al., Phys. Rev. Letters 8, 381 (1962); Phys. Rev. (to be published).
10. P. Lehmann, et al., Phys. Rev. 126, 1183 (1962); and B. Dudelzak et al., Nuovo Cimento 28, 18 (1963).
11. D. J. Drickey and L. N. Hand, Phys. Rev. Letters 9, 521 (1962).
12. D. Yount and J. Pine, Phys. Rev. 128, 1842 (1962).
13. P. Gram and E. Dally (to be published).
14. D. J. Hughes (to be published).
15. R. Littauer, H. Schopper and R. Wilson, Phys. Rev. Letters 7, 141 (1961).
16. P. Stein et al., Phys. Rev. Letters 9, 403 (1962); International Conference on Nucleon Structure, Stanford University, Stanford, California (1963).
17. C. de Vries, R. Hofstadter, R. Herman and A. Johansson, Phys. Rev. (to be published).

POSSIBILITIES WITH A 2 BeV/c SPECTROMETER FOR ELECTRON-PROTON SCATTERING AT SLAC ENERGIES

by

C. de Vries

I. INTRODUCTION

It is obvious that the maximum energy of the electron beam[1] that will be available at SLAC is an important parameter in the design of experiments.

Berkelman (see Section J) has pointed out that, when utilizing this maximum energy, a flexible experimental setup needs a 20 BeV/c spectrometer, if one wishes to go to the far forward scattering angles. Such a huge device would require an important part of the experimental budget, some estimates being as high as $\$2.5 \times 10^6$. It is therefore evident that a final proposal for such a machine would require a detailed study, with emphasis on whether or not such an instrument would really be useful. From the following discussion one might tentatively surmise that, for the particular case of electron-proton scattering, such an extreme energy spectrometer would not be needed. The present report does not advocate that extreme energy spectrometers will not be required eventually. However, it is strongly felt that, at this early stage of the preparations for the experiments, it is wise to refrain from any serious commitment on the construction of such a device.

It is surprising to see how much one can learn with a more moderate design, say a 2 BeV/c spectrometer. Both the high maximum energy and high intensity of the accelerator beam allow one to overtake all the presently existing electron machines with such a "low momentum" spectrometer. Another and more serious argument is that in view of the experimental as well as theoretical difficulties (one-photon exchange assumption, radiative processes) it might very well be that nothing will be learned from extreme electron scattering experiments, simply because one does not know how to interpret the measured quantities. Slowly proceeding into the unknown by combining electron scattering experiments with

positron scattering, polarization experiments and muon-scattering experiments seems to be the way to set up an experimental program for SLAC.

II. CHOICE OF SPECTROMETERS

Using the numerical material obtained from the kinematics program for e-p scattering (see Section F), we have made the plot shown in Fig. 1. The solid curves are the loci of the variable pairs (q^2,θ) for which the energy of the outgoing electron is a constant. Hence any variable pair to the right of those lines can be reached with a spectrometer capable of handling electrons with maximum momentum as indicated alongside the curves. The dashed curves indicate that the regions to their left cannot be reached with any spectrometer because of lack of primary energy. The two dashed curves shown correspond to 20 BeV primary energy (SLAC, Stage I) and 6 BeV primary energy (CEA). From this plot it can immediately be noticed that, in addition to the region of four momentum transfer up to 250 f^{-2} that is the maximum for the CEA machine, the region of q^2 up to 950 f^{-2} can be covered with a 20 BeV electron beam.

Obviously, in principle, a 20 BeV/c spectrometer can reach any variable pair to the right of the (SLAC) dashed line. However, because of the length of such an instrument (see Penner[2] and Berkelman, Section J), its usefulness will be limited to the very forward angles. In addition, it is highly impractical to use such a "universal" instrument for forward as well as backward angles in view of the counting rates involved. For guidance, the numbers in the little squares indicate the estimated counting rates per second for a 1 g/cm^2 target when utilizing a solid angle of 10 mster and a primary beam intensity of 30 μA. These estimates were obtained from the considerations given in Section G.

Rather than discussing to what extent a high momentum spectrometer is useful in terms of solid angle and scattering angle, we refer to Berkelman (Section J).

From a glance at Fig. 1 it is clear that the possibilities with a 2 BeV/c spectrometer are tremendous when using the SLAC beam. Such a device could be made flexible in the sense that it might be used at any

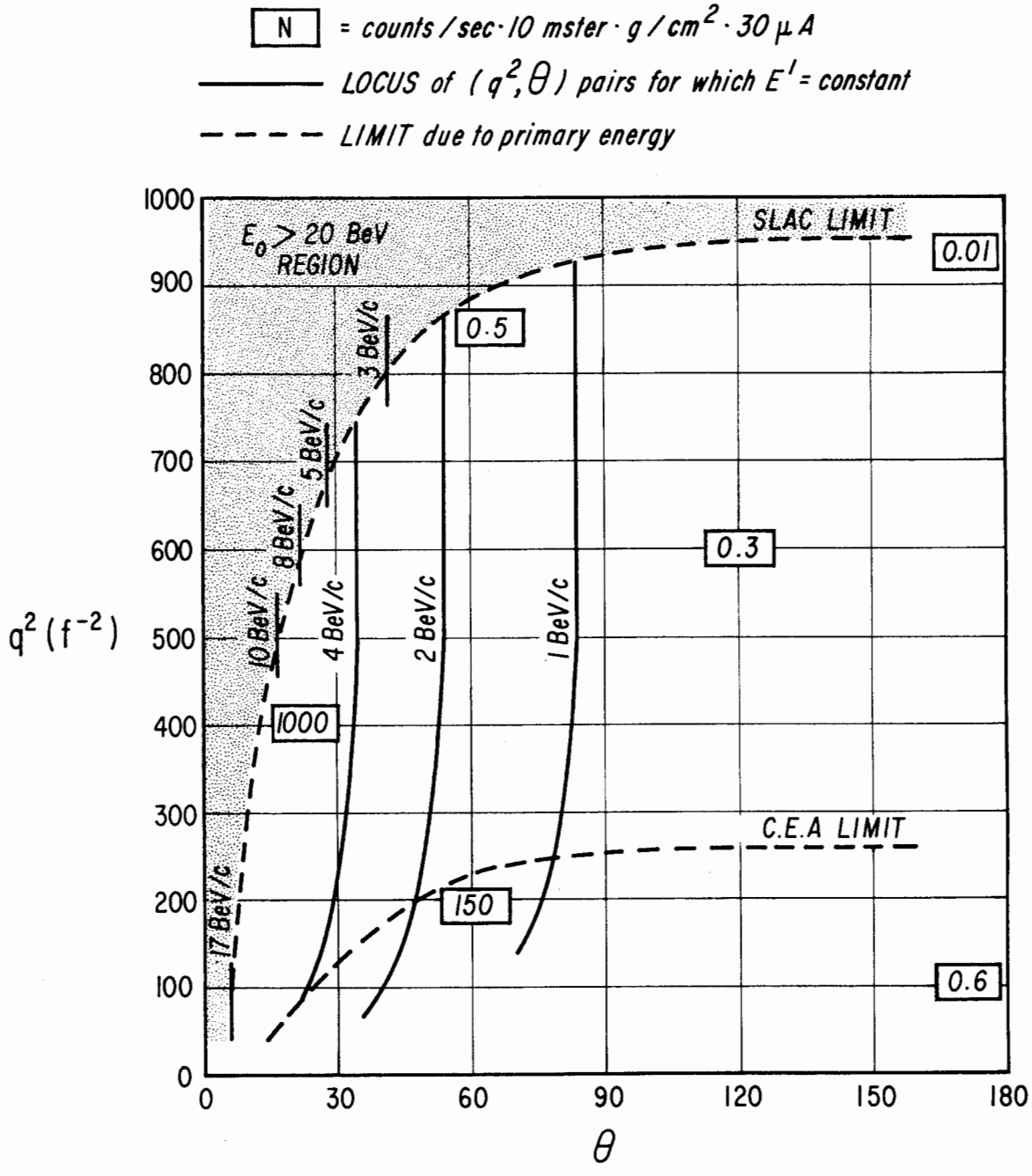
N = counts / sec · 10 mster · g / cm² · 30 μA
LOCUS of (q², θ) pairs for which E' = constant
LIMIT due to primary energy
E₀ > 20 BeV REGION
SLAC LIMIT
C.E.A LIMIT
0.01
0.5
0.3
0.6
1000
150
17 BeV/c
10 BeV/c
8 BeV/c
5 BeV/c
4 BeV/c
3 BeV/c
2 BeV/c
1 BeV/c
q² (f⁻²)
θ
0
100
200
300
400
500
600
700
800
900
1000
0
30
60
90
120
150
180

FIG. 1

angle between, say, 30° and 150°. Hence, almost the entire region to the right of the 2 BeV/c curve in Fig. 1 could be studied with such an instrument. Moreover, it also seems feasible to plan 180° scattering experiments with the same spectrometer. We will discuss this subject later (see Section I).

On the other hand, the far forward angles (less than 40°) are not covered by a 2 BeV/c spectrometer when experiments are planned at $q^2 > 100\ f^{-2}$. It is here that considerations for more extreme spectrometers come into the game. There are several reasons that this region in particular might be the most important one. Certain experiments to search for deviations from the Rosenbluth formula (for instance, Regge behavior of the photon) ask for high energies and small scattering angles. Before deciding, on the basis of the last statement, to construct a spectrometer able to reach the very far forward angles, it is advisable to study to what extent one wants to reach the forward direction. Such a study seems worthwhile, because any small step toward smaller angles means a considerable increase in the maximum momentum capabilities of the corresponding spectrometer, and this will also mean a considerable increase in costs and floor space. We believe the total cost of a spectrometer will probably go up roughly linearly with the maximum momentum reach, if we take into account the fact that a "far forward" spectrometer requires much less solid angle than a "backward" spectrometer.

Let us take one example to strengthen our argument: We assume that the Rosenbluth formula is valid for the four momentum transfers one deals with at SLAC. (Actually to the knowledge of the author there is no way of predicting how serious an eventual breakdown can become. For all we know it could even be possible that the formula will <u>not</u> break down!)

$$\left(\frac{d\sigma}{d\Omega}\right)_p = \sigma_{NS}\ (1 + t)^{-1}\ G_{ep}^2 + t + 2t(1 + t)\ \tan^2\theta/2\ G_{mp}^2$$

with

$$t = \frac{q^2}{4M^2}$$

The formula shows that for fixed θ the influence of G_{ep} on the total cross section will become smaller with increasing t and will increase with decreasing angle at fixed q^2. A measurement of G_{mp} is relatively easy because this form factor essentially dominates the cross section at the backward angles. If one is then satisfied with a 20 percent effect due to G_{ep}, the question might be asked at what scattering angle such an effect will be seen. The arguments can be most easily given on the basis of Fig. 2. Here are plotted on a (q^2,θ) plane the curves which connect those (q^2,θ) points for which 20 percent of the cross section will be due to G_{ep}. Each curve corresponds to a different assumption for the value of the ratio G_{ep}/G_{mp}. As can be seen, for the Sachs limit, $G_{ep}/G_{mp} = 1$, one does not need to go below 15° (corresponding to a 12 BeV/c spectrometer) if a 20 percent experiment satisfies the experimenter. If the ratio G_{ep}/G_{mp} should be larger than 1, the figure shows that the maximum spectrometer momentum required decreases rapidly with increasing numerical value of this ratio.

The dashed-dotted curve corresponds to the capabilities of a 2 BeV/c spectrometer for the particular experiment under consideration. It shows that if $G_{ep}/G_{mp} = 1$, the maximum q^2 to be reached for a 20 percent effect due to G_{ep} is about 220 f^{-2}. If we take seriously the values for the form factors in the high q^2 region, obtained from extrapolating the χ^2 fits to low energy data (Section G), then $G_{ep}/G_{mp} > 1.4$. This would mean that even a 2 BeV/c spectrometer is quite useful for this particular experiment. The author realizes that there are some assumptions in the above argument, but it surely illustrates the point that it is by no means certain that a 20 BeV/c spectrometer will be an instrument, "its money's worth." After all, from another look at the graph, such a device will be needed only if the ratio between form factors happens to be much less than unity and then only low q^2-values will be reached (< 100 f^{-2}). And even under those conditions a 2 BeV/c design could be almost as efficient; it will mean that the maximum q^2-value to be reached is only slightly less (≈ 80 f^{-2} for $G_{ep}/G_{mp} = 0.5$).

To summarize the above arguments:

Either $G_{ep}/G_{mp} > 1$ and then one can separate the values of the two form factors at very high values of the momentum transfer, or this ratio

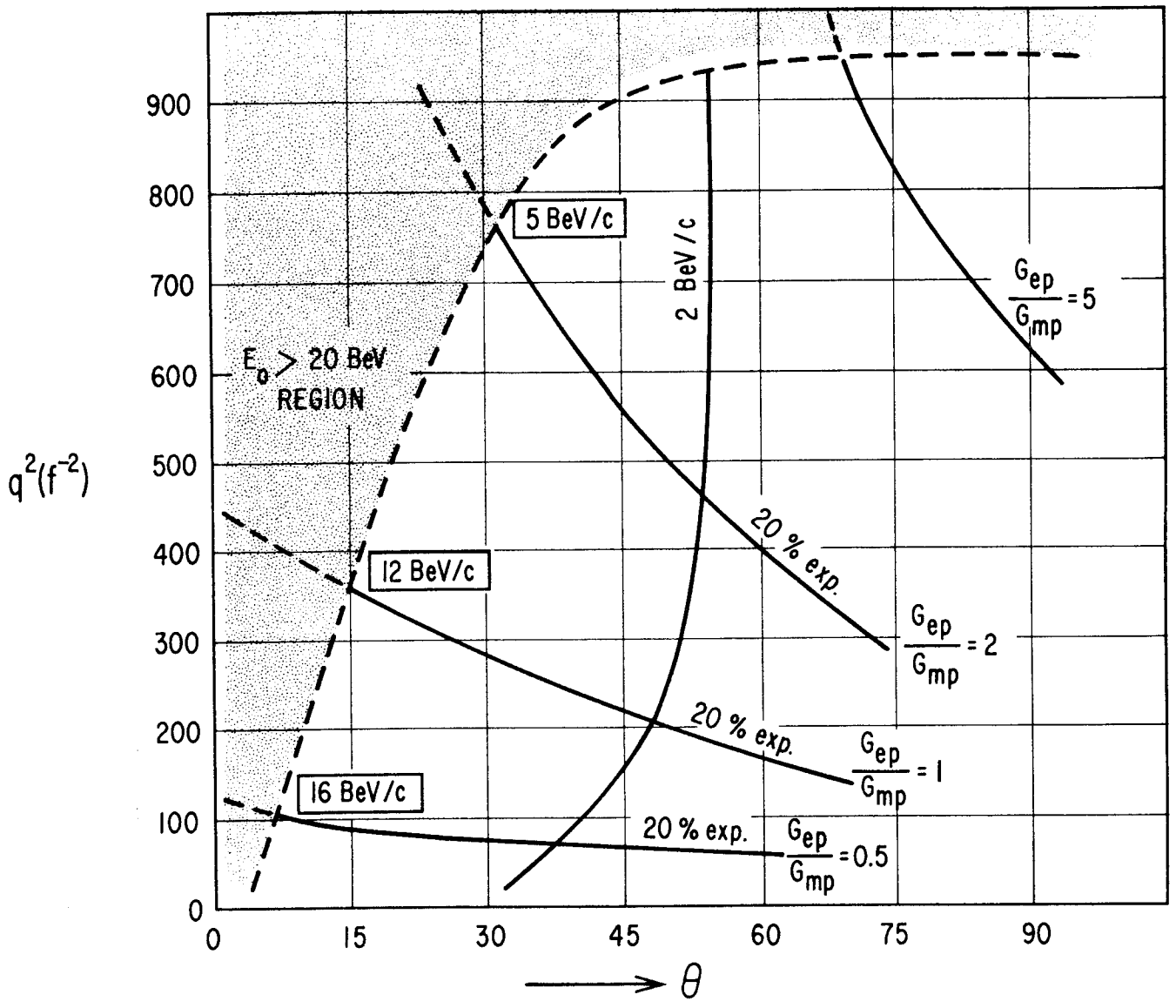
900
800
700
600
500
400
300
200
100
0
$q^2(f^{-2})$
$E_0 > 20$ BeV
REGION
5 BeV/c
12 BeV/c
16 BeV/c
2 BeV/c
20 % exp.
20 % exp.
20 % exp.
$\frac{G_{ep}}{G_{mp}} = 5$
$\frac{G_{ep}}{G_{mp}} = 2$
$\frac{G_{ep}}{G_{mp}} = 1$
$\frac{G_{ep}}{G_{mp}} = 0.5$
0
15
30
45
60
75
90
θ

FIG. 2

is less than 1 and then one will never be able to do so at high values of q^2, no matter what spectrometer is available. In both cases a 2 BeV/c spectrometer seems to be a very useful instrument and the author, for one, should be happy to perform experiments "limited" in scope by such a "small" spectrometer.

In the opinion of the author, a 20 BeV/c spectrometer will not be needed, because the region of (q^2,θ) it will cover in excess of, for example, a 10 BeV/c spectrometer, is too small to justify the extra expenses and the extra floor space. It seems that a combination of 10 BeV/c design, covering the region of θ from about 10° to 40°, and a 2 BeV/c machine is close to the optimum solution for the problem of designing a flexible setup for electron-scattering experiments at SLAC.

III. POSSIBLE LAYOUT FOR A 2 BeV/c SPECTROMETER

First we should like to state that the ideas presented below are not obtained from a careful search of all the possible solutions for a 2 BeV/c spectrometer. Nor is a claim made that the details given warrant that the discussed design needs no further investigation. It is merely felt that the basic ideas deserved at least the time spent during the author's stay at SLAC.

1. Because of the "moderate" momentum capabilities of the spectrometer under consideration, a large bending angle can be chosen; this is important in view of expected background problems.

2. The solid angle has to be at least 5 mster in view of the expected low counting rates (see Section F). From the qualitative picture of the form factors at high four momentum transfers, as sketched in Section G, this solid angle will mean that in the worst case (large q^2 and large angles), counting rates of about 1 per minute have to be handled. Counting rates an order of magnitude lower than this figure could still be handled without causing excessive difficulty. At any rate, there is no way out of this problem. Increasing the solid angle by a factor of 10 seems unrealistic unless one thinks in terms of solenoidal spectrometers, and we feel that such instruments are inflexible as far as scattering

angles are concerned. Because it is impossible to sufficiently shield the counters from the target, this type of spectrometer has a very bad rejection for background.

3. Next we chose a zero gradient magnetic field shape. We feel that for the large area over which the magnetic field shape has to satisfy the theoretical design, the $n = 0$ field is most easily achieved. Double focusing is not needed because the kinematics severely limit the opening angle in one direction. Furthermore, counters extended in the direction perpendicular to the median plane of the spectrometer should not cause severe drawbacks.

4. Further considerations revealed that a large distance between the target and spectrometer might be desirable for the following reasons:

a. Shielding requirements

b. Possible complicated target equipment

c. Possible installment of spark chamber(s) in front of the spectrometer

d. The use of the spectrometer for 180° scattering experiments, which condition requires further complexity of the target area (see Section I).

5. Combining the requirements of large solid angle and a large distance from the target to the spectrometer forces the introduction of strong focusing elements to limit the gap in the spectrometer to reasonable size.

From the above considerations we arrived at the system indicated in Fig. 3. It contains a 2 BeV/c, 90° bend, $n = 0$ spectrometer and a set of quadrupoles. The significant numbers of this system for 2 BeV electrons are indicated in Table 1.

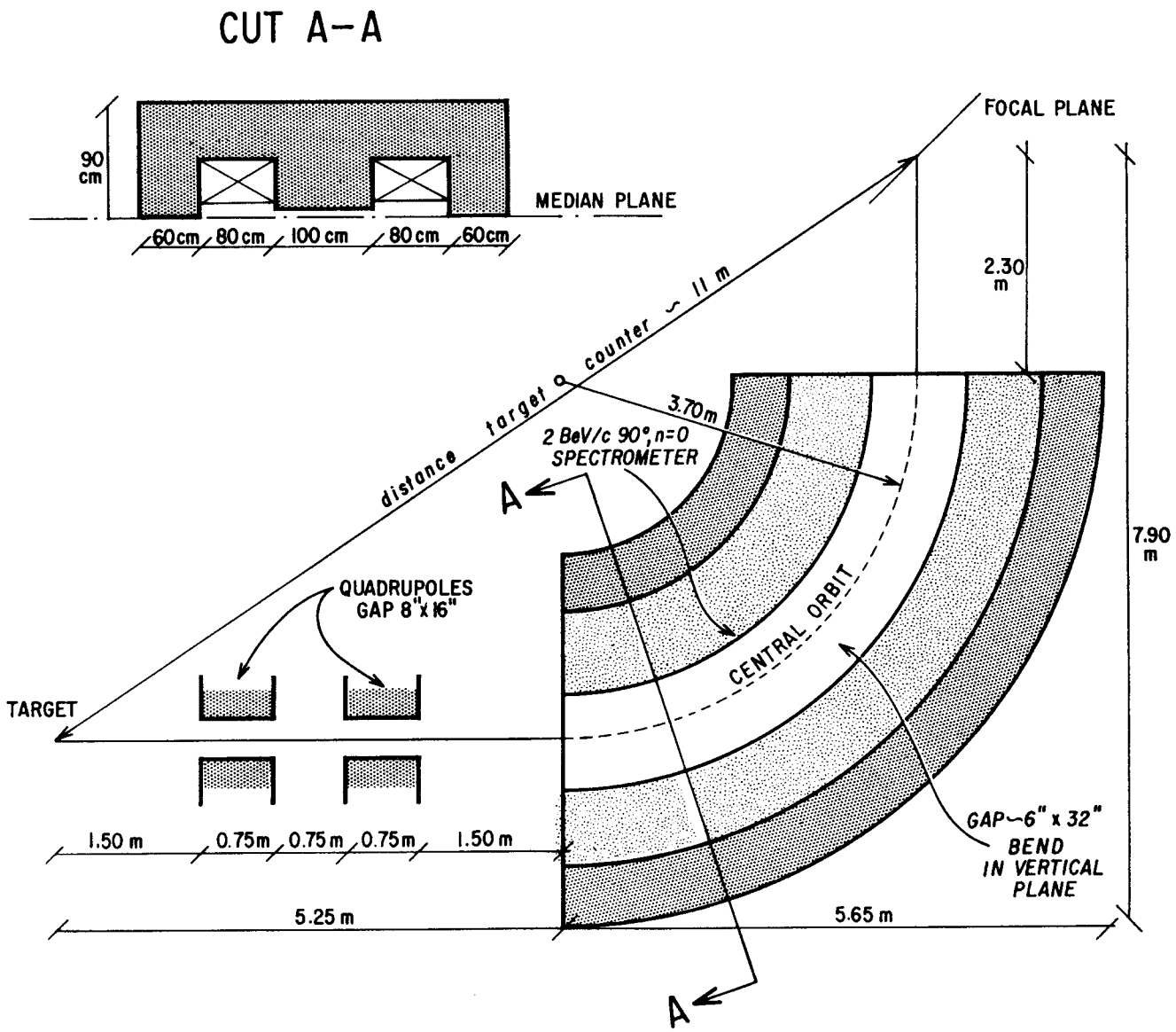

FIG. 3

SLAC-25-H
de Vries

TABLE I

	2 BeV/c, 90°, n = 0 Spectrometer	Quadrupoles
Length along reference trajectory	5.81 meters	0.75 meters
Radius of curvature	3.70 meters	-
Field strength 2 BeV electrons	18 kG	9 kG (at pole tip)
Apertures	15 × 80 cm	20 × 40 cm (Panofsky type) or 40 × 40 cm (conventional type)
Gradient	0	-
Coils (copper)	$\approx 10^5$ ampere - turns/coil	-
Weight	copper 10 ton iron 220 ton	-
Power consumption	0.23 Mw	
Total costs, including power installation	$300,000	

The beam optics of this system have been studied using the SLAC "Beam Transport" program for the IBM 7090 computer. The system under consideration is capable of handling a beam emerging from a target, 0.5 × 2 cm, into 2 × 8 degrees opening angle.

For these conditions we find:

Dispersion = 6 cm/percent

Magnification = 0.8

Resolution = better than 0.1 percent

Solid angle = about 5 mster

Maximum momentum = 2 BeV/c

The second order matrix elements (also obtained from the aforementioned program) showed that second order focusing essentially is achieved at least for the central momentum beam. The dimensions of the gaps are such that a 1 percent momentum bite can be handled at 5 mster without losing any particle against the walls. If larger momentum bites are wanted, one should limit

the solid angle in order to have 100 percent efficiency for all momenta under consideration. We estimate that the system is 100 percent transparent for a 5 percent momentum band using about 2 mster solid angle. From the experiences obtained by Riston with his similar 90° magnets for the Mark III electron accelerator, we think it possible to have second order focusing over a large region in the focal plane. The focal plane tilt can be varied by curving the pole pieces of the spectrometer, as shown by Ritson.

It does not seem too difficult to design a mount to install the whole 230-ton apparatus, such that

(a) The spectrometer can be rotated from 30° to 150°, and

(b) The spectrometer can be moved toward the target if desired for special purposes.

The total length of the system is about 11 meters and the height from the mount to the focal plane is approximately 8 meters. Allowing some space for actual counter equipment and shielding, the overhead crane should at least clear 12 meters above the mount. If the beam height is fixed at 7 feet above floor level, a pit is needed for the installment of the mount.

We feel that this design has been carried through far enough to show that such an instrument would be a worthwhile piece of experimental equipment at SLAC.

LIST OF REFERENCES

1. R. Neal, Internal Memorandum, Stanford Linear Accelerator Center, Stanford University, Stanford, California.
2. S. Penner, SLAC Report No. 200-13, Stanford Linear Accelerator Center, Stanford University, Stanford, California (Summer 1960).

ELECTRON-PROTON SCATTERING AT 180°

by

C. de Vries

I. INTRODUCTION

The considerations in Section H show that the feasibility of separating the numerical values of G_{ep} and G_{mp} at high values of the four-momentum transfer, q^2, depend on the actual behavior of those quantities in the "asymptotic" region. It has been pointed out that

(a) the numerical value of the ratio G_{ep}/G_{mp} determines the maximum value of q^2 at which one is able to disentangle the separate values of the form factors;

(b) the absolute values of these form factors will decide whether the experiments are still feasible in terms of counting rates;

(c) the measurement of G_{mp} alone is relatively simple at backward angles.

In Section G a statistical analysis was made utilizing different data sets on e-p and e-d scattering at low q^2-values ($< 45\ f^{-2}$). The parameters found from the χ^2 tests determine the behavior of the isotopic form factors on the basis of a three-pole model (formulae 1 of Section G. The resulting values of G_{ep} and G_{mp} for the asymptotic region of q^2 are indicated in Fig. 4 of Section G. From this figure one obtains:

$$\left| \frac{G_{ep}}{G_{mp}} \right| > 1.4 \quad \text{at high } q^2\text{-values}$$

for the different combinations of data sets considered.

Another important feature is that for some of the extrapolated results G_{mp} becomes negative. If this happens to be true in nature, then even a relative 180° experiment might be very instructive. Scanning the cross section as a function of q^2 will reveal a sudden drop in the region

where G_{mp} goes through zero. Of course, absolute measurements will always be needed to determine the exact behavior of $G_{mp}(q^2)$. Knowledge about G_{mp} is essential if one is to disentangle the separate value of G_{ep} from measured cross sections at forward angles. Therefore, we believe that a 180° experiment will be essential to learn about the form factors at high values of q^2.

II. EXPERIMENTAL ARRANGEMENT

180° experiments have been successfully undertaken with the 40 MeV electron linac at Stanford. There the incident beam is deflected over 10° by a horizontal magnet (hereafter called magnet A) and the 180° scattered beam is deflected again by the same magnet and then momentum analyzed by a 120° spectrometer. For low incident energies the energy of the elastically scattered electrons is essentially the same as the primary energy.

For the high energy and intensity of the SLAC beam, there are two features which determine the aspects of an experimental arrangement for 180° scattering:

(a) The power contained in the beam demands a very elaborate beam dump construction, which therefore should be at a fixed position.

(b) The energies of the backward scattered electrons are weakly changing with primary energy: for E_o from 1 to 20 BeV, E' goes from 320 to 460 MeV.

These two features make it mandatory that the bending angle of the primary beam in magnet A is kept small and fixed for all energies.

We choose for magnet A a circular magnet with radius $\rho_o = 0.75$ meters and homogeneous field shape. It is easy to show that electrons entering such a field along a radius will also leave the magnetic field radially (see Fig. 1). The primary beam is deflected over 2-1/2 degrees. The trajectories shown are for electrons scattered at 180° on protons, for 20, 3, and 1 BeV incident energies. The numerical values for energies, field strengths, and bending angles are as given in Table I for those three cases.

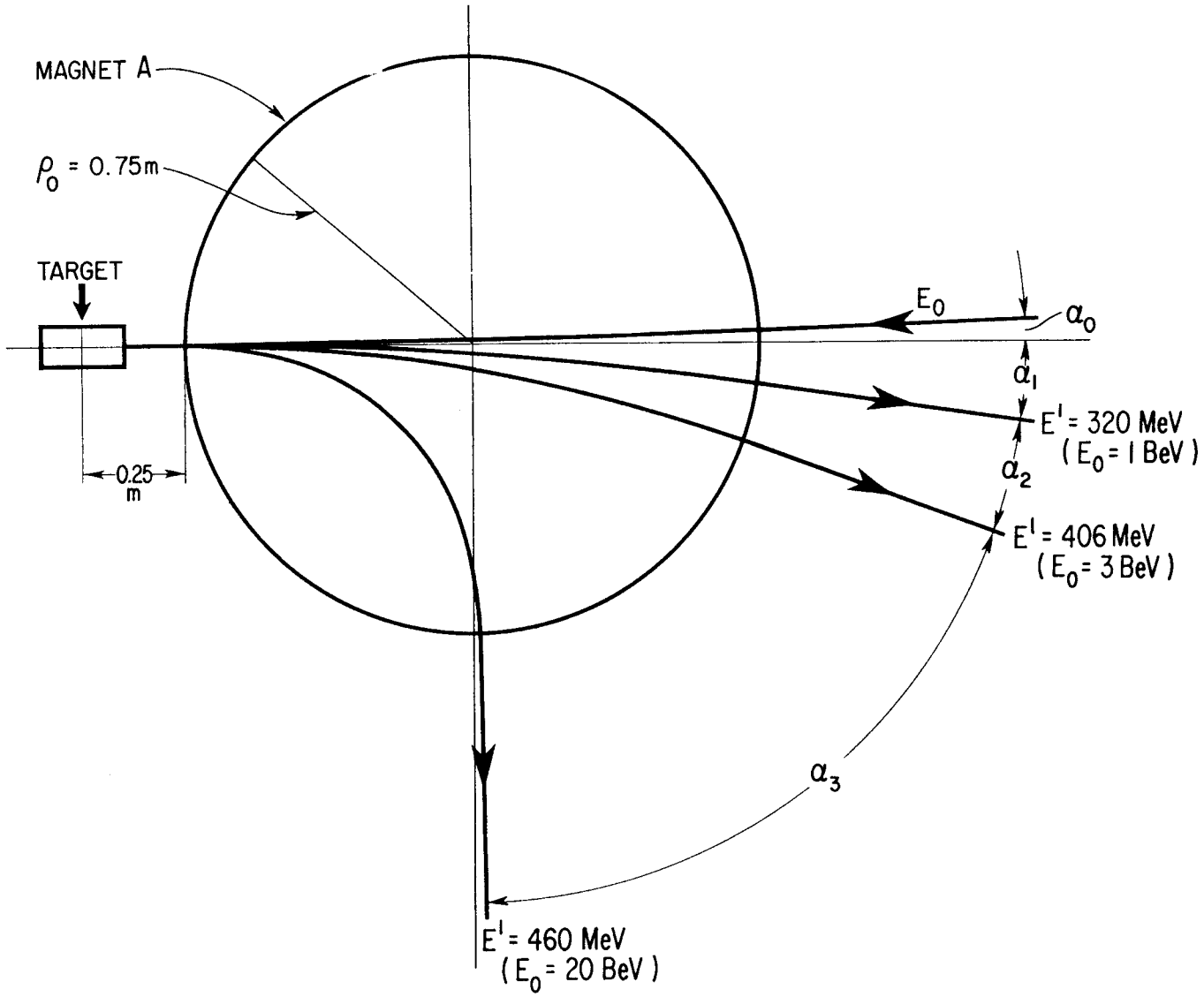
MAGNET A
ρ_0 = 0.75m
TARGET
0.25 m
E_0
α_0
α_1
E' = 320 MeV
(E_0 = 1 BeV)
α_2
E' = 406 MeV
(E_0 = 3 BeV)
α_3
E' = 460 MeV
(E_0 = 20 BeV)

FIG. 1

TABLE I

q^2	E_o	B(magnet A)	α_o	E'	α
950	20 BeV	20 kG	2-1/2°	460 MeV	89°
125	3 BeV	3 kG	2-1/2°	406 MeV	19°
33	1 BeV	1 kG	2-1/2°	320 MeV	8°

The bending angles indicated in the table have been derived from the relation

$$\tan \frac{\alpha}{2} = \frac{\rho_o}{\rho}$$

where ρ is the radius of curvature of the electrons.

For the case of finite opening angles one must still study the focal properties of the magnet. The equation for the focal plane of the magnet under consideration is[1]

$$\frac{1}{b} + \frac{1}{v} = \frac{1 - \cos \alpha}{\rho_o}$$

where v and b are the distances from the center of the magnet to the source and focus, respectively. This formula shows that no real focus can be obtained for bending angles smaller than α_m:

$$\cos \alpha_m = \frac{1}{1 + \frac{\rho_o}{d}}$$

where d is the distance between the target and the entrance of the magnet. As d has to be kept small for solid angle requirements, the emerging electron beams are divergent for almost the entire range of practical bending angles. This fact makes magnet A in itself unsuitable for analyzing purposes. If combined with an analyzing spectrometer, which rotates around the center of magnet A, an extra focusing element

is required to compensate for the variation of focal properties of magnet A with the bending angle. Thus the focal plane of the analyzing spectrometer can be kept fixed for all bending angles.

The 2 BeV/c spectrometer (as sketched in Section H) can serve for this purpose because it contains a set of quadrupoles in front of the 90° bending magnet. The fields in those quadrupoles can be programmed as a function of bending angle in magnet A. The three cases indicated in Table I are schematically sketched in Fig. 2.

It is realized that for 180° experiments one does not really need a 2 BeV/c spectrometer because

$$(E')_{180^{\circ}} = \frac{E_o}{1 + 2E_o/M}$$

However, once such a spectrometer exists, all one has to do for 180° experiments is to shift the target downstream and install the circular magnet with its center at the normal target position.

Using the analyzing magnet for both kinds of experiments poses a problem; namely, the initial bend for 180° scattering is in the horizontal plane, whereas the analyzing magnet will be mounted vertically to satisfy kinematical requirements for other scattering experiments. It seems a rather crude solution to propose that for this particular experiment the 2 BeV/c magnet should be laid on its side. Therefore, we allowed in our investigations for a rather large opening angle in the vertical direction (about 4 degrees) and a 1 degree opening angle in the horizontal direction. Hence the gap in the circular magnet (6 inches) will be correspondingly larger than is otherwise necessary. Although we did not study in detail the exact location of the foci for the different momenta (which will not be on a line in the median plane of the spectrometer!), we feel that under the chosen conditions this is not a very serious problem.

Using the "Transport" program[2] for IBM 7090, we found that the dispersion and resolution of this system are essentially independent of the bending angle in magnet A. The significant beam optical quantities are given in Table II for the three cases mentioned earlier.

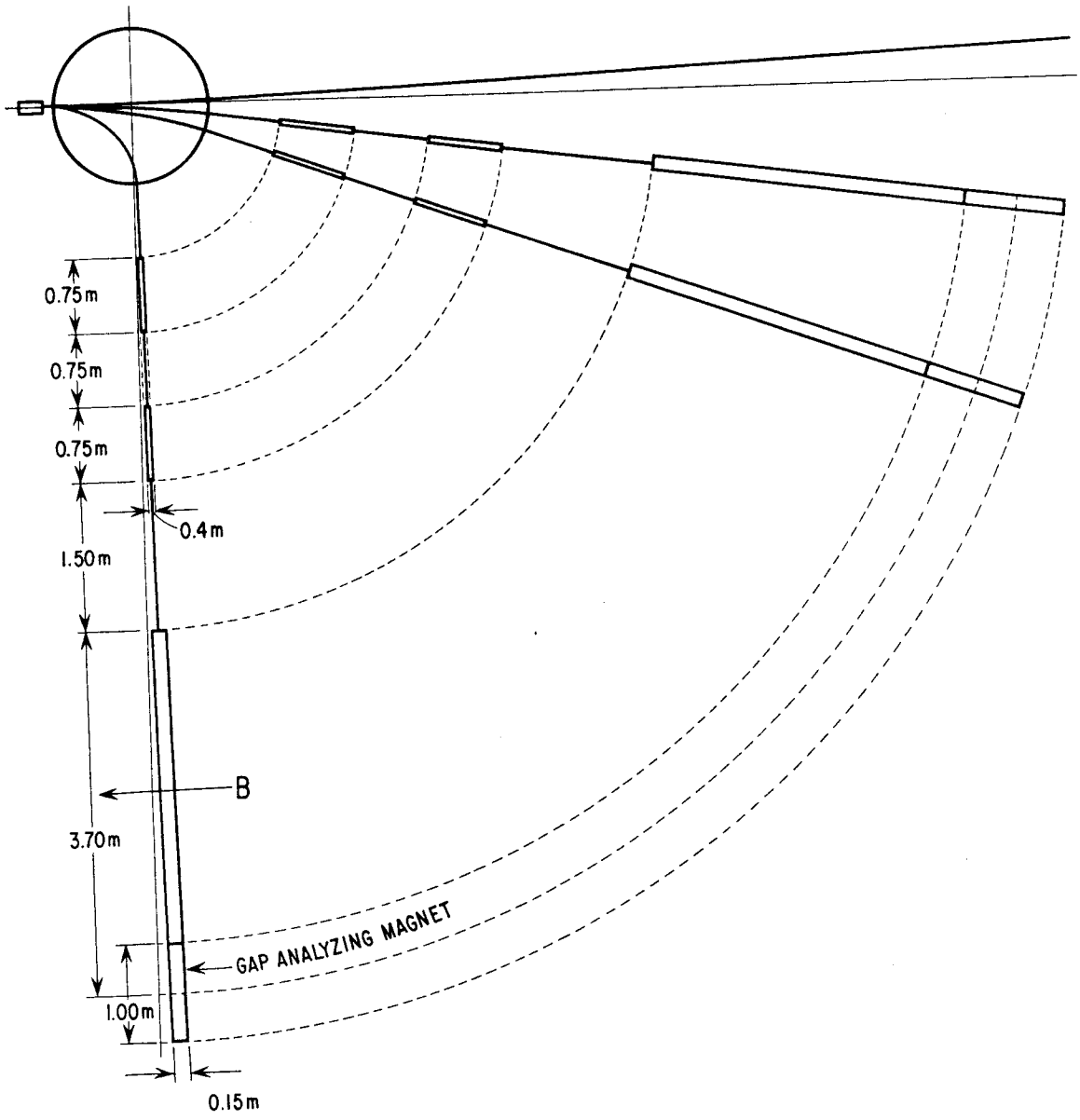
0.75m
0.75m
0.75m
0.4m
1.50m
B
3.70m
GAP ANALYZING MAGNET
1.00m
0.15m

FIG. 2

TABLE II

Target	Ω	q^2	α	Dispersion	Resolution
0.5 × 2 cm	5mster	950	89°	6 cm/percent	0.46 percent
(2 cm in beam direction)		125	19°	6 cm/percent	0.45 percent
		33	8°	6 cm/percent	0.52 percent

The second-order focusing elements are satisfactory in all cases, but it should be said that (a) the system is not optimized, and (b) a more detailed study is desirable if the construction of the system is seriously considered.

LIST OF REFERENCES

1. K. Brown et al., Internal Memorandum, Stanford Linear Accelerator Center, Stanford University, Stanford, California (March 1962).
2. C. Moore, H. Butler, Internal Memorandum, Stanford Linear Accelerator Center, Stanford University, Stanford, California.

ELECTRON SCATTERING AT 20 GEV

by

Karl Berkelman

I. INTRODUCTION

It is natural to expect that electron-nucleon scattering will be one of the important fields of experimental activity at the two-mile accelerator. Elastic and inelastic scattering of electrons and positrons have already been investigated at linear accelerators with incident energies up to 1 GeV and at electron synchrotrons with energies up to 6 GeV; however, not all the techniques employed in these experiments are directly applicable to the 20 GeV beam that will be available at SLAC. In this report I shall discuss some of the problems which will be encountered and outline a possible experiment for the measurement of the elastic electron-proton differential cross section at 20 GeV incident energy. Most of the ideas presented here are neither new nor original but have been obtained from the literature and from discussions with others at SLAC and elsewhere.

II. ELASTIC E-P SCATTERING

A. Motivations For The Experiment

If the Rosenbluth formula[1] for the elastic scattering cross section in terms of nucleon form factors can still be believed at 20 GeV, we can obtain valuable information on the nucleon intrinsic core, or equivalently, the asymptotic behavior of the form factors at high momentum transfers. For example, it should be possible to make some definitive statement about the Sachs hypothesis[2] that G_E and G_M tend to the same limit. Even if we have to abandon the two form factor description, the very high incident energies may enable us to make sensitive checks of the validity of quantum electrodynamics at small distances as well as measurements of multiple photon exchange and other mechanisms leading to breakdown of the Rosenbluth formula. Even if no other argument were

available, the unpredictability of the outcome of the experiment would be sufficient justification for doing it.

B. Experimental Problems

1. Momentum Resolution

As Cassels[3] has pointed out, if one observes elastic scattering by momentum analysis of the scattered electron at fixed angles, the momentum resolution must be sufficient to separate the elastic peak from the pion electroproduction continuum, which starts at $E' = E'_{elastic}\ (1 - \mu/E)$, where μ is the pion mass and E the incident electron lab energy. For $E = 20$ GeV we require a detection spectrometer resolution better than $\Delta P/P = \pm 0.7\%$. The incident beam energy half-width must also be less than one pion mass. The beam transport system for end station A has been designed for limiting momentum resolution of $\pm 0.05\%$.[4] We must insure, however, that the bremsstrahlung in the target and its walls do not cause too great an energy spread in the beam. In passing through x radiation lengths ($r\ell$) the fraction of the beam degraded to energies less than $E - \Delta E$ (i.e., for $x \ll 1$) is approximately $x\ell n(E/\Delta E)$. For $E = 20$ GeV and $\Delta E = 140$ Mev, x must be less than 0.01 $r\ell$ (8.2 cm in liquid hydrogen) to guarantee that 95% of the beam is still within one pion mass of the incident energy. The effect on the scattered beam is similar. Target walls thinner than 0.001 $r\ell$ should present no problem.

To utilize this momentum resolution the definition of the scattering angle must be better than

$$\Delta\theta = \frac{d\theta}{dE'/E'}\,\frac{\mu}{E}$$

which can be as small as 2 mrad, depending on θ (see Table I). Fortunately, multiple scattering in a 0.01 $r\ell$ target will not seriously exceed this limit.

TABLE 1

KINEMATICS OF ELASTIC E-P SCATTERING AT E = 20 GeV

(laboratory system)

θ	E' GeV	q^2 $(GeV/c)^2$	F^{-2}	θ_p	P_p GeV/c	$\frac{d\theta}{dE'/E'}$ mr/%	$\frac{d\Omega_p}{d\Omega}$
3°	19.4	1.0	26	58°	1.2		112
10°	15.0	9.1	235	27°	5.7	3.5	6.2
30°	5.18	27.8	715	9.5°	15.7	3.6	0.13
90°	0.89	35.8	921	2.5°	20.1	8.9	0.002
180°	0.46	36.7	947	0	20.5	∞	

Unfortunately, detection of the angle and momentum of the recoil proton cannot be used to define the elastic scattering process. It is quite possible, especially at high energies, for elastic scattering and electropion production to take place with the same initial energy, electron and proton angles, and proton momentum.[5] There is no substitute for good momentum resolution on the scattered electron.

Because of the narrow momentum resolution required for scattered electron detection, the radiation correction to the measured elastic cross sections will be very large, about 50% if one takes the calculations of Meister and Yennie[6] at face value (using $\Delta E'/E' = \mu/E$). The magnitude of the correction is alone enough to invalidate the approximations used, and new calculations to higher orders will have to be made. In any case, the measured cross sections will be quite sensitive to the momentum resolution of the detection system.

2. Target Heating

A minimum-ionizing beam of 10^{14} particles per second will dissipate about 40 watts in a 0.01 rℓ (8.2 cm) of liquid hydrogen. This heat cannot be removed by conduction through liquid hydrogen and must be removed by convection, i.e., rapid forced circulation of the liquid. This is not an insoluble problem.[7]

3. High Momenta

A 20 GeV/c spectrometer will be needed in the measurement of 20 GeV electron scattering in the forward direction (see Table I). We can expect the forward cross section to be important to the physical understanding of the electron-proton interaction. If the Rosenbluth formula is valid, we will need small angle data to determine the electric form factor (even at 30° the coefficient of G_E^2 is already only about 1/20 of the coefficient of G_M^2). In any case, the center-of-mass forward hemisphere folds into a 17° cone in the lab, so whatever the dynamics of the interaction the lab angles forward of 17° are a priori as informative as all the rest. If elastic scattering is to be detected by electron-proton coincidences, a high momentum spectrometer is essential whatever the scattering angle; one of the two particles will always emerge with at least half the incident kinetic energy.

High momentum and narrow resolution necessarily imply very large magnetic spectrometers. If we let S be the length in meters of trajectory in a bending magnet of maximum field B kilogauss, D the distance in meters between the middle of the magnet and its focal plane, p the momentum in GeV/c, and d the required focal plane dispersion in meters or cm percent, it is easy to show that

$$SD = 33\ pd/B$$

Selecting "reasonable" values on the right-hand side (p = 20, d = 3, B = 17) we find $SD = 120\ m^2$, implying $S \approx D \approx 11$ meters, if we restrict S and D to be of the same order. That is, we require 11 meters of bending (exclusive of focusing elements) and an overall length of at least 20 meters to get one stage of minimal momentum separation.

4. Low Counting Rates

We can make guesses about the magnitude of the elastic e-p differential cross section at 20 GeV based on the Rosenbluth formula and some assumptions about the form factors. We shall distinguish two extremes (not necessarily limits) which are consistent with the available proton form factor data below 6 GeV:[8] (1) the "core" assumption, $G_E = G_M = 0.15$ for $q^2 > 2(\text{GeV/c})^2$ or 50 F^{-2}, and (2) the "no-core" assumption, $G_E \approx G_M \to 0$ based on a phenomenological fit[9] to the data. Table II gives the predicted cross sections and counting rates (see also Fig. 1).

TABLE II

DIFFERENTIAL CROSS SECTIONS AND COUNTING RATES

(assuming 10^{14} e/sec, 0.01 rℓ, Ω = 1 msr) for E = 20 GeV

θ	$d\sigma/d\Omega(cm^2/sr)$		$R_{elastic}$ (counts/sec)	
	"core"	"no-core"	"core"	"no-core"
3^o	2.4×10^{-28}	2.4×10^{-28}	8×10^6	8×10^6
10^o	3.9×10^{-32}	8.5×10^{-33}	1400	300
30^o	3.4×10^{-35}	7.9×10^{-37}	1.2	0.03
90^o	5.6×10^{-37}	7.6×10^{-39}	0.02	3×10^{-4}
180^o	1.4×10^{-37}	1.8×10^{-39}	0.005	6×10^{-5}

As new data in the region 1-6 GeV become available from CEA we will be able to predict more intelligently. Meanwhile, we shall use the lower, "no-core" estimates in determining the experimental setup required to make the measurements. If the cross section turns out to be much smaller than our pessimistic estimate, it will indicate a proton electromagnetic core of < 1% and will probably be of no further interest.

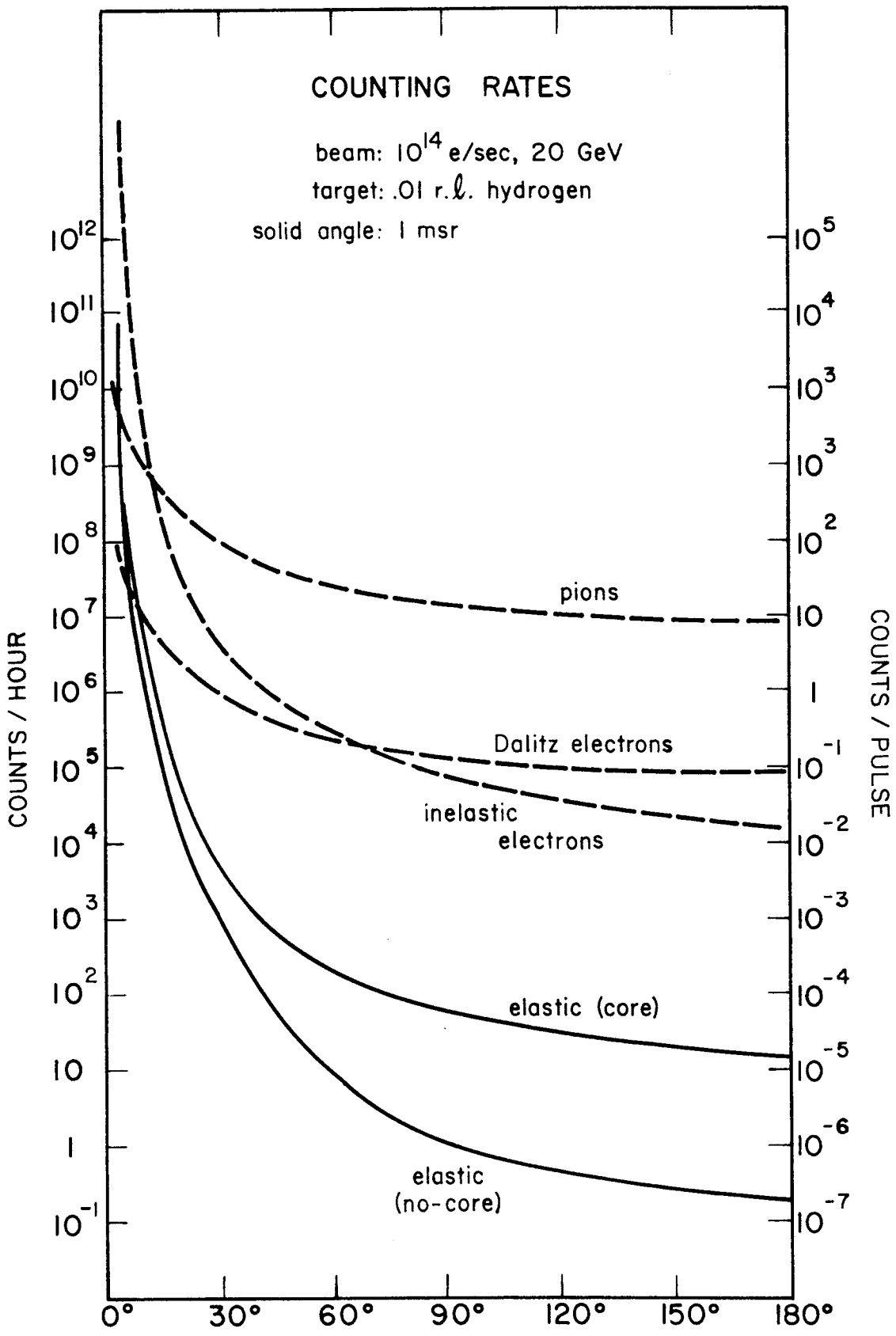

FIG. 1--Predicted counting rates as a function of laboratory angle.

5. Backgrounds

We estimate the flux of inelastically scattered electrons at each angle using an approximate form of the Bjorken-Weiszäcker-Williams formula:[10]

$$\frac{d^2\sigma}{d\Omega dE'} = \frac{\alpha}{4\pi^2}\frac{kE'}{q^2 E}\left(2 + \frac{\cot^2\theta/2}{1 + q_o^2/q^2}\right) F^2(q^2)\ \sigma\ (k)$$

Here $k = q_o - q^2/2M$ is the real-equivalent energy of the virtual photon, $\sigma(k)$ is the total γ - p photoproduction cross section at the lab energy k and $F(q^2)$ is some sort of effective inelastic nucleon form factor. In our complete ignorance we have neglected the contribution of longitudinal photons, assumed $\sigma(k)$ constant at 200 μb for $k > 1$ GeV, and taken $F(q^2)$ to be the nucleon form factor estimated from the "core" assumption above. For $E = 20$ GeV we find, over a wide range of scattering angles

$$\int_0^{E'_{max}} \frac{d^2\sigma}{d\Omega dE'}\, dE' \approx 10^3 \frac{d\sigma}{d\Omega}\ \text{elastic}$$

and

$$\int_{\frac{1}{2}E'_{max}}^{E'_{max}} \frac{d^2\sigma}{d\Omega dE}\, dE \lesssim 10^2 \frac{d\sigma}{d\Omega}\ \text{elastic}$$

where $E'_{max} = E'_{elastic}\ (1 - \frac{\mu}{E})$ is the end point of the inelastic spectrum.

More important than the inelastically scattered electrons are the electro- and photoproduced pions. To the extent that electroproduction of pions is dominated by low momentum transfer events we can use the Weiszächer-Williams approximation in its crudest form and replace each incident electron by a bremsstrahlung spectrum of virtual photons, the

number of photons corresponding to the real photon spectrum emitted by an electron passing through 0.02 $r\ell$ of material.[11] To this 0.02 $r\ell$ we add another 0.005 $r\ell$ to account for real photons produced in the 0.01 $r\ell$ target. The real and virtual photon spectrum is then

$$n(k)\, dk = 0.025\, dk/k$$

per incident electron, and the pion yield is

$$\frac{dN_\pi(\theta)}{d\Omega} \approx N_P \int_\mu^E \frac{d\sigma(k,\theta)}{d\Omega}\, n(k)\, dk$$

where

$$N_P = 3.5 \times 10^{23} \text{ protons/cm}^2 \text{ (0.01 } r\ell \text{ hydrogen)}$$

and $\frac{d\sigma(k,\theta)}{d\Omega}$ is the π^- photoproduction cross section in the lab system (mainly $\gamma + p \rightarrow p + \pi^+ + \pi^-$). Since the high energy contribution to the integral is suppressed by the bremsstrahlung spectrum, we ignore the effect of increased pion multiplicity at high energy. For convenience we distinguish two contributions to $\frac{d\sigma}{d\Omega}(k,\theta)$: the peripheral events strongly peaked in the forward direction, and the non-peripheral events more or less isotropic in the center of mass. The former is estimated using Drell's formula[12] for $\frac{d^2\sigma}{d\Omega d\omega}$ integrated over the pion energy ω. The latter is approximated by

$$\frac{\sigma(\sigma \rightarrow \pi^-)}{4\pi} \frac{d\Omega^*}{d\Omega}(\theta,k)$$

with $\sigma(\gamma \rightarrow \pi^-) = 100\mu b$. Table III and Fig. 1 show the resulting rates. The calculated totals are probably good to an order of magnitude.

TABLE III

NEGATIVE PION FLUXES PER SECOND

(10^{14} incident 20 BeV electrons) per 0.01 rℓ hydrogen, per msr

θ	R_π(Drell)	R_π(isotropic)	R_π(total)
3^o	3×10^6	10^5	3×10^6
10^o	3×10^5	5×10^4	3×10^5
30^o	(3×10^4)	3×10^4	3×10^4
90^o	(2×10^3)	5×10^3	5×10^3
180^o	(0)	3×10^3	3×10^3

Like the inelastic electron spectrum, the pion spectrum is sharply peaked at the lowest momenta, especially at backward angles. A pion cannot be emitted at a given angle with as much momentum as an elastically scattered electron, so that in principle they can be eliminated just by momentum selection. Note, however, that although the pions and elastically scattered electrons are comparable at small angles, the pions dominate by a factor of 10^5 to 10^8 at large angles. A single stage of momentum analysis (bending and focusing on a slit) typically has a transmission of 10^{-3} outside the momentum passband, so that several successive stages would be required to eliminate completely the pions and their secondary products. One can also reject pions by a variety of counting techniques. A lead glass Cerenkov counter with a high pulse height bias will detect showers initiated by high energy electrons but will also detect charged pions with a probability of about 10^{-2} via the charge exchange reaction ($\pi^- + p \rightarrow \pi^o + N$) followed by π^o decay and showering. A gas Cerenkov counter with a velocity threshold above the maximum π (or μ) velocity will register pions with a probability perhaps of the order of 10^{-4} (knock-ons, etc.). For the low-energy end

of the pion spectrum the rejection may actually be much better than indicated by these figures. Other detection techniques such as relativistic-rise ionization, synchrotron radiation, time-of-flight, or rf separation are much less promising. In any case, it is clear that some combination of one or several stages of momentum analysis (nesessary anyway for rejection of inelastic electrons and Dalitz electrons from π^o's) plus electron-sensitive counters can probably accomplish the required rejection factor for charged pions.

C. Suggested Experimental Arrangement

We consider only the electron-proton coincidence detection scheme for the following reasons.

1. Although three or more successive stages of momentum analysis on the scattered electron plus one or several types of electron-sensitive counters can in principle make a clean enough experiment, it seems clear (although rather difficult to establish rigorously) that an electron-proton coincidence system, with the same outlay in magnets now divided between two somewhat simpler spectrometers (say one or two stages each) should have a better background rejection factor. Such a system would provide us with a fourfold overdetermination of the elastic scattering kinematics (both momenta, the recoil proton angle and relative azimuth) rather than only the single redundancy (electron momentum) of the single-spectrometer system.

2. Selecting protons by velocity from a background of pions and lighter particles by means of focusing gas Cerenkov counters or time-of-flight is much easier than trying to separate electrons from pions by similar methods.

3. Coincidence counting will be trivial. One stage of momentum separation will already bring the total charged particle flux (per msr) down to less than one per beam pulse for angles greater than 10^o. We will assume that background from sources other than the target (switch-yard energy slits, beam dump, etc.) can be handled by careful shielding of the sources and detectors.

4. For electrons elastically scattered into a solid angle Ω at an angle $\theta > 17^{\circ}$ the corresponding recoiled protons fall into a solid angle $\Omega_P < \Omega$ (see Table I). Provided the proton spectrometer solid angle is not smaller than that of the electron spectrometer, the coincidence requirement entails no sacrifice in counting rate except in the case of very small scattering angles ($\theta < 17^{\circ} < \theta_P$), where the expected rates are comfortably high anyway. In the latter case the proton spectrometer sets the aperture limit, and the effective detection solid angle for electron scattering is $\Omega_P \frac{d\Omega}{d\Omega_P}$ [see Table I for $(d\Omega_P/d\Omega)$].

We consider three different spectrometers to cover the whole angular range for both electron and proton. First of all we need one spectrometer with $P_{max} \geq 20$ GeV/c. The second need have only $P_{max} \approx 10$ GeV/c, since of course only one of the two outcoming particles can have more than half the incident kinetic energy. In fact, unless we insist on measuring the scattering right at the symmetry angle ($\theta = \theta_P \approx 17^{\circ}$) where both electron and proton emerge with 10 GeV/c, we can use a smaller spectrometer for the second one. For instance, with 20 GeV/c and 6 GeV/c spectrometers we can measure elastic cross sections for $\theta < 10.5^{\circ}$ and $\theta > 277.7^{\circ}$. From the electron-proton solid angle ratio (Table I) it is evident that the lower-momentum larger-angle spectrometer will always determine the limiting solid angle, whether it is set for electrons or protons. It is thus to our advantage to give the 6 GeV/c spectrometer a large acceptance solid angle. In fact, if θ (or θ_P) is reasonably large, say beyond 50°, $\frac{d\Omega}{d\Omega_P}$ (or its reciprocal) gets very large and most of the aperture in the forward spectrometer goes to waste. This, plus the fact that the large-angle particles have very much lower momenta, suggests that we could gain solid angle by substituting a 2 GeV/c spectrometer for the 6 GeV/c spectrometer when θ (or θ_P) $> 50^{\circ}$.

We propose to make each of the three spectrometers with two successive stages of momentum separation; that is, the first half will bring the trajectories to a momentum dispersion focus where the momentum defining slit (or counters) will be located, and the second half (the reverse of the first half) will re-focus achromatically to a unit-magnification image of the target.[13] Such a system is probably capable of better than 10^{-6} rejection outside the momentum passband.

1. The 20 GeV/c Spectrometer

A possible design is shown in Fig. 2. The bending angle ($\Phi = 17.2^{\circ}$ each stage) and overall scale are determined from the relations $SD = 33\ pd/B$ and $\Phi = d/D$. A lower limit for the dispersion d is given by the projected target width in a plane perpendicular to the trajectory at the largest scattering angle used with this spectrometer divided by the required momentum resolution (assuming each stage has approximately unit horizontal magnification). This gives $d \approx 3$ cm/% as a minimum dispersion, and $SD = 120\ m^2$ with, for example, $S = 12$ meters magnet length and $D = 19$ meters drift distance. The first quadrupole pair focuses at the symmetry plane of the system where the momentum defining slit is located. The horizontally defocusing quadrupole is placed first so that the solid angle aperture defined by the system will be elongated in the vertical direction and will therefore subtend a minimum interval in θ. Even so, the momentum range over this angular spread (11 mrad in our design) exceess the required 0.7% (see Table I) by a factor of about four. This means that in order to use the full magnet aperture we must preserve the momentum and angle correlation of the trajectories and recover the information with suitably placed counter hodoscopes or spark chambers. A horizontally focusing quadrupole is placed at the symmetry plane to reverse the sign of the angular displacement of the off-momentum rays so that the second half of the system can form an achromatic image of the target. Using the same 3 meter bending magnets (6-cm-high × 30-cm-side gap) and 2 meter quadrupoles (8 cm inscribed diameter) used in the switchyard we arrive at a system about 50 meters long having about 0.4 msr solid angle. This is not an optimized solution, and a more careful design to higher orders may require a somewhat more elaborate system. Nevertheless, it is hard to see how a 20 GeV/c (iron) spectrometer with the required resolution and solid angle could be made any smaller. One annoying difficulty will arise from the necessity of using this spectrometer at scattering angles closely approaching 0°, especially in the case of proton recoil detection. This can presumably be arranged by making holes in the sides of the first magnets to let through the main beam. Or, since most of the 0.4 msr solid angle will not be needed at the very small scattering angles, one can simply back away from the target to clear the main beam.

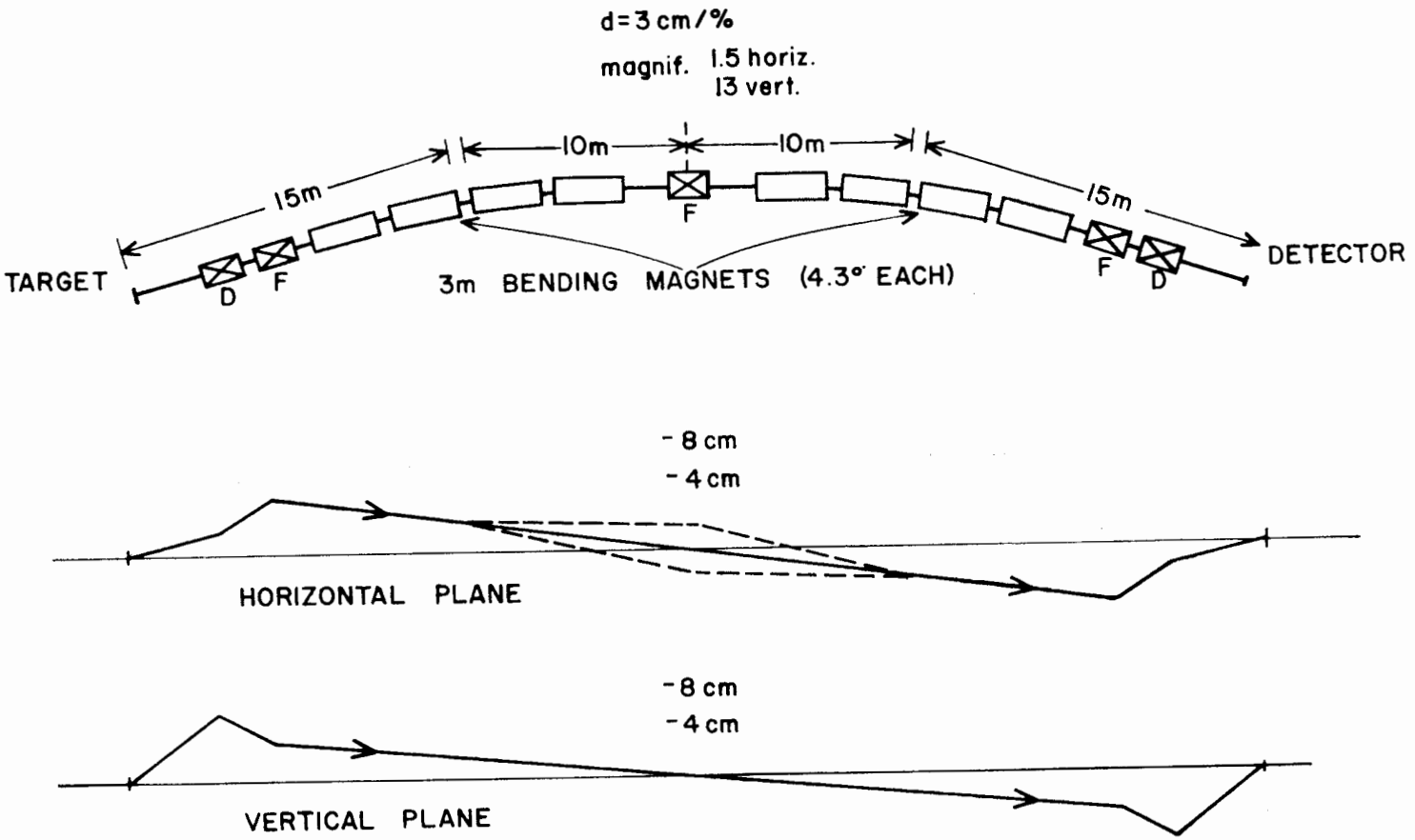

FIG. 2--Geometrical layout and optical ray diagrams for 20 GeV/c spectrometer.

2. The 6 GeV/c Spectrometer

To minimize the target width in the bending plane and hence the required dispersion, we propose to bend in the vertical plane. Then, using $d = 1$ cm/% we arrive at $SD = 12\ m^2$, or say $S = 3$ meters, $D = 4$ meters, and $\Phi = 14.4^\circ$ for minimal momentum resolution. We can eliminate the symmetry quadrupole and also keep the spectrometer from getting too high off the floor by reversing the direction of bend in the second stage. Rather than using an initial quadrupole pair for focusing, one might be able to increase the solid angle more economically using a strong-focusing bending magnet. A solid angle of at least 3 msr should be the goal. The overall length of the two-stage system will have to be at least 15 meters.

3. The 2 GeV/c Spectrometer

Here too, we can economize by bending in the vertical plane. Taking $d = 1$ cm/% again, we require $SD = 4\ m^2$, or $S = 2$ meters, $D = 2$ meters, $\Phi = 28.7^\circ$. This is again a minimum design. It is important to get as large a solid angle as possible (say 15 msr), so that it may be necessary to increase the dispersion to compensate the inevitable aberrations.

Table IV shows the counting rates expected.

TABLE IV

Coincidence counting rates (per second) for elastic e-p scattering based on the "no-core" model and assuming 10^{14} e/sec, 0.01 $r\ell$ hydrogen, and solid angles 0.4, 3, and 15 msr for the 20, 6, and 2 GeV/c spectrometers.

E = 20 GeV

θ	θ_p	e-spectrometer	p-spectrometer	Ω(msr)	R (sec^{-1})
3°	58°	20	2	0.13	10^6
10°	27°	20	6	0.4	100
30°	9.5°	6	20	3	0.1
90°	2.5°	2	20	15	0.004

These three spectrometers are certainly not a unique solution to the problem of measuring 20 GeV elastic scattering cross sections. It may turn out, for example, that the background rejection factor gained by counting the electron and proton in coincidence is sufficiently great to enable one to use single-stage spectrometers, especially for the recoil proton. On the other hand, it is clear that scaled up versions of some of the simple spectrometers used in "low-energy" scattering, such as the single quadrupole[14] or the solenoid,[15] do not have the required background rejection factor. A 180° double-focusing spectrometer for 20 GeV/c might do the job, but it is certainly not an economical solution.

The elastic e-p scattering spectrometers will of course be useful in other experiments: electron-proton scattering at lower energies (obviously the place to start in this field, perhaps using the 2 and 6 GeV/c spectrometers), positron-proton scattering, muon-proton scattering, electron-deuteron scattering, inelastic electron scattering, wide-angle pair production, and so on.

In conclusion, we have shown that e-p elastic scattering experiments are very probably feasible up to 20 GeV incident energies using straightforward, brute-force techniques. However, such experiments almost certainly require (1) a large experimental area (at least 80 meters long by 30 meters wide), (2) many magnets, (3) a major engineering effort, and (4) considerable running time. The interpretation of the results will most likely not be straightforward, but they will certainly be interesting.

III. INELASTIC E-P SCATTERING

A. Motivations

Assuming that a single photon is exchanged between the inelastically scattered electron and the nucleon system, it is convenient to express the inelastic cross section $\frac{d^2\sigma(E,E',\theta)}{d\Omega dE'}$ (integrating over all non-electron variables) in terms of the usual invariant q^2, the real-equivalent photon energy $k = q_o - q^2/2M$, and a third variable which can be chosen to represent the polarization of the virtual photon. Instead

of k, one could use the invariant $q \cdot P$ (P is the initial nucleon four-momentum).[3] The cross section $\frac{d^2\sigma}{d\Omega dE'}$ is expressible in terms of two functions of q^2 and $q \cdot P$ using Bjorken's generalization of the Rosenbluth formula.[3] These two inelastic "form factors" may well contain more interesting information on nucleon structure than the usual elastic form factors.

Looking at it another way, inelastic scattering enables us to study "photoproduction" cross sections with virtual, monoenergetic, polarized photons of variable (spacelike) mass--tagged by the recoiling electron. The effective intensity of this virtual photon beam can be estimated from the Bjorken-Weiszäcker-Williams formula,[10] and varies from 10^{-5} to 10^{-10} of the incident electron flux, depending on energy and angle. The intensities are low, but at small momentum transfers inelastic scattering may compete with other sources of monoenergetic polarized photon beams. The scattered energy spectrum might provide a convenient way of investigating the whole gamut of nucleon isobars.

B. Total Inelastic Spectrum Measurements

We consider first the detection of just the inelastically scattered electrons, measuring $\frac{d^2\sigma}{d\Omega dE'}$, as a function of E, E' and θ and making no restriction on the final state of the other particles. All of the problems encountered in the elastic experiment will still be with us; some will be considerably more formidable. Momentum resolution must be of the order of $\frac{\mu}{E}$ to resolve nucleon resonance structure. Rates should be comparable to those in elastic scattering at the same E and θ except where $E' \ll E'_{elastic}$, where they can become rather large. Since we commit ourselves to detection of the electron alone, we are already at a disadvantage relative to the elastic scattering experiment in background rejection. Neither will it be possible to reject the pion background by momentum selection, and a detector that can distinguish electrons in the presence of 10^6 as many pions of the same momentum is difficult to achieve. Moreover, for every 10^2 charged pions there will be a few neutral pions produced that will Dalitz decay in the target, producing electrons indistinguishable from inelastically scattered electrons. This alone is probably enough to make the inelastic electron experiment at 20 GeV impossible.

C. Electroproduction Coincidence Experiments

Coincidence counting of the inelastic electron and one or several of the other final-state particles can be used to improve background rejection as well as to increase the information output. The measured yields then involve at least two solid angle factors and will be correspondingly smaller than in the single-channel experiment. Unless the detection solid angles are quite large, this can be a severe limitation. It is possible, however, to choose kinematic situations for which the rates are comfortably large, since the dominant background (pions) really comes from the same process we are considering. The relatively large pion flux at angles $> 20^{\circ}$ comes mainly from low momentum transfer electroproduction events in which the inelastically scattered electron comes out at a rather small angle. One important experiment that can be done under these conditions is the measurement of the charge form factor of the pion.

Suppose, then, we consider the feasibility of measuring by e-π coincidence counting the cross section $\frac{d^3\sigma}{d\Omega dE' d\Omega_\pi}$ for the reaction $e^- + p \rightarrow e^- + n + \pi^+$, with the aim of determining $F_\pi(q^2)$. Only the diagram involving the interaction of the exchanged photon with a peripheral pion emitted by the proton (Fig. 3) contains a dependence on F_π, so that in general we must perform an extrapolation in θ_π to the unphysical pole angle at which the "target" pion becomes real. The residue is proportional to F_π^2 and independent of other contributing diagrams (isobar production, etc.).

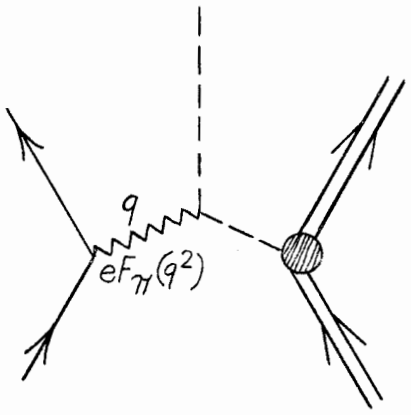

FIG. 3--The pion pole diagram in electroproduction.

The details of the extrapolation procedure have been discussed by Frazer.[16]

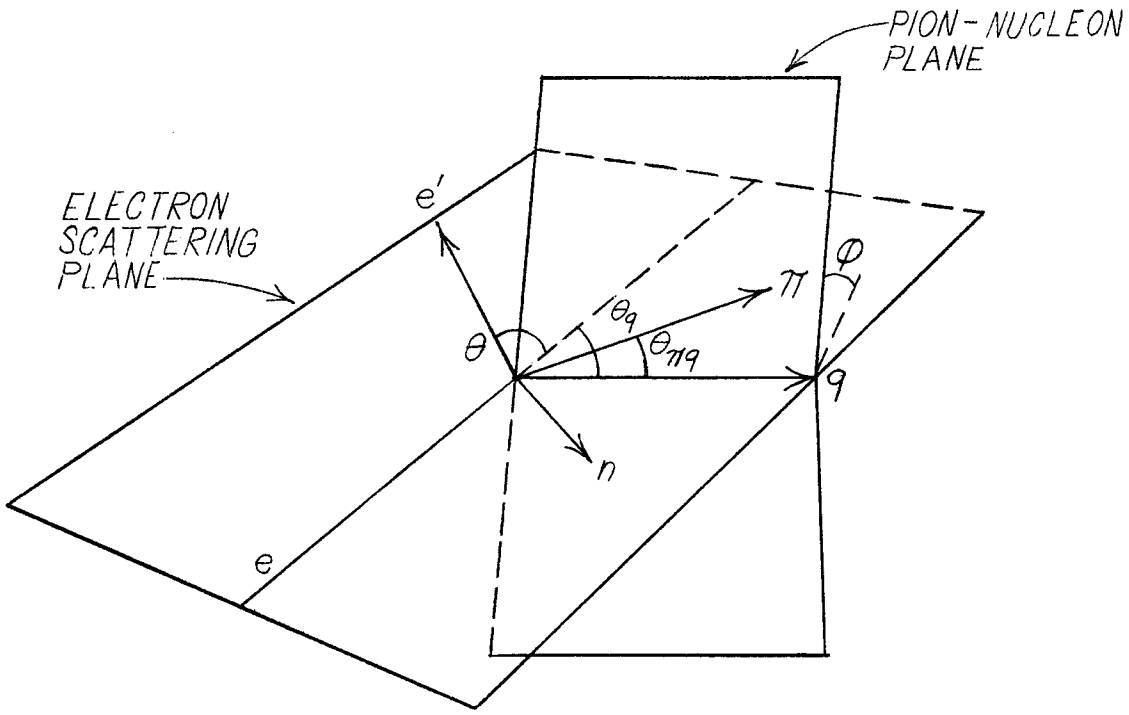

FIG. 4--Kinematic variables for electropion production.

Figure 4 illustrates the laboratory kinematic variables involved in the single electropion production reaction. θ_q is the angle between the momentum transfer direction ($\hat{q}$) and the beam direction, $\theta_{\pi q}$ is the angle between the pion direction and $\hat{q}$, and Φ is the angle between the π-n plane and the e-e' plane (these planes intersect along $\hat{q}$). As our five independent variables, let us choose the three electron-determined variables q^2, k, and θ_q (fixed by E, E', and θ) plus the two pion variables $\theta_{\pi q}$ and Φ. We pick q^2 to be the momentum transfer at which we wish to know $F_\pi(q^2)$, for example, $q^2 = 0.5\ (\mathrm{GeV/c})^2 = 12.5\ F^{-2}$. We chose $k \approx 0.5$ GeV to avoid both the isobar peak and the double pion electroproduction background. Since the virtual photon is polarized, the pion distribution is azimuthally asymmetric about $\hat{q}$; we must actually measure and extrapolate the quantity $\frac{1}{2}[d\sigma(\theta_{\pi q}, \Phi) + d\sigma(-\theta_{\pi q}, \Phi)]$. That is, we need the pion angular distribution on both sides of $\hat{q}$ in the π-n plane.

To avoid having to detect pions near the incident beam line we therefore chose $\Phi = 90^{\circ}$; the π-n plane is then perpendicular to the e-e' plane. The only remaining free variable, besides $\theta_{\pi q}$ over which we extrapolate, is θ_q . This we chose to be a maximum (42° for our choice of q^2 and k), thus fixing the incident energy at the highest possible (20 GeV). This choice also makes the electron angle a minimum (2.0° and hence maximizes the cross section $\frac{d^2\sigma}{d\Omega dE'}$ (2×10^{-29} cm^2/sr-BeV, roughly proportional to $1/\theta^4$). The scattered electron energy turns out to be 19.2 GeV. Counting rate is really the only reason for using such a high incident energy to do a low momentum transfer experiment. The actual rate will depend on the electron and pion detection solid angles and the electron momentum resolution. Assuming Ω = 0.1 msr and $\Delta E'$ = 0.1 GeV on the electron side we get a rate of 7000/sec integrated over all pion production angles (computed from the Bjorken-Weiszäcker-Williams formula[10]). A 1 msr pion detection system will then give an e-π coincidence rate the order of 1/sec. Good statistics should be easy to accumulate at many pion angles; this is necessary for a meaningful extrapolation.[16] Pion detection should not be very difficult, since the energies are all below 0.5 GeV. Such an experiment, while it may not actually be done in the way we have described, is clearly feasible.

LIST OF REFERENCES

1. M. N. Rosenbluth, Phys. Rev. 79, 615 (1950); F. J. Ernst, R. G. Sachs, and K. C. Wali, Phys. Rev. 119, 1105 (1960).
2. R. G. Sachs, Phys. Rev. 126, 2256 (1962).
3. J. M. Cassels, M Report No. 200-5, Stanford Linear Accelerator Center, Stanford University, Stanford, California (July 1960).
4. H. S. Butler, "Beam Transport Systems for Beam Switchyard" (unpublished).
5. S. Galster and G. Hartwig, "Kinematik der e-p-Streuung mit der erzeugung eines Pions im Bereich von 3 bis 6 Gev Elektronenergie," preprint KFK 168 , Karlsruhe (August 1963).
6. N. Meister and D. R. Yennie, Phys. Rev. 130, 1210 (1963).
7. L. Schwarcz (private communication).
8. Proceedings of the International Conference on Nucleon Structure, Stanford University, Stanford, California (June 1963).
9. K. Berkelman, M. Feldman, R. M. Littauer, G. Rouse, and R.R. Wilson, Phys. Rev. 130, 2061 (1963).
10. J. M. Cassels, Ref. 3, and L. N. Hand, Phys. Rev. 129, 1834 (1963).
11. G. B. Yodh and W.K.H. Panofsky, Phys. Rev. 105, 731 (1957).
12. S. Drell, M Report No. 200-7A, Stanford Linear Accelerator Center, Stanford University, Stanford, California; Equation (3)(August 1960).
13. See S. Penner, M Report No. 200-13, Stanford Linear Accelerator Center, Stanford University, Stanford, California (August 1960); or H. S. Butler (Ref. 4) for a discussion of this type of magnet system.
14. R. R. Wilson, K. Berkelman, J. M. Cassels and D. N. Olson, Nature 188 (1960).
15. R. Hofstadter et al., Proceedings of an International Conference on Instrumentation for High Energy Physics, Lawrence Radiation Laboratory, Berkeley, California (1960); p. 316.
16. W. R. Frazer, Phys. Rev. 116, 1763 (1959).

ELASTIC ELECTRON-PROTON SCATTERING
CHOICE OF ANGLES AND ENERGIES

by

R. Wilson

I. INTRODUCTION

This note is intended as a supplement to other studies of e-p scattering, particularly that by Berkelman (Section J of this report). Berkelman has shown that elastic scattering experiments are probably feasible at any angle and any energy up to 20 BeV. Since the experimental apparatus required is large, it is useful to look into a crystal ball and to guess what angular and energy regions are likely to be those at which experiments will start.

II. EXISTING THEORETICAL KNOWLEDGE

A. First Born Approximation

We have, for one photon exchange, the Rosenbluth formula, which expresses the differential cross section in terms of two form factors $G_E(q^2)$ and $G_M(q^2)$

$$\frac{d\sigma}{d\Omega} = \left[\frac{\alpha r_e m}{2E \sin(\theta/2)}\right]^2 \left\{\frac{E'}{E} \frac{\cot^2 \theta/2}{(1+t)} \left(G_E^2 + tG_M^2\right) + 2tG_M^2\right\} \qquad (1)$$

where $t = q^2/4M^2$ is the invariant 4-momentum transfer in convenient units.

We can, if we assume that one photon exchange (first Born approximation) is valid, take as our experimental goal the determination of $G_E(q^2)$ and $G_M(q^2)$ up to the highest possible momentum transfer. A set of tables of various kinematic factors, and of the coefficients of G_E and G_M in the above formula, has been computed for incident energies E up to 20 BeV and at selected angles by a computer program prepared by W. Shlaer of Harvard. The tables and the cards are available at SLAC.

B. Multiple Photon Exchange

The question then arises as to the possible deviations from the first Born approximation. If we are to design a meaningful experiment to

measure such deviations, it is a good idea to know what they are likely to be. Only preliminary indications are now possible. We will discuss briefly two lines of approach.

The first method (historically the second!) is to consider the crossed channel:

$$P + \bar{P} \rightarrow e^+ + e^-$$

We then express the angular distribution in this channel in spherical harmonics of the scattering angle $\Phi\left[P(\cos\Phi)\right]$. Now in the scattering channel, the scattering angle θ is given by

$$\cos\Phi = \sqrt{1 + \frac{\cot^2(\theta/2)}{(1+\ell)}} \qquad (2)$$

We note that a photon is 1^- and the ℓ value is then forced to 0 or 2. This gives an angular distribution $A + B\cot^2\theta/2$.

This is not a good way to see the separation into G_E and G_M, which is seen best by considering the helicity of the gamma ray. (The helicity and J separation is different from the L, J separation.)

This treatment is discussed in detail by Gourdin and Martin (CERN 3568/TH 261) and by Flamm and Kummer (Nuovo Cimento, 1963).

We note that as higher angular momenta in the crossed channel participate, higher powers of $\cos\Phi$ (and hence $\cot^2\theta/2$) appear. This, for constant q^2, means that the forward cross section goes as E^{ℓ}, a fact which we recognize as a last remnant of the Regge approach. As we shall see later, a behavior more singular than the Mott cross section is unpalatable. At forward angles enough partial waves must enter to cancel this singular behavior. [We see, for example, $1+s+s^2+\ldots=1/(1-s)$.] The method of considering the partial waves in the crossed channel is therefore only useful if we have some reason to imagine that one or another might predominate - by a resonant state in this channel, for example. It is useful up to a few angular momentum states only. The cross section including all

states 0^+, 0^-, 1^+, 1^-, 2^+, is of the form

$$\frac{d\sigma}{d\Omega} = \left[\frac{\alpha r_e m}{2E \sin(\theta/2)}\right]^2 \frac{E'}{E}\left\{A + B\cot^2\left(\frac{\theta}{2}\right) + \left[C + D\cot^2\left(\frac{\theta}{2}\right)\right]\sqrt{1 + \frac{\cot^2\theta/2}{(1+t)}}\right\} \tag{3}$$

The term A includes the G_M^2 term, terms from 0^-0^+ and 1^+ exchange which add without interference. B is the G_E^2 term (unaltered). C and D arise respectively from 1^+1^- interference and 2^+1^- interference. We note that the singular behavior implied by the constant D must be damped somewhat at forward angles; this was already recognized by Gourdin and Martin who limited themselves to angular momentum change 1. We may, however, include a $J = 2$ state, provided we realize that it must be damped at small angles.

What conclusions can we draw? If we have a resonance in one or another of the low angular momentum states considered, then we can expect a large contribution to the scattering. Thus for a 2^+ resonance (Fig. 1) the coefficient D in Eq. (3) becomes large (and is presumably cancelled at small angles).

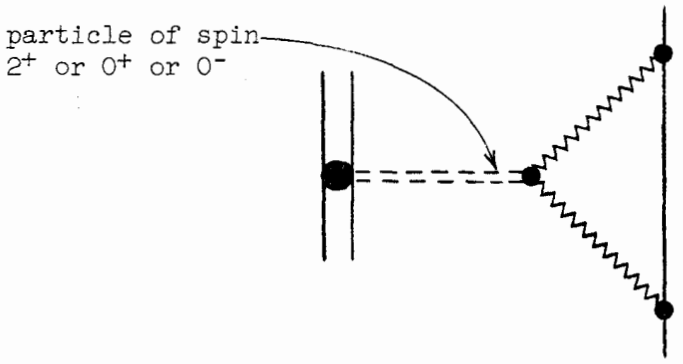

Fig. 1

The second way of considering corrections to first Born approximation is to attempt some general relation at forward angles. These have been considered by Drell and Pratt [Physical Review 125, 1394 (1962)] and give,

in addition to the leading term,

$$\frac{d\sigma}{d\Omega} \approx \frac{1}{2E^2 \sin^4\theta/2} \approx \frac{1}{q^2} \qquad (4)$$

a term $\approx 1/E$.

So that, overall, we find

$$\frac{d\sigma}{d\Omega} \approx \frac{1}{q^2}\left(1 \pm H\frac{q^2}{E}\right) \approx \frac{1}{q^2}\left(1 \pm H\,\theta\sqrt{q^2}\right) \qquad (5)$$

Equation (5) shows that the higher terms are <u>smaller</u> at small angles, and <u>not</u> larger as the expansion in partial waves of the crossed channel indicate. This shows that we must be cautious about using the Gourdin and Martin results. We can <u>hope</u>, however, that any unusual (e.g., resonant) enhancement of multiphoton exchange processes occurs in a specific angular momentum state in the crossed channel, as discussed above.

III. CHOICE OF ANGLES - ONE PHOTON EXCHANGE

Let us consider the first goal at 3 values of the momentum transfer; q^2 = 100, 500, 900 fermi^{-2}, for which $q^2/4M^2 \approx (1.1, 5.5, 10)$ using kinematic tables of Shlaer and Wilson which tabulate the coefficients of G_M^2 and G_E^2.

We now have to consider the probable extrapolations of known numbers for G_E and G_M. They were last seen separately at $q^2 = 45$ f^{-2} and were $G_M = 0.24$, $G_E = 0.16$. G_M was falling as $1/q^2$.

If $G_E = G_M/\mu$ we have no hope of separating the form factors. At $q^2 = 100$ f^{-2} G_E could only contribute 10% of the cross section at the forward angles (where it appears in the term $G_E^2 + q^2/4M^2\ G_M^2$); at higher momentum transfers the situation is worse.

If $G_M \approx G_E$, then we can see that angles beyond 90° give little extra information, for the coefficient of G_E^2 is vanishingly small.

If G_E = const as $G_M \to 0$, then we need to measure at backward angles,

too, to separate the contributions adequately.

We may now consider the most forward angles at which we will wish to carry out experiments. No gain is obtained by going to a more forward angle than that which gives the whole cross section contribution in the term $G_E^2 + q^2/4M^2\, G_M^2$. If G_E is much larger than G_M, this is quite a backward angle. If G_E is small compared with, or of the order of, G_M, then we get the criterion $\cot^2 > 2(1 + q^2/4M^2)$. For the detailed numbers, we may examine once more the coefficients of G_E^2 and G_M^2. We note that there is only a 10% gain in measuring forward of 30° at 150 fermi^{-2}, if $G_M \approx G_E$. At $q^2 = 600$ fermi^{-2} it is impossible, kinematically, to achieve a 20° angle with 20 BeV.

At $q^2 = 540$ fermi^{-2}, there is a 20% gain in measuring at 20° instead of 30°. We regard this for the moment as insignificant. Even at 20°, the scattered electron energy (for 20 BeV in) is only 8.7 BeV. Thus we can take 10 BeV maximum scattered electron energy, and 15° minimum angle for our design criteria for spectrometers to measure elastic e-p scattering, if our goal is to compare G_M and G_E and assume one photon exchange.

IV. CHOICE OF ANGLES - MANY PHOTON EXCHANGE

Now we wish to consider how these conclusions are altered by many photon exchange terms. The conclusion that backward angles contain little information is only altered if there is a <u>reduction</u> in the coefficient A of Eq. (3) so that to determine A we have to make $\cot^2(\theta/2)$ ever smaller; or else if a term in $\cot(\theta/2)$ or $\cot^{-1}(\theta/2)$ were to appear. The first <u>cannot</u> occur from 0^+ and 0^- angular momentum exchange, for Gourdin and Martin have shown that there is no interference; the terms <u>add</u> to G_M^2. But the term C from $1^+\,1^-$ interference has almost the same angular distribution and can reduce the cross section at wide angles.

The extra term D in Eq. (3) blows up at small angles. But very precise measurements would be needed even there to gain much information. At $E' = 235$ fermi^{-2} measurements at 10° are just possible, but the D term will only be a factor 2 bigger than at 20°.

Some of these points will be clearer after more experimental work at the CEA. If, for example, it transpires that the backward angle cross

section holds up, in accordance with expectation, then backward angle scattering will not be a high priority.

V. INELASTIC ELECTRON SCATTERING

Now we must consider inelastic electron scattering. There is one class of inelastic scattering experiments which demand a high energy spectrometer: those where the energy transferred is small and the 4 momentum small. We will assume that these are better done at CEA where the duty cycle is better; the intensity is unlikely to be important. Other classes of experiments need lower energy spectrometers and need not be considered.

VI. POSITRON SCATTERING

The above paragraphs have considered multiphoton exchange. It is clear that it is hard to make a clean separation of single and multiphoton exchange terms by angular distributions alone. Positron scattering is going to be a powerful tool for separating these.

The intensity is likely to be low, so that the experiments will probably not be done much above $q^2 = 300$ fermi^{-2}. A high energy spectrometer would therefore be required even less than for electrons.

VII. PROTON POLARIZATION EXPERIMENTS

To separate the many photon exchange we may want to detect the proton in a spectrometer and then measure its polarization. The analyzing power for a polarimeter is likely to be low for any energy above 1 BeV, and another solid angle factor reduces counting rate. A reasonable limit of $q^2 = 100$ fermi^{-2}, (proton energy 2 BeV; proton momentum 3 BeV/c) can thus be set.

VIII. CHOICE OF DETECTION METHOD

The above choice of angles makes no mention of the particular method of detection - detecting the electron, the proton or both. Berkelman showed that in order to separate elastic from the production of π mesons,

one needs 0.1% resolution for electron detection and 0.01% for proton detection.

It is not necessary, however, to have a complete separation, provided that the background is small. The background (of inelastically scattered electrons exciting the N^* resonance) is appreciable for electron detection at $q^2 = 50$ fermi^{-2} (CEA measurements). For proton detection the background is due to recoil protons from neutral meson (π^o, η^o, ρ^o) production and is small for small electron angles where the cross section is adequate. If a 1% momentum interval is accepted, and neutral meson production is about the same as at 1 BeV, the background can be calculated to be equal to the effect at $E_{incident} = 20$ BeV and $q^2 = 150$ fermi^{-2}. The recoil proton momentum is 3 BeV/c. Use of proton detection, in this region of small electron scattering angles, has been made by Dunning, et al. (Phys. Rev. Lett. 1963). If interest does develop again in scattering in these angles, in order to look for a 2^+ state or otherwise, some experiments can be done with proton detection.

If we decide to detect electrons only, we will wish to have a spectrometer of 0.1% resolution, of 6 BeV. Pions will count only by producing cascades in the shielding, because they cannot have as high a momentum as elastically scattered electrons. A combination of a gas Cerenkov threshold counter and a shower counter can discriminate against pions, to a factor of 20 or so each (total 400). At 20^o, 30^o electron scattering angles, there is likely to be no problem. At 90^o scattering angles, however, we may expect difficulty.

Background may also be reduced by a coincidence. Pion emission along the direction of one of the particles can still be detected unless there is some energy resolution, but again this is not important if the background is small.

We may anticipate a need for a coincidence for backward electron scattering. The proton, now, will have a high momentum; at $q^2 = 600$ fermi^{-2} $\theta_{electron} = 90^o$ the proton momentum is 13.36 MeV and the angle 3.76^o. We may, however, be able to get away with quite a crude spectrometer, forming in the vertical direction only and displaying the scattering angle.

This second spectrometer should reject wrong sign particles (electrons) by a factor of about 10^6, and π mesons from the Drell process. The

former is quite easy, as the radiation length for electrons is quite low. The latter can also be done quite well at large electron scattering angles, for the recoil proton will then have a larger momentum than any possible π meson.

IX. CONCLUSION

A spectrometer of 6 BeV/c, solid angle 5 msr 0.1% resolution is the most important spectrometer to design now. The method of detecting electrons to separate them from the junk (perhaps pi mesons) is not easy to specify. A double magnet system, as proposed by Berkelman, will help; but it is not yet clear that a combination of a gas Cerenkov counter and total energy shower counter, as used at CEA, will not eventually prove adequate.

A second spectrometer of 15 BeV/c, 2% resolution, is useful to add for coincidence experiments only. These will probably be needed for electron scattering through angles of 90° or more and for electron scattering from the deuteron.

This conclusion differs from that of Berkelman who proposed a 20 BeV/c 0.1% resolution spectrometer at the start.

PHOTOPRODUCTION OF μ PAIRS AND e PAIRS AT SLAC

by
R. Wilson

I. GENERAL

One of the most elegant experiments at the Cambridge Electron Accelerator, and in principle one of the most simple, is the photoproduction of μ pairs ably performed by Weinstein, Kendall and Friedman. It is the purpose of this brief note to consider whether an extension to SLAC energies is sensible and possible. This can be done with more certainty than considering an experiment from scratch, because one can make comparisons with existing experience.

In their experiment, Weinstein, Kendall and Friedman bombarded a carbon target with the bremsstrahlung beam from CEA. The angles and energies of the muons were measured by two scintillation counter hodoscopes and two sets of range counters. The geometry was such that the two muons were produced nearly symmetrical to the photon direction, with the angle between the muon and photon direction varying between 3.5 and 11.5 degrees. Most of the background was removed by the large amounts of iron shielding placed between the target and the counters.

We assume, for simplicity, that the energy E of each muon is equal to half of the incident photon energy, and that both of the muons are produced coplaner with, and at angles $\pm\theta$ to, the incident photon direction. The cross section then varies as $\sigma \approx 1/E^4\theta^6$, the four-momentum to the target varies as $q^2 \approx E^2\theta^4$, and the four-momentum of the virtual muon as $T^2 \approx E^2\theta^2$. We can now compare a SLAC experiment with the Weinstein experiment. If we keep T^2 constant (i.e., an experiment of the same usefulness for quantum electrodynamics),

$q^2 \approx T^4/E^2$	goes down a factor of 10 relative to Weinstein,
$\theta \approx 1/E$	goes down a factor of 3,
$\sigma \approx E^2/T^6$	goes up a factor of 10.

The fact that q^2 goes down is good, for the form factors of the proton are less important. With a factor of 100 increase in intensity at SLAC,

the counting rate is up a factor of 1000.

If we keep our angle equal to that of Weinstein, the cross section goes down by a factor of 100. However, the counting rate remains constant due to the increase in beam intensity. Then both T^2 and q^2 increase by a factor of 10 (we note that T^2 will then reach a value equal to 10 times the square of the ρ mass). The increase in q^2 does not cause any problem for pair production in hydrogen, as the form factors are well known. It seems unlikely, however, that pair production in beryllium or carbon would still be possible at the higher q^2. If the geometry is such that a long hydrogen target is possible, there is no loss in using hydrogen.

II. BACKGROUNDS

The room background is not important at CEA and could be much reduced if it were; at SLAC three times the iron absorber is necessary and the background can be much reduced, which should compensate for the duty cycle and the increased intensity of the two-mile accelerator.

The pion background is likely to occur dominantly as π pairs; in any case, as this occurrence would be more serious, single π mesons will be neglected. The π pairs will count by each member of the pair decaying in flight into a μ. The best rejection one can achieve in any experimental situation is the ratio of the absorption length of π mesons (10 cm) to the decay length (= 600 cm $\times$ E/140 MeV). This is about $10 \text{ cm}/(3.6 \times 10^4 \text{ cm}) = 3 \times 10^{-4}$ for E = 8.5 BeV. Because we have two particles, the net μ coincidence rate by decay is 10^{-7}. We expect the two-π production to be resonant (by a ρ meson or otherwise) and two μ's to be produced in 3×10^{-5} collisions.[1] Thus the genuine μ pair rate from strong interactions will dominate the rate from decay in flight.

In the real experiment the situation is worse. A space must be allowed between the target and the absorber to allow a finite size target, and still keep an adequate definition in θ. (Varying this space varies the decay and allows a correction to be made.) The exact criterion here is hard to define. As compared to Weinstein, the scattering angle would

be the same (and the acquired definition comparable); the energy of the μ mesons is greater, so that multiple scattering need not limit. Thus our background rate from two-π production is 10^{-5} for a decay distance of 1 meter. Clearly there is no advantage in reducing the rate of counting of π pairs to less than the rate of the accompanying weak two-μ decay.

The $\gamma \rightarrow \rho$ rate will not appreciably increase as a function of energy whether it is due to one-pion exchange or diffraction. This we see by examination of Equations 29 and 33 of Berman and Drell.[2] The angles at which the resonant contribution will appear will go down as $1/E$, and the cross section $\gamma \rightarrow 2\pi$ will therefore go up as E^2 (Berman and Drell Equation 43) just as the μ pair cross section does at these angles. This leads to the almost obvious conclusion that the $\gamma \rightarrow 2\pi$ background varies with energy as the $\gamma \rightarrow 2\mu$ background if we adjust θ to keep the virtual μ four-momentum (T^2) constant.

Nonresonant two-π states will give appreciably smaller cross sections, which are negligible compared with the $\gamma \rightarrow 2\mu$ cross section.

III. APPARATUS

The apparatus for the μ pair experiment is simple and is shown in Fig. 1. It consists of a liquid hydrogen target 10 inches long, irradiated by gamma rays only (so that boiling is no problem), and two steel absorbers, with spark chambers to define θ and range interspersed with the iron. The whole is to be triggered by any pair of long range. Although Weinstein's existing apparatus (which has a scintillation counter hodoscope) could be used, spark chambers are probably preferable if one starts from scratch.

IV. CONCLUSIONS

A μ-pair experiment could be designed for μ which would measure QED a factor $\sqrt{10} = 3.2$ better than the CEA measurements. The CEA experiments will carry our knowledge of the μ propagator to about 3×10^{-15} cm before they are complete; this experiment would therefore

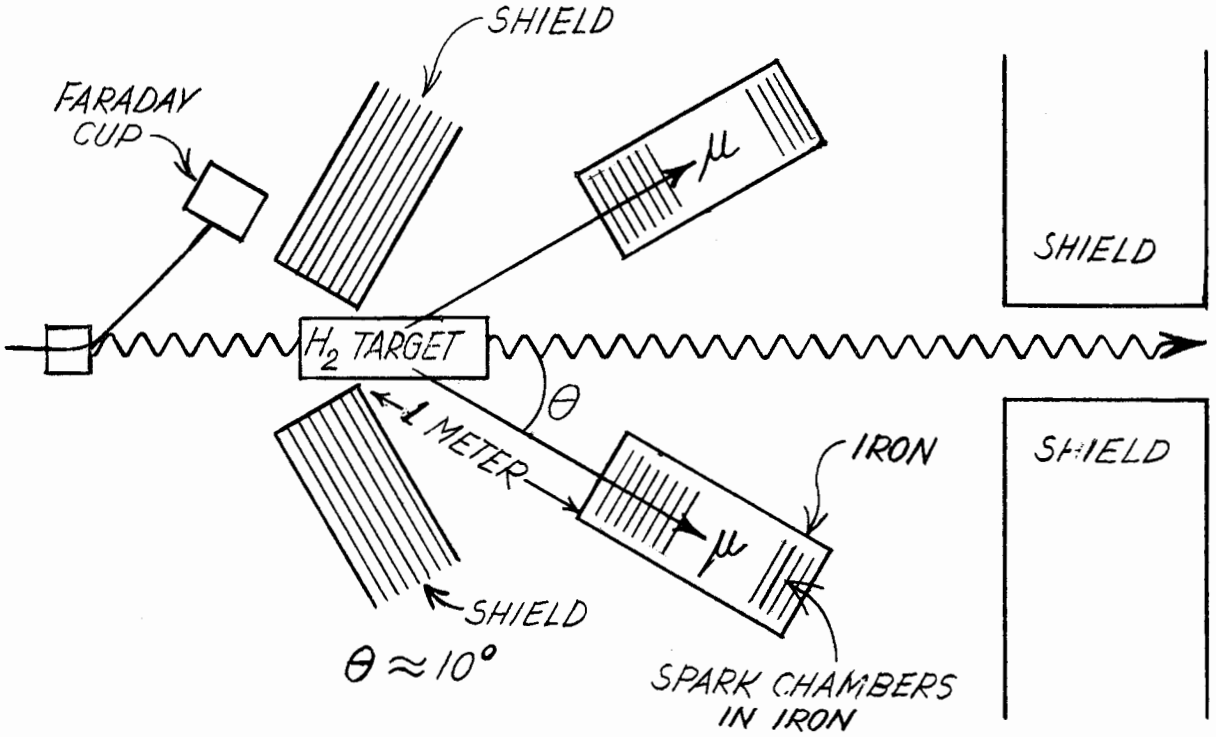

FIG. 1--Apparatus for μ pair experiment.

go to about 8×10^{-16} cm. The four-momentum of the virtual μ line is already greater at CEA than the ρ mass, and no effect of the weak decay of the ρ is found. If other resonant two-π states exist, a two-π background might interfere with the experiment, but this interference could give real μ pairs in such a way that the effect is indistinguishable from a breakdown of QED.

V. COMPARISON WITH OTHER QED CHECKS

Other experiments to study colliding beams include:

1. 3 BeV e^+e^- storage ring, μ pair production at 90°; this will study the photon propagator to about 5×10^{-16} cm.

2. Comparison of μ,P scattering and e,P scattering. There are two suggestions: (a) straightforward, by Masek; and (b) with a μ storage ring, by Tinlot.[3] The second would make it possible to measure up to $q^2 = 400$ fermi^{-2} ($\sqrt{q^2} = 20$ fermi^{-1}) and the first up to

$q^2 = 200$ fermi^{-2}. With a 10 percent measurement these will extend the knowledge of the $\mu\gamma$ vertex to 3×10^{-15} cm.

The μ pair experiment would not only provide limits on QED of comparable precision to the other possible experiments, but it also measures a different parameter.

An extension of these arguments to e^+e^- pairs depends upon the ability to separate e from π by the same factor of 10^3 in each particle. Pipkin at CEA is attempting this (Fall 1963), and his experiments will aid in this understanding.

Silverman[4] discussed wide angle electron pair production. The detection apparatus in use at CEA is similar to that he discusses — a gas Cerenkov threshold counter plus a shower counter. He neglects, as we did at first, the efficiency of the Cerenkov counter for π mesons by δ ray production. Contrary to Silverman's impression, it is not yet clear that the problem of electron detection is easily soluble. Dalitz pairs, considered by Silverman, will not have as large a pair angle as those considered here and can only contribute to random coincidences.

LIST OF REFERENCES

1. M. Gell-Mann, R. Sharp and W. Wagner, Phys. Rev. Letters 8, 261 (1962).
2. S. M. Berman and S. D. Drell, "Speculations on the production of vector mesons" (to be published in The Physical Review).
3. W. Chinowsky, J. DeWire, D. Lichtenberg, G. Masek, J. Muray, M. Perl, M. Schwartz, J. Tinlot and G. Trilling, "Some aspects of the prospective experimental use of the Stanford two-mile accelerator," SLAC Report No. 5, Stanford Linear Accelerator Center, Stanford University, Stanford, California (Summer 1962).
4. A. Silverman, SLAC Report M-285, Stanford Linear Accelerator Center, Stanford University, Stanford, California (August 1961).

PAIR PRODUCTION OF VECTOR BOSONS IN THE COULOMB FIELD OF A NUCLEUS

by

J. Mathews*

The total cross section for the reaction

$$\gamma + Z \rightarrow Z + W^+ + W^- \tag{1}$$

has been evaluated to lowest order in e^2, by standard methods of perturbation theory. The kinematics have been simplified slightly by assuming that the nucleus is infinitely heavy, so that it can take up momentum but no energy.

With this assumption, the cross section for reaction (1) is

$$\sigma = \frac{Z^2 \alpha^3}{4k_o^2} \int d(Q^2) \int d(S^2) \int dx \frac{[F(Q^2)]^2}{Q^4} \frac{1}{S^2 - Q^2} \Sigma |M|^2 \tag{2}$$

where our notation is as follows:

Four-momenta of γ, W^+, and W^- are k, q_+, q_-, respectively

Our metric is such that $k^2 = 0$, $q_+^2 = q_-^2 = m^2$

k_o is the photon laboratory energy

Q is the recoil four-momentum: $Q = q_+ + q_- - k$

(note that $Q^2 < 0$)

S is the total four-momentum of the W pair: $S = q_+ + q_-$

$x = k \cdot q_+$

$F(Q^2)$ is the form factor of the Coulomb field; $F(0) = 1$

$\Sigma |M|^2$ is the square of the invariant Feynman matrix element, summed over all spins and polarizations

$\alpha = \frac{e^2}{4\pi} \approx \frac{1}{137}$

---

*California Institute of Technology, Pasadena, California.

The limits of integration in Eq. (2) are:

$$-\left(k_o + \sqrt{k_o^2 - 4m^2}\right)^2 < Q^2 < -\left(k_o - \sqrt{k_o^2 - 4m^2}\right)^2$$

$$4m^2 < S^2 < Q^2 + 2k\sqrt{-Q^2}$$

$$\left(\frac{S^2 - Q^2}{4\sqrt{S^2}}\right)\left(\sqrt{S^2} - \sqrt{S^2 - 4m^2}\right) < x < \left(\frac{S^2 - Q^2}{4\sqrt{S^2}}\right)\left(\sqrt{S^2} + \sqrt{S^2 - 4m^2}\right)$$

A (nearly) trivial azimuthal integral has been omitted from Eq. (2); it is of the form

$$\oint d\varphi \, (A + B \cos \varphi + C \cos^2 \varphi) = 2\pi \left(A + \frac{1}{2} C\right) \qquad (3)$$

The factor 2π of Eq. (3) is included in the formula (2).

If the magnetic moment coupling of photons and vector mesons is separated from their charge coupling, there are nine Feynman diagrams contributing to reaction (1), namely:

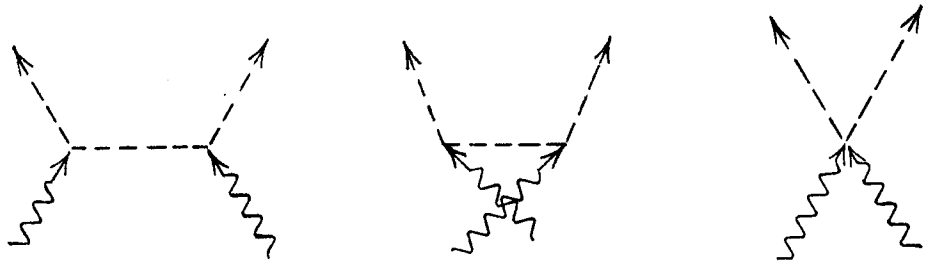

I II III

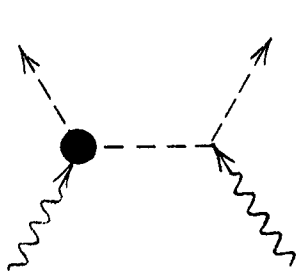

IV

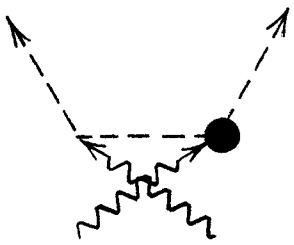

V

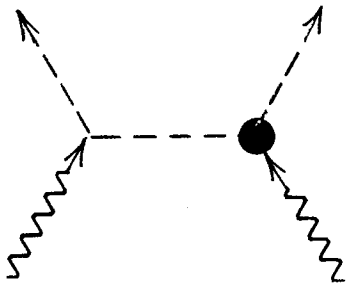

VI

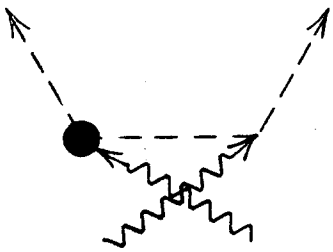

VII

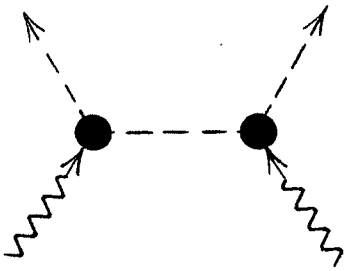

VIII

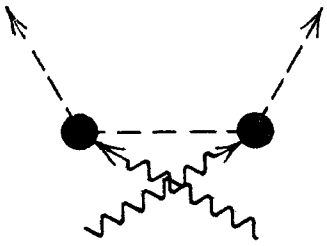

IX

The three different vertices are as follows:

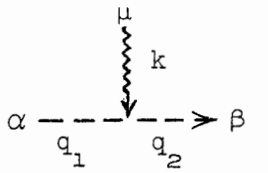

$$(q_1 + q_2)_\mu \, \delta_{\alpha\beta} - q_{1\beta} \, \delta_{\mu\alpha} - q_{2\alpha} \, \delta_{\mu\beta}$$

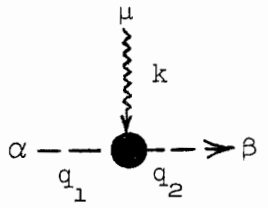

$$\kappa \, (k_\beta \, \delta_{\mu\alpha} - k_\alpha \, \delta_{\mu\beta})$$

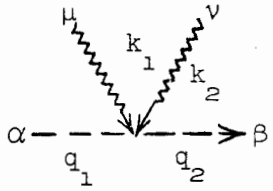

$$- 2 \, \delta_{\mu\nu} \, \delta_{\alpha\beta} + \delta_{\mu\alpha} \, \delta_{\nu\beta} + \delta_{\mu\beta} \, \delta_{\nu\alpha}$$

The virtual vector meson propagator is, as usual, given by

$$\left(\delta_{\alpha\beta} - \frac{q_\alpha \, q_\beta}{m^2} \right) \, (q^2 - m^2)^{-1}$$

The squaring and summing over spins was performed by an algebra program written for the IBM 7090 by the author and Dr. J. Shirley. The integrals in (2) were done numerically on a 7090.

The form factor $F(Q^2)$ was that used by Berman and Tsai:[1,2]

$$F(Q^2) = \frac{4\pi^2 \, \rho_o \, c \, z}{\sqrt{-Q^2}} \left[\frac{\pi z}{c} \sin \left(c \sqrt{-Q^2} \right) \cosh \left(\pi z \sqrt{-Q^2} \right) \right.$$

$$\left. \times \operatorname{csch}^2 \left(\pi z \sqrt{-Q^2} \right) - \cos \left(c \sqrt{-Q^2} \right) \operatorname{csch} \left(\pi z \sqrt{-Q^2} \right) \right]$$

where

$$\rho_o = \frac{3}{4\pi c^3} \frac{1}{1 + (\frac{\pi z}{c})^2}$$

$$c = 1.07\ A^{1/3} \times 10^{-13}\ \text{cm}$$

$$z = 0.568 \times 10^{-13}\ \text{cm}$$

The actual calculations were for iron: Z = 26, A = 56.

The cross section may be written in the form

$$\sigma = A + B\kappa + C\kappa^2 + D\kappa^3 + E\kappa^4$$

We computed A, B, C, D, E separately; the results are given below in cm^2 [9.46 (-37) means 9.46×10^{-37}].

	A	B	C	D	E
m = 0.6 BeV					
k_o = 3.0 BeV	9.46 (-37)	1.26 (-36)	2.80 (-36)	2.67 (-36)	2.70 (-36)
6.0	1.42 (-34)	1.96 (-34)	4.61 (-34)	4.72 (-34)	4.82 (-34)
10.0	4.66 (-33)	6.10 (-33)	1.44 (-32)	1.49 (-32)	1.51 (-32)
20.0	1.00 (-31)	8.91 (-32)	2.27 (-31)	1.93 (-31)	2.55 (-31)
m = 0.8 BeV					
k_o = 3.0	9.85 (-40)	1.14 (-39)	2.50 (-39)	2.14 (-39)	2.20 (-39)
6.0	1.75 (-36)	2.70 (-36)	6.18 (-36)	6.63 (-36)	6.18 (-36)
10.0	5.24 (-35)	7.07 (-35)	1.66 (-34)	1.72 (-34)	1.75 (-34)
20.0	5.08 (-33)	6.26 (-33)	1.48 (-32)	1.50 (-32)	1.57 (-32)
m = 1.0 BeV					
k_o = 3.0	4.03 (-43)	3.85 (-43)	8.20 (-43)	5.40 (-43)	5.69 (-43)
6.0	1.68 (-38)	2.56 (-38)	5.71 (-38)	6.00 (-38)	5.53 (-38)
10.0	1.81 (-36)	3.07 (-36)	7.05 (-36)	7.70 (-36)	7.18 (-36)
20.0	2.01 (-34)	2.96 (-34)	6.92 (-34)	7.49 (-34)	7.15 (-34)
m = 1.4 BeV					
k_o = 4.0	5.27 (-47)	4.56 (-47)	8.93 (-47)	4.90 (-47)	4.77 (-47)
6.0	9.51 (-43)	1.17 (-42)	2.31 (-42)	2.01 (-42)	1.78 (-42)
10.0	1.33 (-39)	2.15 (-39)	4.72 (-39)	5.08 (-39)	4.45 (-39)
20.0	1.19 (-36)	1.88 (-36)	4.35 (-36)	4.82 (-36)	4.43 (-36)

Work is continuing on the pair production of $W^{\pm}$ from protons, from spin-zero charged particles; and the inclusion of electric quadrupole terms in the photon-vector boson interaction.

The author would like to acknowledge the support of the Radio Corporation of America.

LIST OF REFERENCES

1. S. M. Berman and Y. S. Tsai, Phys. Rev. Letters (to be published).
2. S. M. Berman (private communication).

SLAC-25 (Part Two)
UC-28, Particle Accelerators
and High-Voltage Machines
UC-34, Physics
TID-4500 (31st Ed.)

1963 SUMMER STUDY REPORT

PART TWO

Summer 1963

by

L. Hand and R. Wilson
Cambridge Electron Accelerator
Harvard University
Cambridge, Massachusetts

Technical Report
Prepared Under
Contracts AT(04-3)-400 and AT(04-3)-476
for the USAEC
San Francisco Operations Office

Printed in USA. Price $1.50. Available from the Office of Technical Services, Department of Commerce, Washington 25, D.C.

TABLE OF CONTENTS

Section A: "Inelastic Electron-Proton, Positron-Proton, and Muon-Proton Scattering" by L. Hand and R. Wilson

		Page
I.	Introduction	1
II.	General theory	2
III.	The equivalent radiator	4
	A. Region I: Dalitz and Yennie limit	5
	B. Region II: $pp' > (450\ \mathrm{MeV})^2$	6
IV.	Polarization of the virtual photons	9
V.	Backgrounds for inelastic electron scattering	10
VI.	Classes of experiments	10
	A. Study of total inelastic cross sections	11
	B. Study of the nucleon resonances	14
	C. Study of peripheral processes by electroproduction	14
VII.	Relation to nuclear physics	14
Appendices:		
	A: Derivation of one-photon exchange formula	17
	B: Integration over scattered electron angles	26
	C: Some useful kinematic formulae for inelastic scattering	29

Section B: "Electroproduction at SLAC" by L. Hand

I.	Introduction	31
II.	The physics of virtual photons	33
III.	Counting rate for $1^\circ < \theta < 2^\circ$ detector	39
IV.	Backgrounds causing accidental coincidences	39
V.	Electron-electron scattering: restriction on t	43
VI.	Second-order effects in X: electron detector	44
VII.	First- and second-order backgrounds in the secondaries detector	45
	A. First-order processes	46
	B. Second-order processes	53
	C. First-order figure of merit for a real photon beam	57

TABLE OF CONTENTS - (Continued)

	Page
VII. Summary and preliminary design objectives	59
Appendices:	
I. Brief summary of proposed photon sources	65
II. Frisch's scheme for tagging photons at the CEA . .	67

INELASTIC ELECTRON-PROTON, POSITRON-PROTON, AND MUON-PROTON SCATTERING

by

L. Hand and R. Wilson

I. INTRODUCTION

The first ideas about experiments in inelastic electron-proton scattering date from 1951.[1,2] In those days it seemed obvious that the experiments on elastic electron-nucleus and electron-proton scattering would be finished within a year or so, and extensions were therefore worth seeking. It was realized, even then, that inelastic scattering would be a more difficult and extensive programme than elastic scattering.

The first experiments were conceived in analogy with internal conversion in nuclear spectroscopy. It was hoped that by measuring the ratio of electron- to photon-produced interactions, one could measure the multipolarity of the transition. The first experiment was an attempt to measure directly the multipolarity of the giant resonance — at that time assumed to be entirely an electric dipole resonance — by detecting induced radioactivity. The first work was performed on Stanfor University's Mark II accelerator. Unfortunately, the differences between multipolarities were small. Similar experiments were planned for electropion production for the Mark III accelerator, to establish beyond doubt that the first nucleon resonance was excited by a magnetic dipole transition. The experiments were done by detecting the produced pions, but the aim was not achieved.[3]

In discussing this experiment, Dalitz and Yennie[4] produced the first theory of electropion production, and showed that the major interest lies in cases where the electron has scattered with an appreciable momentum transfer. Following this, experiments have been performed by detecting the scattered electron only,[5,6,7] and the theory has been generalized somewhat.[7,8] Also, specific calculations for electro- and photoproduction of pions near the first resonance have been made.[9,10,11] Extensions to inelastic electron-nucleus scattering are similar and are summarized by W. C. Barber.[12]

II. GENERAL THEORY

In this section the relation of electroproduction to photoproduction cross sections will be recapitulated. The notation of Hand[7] will be used; it may be regarded as a generalization of the earlier Weiszacker-Williams calculations in terms of virtual photons.

The cross section for electroproduction (within the approximation of one-photon exchange) can be expressed in the following form (see Appendix A):

$$\frac{d^2\sigma}{d\Omega dE} = \Gamma_T(q^2,K)\sigma_T(q^2,K) + \Gamma_o(q^2,K)\sigma_o(q^2,K) \qquad (1)$$

where, for $q^2 \gg 4m^2$ (m is the electron rest mass),

$$\Gamma_T = \frac{\alpha}{4\pi^2}\frac{K}{q^2}\frac{E'}{E}\left[2 + \frac{\cot^2\theta/2}{1 + (\Delta E)^2/q^2}\right]$$

$$\Gamma_o = \frac{\alpha}{4\pi^2}\frac{K}{q^2}\frac{E'}{E}\left[\frac{\cot^2\theta/2}{1 + (\Delta E)^2/q^2}\right]$$

The square of the four-momentum transfer is $q^2 = 2EE'(1 - \cos\theta)$; E, E', and θ are incident and final electron scattering energies in the lab, and θ is the scattering angle; $(\Delta E)^2$ is the square of the energy transferred ($\Delta E = E - E'$).

The laboratory photon energy, $K = E - E' - q^2/2M$, produces the same center-of-mass energy in the reaction products (excluding the recoil electron). See Appendix C for some kinematic results.

At the limit $q^2 \to 0$ we assign a physical meaning to the parameter σ_T; it is just the photoproduction cross section. There is no simple physical meaning for σ_o. The Γ factors may be interpreted as the number of virtual photons per MeV/steradian (of the scattered electron).

The separation of the kinematic factors between Γ and σ is arbitrary, provided that the limit at $q^2 = 0$ has the physical meaning provided above. It is convenient, however, to make the separation such that

$$\sigma_T = \sigma_T(q^2,K) = \sigma(0,K)F(q^2)$$
$$= \sigma_\gamma(K)F(q^2) \tag{2}$$

where σ_γ is the photoproduction cross section and $F(q^2)$ is a form factor defined by the above relation. This factorization is not possible to do exactly in terms of nucleon form factors (as can be seen by a detailed examination of the FNW theory[9]), but it holds approximately.

The separation above into scalar and transverse matrix elements holds only if the total production of electrons is measured. If the outgoing mesons in coincidence with an electron are measured, and in particular if the azimuthal dependence of these mesons is measured, an interference term is produced. This will be ignored for the purposes of the following discussions.

A derivation of the "inelastic Rosenbluth" formula is given in some detail in Appendix A. In this derivation, all effects of the finite electron or muon mass are retained to the end of the calculation, to allow integration over electron or muon angles (Appendix B) the results of which are discussed below and compared with the earlier calculation of Dalitz and Yennie.[4]

Note that here we use a transverse/scalar separation, whereas, for example, Dalitz and Yennie[4] use a transverse/longitudinal separation. The two are related by the requirement of gauge invariance on the electron and proton current operators, $j_\mu q^\mu = 0 = J_\mu q^\mu$, giving

$$j_L J^L = j_o J^o \left(\frac{q_o^2}{|\vec{q}|^2} \right) \tag{3}$$

We find (Appendix A) that some of the properties of electron scattering are especially easy to understand in the Breit frame, where

$q_o^2 = 0$. In this frame j_L is zero (to order q/m). However, if we were considering electron-positron annihilation, the longitudinal separation would be preferable. We are interested in three frames of reference (the lab frame, the center-of-mass frame, and the Breit frame), which are obtained from each other by Lorenz transformations along the momentum transfer direction $\vec{q}$. The separation remains correct in any of these frames.

III. THE EQUIVALENT RADIATOR

If the approximation $\sigma(q^2,K) = \sigma(0,K)$ can be made over the whole range of interest, then the Γ factor of Eq. (1) above can be integrated over q^2, with the result, by now well known, that electrons carry a field of virtual photons of intensity, and with a spectrum, equivalent to those produced by about 0.02 radiation length. It is sometimes stated that the equivalent radiator is 0.02 radiation length. Integration of Eq. (1) as it stands leads to an infinite result, because when $q^2 \to 0$, $q^2 \not> m^2$. The full formula in Appendix A must be used. Deviations from this statement are due either to variations of $\sigma(q^2,K)$ with q^2, a form factor variation, or due to the presence of scalar (longitudinal) transitions.

For mu-mesons, such a simple assumption would lead to an equivalent radiator of 0.01 radiation length. But the simple assumption is not correct; the smallest value of q^2 available is larger than that available with electrons because of the mass, and is large enough that variations of σ are dominant. As calculated below, the effective radiation length is near 0.001 radiation length and is critically dependent on the inelastic form factors and hence on multipolarity. Thus the Panofsky, Woodward, and Yodh experiment[3] could have shown a large effect if performed with incident μ-mesons. The effectiveness of the inverse process of internal conversion in nuclear physics is attributable to the fact that we are there dealing with energies and momentum transfers of the order of, or less than, the electron mass.

The complete integration can be carried out easily in the limit of interest, retaining the lepton mass. This is necessary to prevent an

infinite integral. Take:

$$t \equiv q^2 = 2(EE' - pp' - m^2) + 2pp'(1 - \cos\theta) \tag{4}$$

and assume

$E,E' \gg m$ or μ

$(\Delta E)^2 \gg q^2$ (small angles, or very low secondary energy)

$(\Delta E) > q^2/2M$ (no recoil)

The effective radiation lengths are then:

$$N^T_{e,\mu} = \frac{\alpha}{\pi}\left\{\frac{(p + p')^2}{2p^2 \cdot} \int_{t_{min}}^{t_{max}} \frac{dt}{t} - \frac{1}{4p^2}\int_{t_{min}}^{t_{max}} dt\right\} \tag{5}$$

$$N^O_{e,\mu} = \frac{\alpha}{\pi}\left\{\frac{(p')}{p} \int_{t_{min}}^{t_{max}} \frac{dt}{t} - \frac{1}{4p^2}\int_{t_{min}}^{t_{max}} dt\right\} \tag{6}$$

(The superscripts T and O refer to transverse and scalar.) More complicated formulas are given in Appendix B at various levels of approximation, but the physics is not altered significantly, with the exception that $N^O_{e,\mu}$ as derived above is incorrect, for reasons to be discussed below. Several regions of validity will be discussed.

A. Region I: Dalitz and Yennie Limit

It may be seen that, because nucleon (and supposedly meson) form factors are non-zero only for $q^2 \lesssim 20\ f^{-2}$ (we are only estimating the argument of a logarithm), setting t_{max} equal to the kinematic limit $4pp'$ is justified only if $pp' < (450\ \text{MeV})^2$:

$$N^T_{e,\mu} \approx \frac{\alpha}{\pi}\left\{\left(\frac{p + p'}{p}\right)^2 \log\left[\frac{2pp'}{m_{e,\mu}(p - p')}\right] - \frac{p'}{p}\right\} \tag{7}$$

The more exact treatment gives a result in closer agreement with that of Dalitz and Yennie ($p' < p$):

$$N^T_{e,\mu} \approx \frac{\alpha}{\pi}\left\{\left[1 + \left(\frac{p'}{p}\right)^2\right] \log\frac{2pp'}{m(p - p')} - \frac{5}{3}\frac{p'}{p} - \frac{1}{2}\left(1 + \frac{p'}{p}\right)^2 \log\left(\frac{p + p'}{p - p'}\right)\right\} \quad (8)$$

The numerical result for $p = 500$ MeV, $p' = 250$ MeV is:

$$N^T_e \approx \underline{0.017} \qquad \begin{aligned} p &= 500 \text{ MeV} \\ p' &= 250 \text{ MeV} \end{aligned}$$

The corresponding number for muons is probably not valid because $p' \not> m_\mu$; however, from the same formula, the mass in the log can be changed, giving $N^T_\mu \approx 1.8 \times 10^{-3}$, a factor of 10 less than for electrons. This large drop is caused by the cancellation with the terms not containing the mass, a feature retained in the more exact treatment.

Contrary to what one would expect from a naive application of the inelastic Rosenbluth formula integrated over angles, the scalar contribution is <u>not</u> down by p'/p, but is comparable to the transverse, if the nuclear matrix elements are similar. To see this, one must retain the electron mass more carefully in the calculation (or read Dalitz and Yennie[4]). In Dalitz and Yennie's notation, the longitudinal contribution is reduced [Eq. (3)]. The result of this calculation is:

$$\underline{\text{Region 1}} \qquad N^O_{e,\mu} \approx \frac{\alpha}{\pi}\left\{\frac{1}{2}\left(\frac{p + p'}{p}\right)^2 \log\frac{2pp'}{m(p + p')} - \frac{p'}{p}\right\} \quad (9)$$

This gives $N^O_{e,\mu}$ about comparable to $\frac{1}{2}N^T_{e,\mu}$. The factor of two arises from the definition of equivalent radiator and has its origin in the fact that there are two directions of transverse polarization and one of longitudinal.

B. <u>Region II</u>: <u>$pp' > (450 \text{ MeV})^2$</u>

This is the region of greatest interest to SLAC. For a 10 GeV incident electron, even a 100 MeV secondary electron corresponds to

Region II. In this region we somewhat arbitrarily set $t_{max} \approx 20f^{-2}$ in the upper limit of the integrals in order to express the fall-off of (q^2K) with q^2. The formula below can be applied in either Region I or II, but it still assumes $M \to \infty$, i.e., no recoil and relativistic primary and secondary electrons or muons. Also, $(p - p')^2 \gg t_{min}$ and $t_{max} > t_{min}$.

$$N^T = \frac{\alpha}{2\pi} \left\{ \left[1 + \left(\frac{p'}{p} \right) \right]^2 \log \frac{t_{max}}{t_{min}} - \frac{10}{3} \frac{p'}{p} - \frac{1}{2} \left(1 + \frac{p'}{p} \right)^2 \log \left[1 + \frac{t_{max}}{(p - p')^2} \right] \right\} \tag{10}$$

The corresponding formula for N^o is

$$N^o = \frac{\alpha}{2\pi} \left\{ \frac{1}{2} \left(1 + \frac{p'}{p} \right)^2 \left[\log \left(\frac{t_{max}}{t_{min}} \right) - \log \; 1 + \left(\frac{t_{max}}{(p - p')^2} \right) \right] - \frac{10}{3} \frac{p'}{p} + 2 \left(1 - \frac{p'}{p} \right)^2 \frac{m_{e,\mu}^2}{t_{min}} \right\} \tag{11}$$

Note that m^2/t_{min} is the same for relativistic muons or electrons of the same momentum provided that t_{min} is evaluated at 0^o:

$$\begin{aligned} t_{min} &= m^2 \left(\frac{p}{p'} + \frac{p'}{p} - 2 \right) \quad (\text{at } 0^o) \\ &= m^2 \frac{(p - p')^2}{p'p} \end{aligned} \tag{12}$$

in which case the last term in the above expression becomes $2 \frac{p'}{p}$ and almost cancels the second term.

A simpler form of the above is given below. Assuming

$$p' \ll p \quad , \; t_{min} = \frac{(p - p')^2}{p'p} \quad , \text{ and } \quad t_{max} \approx (950 \text{ MeV})^2 \quad ,$$

$$N^T \approx \frac{\alpha}{\pi} \log \frac{950 \text{ MeV}}{m} \frac{\sqrt{pp'}}{p - p'} \approx 2.3 \times 10^{-3} \begin{cases} \log \frac{2000 \sqrt{pp'}}{p - p'} \text{ (electrons)} \\ \log \frac{10 \sqrt{pp'}}{p - p'} \text{ (muons)} \end{cases} \tag{13}$$

$$N^o \approx \tfrac{1}{2} N^T$$

If $p = 10$ GeV and $p' = 1$ GeV,

$$N_e^T \approx 0.015$$

$$N_\mu^T \approx 0.0029 \tag{14}$$

Thus, even if $F^2 = 1$ and $q^2 < 20 \text{ f}^{-2}$, muons are about 1/5 as effective in producing nuclear interactions as electrons, which is the main conclusion of this section. Another point of interest is that the angular distribution of muons is by no means peaked as sharply around 0^o as one might expect. The possible range of scattered muon angles may be divided into annular zones centered around the beam with the outer boundary of the n-th region defined by $t_n = e^n t_{min}$.

Table I lists values of θ_n and $P_n \equiv$ % inelastic muons scattered into $\theta < \theta_n$, for $p = 10$ GeV and $p' = 1$ GeV. In this case, $t_{min}(0^o) \approx 2 \text{f}^{-2}$.

TABLE I

n	$t_n <$	θ_n	F^2_{exp} (average)	P_n	$(P_n - P_{n-1})F^2$
1	5.6 f^{-2}	6.7^o	0.47	44%	0.21
2	14.8 f^{-2}	13.0^o	0.17	87%	0.07
2.3	20.0 f^{-2}	15.4^o	0.06	100%	0.008

Also given in the table is the average value of

$$F^2_{exp} \approx 1/(1 + q^2/18.5)^4 \quad ,$$

which is an adequate fit to the low q^2 electron-proton elastic scattering data. The form factors can be expected to behave in approximately this fashion. This will further reduce the muon inelastic scattering, as the above calculation assumes $F^2 = 1$ below 20 f^{-2}.

By adding the numbers in the right-hand column, a crude estimate of this further reduction is obtained. It is about <u>another</u> factor of 3. In other words, under these conditions the equivalent radiator for muons is $\approx 10^{-3}$, which is a factor of 15 under that for electrons.

IV. POLARIZATION OF THE VIRTUAL PHOTONS

In Appendix A we derive the fact that the effective <u>transverse</u> polarization of the virtual gamma ray is just equal to the ratio of $\Gamma_o/\Gamma_T \equiv P$. This is the <u>maximum</u> obtainable azimuthal asymmetry in the final state unless non-zero longitudinal matrix elements are present. (The appearance of Γ_o in P has nothing to do with this, but rather is due to the fact that the same Lorentz transformation from frames II $\rightarrow$ I that "creates" scalar electron currents also, by Lorentz contraction, "polarizes" the gamma ray.)

It may be observed that:

(1) If $(\Delta E)^2 \gg q^2 \cot^2 \frac{\theta}{2}$, the effective polarization of the gamma rays is small, i.e., to obtain this polarization at high energies, we must go to small angles and high-energy secondaries for a given ΔE. Large polarization can be obtained in some cases and might be of interest in studying the lower-lying resonances at SLAC.

(2) At 180^o and over a wide range of backward angles, inelastic electron scattering is effectively an unpolarized source of transverse gamma rays.

V. BACKGROUNDS FOR INELASTIC ELECTRON SCATTERING

A list of backgrounds is tabulated in Table II, in which the dependence of the backgrounds on the target thickness t and the mass dependence of backgrounds for muons vs electrons are shown.

TABLE II

Electrons	Varies as	Muons vs electrons
1. Elastic electron-proton scattering	t	1
2. Wide-angle bremsstrahlung	t	1
3. Bremsstrahlung followed by elastic scattering	t^2	$(m/\mu)^2$
4. Electron-electron scattering followed by elastic scattering	t^2	1
5. Dalitz pairs	$0.02\ t + 0.5\ t^2$	1/15
γ rays from		
6. Wide-angle bremsstrahlung	t	1
7. Decay photons from π^0 decay	$0.02\ t + 0.5\ t^2$	1/15
8. Bremsstrahlung followed by Compton scattering	t^2	$(m/\mu)^2$

VI. CLASSES OF EXPERIMENTS

The previous section establishes a connection with photoproduction which is conceptually very useful. It enables us to consider extending to electroproduction any process which has been usefully studied in photoproduction. The extension gives a factor of 2 in parameters — σ_o as well as σ_T — and an infinite extension also, $q^2 = 0$ to $q^2 = \infty$. Because photoproduction is already a big field, electroproduction is bigger; it remains to narrow it down to a few regions which are interesting, possible to study, or are otherwise partially understood by the authors. These are classified below. All involve deflection of a scattered electron.

A. Study of the total cross sections $\sigma_T(q^2,k)$; $\sigma_o(q^2,k)$ as a function of q^2,k.

B. Study of the nucleon resonance regions $k \approx 300$, 700, 1000 GeV, etc., with a π or two in coincidence with the scattered electron.

C. Study of peripheral interactions (Drell process) by electroproduction. Some of these are considered below.

A. Study of Total Inelastic Cross Sections

The minimum aim is to measure $d^2\sigma/d\Omega dE'$ and to deduce σ_o and σ_T from Eq. (1). This study is what has been started by Panofsky and Allton,[5] Ohlsen,[6] and by Hand.[7] Let us consider the uses of such a study. First, a total gamma cross section is hard to obtain. An absorption measurement, as is possible for neutrons, measures primarily electronic absorption processes such as pair production. A gamma ray detector which will equally detect all products of an electron-positron shower has been suggested by Joos[13] for an experiment at DESY. There are, however, likely to be problems.

There are similar problems in measuring $\sigma(q^2,k)$ at low q^2; the analogue of the problem of separating the gamma ray nuclear absorption and pair production is the problem of separating the inelastic electron-proton scattering from the radiative tail of the elastic scattering. The lower limit of $q^2 > 2$ fermi^{-2} seems reasonable.

We are concerned with whether or not the inelastic counts with nucleon excitation stand out above the radiative tail. In order to see this easily we rearrange Eq. (1) into a cross section differential in the virtual photon energy

$$\frac{d^2\sigma}{d\Omega dK} = \frac{d^2\sigma}{d\Omega dE'}\left|\frac{dE'}{dK}\right| = \eta \frac{d^2\sigma}{d\Omega dE'} \qquad \text{(from Appendix C)}$$

$$= \left(\frac{\alpha K}{4\pi^2}\right) \frac{\eta}{4E^2 \sin^2 \theta/2} \left\{ \sigma_T \left[2 + \frac{\cot^2 \theta/2}{1+\tau} \right] + \sigma_o \frac{\cot^2 \theta/2}{1+\tau} \right\} \qquad (15)$$

where $\tau = (\Delta E)^2/q^2$.

We can note the similarity even in constants with the elastic scattering formula

$$\frac{d\sigma}{d\Omega} = \left(a^2 r_e^2 m^2\right) \frac{\eta}{4e^2 \sin^2 \theta/2} \left\{ \tau G_M^2 \left[2 + \frac{\cot^2 \theta/2}{1+\tau} \right] + G_E^2 \frac{\cot^2 \theta/2}{1+\tau} \right\} \qquad (16)$$

where $t = T^2/q^2 = q^2/4M^2$.

If the radiated γ ray energy is small compared with the incident energy, we can write the radiative tail,[17]

$$\frac{d^2\sigma}{d\Omega dK} = \frac{d\sigma_{elastic}}{dK} \frac{2\alpha}{\pi} \left[\log (q^2/m^2) - 1 \right] \qquad (17)$$

The ratio of the inelastic scattering to the radiative tail is given by R:

$$\frac{\sigma_I}{\sigma_R} = AK^2 \left\{ \quad \right\}_I \Big/ \left\{ \quad \right\}_E \qquad (18)$$

where

$$A = \frac{\log (q^2/m^2) - 1}{8\pi^2 \alpha^2 r_e^2 m^2}$$

is almost a constant and the braces are those of Eqs. 15 and 16.

At low q^2, G_E dominates the elastic scattering and equals unity, σ_T tends to a constant σ_γ, and σ_o tends to 0 for most models. Therefore,

$$\frac{\sigma_I}{\sigma_R} \rightarrow AK^2 \sigma_\gamma \left[\theta^2/2 + \frac{q^2}{K^2} \right] \qquad (19)$$

which tells us that it is difficult to find inelastic scattering at low momentum transfers. Assuming that σ_T varies roughly as $q^2 G_M^2$ (see

Section VII), the ratio will increase with increasing momentum transfer until both $(\Delta E)^2/q^2$ becomes less than unity and G_M begins to dominate the elastic scattering, i.e., for $q^2 > 10$ fermi^{-2}($= \frac{1}{2}$ BeV/c)^2 for low lying resonances; higher momentum transfers are necessary for the higher resonances.

If the radiated energy is larger in comparison with the incident energy, σ_R is <u>larger</u> than given by Eq. (17). (See for example Ref. 7.) The form of Eqs. (18) and (19) tells us at once that if we choose E and θ conveniently so that σ_R reaches its lower limit of Eq. (17), the inelastic scattering will be most apparent. This happens at small angles and high energies for a given q^2. This suggests another field where SLAC can do experiments impossible for other accelerators.

At momentum transfers of $q^2 = 250$ to 900 fermi^{-2}, Berkelman[14] suggests that Dalitz pairs are a major source of background to elastic or inelastic scattering experiments. Since Dalitz pairs give equal numbers of positrons and electrons, they can be subtracted out. At momentum transfers up to $q^2 = 75$ fermi^{-2} and angles of 31° to 90°, this background is less than 10% (as measured by A. Cone at CEA). This contrasts with 135° measurements by Hand[7] at $q^2 = 20$. Thus at forward angles we anticipate no problem from Dalitz pairs.

Apart from the interest in mapping $\sigma_T(q^2,k)$ and $\sigma_o(q^2,k)$, there is some interest in evaluating integrals of σ_T and σ_o. Thus Cottingham[15] has expressed the electromagnetic mass of the nucleon in terms of these parameters. Also, by a unitarity relation, one may be able to obtain some idea of the imaginary part of the elastic e-p scattering amplitude (due of course to multiphoton terms), in the same way that one can express the imaginary part of the forward amplitude in terms of the total cross section.

In terms of σ_T and σ_o we find for the electromagnetic self mass

$$\Delta M = \Delta M^E + \Delta M^I$$

$$\Delta M^I = -\left(\frac{1}{2\pi}\right)^3 \int_0^\infty dq^2 \int_c^\infty d(\Delta E)\, \frac{K}{\sqrt{q^2 + (\Delta E)^2}} \left[\frac{(1 - x)(2 + x)}{1 + x}\right] \sigma_T$$

$$+ \left(\frac{1}{2\pi}\right)^3 \int_0^\infty dq^2 \int_c^\infty d(\Delta E)\, \frac{K}{\sqrt{q^2 + (\Delta E)^2}} \left[\frac{1 + x + x^2}{1 + x}\right] \sigma_o$$

where $x = \sqrt{\tau/(1+\tau)}$ with $\tau = (\Delta E)^2/q^2$, so that $x < 1$, and $c = [2M\mu + \mu^2 + q^2]/2M$ where μ is the pion mass. The expression for ΔM^E is similar, but includes the elastic form factors.

In this type of experiment, μ scattering may be better than electron scattering. The radiative correction at a given q^2 is given by a term $\log (q^2/m^2)$; at $q \approx 250$ MeV/c, the improvement with μ mesons is thus $\log (10^6/4)/\log 4$, or a factor of 20. The Dalitz pair background is also down by the factor of 15 discussed earlier.

B. Study of The Nucleon Resonances

This has been little studied in the past. If we wish to define a nucleon resonance unequivocally we must define not only K but J. The only way to determine J is to look at the outgoing particles. For the first resonance, Δ_{1238}, there is little contamination by nonresonant processes. For higher resonances, there is a large amount, so that the resonances are not expected to stand out in a total cross section measurement. The study of the outgoing particles is then particularly useful.

C. Study of Peripheral Processes by Electroproduction

A study of a particular experiment for the CEA has been made by the electron-scattering group at Harvard, and we refer to it for completeness.[16]

VII. RELATION TO NUCLEAR PHYSICS

Formulae equivalent to Eq. (1) have been derived for inelastic electron scattering from nuclei. These are summarized by Barber.[12] These formulae are unfortunately not easily recognized as equivalent because the nuclear physics formulae seem not to reduce to the expression of Eq. (1) without some approximation, and are expressed in terms of the three-dimensional momentum transfer.

For nuclear physics it is convenient to expand the nuclear current operators J_T and J_o into multipoles; for electric one-pole radiation

except monopole we can then make the identification

$$\sigma_T = \left(\vec{q} \,/K\right)^2 \frac{F^2\, \vec{q}^{\,2}}{F^2\, K^2}\, \sigma_\gamma$$

$$\sigma_o = \left(\vec{q} \,/K\right)^2 \frac{F^2\, \vec{q}^{\,2}}{F^2\, K^2}\, \sigma_\gamma \; \frac{\ell}{\ell + 1}$$

and for magnetic one-pole radiation

$$\sigma_T = \left(\left|\vec{q}\right|/K\right)^2 \frac{F^2\left|\vec{q}^{\,2}\right|}{F^2\left|K^2\right|}\, \sigma_\gamma$$

$$\sigma_o = 0 \tag{20}$$

Note that $\sigma_T \to \sigma_\gamma$ for photoproduction as $\left|\vec{q}\right| \to K$; $F^2(\vec{q}^{\,2})$ is a form factor for the process.

Both electric and magnetic multipoles contribute to σ_T, but only electric multipoles contribute to σ_o; electric monopole transitions contribute only to σ_o.

These terms are the first terms in the expansion of

$$\int j_\ell(\left|\vec{q}\right| r) p(r) r^2 dr$$

For a study of the nucleon resonances these formulae are not applicable. It is tempting, however, to see what they suggest. For excitation of the first nucleon resonance, Δ_{1238}, we need a spin change of one and a parity change. This can be given by a magnetic dipole transition or an electric quadrupole transition. The magnetic dipole is dominant. Equation (20) says that $\sigma_o = 0$; for the transverse element,

$$\sigma_T = \left(\left|\vec{q}\right|^2/K^2\right) \frac{F^2\left|\vec{q}^{\,2}\right|}{F^2\left|K^2\right|}\, \sigma_\gamma \tag{21}$$

One might ask in what reference frame $\vec{q}$ is measured. For nuclear physics the lab frame and the rest frame of the excited nucleus give nearly the same answer. For the nucleon, there is a difference. We

We suggest here taking the excited nucleon rest frame; the result of References 9, 10, and 11 is then obtained, and the form factor is the magnetic vector form factor $G_{MV}(q^2)$.

$$\sigma_T = \frac{|\vec{q}|^2}{K^2} \frac{G_{MV}|\vec{q}^2|}{G_{MV}|K^2|} \sigma_\gamma \tag{22}$$

This result is confirmed by experiment,[7] as is the low value of σ_o.

What happens for higher resonances is unclear. It is tempting to say that high spin resonances are produced with high cross sections because of the factor $|\vec{q}|^{21}$; however, the form factors F^2 prevent the rise going to infinity. The nuclear case is well understood,[12] but the problems in the relativistic case are unclear.

APPENDIX A: DERIVATION OF ONE-PHOTON EXCHANGE FORMULA

The following is intended for those who are interested in the most intimate details of the one-photon exchange derivation.

We do not wish to make any approximation regarding the mass of the source of the electromagnetic field. It is amusing that if the calculation is done in the brick wall frame, as described below, and then written in terms of laboratory quantities at the end, the chief complication finite mass introduces is a kinematic one — a fact which is not clear when one does the traces directly in the laboratory. This remark may have some significance for the calculation of muon pairs and wide-angle electron pairs, where computer programs tend to give incorrect answers because large cancellation between terms occurs. It is therefore essential to have all the mass dependence appear in the formulae. A reference frame in which the reaction exhibits a high degree of symmetry should simplify the calculation.

Let us consider the following two "brick wall" or Breit frames, defined by the condition that no energy is transferred between the scattered electron and the nuclear system absorbing the virtual photon.

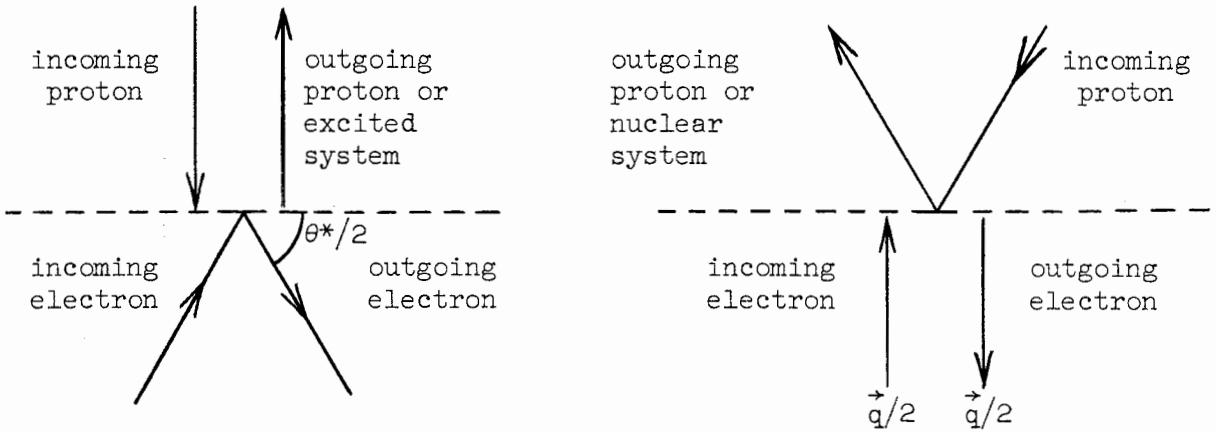

I. Breit frame for the proton. All quantities are starred.

II. Breit frame for the electron. All quantities are double-starred.

Frame I can be reached from the lab frame by a Lorentz transformation along the direction of the laboratory momentum transfer. Frame II is reached from Frame I by a Lorentz transformation parallel to the brick wall with a velocity

$$\beta(\mathrm{I} \rightarrow \mathrm{II}) = \frac{p^* \cos \frac{\theta^*}{2}}{\epsilon^*}$$

where p^*, ϵ^*, and θ^* are momentum, total energy, and scattering angle of the electron in Frame I.

Observe the collision in Frame II. The electron is scattered 180° and emerges without energy loss. The electron current j_μ is just given by the matrix element $< \bar{u}' \gamma_\mu u >$, where the prime stands for the outgoing electron, the u's are Dirac spinors, and γ_μ are the four Dirac γ matrices. The theory is Lorentz invariant; hence it is constructed so that the four complex numbers j_0, j_1, j_2, j_3 transform among themselves like the components of a four-vector upon going to another coordinate system. Because we are in the most symmetric frame for the electron, we can expect the j's to take on the simplest form in this frame.

Furthermore, each of the four numbers j_0, j_1, j_2, j_3 must be referred to definite initial and final electron spin states, making 16 numbers in all; however, we shall see that even in the most general case of a nucleon current, these 16 numbers reduce to two numbers.

The procedure to be followed below is first to evaluate the matrix elements for j_μ and J_μ in the (different) Breit frames of the two particles, in each case for a spin direction chosen along the direction of particle motion in that frame. We will find a particularly simple form for the current matrix element in these frames. The effect of small electron rest mass will be seen to suppress completely the term in the electron current analogous to G_E in the proton current. The interaction, $j_\mu J^\mu$, may then be computed by transforming one electron current into the proton Breit frame.

In the limit of the electron mass equal to zero, it is rigorously true that one unit of angular momentum must be transferred along the

direction of the momentum transfer. This statement remains true even for multiple photon exchange. This is often called helicity conservation, since the scattered electron retains its original helicity. Thus, if helicity is conserved, either right-hand circularly polarized virtual photons or left-hand circularly polarized virtual photons are emitted, depending on whether the initial helicity of the electron is positive or negative. Thus, in the electron's Breit frame, the virtual photons appear as purely transverse, with no net polarization if the electrons are themselves unpolarized. Note that a conserved j_μ requires the vanishing of j_o in the electron's Breit frame, while helicity conservation, which only holds to order (m/q), in addition requires j_z to vanish. The effect of violations of either a conserved current or of helicity conservation is easily seen with this approach.

We may simplify the expressions further by writing j_μ in terms of the matrix elements of Pauli σ matrices between Pauli spinors evaluated in the rest frames of the initial and final electron states. We obtain:

$$j_o = e\chi_f^* \chi_i$$

$$\vec{j} = ei\ \chi_f^* \left(\vec{\sigma} \times \frac{\vec{q}^{**}}{2m}\right)\chi_i \qquad \text{(A.1)}$$

In deriving Eq (A.1) from $\bar{u}(p')\gamma_\mu u(p)$, we made use of the explicit form of the Lorentz transformation of a Dirac spinor from the particle rest frame:

$$u(p) = L(p)u(o) = L(p)\begin{pmatrix}\chi\\0\end{pmatrix}$$

In the above χ is a two-component Pauli spinor and $\begin{pmatrix}\chi\\0\end{pmatrix}$ is the familiar mixed notation for the rest frame spinor $u(o)$. Explicitly,

$$L(p) = e^{\gamma_5 \vec{\sigma}\cdot\vec{n}\varphi/2}$$

$$\gamma_5 = \begin{pmatrix}0 & 1\\1 & 0\end{pmatrix}$$

where $\vec{n}$ is a unit vector along the particle direction and φ is defined by $\sinh \varphi = p/m$, the momentum of the particle divided by its mass.

For the proton, in its Breit frame, we obtain the familiar

$$\begin{aligned} J_o &= eG_E(q^2) X_f^* X_i \\ \vec{J} &= eG_M(q^2) i X_f^* \left(\vec{\sigma} \times \frac{\vec{q}^*}{2M} \right) X_i \end{aligned} \tag{A.2}$$

The X_f and X_i are the rest frame proton Pauli spinors. G_E and G_M are the proton form factors.

Lorentz-transforming the electron current back into Frame I results in

$$\text{Frame I} \quad p^{**} = \frac{q^{**}}{2} \qquad \begin{cases} j_o = \dfrac{1}{\sqrt{1-\beta^2}} \left[\chi_f^* \left(1 + \beta \sigma_y \dfrac{P^{**}}{m} \right) \chi_i \right] \\ j_z = 0 \\ j_x = \dfrac{P^{**}}{m} \chi_f^* \sigma_x \chi_i \\ j_y = \dfrac{1}{\sqrt{1-\beta^2}} \left[\chi_f^* \left(\dfrac{p^{**}}{m} \sigma_y + \beta \right) \chi_i \right] \end{cases} \tag{A.3}$$

Note that $p^{**} = \frac{1}{2}\sqrt{q^2}$. We spare the reader the sight of more algebra, and write

$$\begin{aligned} j_\mu J^\mu = \sqrt{\frac{q^2}{4m^2}} \Bigg\{ & G_E X_f^* X_i \, \chi_f^* \left(\frac{\beta}{\sqrt{1-\beta^2}} \sigma_y + \sqrt{\frac{4m^2}{q^2}} \frac{1}{\sqrt{1-\beta^2}} \right) \chi_i \\ & + iG_M \sqrt{\frac{q^2}{4M^2}} \, X_f^* \sigma_x X_i \, \chi_f^* \left(\frac{\sigma_y}{\sqrt{1-\beta^2}} + \sqrt{\frac{4m^2}{q^2}} \frac{\beta}{\sqrt{1-\beta^2}} \right) \chi_i \\ & - iG_M \sqrt{\frac{q^2}{4M^2}} \, X_f^* \sigma_y X_i \, \chi_f^* \sigma_x \chi_i \Bigg\} \end{aligned} \tag{A.4}$$

By squaring this and summing over spin directions, using

$$\frac{\beta^2}{1-\beta^2} = \frac{\cot^2\frac{\theta^*}{2}}{\left(1+\frac{4m^2}{q^2}\right)}$$

$$\frac{\beta^2}{1-\beta^2} = \frac{1}{\left(1+\frac{4m^2}{q^2}\right)}\left[\csc^2\frac{\theta^*}{2}+\frac{4m^2}{q^2}\right]$$

we obtain

$$\sum_{\text{spins}}\left|j_\mu J^\mu\right|^2 = \frac{q^2}{4m^2}\left\{G_E^2\left[\frac{\beta^2}{1-\beta^2}+\frac{4m^2}{q^2}\frac{1}{1-\beta^2}\right] + \frac{q^2}{4M^2}G_M^2\left[1+\frac{1}{1-\beta^2}+\frac{4m^2}{q^2}\frac{\beta^2}{1-\beta^2}\right]\right\}$$

which becomes

$$\sum_{\text{spins}}\left|j_\mu J^\mu\right|^2 = \frac{q^2}{4m^2}\left\{G_E^2\left[\cot^2\frac{\theta^*}{2}+\frac{4m^2}{q^2}\right]+\frac{q^2}{4M^2}G_M^2\left[2+\cot^2\frac{\theta^*}{2}\right]\right\} \quad \text{(A.5)}$$

No approximations have been made here regarding the electron rest mass. The proof of this is left to the reader as an excercise in frustration.

The transformation to the lab system is

$$\cot^2\frac{\theta^*}{2} = \frac{\cot^2\frac{\theta}{2}}{\left(1+\frac{q^2}{4M^2}\right)} \qquad (m^2 \ll q^2)$$

and we thus find the usual formula, in terms of lab quantities ($m^2 \ll q^2$),

$$\frac{q^2}{4m^2}\left\{ G_E^2 \frac{\cot^2\frac{\theta}{2}}{1+\frac{q^2}{4M^2}} + \frac{q^2}{4M^2} G_M^2 \left(2 + \frac{\cot^2\frac{\theta}{2}}{1+\frac{q^2}{4M^2}} \right) \right\}$$

If we wished to detect violations of current conservation for virtual photons, we could find a corresponding formula to that preceding Eq. (A.5), in which the arbitrary assumptions $j_3 = \lambda j_0$ and $J_3 = \lambda J_0$, with $\lambda \neq 0$, have been made, thus violating the conserved current for virtual photons. This calculation is easily performed and the answer given:

$$\frac{q^2}{4m^2}\left\{ G_E^2 \left[\frac{\beta^2}{1-\beta^2} + \left(\frac{2m}{\sqrt{q^2}} \frac{1}{\sqrt{1-\beta^2}} - \lambda^2 \right)^2 \right] + \frac{q^2}{4M^2} G_M^2 \left[1 + \frac{1}{1-\beta^2} + \frac{4m^2}{q^2}\frac{\beta^2}{1-\beta^2} \right] \right\} \tag{A.6}$$

Thus current conservation must fail at <u>both</u> electron and proton vertices in order to be observable. The best place to look for such effects is in the 180° scattering of either electrons or muons.

If we write, using Eq. (A.6) (at $\theta = 180^\circ$),

$$\sigma_{\lambda^2} = \sigma_0(1 + \alpha\lambda^2$$

we find

$$\alpha \approx -\sqrt{\frac{m}{M}}\frac{\sqrt{q^2}}{2M}\left(\frac{G_E}{G_M}\right)^2$$

In order to detect $\lambda^2 \neq 0$ we might compare 180° electron scattering with 180° muon scattering. Assuming $\lambda^2(q^2) \approx 1$ at $q^2 = 90f^{-2}$,

we would obtain a ratio

$$\frac{\sigma_\mu(180^\circ)}{\sigma_e(180^\circ)} \approx 0.961$$

This would obviously be very hard to detect experimentally. Certainly there is no reason to suspect such an exchange of a non-conserved vector current between the muon and the proton.

Another fairly easy calculation using this well known trick of Lorentz-transforming rest frame spinors is the calculation of spin correlations in the scattering of polarized electrons and subsequent measurements of proton polarization. This is analogous to D_t, R_t, and A_t in nucleon-nucleon scattering. The analogue to P does not arise in first Born approximation for anything, including virtual photons.

Example II: Inelastic Scattering

Having gone to the trouble of introducing this method, we can finish the derivation of the inelastic scattering formula. It is more complicated than the elastic scattering case only because we may not wish to sum over outgoing particles and because of the final transformation to the lab system. It is clear that the J_μ, the nuclear interaction matrix elements which are complicated functions of all the spins and momenta involved in the final state, must rotate in a way determined only by the label on J, i.e., if we had a $J_x \approx X_f \sigma_y X_i$, then a 90° rotation about the y axis would imply that $J'_z = -X_f \sigma_y X_i$, etc. Because we are not observing the final state, or the initial spin direction of the proton (or nuclear) target, we may average first over independent rotations of the initial and final states about the momentum transfer axis. In Frame I, terms proportional to $J^o \vec{J}$ average to zero like ordinary vectors, and we need not inquire about the complexity of the expressions for J^o and $\vec{J}$. Thus we see that in the end, for inelastic or elastic scattering, we must not have any interference between J^o and $\vec{J}$. Just as in the case of elastic scattering, we get (now the J's are unspecified and $\overline{J^{o2}}$ is the average of J^{o2} over rotations

about the momentum transfer axis of the final state, however complex):

$$\left|j_\mu J^\mu\right|^2 = \frac{q^2}{4m^2}\left\{\overline{J^{o2}}\left[\cot^2\frac{\theta^*}{2} + \frac{m^2}{q^2}\right] + \frac{\overline{\vec{J}^2}}{2}\left[1 + \csc^2\frac{\theta^*}{2}\right]\right\}$$

The factor of $\frac{1}{2}$ before $\overline{\vec{J}^2}$ arises because $\overline{J_x^2} = \frac{1}{2}\overline{J^2}$ and the 1 and $\csc^2\frac{\theta^*}{2}$ terms select $\left|J_x\right|^2$ and $\left|J_y\right|^2$ respectively in the sum. Thus we have derived the effective <u>linear polarization</u> of the virtual gamma ray on our way to the cross section. To see polarization effects, of course, we must observe the final state and look for a φ dependence (φ is the angle of rotation about the momentum transfer) of some vector in the excited system. The effective linear polarization of the virtual gamma is

$$P \equiv \frac{-\left|j_x\right|^2 + \left|j_y\right|^2}{\left|j_x\right|^2 + \left|j_y\right|^2} = \frac{\cot^2\frac{\theta^*}{2}}{2 + \cot^2\frac{\theta^*}{2}}$$

which is also the ratio of scalar/transverse photons. In the absence of scalar currents, the final state will have an angular distribution characteristic of linear polarized gamma rays with polarization in the electron scattering plane of magnitude P, assuming the multipole mixture is the same.

<u>Cross section for inelastic scattering</u>

We denote by $\prod\!\!\prod$ a symbol standing for all delta functions, numerical factors, integrations, etc., common to both photoproduction and electroproduction.

Using standard Feynman rules, we write

$$\frac{d^2\sigma}{d\Omega' dp'} = \frac{\alpha}{2\pi^2}\frac{m^2}{q^4}\frac{\epsilon'}{\epsilon}\left(\frac{p'}{\epsilon'}\right)^2\frac{\epsilon}{p}\prod\!\!\prod \text{Trace}\left[\Lambda(p)\not{\ell}\Lambda(p)^*\not{\ell}\right]$$

$$\sigma_T = \frac{1}{2k}\prod\!\!\prod\left|\vec{J}^T\right|^2 \quad \text{for real gamma rays, in the same notation.}$$

We define

$$\sigma_o \equiv \frac{1}{k} \iint \left| J^o \right|^2$$

and we have effectively evaluated an easy trace the hard way as equaling

$$\frac{q^2}{2m^2}\left[\left(\cot^2 \frac{\theta^*}{2} + \frac{4m^2}{q^2}\right)\left(J_o\right)^2 + \left|\vec{J}\right|^2 \left(1 + \tfrac{1}{2} \cot^2 \frac{\theta^*}{2}\right)\right]$$

We need only to combine terms and express $\cot^2 \frac{\theta^*}{2}$ in terms of lab quantities to obtain the desired formula, quoted above. To find $\cot^2 \frac{\theta^*}{2}$, consider the square of that component of the incident electron momentum which is perpendicular to the momentum transfer, divide this by $q^2/4$, and evaluate it in the lab and in Frame I, as it must be invariant to Lorentz transformation along $\vec{q}$.

We obtain

$$\cot^2 \frac{\theta^*}{2} = \frac{\cot^2 \frac{\theta}{2}}{1 + \frac{(\Delta E)^2}{q^2}} \qquad \text{if} \quad m \to o$$

or more generally

$$\cot^2 \frac{\theta^*}{2} = \frac{\sin^2 \theta}{\left[\frac{(p - p')^2}{2pp'} + (1 - \cos \theta)\right]\left[\frac{1}{2} \frac{m(p - p')^2}{pp'} + (1 - \cos \theta)\right]}$$

and Eq. (1) of the text and the formulae of Appendix B are obtained.

APPENDIX B: INTEGRATION OVER SCATTERED ELECTRON ANGLES

For reference, various formulas are given below that are obtained by integrating the differential cross section derived in Appendix A.

Integrating Φ from 0 to 2π and changing the independent variable from θ to t yields

$$t = t_{min} + 2pp'(1 - \cos\theta)$$

$$t_{min} = 2(\epsilon\epsilon' - pp' - m^2) \approx m^2 \frac{(p - p')^2}{pp'} \quad \text{for relativistic particles.}$$

We obtain, without any approximations,

$$\frac{d^2\sigma}{dtdp'} = \frac{\alpha}{4\pi}\frac{1}{pp'}\left(\frac{\Delta\epsilon}{t} - \frac{1}{2M}\right)\frac{\epsilon'}{\epsilon}$$
$$\left\{\left[\frac{(t-t_{min})[4pp' - (t-t_{min})]}{[(p-p')^2 + (t-t_{min})](t+2t_{min})}\sigma_o(t,k) + \sigma_\tau(t,k)\right]\right.$$
$$\left. + 2\sigma_T + \frac{4m^2}{t}\sigma_o\right\}$$

The complicated bilinear term in t is just $\cot^2\frac{\theta^*}{2}$ in terms of t. In order to do the integral, a t dependence of σ_o and σ_T must be assumed. We follow the time-honored custom of assuming $\sigma_o(t,k) = \sigma_o(0,k)$ and likewise for σ_T.

This gives us expressions independent of the multipolarity of the particular transition or excitation of the system being studied. If one were possessed of sufficient stamina (historically there are several examples), one could (neglecting 1/M) take advantage of the fact that the multipoles depend on known powers of the spatial momentum transfer $|\vec{q}|^{2m}$, where m depends on the particular multipole being considered. Because for $t \ll k^2$, $|\vec{q}|^{2m} \approx k^{2m} + mtk^{2m-2}$, we obtain a multipole dependence in a non-logarithmic term added to the equivalent radiator. These give terms, varying with multipolarity, of order 1 relative to $\log q^2/m^2$. It is thus obvious why attempts to use electroproduction to

determine the multipolarity of resonances by integrating over-all scattered electrons cannot succeed, as Dalitz and Yennie first showed by explicit calculation.

Neglecting terms in 1/M and assuming $\sigma_L(t,k) = \sigma_o(0,k)$ and $\sigma_T(t,k) = \sigma_T(0,k)$, we can integrate the above expression analytically. An analytic form could also be obtained for the 1/M term, but if the momentum transfers are sufficiently high so that they are important, then so are form factors, which are ignored here. Both effects tend to suppress the cross section.

$$\frac{d\sigma_T}{dp'} = \frac{\alpha}{2\pi}\frac{\epsilon'}{\epsilon}\frac{\epsilon-\epsilon'}{2pp'}\sigma_T\left\{\left[1 + \frac{(p^2 - p'^2)^2}{\left[(p-p')^2 - t_{min}\right]\left[(p-p')^2 - 3t_{min}\right]}\right]\log\frac{t_{max}}{t_{min}}\right.$$

$$+\frac{3}{2}\frac{1}{1 - \frac{(p+p')^2}{3t_{min} + 4pp'}}\log\frac{3t_{max}}{t_{max} + 2t_{min}}$$

$$\left. - \frac{(p^2 - p'^2)^2}{\left[(p-p')^2 - t_{min}\right]\left[(p-p')^2 - 3t_{min}\right]}\log\left[1 + \frac{t_{max} - t_{min}}{(p-p')^2}\right]\right\}$$

$$\frac{d\sigma_o}{dp'} = \frac{\alpha}{2\pi}\frac{\epsilon'}{\epsilon}\frac{\epsilon-\epsilon'}{2pp'}\sigma_o\left\{4m^2\left(\frac{1}{t_{min}} - \frac{1}{t_{max}}\right)\right.$$

$$+\frac{(p^2 - p'^2)^2}{\left[(p-p')^2 - t_{min}\right]\left[(p-p')^2 - 3t_{min}\right]}\log\frac{t_{max}}{t_{min}}$$

$$+\frac{3}{2}\frac{1}{1 - \frac{(p+p')^2}{3t_{min} + 4pp'}}\log\left(\frac{3t_{max}}{t_{max} + 2t_{min}}\right)$$

$$\left. - \frac{(p^2 - p'^2)^2}{\left[(p-p')^2 - t_{min}\right]\left[(p-p')^2 - 3t_{min}\right]}\log\left[1 + \frac{t_{max} - t_{min}}{(p-p')^2}\right]\right\}$$

In both cases, the term in $\log\left(\frac{t_{max}}{t_{min}}\right)$ is the dominant one. The above formulas may be used for non-relativistic particles or hypothetical heavy leptons, with the only restriction being $\frac{t}{2M} \ll k$.

APPENDIX C: SOME USEFUL KINEMATIC FORMULAE FOR INELASTIC SCATTERING

Incident electron four-momentum p_i

Outgoing electron four-momentum p_f

Incident proton four-momentum $\mathbb{P}_i$

Outgoing proton four-momentum $\mathbb{P}_f$

Four-momentum transfer $q = p_i - p_f = \mathbb{P}_f - \mathbb{P}_i$

Relativistic invariant
$$-t = q^2 = p_i^2 + p_f^2 - 2p_i \cdot p_f = 2p_i \cdot p_f$$
$$= 2\vec{p}_i \cdot \vec{p}_f + 2EE' \quad (\text{for } m = 0)$$
$$= 2EE'(1 - \cos\theta)$$

$$\boxed{-t = q^2 = 4EE' \sin^2 \theta/2}$$

Also,
$$q^2 = \mathbb{P}_f^2 - 2\,\mathbb{P}_f \cdot \mathbb{P}_i + \mathbb{P}_i^2$$
$$= -(M + \epsilon)^2 - M^2 - 2\,\vec{\mathbb{P}}_f \cdot \vec{\mathbb{P}}_i + 2E_f^p E_i^p$$

where ϵ is the excitation energy of the outgoing nucleon, including any pions and so forth emitted.

In the lab, $\vec{\mathbb{P}}_i = 0$, and we put T = kinetic energy of the outgoing nucleon system in the laboratory.

$$q^2 = -M^2 - 2M\epsilon - \epsilon^2 - M^2 + 2M(M + \epsilon + T)$$

$$\boxed{q^2 = -\epsilon^2 + 2MT}$$

Now in the lab frame

$$E - E' = q_o^{lab} = \epsilon + T = \epsilon + q^2/2M + \epsilon^2/2M$$

whence

$$E' = E\,\frac{\left[1 - \frac{\epsilon}{E}\left(1 + \frac{\epsilon}{2M}\right)\right]}{\left[1 + \frac{2E}{M}\sin^2\theta/2\right]}$$

Put $K = E - E' - q^2/2M$

$$\boxed{K = \epsilon(1 + \epsilon/2M) = q_o - q^2/2M}$$

Then

$$\boxed{E' = \frac{E - K}{1 + 2\,E/M \sin^2 \theta/2}}$$

For $\epsilon = K = 0$, these reduce to the well known elastic scattering formulae. For $\theta = 0$, $E' = E - K$.

The kinematics here is clearly the same as in photoproduction, so we call K the virtual photon energy, equal to the real photon energy for $\theta = 0$. Note that the relation between K and ϵ does not depend on kinematics, so K remains a useful quantity in electron scattering.

If we place $E'/E = \eta$ for elastic scattering, we can write the more general case

$$\boxed{\frac{E'}{E} = \eta(1 - K/E)}$$

$$\boxed{\frac{dE'}{dK} = -\eta}$$

ELECTROPRODUCTION AT SLAC

by

L. Hand

I. INTRODUCTION

At the present time, electron synchrotrons enjoy a monopoly on the possible use of large solid-angle detectors capable of analyzing reactions leading to many-particle final states. These machines have the advantage of a duty cycle better by a factor of 100 than that to be obtained at SLAC. To date, at the Stanford Mark III accelerator and at Orsay, the low duty cycle of the linear accelerator has effectively provided a constraint restricting the latter's use to the study of reactions having two-body kinematics, since the large background rates seem to require magnetic spectrometers with very small solid angles and momentum acceptances.

Because the duty cycle cannot be improved, one must take advantage of the large intensity and high energy expected of the SLAC electron beam. In terms of the product of intensity and duty cycle, SLAC is better off by a factor of 6 than the CEA. A successful scheme for producing photons (real or virtual) at SLAC must in some way turn this to advantage. Many people are aware of these problems, which have become even more acute in the light of recent trends in elementary particle physics, and various proposals for "photon" sources have been advanced.[1] At this time, our understanding is not sufficient to predict with certainty which of these proposals will yield the most physics. It is the purpose of the report below to discuss still another possibility: the use of electrons inelastically scattered at very small angles as a source of monochromatic virtual gamma rays. The reasons for giving serious consideration to this are the following:

1. The distribution of the scattered electrons at small angles is essentially logarithmic $\approx \int \frac{d\theta}{\theta}$. This implies that despite the nearly singular nature of the forward electron scattering. a detector at quite surprisingly large angles can receive a significant fraction of the inelastically scattered electrons having the desired secondary energy.

Because with a sufficiently thin target the reactions are all directly produced by the electromagnetic field of the electrons, we have a good efficiency ($\approx 0.1\%$ in the system discussed below) for detecting the scattered electron for <u>any</u> nuclear reaction occurring in the target.

2. None of the proposals thus far, with the possible exception of inelastic mu scattering, which has other serious disadvantages, offers really monochromatic photons in the sense of a kinematic constraint. Here $\frac{dk}{k} = 1\%$ has been taken as a desirable resolution. It may be argued that this merely means that an additional momentum must be measured in the final state if the photons are untagged. That this cannot always be done is clear from considering, for example,

$$\gamma + p \rightarrow p + \omega$$

i.e.,

$$\gamma + p \rightarrow p + \pi^+ + \pi^- + \pi^\circ$$

This reaction cannot be distinguished from any other reaction $\gamma + p \rightarrow p + \pi^+ + \pi^-$ + neutrals, unless the gamma ray energy is known. Partial monochromaticity, such as that achieved for the collimated positron annihilation gamma rays (see Appendix I) is certainly crucial in reducing backgrounds by factors of 50 to 100 over those encountered with hardened bremsstrahlung spectra, but cannot serve as a constraint.

3. As discussed in detail both below and in the report[2] by R. Wilson and L. Hand, the virtual photon exchanged when an electron scatters inelastically is highly polarized along a definite space-time direction. The spatial component of this polarization four-vector lies in the scattering plane. Since longitudinal and transverse components are present in an essentially coherent fashion, a powerful tool exists for studying the structure of the transition currents involved in the various production reactions. This feature is unique to electroproduction, and means that the proposal for small-angle electroproduction would not merely duplicate the physical information obtained by other means but should be considered in its own right.

Briefly, it is proposed to detect in a spectrometer all electrons scattered between 1° to 2° into a 1% momentum interval at a momentum

1/2 to 2/3 of the beam. The target is surrounded by a 4π detector and an axial magnetic field, which enables the momentum of reaction particles emitted at angles greater than some smallest angle to be measured. (The cost and size of this detector is a strong function of this minimum angle.) The detector consists of various counters and spark chambers to be placed in coincidence with the signal from the small-angle electron spectrometer.

Both first- and second-order backgrounds (in target density) are considered in some detail below, and it is found that by reducing the target density considerably from those densities conventionally employed, and maintaining an intense beam, the second-order backgrounds may be made small compared to the first-order backgrounds. The principal design problem seems to center around eliminating events from elastic electron-electron scattering in both detectors. The restrictions thus placed on this scheme are discussed below. That this is a severe problem may be seen by considering that both Compton scattering of low-energy gamma rays and Møller scattering of electrons by the electrons in the target are governed by cross sections proportional to $r_o^2 \approx 80{,}000$ microbarns, while an electron has a "nuclear" reaction cross section ≈ 3 microbarns.

A summary of the general conclusions reached appears at the end of this report, as a starting point for a serious design effort. Details concerning specific design problems connected with implementing this proposal will not be presented here; although hardware problems may very well be decisive, it seems clear that the problem itself must be outlined before design considerations are undertaken.

II. THE PHYSICS OF VIRTUAL PHOTONS

For a more complete description of electroproduction, see the report by L. Hand and R. Wilson;[2] here only the main features one encounters are given. Consider the Feynman diagram of Fig. 1(a). An electron initially of energy ϵ scatters through an angle θ and emerges with an energy ϵ'. The energy transferred plus the target rest mass consist of two parts: the energy of the reaction products in their own center of mass, and the energy of the center-of-mass recoil. The dynamics of the final

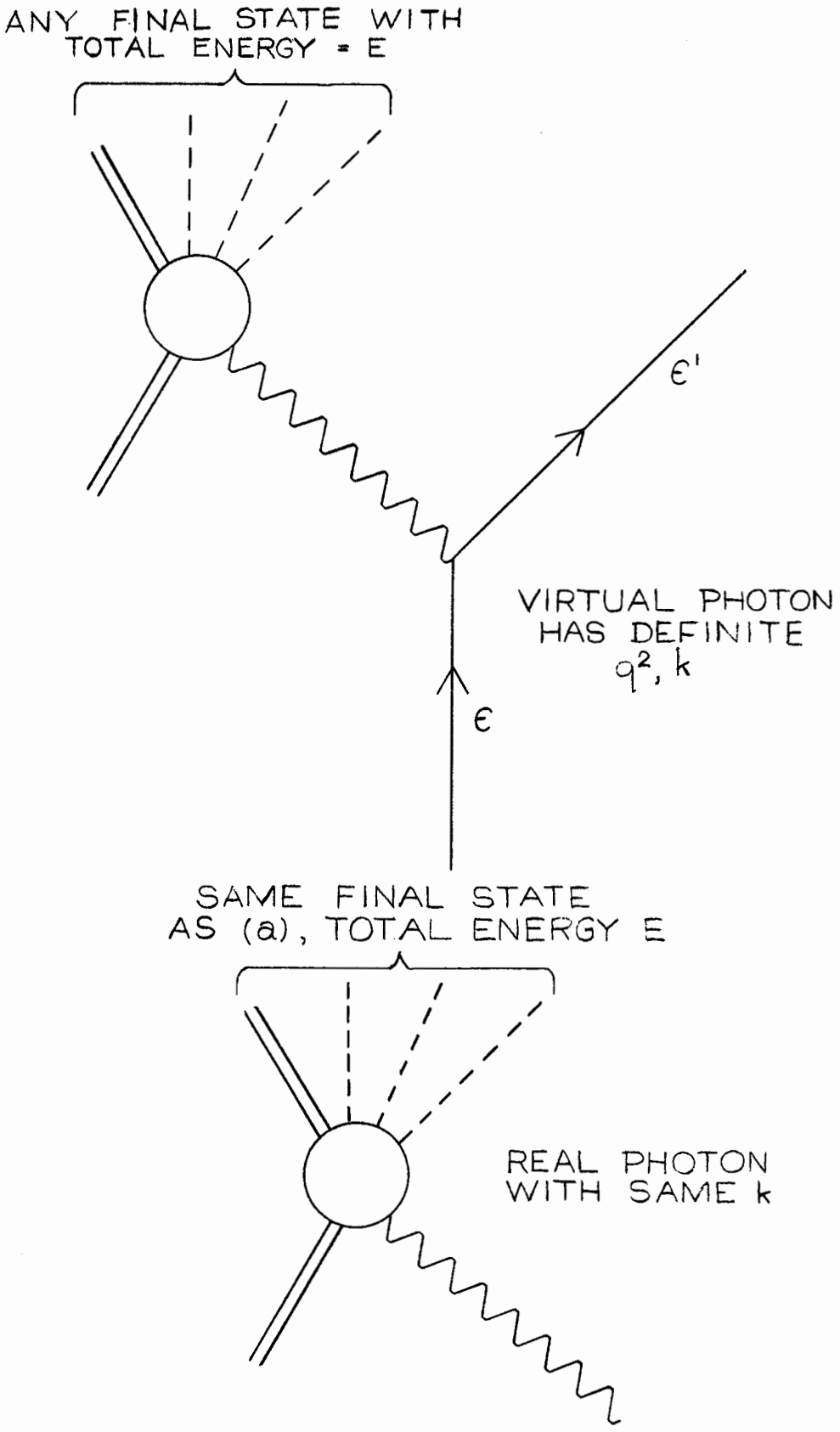

FIG. 1--Feynman diagrams for photo and electroproduction.

state interactions depend primarily on the total center-of-mass energy of the reaction products (excluding the electron) which we call E. It is very convenient to define another quantity, $k = \frac{E^2 - M^2}{2M}$; this happens to be numerically equal to the laboratory energy of the real photon, leading to the same total center-of-mass energy E for the reaction products in photoproduction. The k definition is useful because it allows a more direct correspondence of electroproduction results with photoproduction [Fig. 1(b)]. Figure 2 portrays the "polarization" of the virtual gamma ray; it is clear that this polarization depends on the electron scattering angle. This dependence may easily be derived by using helicity conservation in the electron brick wall frame and making a Lorentz transformation to, say, the center-of-mass frame for the reaction products. For the case of sufficiently small θ ($\theta \ll k/\sqrt{\epsilon\epsilon'}$) , the effective transverse polarization of the virtual gamma ray is no longer a function of θ:

$$\text{Effective transverse polarization} \approx \frac{2\epsilon\epsilon'}{\epsilon^2 + \epsilon'^2} \text{ at small angles .}$$

If $\epsilon' = \epsilon/2$, the effective polarization of the transverse component of the vector potential is $\approx 80\%$. It is then seen that for a given k, i.e., a given resonance or reaction threshold, a gain is realized from the higher energy ϵ in terms of effective polarization.

If the secondary reaction products are not observed, then one can write the cross section for the electrons as

$$\frac{d^2\sigma}{d\Omega d\epsilon'} = \frac{\alpha}{4\pi^2}\frac{k}{q^2}\frac{\epsilon'}{\epsilon}\left\{\left(2 + \frac{\cot^2\frac{\theta}{2}}{1 + \frac{(\epsilon - \epsilon')^2}{q^2}}\right)\sigma_{trans}(k,q^2) + \left(\frac{\cot^2\frac{\theta}{2}}{1 + \frac{(\epsilon - \epsilon')^2}{q^2}}\right)\sigma_{long}(k,q^2)\right\}$$

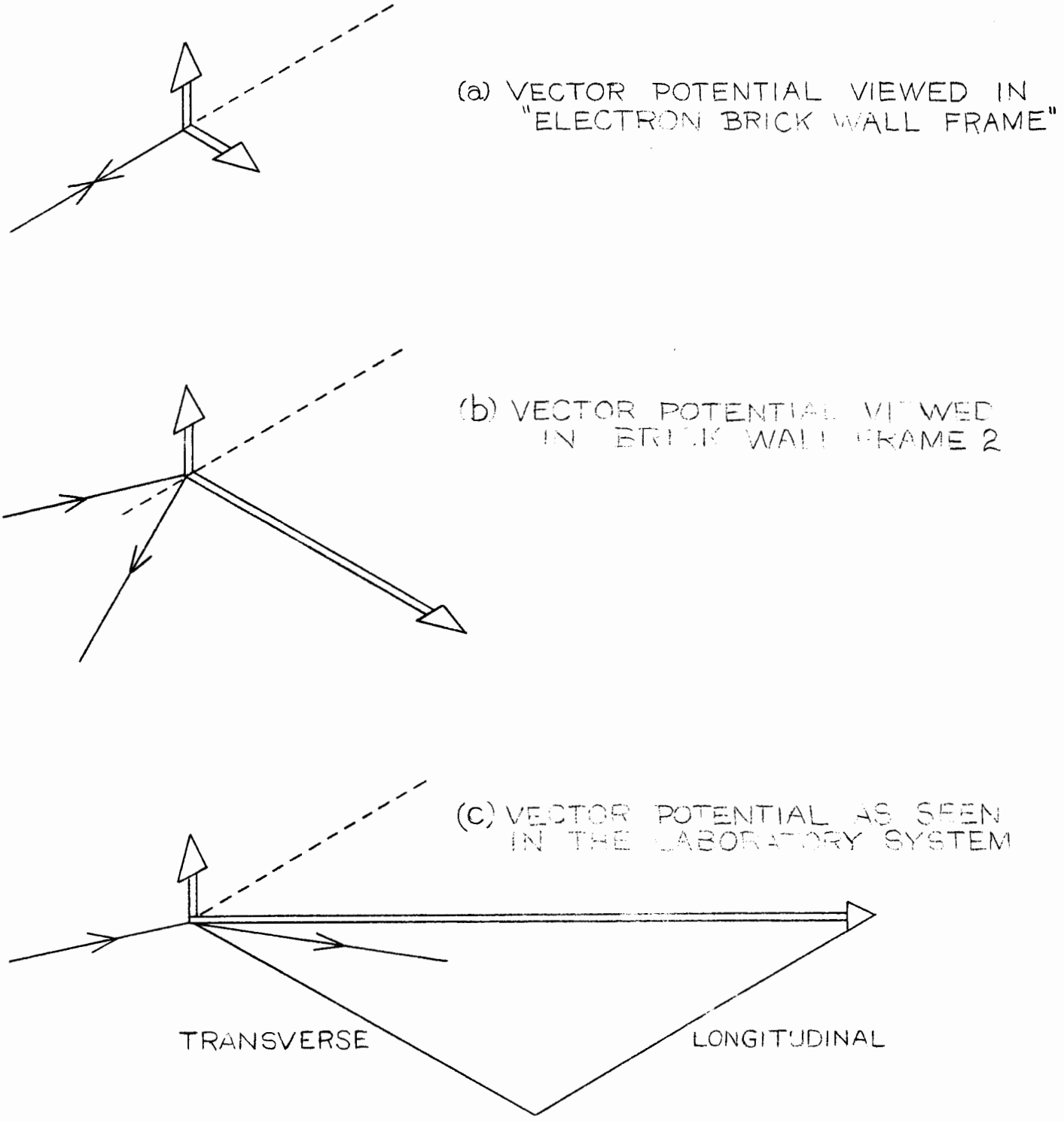

FIG. 2--Polarization of virtual gamma rays. In the figure, dotted lines represent the momentum transfer direction and hollow arrows represent the 2 independent (added incoherently) components of the vector potential associated with the transition current of the inelastically scattered electron. The frame called "frame 2" is the brick wall frame reached from the laboratory by a Lorentz transformation along the momentum transfer direction. Unlike the case of real photons, the effective polarization for virtual photons is not a Lorentz invariant and can be quite large in the laboratory.

If electrons only are observed, there is no interference between transverse and longitudinal matrix elements. The matrix elements $\sigma_{trans}(k,q^2)$ and $\sigma_{long}(k,q^2)$ have the dimensions of total cross sections, i.e., cm^2, and indeed $\lim_{q^2 \to 0} \sigma_{trans}(k,q^2) = \sigma_\gamma(k)$, the total cross section for gamma ray absorption at a laboratory energy k.

The distinction between transverse and longitudinal currents is useful only in the case of resonances where, in general, only one electric and one magnetic multipole can contribute. The longitudinal matrix elements arise only via the electric multipole. For the first pion-nucleon resonance in π^o photoproduction, one expects only a small electric quadrupole ($\approx 4.5\%$) contribution and hence a longitudinal contribution of this order of magnitude. According to most modern theories of the photoproduction of "anything" via a specific mechanism, one should be able to predict the relative amounts of longitudinal and transverse currents according to this mechanism. Peripheral processes seem to have[3] a definite large ratio of longitudinal to transverse currents, i.e., the longitudinal production is equally as important as the transverse. This is intuitively clear from the geometric nature of the currents involved in such processes. Thus it is seen that electroproduction adds a new degree of freedom which clearly has an important bearing on the correctness of any theoretical models proposed for a given process.

If small angles are considered, and one integrates over the solid angle of acceptance of a detector for the scattered electrons ($\theta \gg m/\sqrt{\epsilon\epsilon'}$, however, where m is the electron rest mass), the following approximation to the inelastic Rosenbluth formula above is obtained, giving the effective cross section for a particular reaction to be produced by electrons. It is assumed that the electron detector accepts the full 2π azimuthal angle (note that this angle must be measured to take advantage of the polarization of the virtual gamma rays) and that $\sigma_{long} = \sigma_{trans} = \sigma_\gamma(k)G(t)$ where $t = q^2$. For $G(t)$, the effective form factor of the reaction, one takes[4] as an approximation $G(t) = 1/(1 + t/8)$ with t measured in units of $fermi^{-2}$; then

$$\sigma_{effective} = \frac{\alpha}{\pi} \frac{dk}{k} \left(1 + \frac{\epsilon'}{\epsilon}\right)^2 \left(\int \frac{d\theta}{\theta}\right) (\sigma_\gamma G^2)$$

If $\int \frac{d\theta}{\theta}$ is replaced by $\frac{1}{2}\int \frac{dt}{t}$ and one integrates from the minimum possible t

$$t_{min} \approx \frac{m^2(p - p')^2}{pp'}$$

to a cutoff point at $t \approx 3\ F^{-2}$, $\left(G^2 \approx \frac{1}{2}\right)$, a logarithm of argument $\approx 10^6$ is obtained. If, on the other hand, an electron detector subtends a hollow cone $1^\circ < \theta < 2^\circ$, the same factors times log 2 appear. Thus the appearance of the logarithm means that the "efficiency" of a device detecting electrons at relatively large angles is quite high, in this case being $\frac{\log 2}{\frac{1}{2}(\log 10^6)} \approx 10\%$. It is this logarithm which makes the proposal below possible.

If $\epsilon' = \frac{1}{2}\epsilon$, then the $1^\circ < \theta < 2^\circ$ electron detector corresponds to an equivalent radiator of $\approx 3.7 \times 10^{-3}$ radiation lengths, i.e., the rate of electroproduction events yielding coincidences with the electron spectrometer is the same as the rate one would obtain into the same interval dk/k from real bremsstrahlung produced in a radiator of 3.7×10^{-3} radiation lengths.

Of course, σ_γ can be a partial cross section, because it is assumed that the main job of any experimenter who wishes to use this facility is the design of an appropriate trigger logic in the 4π secondaries detector. A typical total cross section for a reaction of interest[5] might be of the order of 1 microbarn, and a typical total cross section for gamma ray absorption in the several BeV region might be 100 to 150 microbarns. Thus, a ratio of about 100/1 between absorption of a virtual gamma ray and production of an "interesting" event into the 4π detector will be assumed.

If the reaction products are observed for a two-body final state (excluding the electron), it can be shown that the most complicated azimuthal dependence about the space momentum transfer is of the form

$$A + B \cos \varphi + C \cos^2 \varphi$$

Longitudinal matrix elements contribute through the terms in A and B (the latter via interference with the transverse matrix elements),

and hence the amount of longitudinal production can be determined without varying the electron angle θ. For a given multipole, or a peripheral model calculation, the center-of-mass angular dependences of A, B, and C are known. A similar theorem can be proved for more complicated final states if one averages over all of the various spins and all but two of the particle momenta.

III. COUNTING RATE FOR $1^\circ < \theta < 2^\circ$ DETECTOR

It is assumed that the SLAC machine will operate with 10^{12} electrons/pulse, 1.3×10^6 pulses/hour, an effective pulse length of 0.5 microseconds,* with a duty cycle of $\approx 1/5000$ and an energy of 20 BeV or less. In addition, the target thickness X will be expressed in units of 10^{20} H/cm^2; X = 1 corresponds to about 2/3-inch of STP hydrogen gas.

Assuming a 1 microbarn cross section, with $\frac{dk}{k} = 1\%$ and $\epsilon' = \epsilon/2$, the rate for events of interest becomes

$$\boxed{\text{Rate} \approx 4000\ X/\text{hour}}$$

IV. BACKGROUNDS CAUSING ACCIDENTAL COINCIDENCES

It is clear from the nature of coincidence experiments that the relevant figure of merit for a given photon monochromatization scheme is

$$\boxed{P \equiv \left(\frac{\text{Rate of events}}{\text{hour}}\right) \times (\text{signal/accidentals})}$$

An explicit calculation of P in terms of the quantities of interest is

$$\boxed{P = \left(\frac{X_{eff}}{X_e}\right)\left(\frac{\text{duty cycle}}{2T_R}\right)\left(\frac{\frac{dk}{k}\,\sigma_{signal}\,G^2}{\int \frac{dk}{k}\,\sigma_{trigger}}\right)\left(\frac{\sigma_{signal}}{\sigma_{tot,\ inelastic}(R+1)}\right)}$$

*The nominal pulse length is 2 microseconds, but the structure in the beam will probably reduce this by an appreciable amount.

Each of the above factors is explained below.

The quantity X_{eff}/X_e is the ratio of "effective" radiator for the particular electron detection geometry, X_{eff}, to the total equivalent radiator lengths for electrons. This ratio has been calculated to be ≈ 0.1 for the 1^o to 2^o detector.

The next factor is the ratio of the duty cycle to twice the resolving time of the coincidence electronics for coincidences between the 4π detector and the electron detector. For a 0.5-microsecond pulse, the duty cycle is $\approx 1/5000$, and a resolving time of $2T_R \approx 2 \times 10^{-9}$ seconds leads to a ratio of $\approx 3 \times 10^8$ hour^{-1} for this factor.

The next term expresses the dependence of P on the ability of the 4π secondaries detector to select events qualitatively. It is assumed that almost no photon monochromatization takes place, but a trigger signal for a possible coincidence with the electron detector is achieved only if, for example, a three-body event (in which one particle is more than minimum ionizing) and two gamma ray showers appear. It is assumed that a clever experimenter can design such a trigger, although it is clear that most of the work involved in any specific experiment is to do so successfully.

Thus it is assumed that

$$\int \frac{dk}{k} \sigma_{trigger} \approx 2 \text{ microbarns}$$

and

$$\frac{dk}{k} \sigma_{signal} G^2 \approx 10^{-2} \times 1 \text{ microbarn} \times \frac{1}{2}$$

giving a ratio of $\approx 2.4 \times 10^{-3}$ here.

The last term expresses the effect of the electrons in the electron detector which are not related to the inelastic events of interest. Assume that $\sigma_{tot,inelastic} \approx 100$ microbarns, with $\sigma_{signal} \approx 1$ microbarn. The ratio of wide-angle bremsstrahlung electrons in the electron detector to those produced by the total nuclear inelastic scattering is expressed

by R. One then obtains

$$\boxed{P \approx \frac{720}{R+1} \text{ hour}^{-1}}$$

It is seen at once that for any R we will never be rate-limited at SLAC but always accidentals-limited. R is the ratio of wide-angle bremsstrahlung electrons (WAB) to all nuclear inelastic electrons:

$$R = \frac{\left.\frac{d^2\sigma}{d\Omega d\epsilon'}\right|_{WAB}}{\left.\frac{d^2\sigma}{d\Omega d\epsilon'}\right|_{inelastic}}$$

In the limit $\sigma_{trans} = \sigma_{long}$, a suitable expression for $\left.\frac{d^2\sigma}{d\Omega d\epsilon'}\right|_{inelastic}$ has been found above. A convenient expression for small-angle WAB must now be obtained. An approximate formula sufficiently accurate for these purposes is found in Ref. 6. Remember that $\frac{d\sigma}{d\Omega}$ for Coulomb scattering at very small angles is

$$\left.\frac{d\sigma}{d\Omega}\right|_{elastic} \approx \left(\frac{2r_o m}{\epsilon\theta^2}\right)^2 ; \quad r_o = 2.818 \text{ fermi}$$

From this expression for $\frac{d\sigma}{d\Omega}$ and neglecting all form factors and recoil factors,

$$\frac{d^2\sigma}{d\Omega d\epsilon'} \approx X_e \frac{1}{k}\left(\frac{2r_o m}{\epsilon'\theta^2}\right)^2 \left(1 + \frac{\epsilon'^2}{\epsilon^2}\right)$$

where the equivalent radiator for WAB, X_e, is

$$X_e \approx \frac{\alpha}{\pi}\frac{\epsilon'}{\epsilon}\left[\log\left(\frac{t}{m^2}\right) - 1 + \frac{k^2}{\epsilon\epsilon'}\log\frac{\epsilon+\epsilon'}{m}\right]$$

$$\approx \frac{10\alpha}{\pi}\frac{\epsilon'}{\epsilon}\left[1 + \frac{k^2}{\epsilon\epsilon'}\right]$$

Using the latter approximation, (good for the q^2 and the energy range of interest here: $2\ F^{-2} < t < 16\ F^{-2}$; ϵ, ϵ' several BeV),

$$\frac{d^2\sigma}{d\Omega d\epsilon'} \approx \frac{7400 \text{ microbarns}}{\theta^4} \frac{1}{k} \left[1 + \frac{k^2}{\epsilon\epsilon'}\right] \left(\frac{m^2}{\epsilon\epsilon'}\right) \left(1 + \frac{\epsilon'^2}{\epsilon^2}\right)$$

An even cruder formula, good for low ϵ' and small angles, is

$$\frac{d^2\sigma}{d\Omega d\epsilon'} \approx \frac{1850 \text{ microbarns}}{\epsilon} \left(\frac{m}{\epsilon'}\right)^2 \left(\frac{1}{1 - \cos\theta}\right)^2$$

The latter formula is good only if $k^2 > \epsilon\epsilon'$, i.e., $k \gtrsim \frac{2}{3}\epsilon$.

Because the arguments of the various logarithmic terms are only approximate anyway, the estimates $\log q^2/m^2 \approx 11$ and $\log\left(\frac{\epsilon + \epsilon'}{m}\right) \approx 10$ have been set. A much more accurate calculation of WAB has been made by E. A. Allton.[7]

Two limiting cases of the above will be considered.

(1) $\underline{\epsilon' \ll \epsilon}$

$$\frac{d^2\sigma}{d\Omega d\epsilon'} \approx \frac{1850 \text{ microbarns}}{\epsilon} \left(\frac{m}{\epsilon'}\right)^2 \frac{1}{(1 - \cos\theta)^2}$$

$$\approx \frac{3700 \text{ microbarns}}{\epsilon'} \frac{m^2}{t} \frac{1}{(1 - \cos\theta)}$$

$$R \approx \frac{2.5 \times 10^4 \text{ microbarns-MeV}}{G^2 t} \left(\frac{k}{\epsilon'}\right)$$

(2) $\underline{\epsilon' \approx \tfrac{1}{2}\epsilon}$

$$\frac{d^2\sigma}{d\Omega d\epsilon'} \approx \frac{7000 \text{ microbarns}}{k} \frac{m^2}{t} \frac{1}{1 - \cos\theta}$$

$$R \approx \frac{4.8 \times 10^4 \text{ microbarns-MeV}^2}{G^2 t}$$

Two things can be seen from the above expression for R: (1) the minimum R comes for the highest ϵ', and (2) it is desirable in any case to maximize $G^2 t$ where G^2 is the form factor for one inelastic scattering. Using $G \approx 1/(1 + t/8)$, the maximum value of tG^2 is $\approx 8 \times 10^4$ MeV^2 at $t \approx 8$ F^{-2} and tG^2 varies only 10% for $4 \text{ F}^{-2} < t < 16 \text{ F}^{-2}$. By happenstance this corresponds to the most interesting range of momentum transfers.

Thus it can be seen that for $\epsilon' \approx \epsilon/2$, $R \approx 5/8$, and

$$\boxed{P \approx 440 \text{ hour}^{-1}}$$

For a signal-to-accidental ratio of 1:1, data could be taken at the rate of 440 counts/hour. This may seem an intolerable background from accidental coincidences, but good spatial resolution on the point of origin along the beam line for the event would allow operating at such levels and ultimately filtering the noise. Actually, one would probably plan to operate at somewhat lower rates, reducing this problem accordingly.

V. ELECTRON-ELECTRON SCATTERING: RESTRICTION ON t

The cross section for elastic electron-electron scattering is

$$\frac{d\sigma}{d\epsilon'} \approx 2\pi r_o^2 \left\{ \frac{m}{\epsilon'^2} + \frac{m}{k^2} \right\}$$

This cross section is much too large to allow its inclusion in the above estimate of accidentals. Fortunately, a simple constraint on any designed apparatus will eliminate all elastic and inelastic electron-electron scattering. Elastic electron-electron scattering obeys the kinematic relation

$$\frac{m}{(1 - \cos\theta)} \approx \epsilon' \quad \text{if} \quad \epsilon' < \epsilon$$

Thus, computing $t = 2\epsilon\epsilon'(1 - \cos\theta)$, one finds that t does not depend on angle. Then, defining $t^{ee} = 2m\epsilon = 0.53 \text{ F}^{-2} \left(\frac{\epsilon}{20 \text{ BeV}}\right)$, if the

electron detector detects only electrons for which $t \gg t^{ee}$, the exclusion of electron-electron events is guaranteed. This is not a severe restriction, assuming of course that the electron detector can reject the large number of low energy electrons emerging from the target. The ratio of the number of these electrons possessing the "wrong" energy to the nuclear inelastic electrons is estimated to be

$$\approx \frac{\pi r_o^2 \, \theta_{max}}{\frac{\alpha}{\pi} \frac{dk}{k} \left(1 + \frac{\epsilon'}{\epsilon}\right)^2 \int \frac{d\theta}{\theta} \sigma_\gamma G^2}$$

$$\approx \frac{2.4 \times 10^5 \text{ microbarns}}{10^{-3} \text{ microbarns}} \times \theta_{max}^2$$

Thus it can be seen that: (1) a gain is actually achieved by going to small angles (but $\theta > \sqrt{m/\epsilon}$); and (2) rejection of electrons with energies $\approx 2m/\theta^2$ must be of the order of 10^{-6} at $\theta_{max} \approx 1/30$, an improvement over spectrometers currently in use, but not in principle unattainable if enough overdetermination of the electron is employed.

The first practical problem to be faced for such a scheme is the proof that such a system can in fact be constructed. This can be checked on a lower energy machine, although it must be kept in mind that high energy beams possess an advantage here in that $t^{ee} \approx \epsilon$. Therefore, if t is decreased to allow for the decrease in energy at Mark III, for example, and one tries to keep the same ratio of t/t^{ee}, it is found that $\theta \approx 1/\epsilon$; i.e., it is desirable that the transverse momentum be constant. The problem of rejection, therefore, is worse for the Mark III accelerator than for SLAC. Furthermore, the data rates are less, because $\int \frac{d\theta}{\theta}$ must be smaller for practical detectors needing a larger θ_{min}.

VI. SECOND-ORDER EFFECTS IN X: ELECTRON DETECTOR

The probability that electrons, having lost their energy by electron-electron scattering, will then Coulomb-scatter into the detector with the proper energy to be detected, is now computed.

The differential yield/incident electron is

$$\frac{d^2y}{d\Omega d\epsilon'} \approx \frac{10^{-9}}{m} \frac{X^2}{2} \left(\frac{m^2}{t}\right)^2 \left\{ \left(\frac{\epsilon}{\epsilon'}\right)^2 + \left(\frac{\epsilon}{k}\right)^2 + 1 \right\}$$

It is easily shown that the ratio of this yield for the momentum transfers of interest to the signal yield is $\lesssim 10^{-5}$ X and thus is completely negligible.

One might consider another higher order effect. Is 1° or 2° a large angle at these energies? In other words, can one trust the use of formulas for the single scattering of electrons or the calculation for WAB at these angles, which is also good only in the same limit?

The cross-over point at which one must consider plural and multiple scattering occurs very roughly at an angle such that the probability for an electron scattering into a greater angle is ≈ 1. This corresponds to $\theta \approx \left(\frac{m}{\epsilon}\right)\sqrt{4\pi r_o^2 X}$, or for $X \approx 1$, a transverse momentum of ≈ 50 KeV. Because the rms multiple scattering angle, $< \theta^2 >^{\frac{1}{2}} \approx \frac{21}{p\beta}\sqrt{\text{target r.}\ell.}$, corresponds to a transverse electron momentum of 35 KeV $\sqrt{X}$, it can be seen that at 10 BeV angles almost 1000 times smaller can be approached before the single scattering formula breaks down.

VII. FIRST- AND SECOND-ORDER BACKGROUNDS IN THE SECONDARIES DETECTOR

So far no difficulty in principle has been encountered with the plan to detect electrons emerging at small angles, but now the flood of low energy electrons and gamma rays with which the target illuminates the 4π secondaries detector must be considered. It is quite possible that one may find here a limitation in the permissible maximum X from the second-order processes. Listed below are the reactions that will be considered.

A. First-Order Backgrounds in 4π Detector

1. Electron-electron scattering
2. Wide-angle bremsstrahlung
3. Inelastically scattered electrons from photoproduction processes
4. Recoil protons from small-angle elastic electron scattering; scattered electrons from the same reaction
5. "Strong interaction" backgrounds arising from electroproduction via 0.02 equivalent radiation lengths, including
   a. Dalitz pairs
   b. High energy gamma rays, mainly from π^{o} decay
   c. Electroproduced π's, K's, etc.

B. Second-Order Backgrounds in 4π Detector

1. Electron-electron scattering followed by Coulomb scattering
2. Real bremsstrahlung followed by either an electron or a gamma ray or both appearing at wide angles from Compton scattering
3. Direct pair production followed by Coulomb scattering of one member of the pair

A. First-Order Processes

In defining a proper figure of merit for first-order background, the most obvious question one asks is, "What is the ratio of spurious tracks to real events?" Because spark chambers have a high spatial resolution, one can hope to separate real from spurious events if the longitudinal origin of an event is detected. This is the reason that a signal-to-noise ratio of 100% for accidental coincidences was accepted previously. Now, however, assume that the selective trigger has acted to select 3 pions plus 1 gamma ray plus a recoil proton. The question is, what else can be seen? This situation is analogous to that in bubble chamber work, because the analysis of events must take place in the presence of many spurious tracks of various kinds. Rather than consolidating all backgrounds into one figure of merit, it is desirable to

make a separation into several broad categories and to indicate how they may be combined as an index of the merit of any given situation. One notices that here, as above, the reals/accidentals tradeoff is encountered, but with the longer resolving time T_S corresponding to the sensitive time of a spark chamber.

Thus one can define

$$P_S = \left(\frac{\text{Rate of real events}}{\text{hour}}\right) \Big/ \left(\frac{\text{Background events}}{\text{real event}}\right)$$

By comparing P_S with P for a given experiment, it can be seen whether one would expect to be limited by backgrounds in the secondaries detector or by accidental coincidences. If the cross section for a background reaction is σ_B,

$$P_S = X_{eff} \frac{dk}{k} \left(\frac{\sigma_{signal}}{\sigma_B}\right) \left(\frac{\text{duty cycle}}{T_S}\right)$$

where X_{eff} = "equivalent radiator" for the electron detector used

$\sigma_{sig} = \sigma_{sig}(0,k)G^2(t)$, assumed to be about 1/2 μbarn in the cases of interest, because $\sigma_{sig}(0,k)$ is assumed to be ≈ 1 microbarn

σ_B = background cross section/incident electron

T_S = spark chamber sensitive time = 1/2 microsecond
$= 1.4 \times 10^{-10}$ hour = assumed to equal pulse length

To get a feeling for the numbers, consider first the background arising essentially from the photon total absorption cross section. This cannot be removed, as it is always present if the signal itself is present. It has been assumed that $(0.03)\int\sigma_{tot} \frac{dk}{k} \approx 3$ microbarns/electron; as an estimate, take X_{eff} to be 4×10^{-3} r.ℓ., $\frac{dk}{k} = 1\%$. Thus the maximum value P_S could possibly possess, regardless of the cleverness of

the experimenter, is $10 \approx P_S(\text{max})$. Because it would probably be possible to cope with between 5 and 25 background tracks in a picture, if the point of origin of the scattered electron were sufficiently well determined, there is a natural upper limit of < 50 to 250 counts/hour for a signal with a 1 microbarn "photoproduction" cross section. If the machine pulse is spread out over the full 1.5 to 2 microseconds nominally claimed, even if the distribution is not constant, we gain an additional factor of 3 to 4 from the shorter sensitive time of the spark chamber.

It has been shown that with $\sigma_B \approx 3$ microbarn, one can expect $P_S \approx 10$ hour^{-1}. Now the cross section σ_B for the various other processes must be computed, reaction A.5 having been taken care of by the above calculation.

1. Electron-electron scattering

It will be shown below that electron-electron scattering is a prohibitively large cross section. Precautions must therefore be taken that no particle obeying the electron-electron scattering kinematics is allowed to pass through the spark chamber detectors. Thus, the smallest angle one can observe, θ_{min}, is determined by the magnetic field and physical size of a detector to provide a cutoff for those electrons scattered at $\theta > \theta_{min}$. This can be shown to require

$$\frac{2.6 \text{ kilogauss-inch}}{Bd} < \theta_{min}$$

where B is the magnetic field (axial) of the detector and d is the radial distance from the beam axis to the first spark chamber. For $B = 13$ kG and $d = 12$ inches, $\theta_{min} \approx 1^\circ$.

One experimental project that should be initiated if construction of this inelastic electron facility is seriously contemplated is a measurement to determine how close it is possible to approach the θ_{min} calculated above. To show that it is not possible to allow <u>any</u> electron-electron scattering to appear directly in the secondaries detector, one may choose $B = 13$ kG and $d = 6$ inches. Thus $\theta_{min} = 2^\circ$. The cross

section for electron-electron scattering into a cone between 1° and 2° is:

$$d\sigma \approx 2\pi r_o^2 \int \frac{m}{\epsilon'^2}\, d\epsilon'$$

$$\approx \pi r_o^2 \left(\theta_{max}^2 - \theta_{min}^2\right)$$

$$\approx 300\ \mu\text{barns} \quad \text{if} \quad \theta_{max} \approx 2^{\circ}$$

It can be seen that inclusion of the cone from 1° to 2° would reduce the rate possible to 1/2 event/hour even if 10 spurious tracks are permitted per real event. (The above formula assumes $\frac{2m}{\theta_{min}^2} \ll \epsilon$.)

2. Wide-angle bremsstrahlung

Another first-order process considered above only as a source of electrons in the electron detector is wide-angle bremsstrahlung. Again, a cutoff in the lowest possible transverse momentum must be assumed, $\left(P^T_{cutoff}\right)$, which a particle must possess in order to reach the spark chamber 4π detector. One may thus compute

$$2\pi \int_{\theta=\theta_{min}}^{\pi} \sin\theta d\theta \int_{P_c^T/\sin\theta}^{\epsilon} \frac{d^2\sigma}{d\Omega d\epsilon'}\, d\epsilon'$$

To obtain what is probably an overestimate of the wide-angle bremsstrahlung, use the simple semi-empirical formula quoted above, setting the upper limit of the integral over $d\epsilon'$ at infinity. This formula neglects form factors and the $\cos^2\theta/2$ in the angular dependence of the cross section; it is hence an overestimate which is probably increasingly pessimistic as P_c^T is increased.

The result, using the limit $\epsilon' \ll \epsilon$ for the WAB, is

$$\left.\frac{d^2\sigma}{d\Omega d\epsilon'}\right|_{WAB} \approx 2000\ \text{microbarns} \left(\frac{m}{\epsilon}\right)^2 \frac{\epsilon}{\epsilon'^2} \frac{1}{(1-\cos\theta)^2}$$

$$\Delta\sigma_{WAB} \approx \iiint \frac{d^2\sigma}{d\Omega d\epsilon'} \Delta\Omega\Delta\epsilon' \approx \frac{1}{2} \times 10^5 \text{ microbarns} \left(\frac{1}{\theta_{min}}\right)\left(\frac{m^2}{P_c^T \epsilon}\right)$$

If d is the cutoff radius,

$$P_c^T = \left(\frac{Bd}{2.6 \text{ kilogauss-inch}}\right) \text{MeV/c}$$

For the case $B = 13$ kG, $d = 12$ inches, $P_c^T = 60$ MeV/c. If $\epsilon = 20$ BeV and $\theta_{min} = 1^\circ$, we have

$$\sigma_{WAB} \approx 0.7 \text{ microbarns} \quad \begin{cases} \epsilon = 20 \text{ BeV} \\ P_c^T = 60 \text{ MeV/c} \\ \theta_{min} = 1^\circ \end{cases}$$

The wide-angle bremsstrahlung, for a reasonable cutoff in transverse momentum and angle, only reduces P_S by 25% to 8 hour^{-1}. Clearly, an advantage is gained by the high initial electron energy. It would be helpful if a more exact integration were performed using the Allton program for σ_{WAB}.[7]

3. Inelastically scattered electrons from "photoproduction" processes

Exactly the same integral must be done over the inelastic Rosenbluth equation as was done above for wide-angle bremsstrahlung in order to find the contribution from the total photon absorption cross section,

$$\int \sigma \frac{dk}{k} \approx 100 \text{ } \mu\text{barns} .$$

The estimate below is quite crude, and the inelastic formula for $\epsilon \ll k$ is used, which greatly underestimates the contribution from the first

resonance; for example,

$$\sigma_{\text{inelastic}} \approx \frac{\alpha}{2\pi} \int \frac{d(\cos\theta)}{1 - \cos\theta} \int \frac{dk}{k} \sigma_{\text{tot}}$$

$$\approx \frac{2\alpha}{\pi} 500 \text{ microbarns} \times \log\left(\frac{2}{\theta_{\text{min}}}\right)$$

$$\lesssim 2 \text{ microbarns } \log \frac{2}{\theta_{\text{min}}}$$

$$\boxed{\sigma_{\text{inelastic}} \leq 10 \text{ microbarns if cutoff is } \theta_{\text{min}} \approx 1^{\circ}}$$

Thus one might expect a greater contribution from the inelastic electrons than from the wide-angle bremsstrahlung in the hypothetical case of interest. The form factors in inelastic scattering will reduce this number considerably, probably more than a factor of 2, because much of $\int \frac{dk}{k} \sigma_{\text{tot}}$ comes from low k and hence high ϵ'.

4. Recoil protons from small-angle elastic electron-proton scattering

Another first-order effect to be considered is the flux of protons from the gas due to very small-angle electron scattering. If τ is the recoil proton kinetic energy ($\tau < M$),

$$d\tau = \frac{\epsilon^2}{M} \frac{d\Omega}{2\pi}$$

for small τ, where M is the proton rest mass.

If the deviation of the recoil proton from the plane perpendicular to the beam is called δ,

$$\delta \approx \left(1 + \frac{\epsilon}{M}\right) \frac{\theta}{2} \qquad \delta, \theta \ll 1$$

where θ is the electron scattering angle. The cross section (neglecting form factors) is

$$\frac{d\sigma}{d\tau} \approx \frac{2\pi}{M} \left(\frac{r_o m}{\tau}\right)^2$$

Suppose that by using a thin absorber one excludes protons of $\tau < 50$ MeV from reaching the detector; then

$$\sigma_{\text{recoil proton}} > \tau_{min} \approx 5 \times 10^5 \left(\frac{m}{M}\right)\left(\frac{m}{\tau_{min}}\right)$$

$$\approx 250 \text{ microbarns} \left(\frac{m}{\tau_{min}}\right)$$

$$\boxed{\sigma_{\text{recoil protons}} \approx 2.5 \text{ microbarns}}$$

if $\tau_{min} \geq 50$ MeV corresponds, for example, to a range of about 1 cm or $\approx 1/8$ radiation length of aluminum. Thus it would seem that a cutoff of even 25 or 10 MeV could be tolerated, especially as all protons of $\tau \leq 50$ MeV emerge at angles between 80 and 90 degrees to the beam. One might try cutting out a small ring around the beam either with an absorber or just by not allowing the detectors to subtend this angular region. It is seen that δ in terms of τ is given by $\delta \approx \sqrt{\frac{\tau}{2M}} \approx \frac{P}{2M}$; therefore, for example, 10 MeV protons emerge at $\approx 86^\circ$ independent of the initial beam energy if it is sufficiently high. Since these recoil protons obey elastic kinematics, they can presumably be eliminated in the analysis, if they cause no triggering difficulties.

This ability to observe low energy protons is actually an important feature of the entire scheme, because it is true that the angle of emission for a low energy (struck with large impact parameter) proton is a very good kinematic indicator of the mass of the neutral system produced in the reaction.

The electron elastic scattering and direct observation of the electron in the secondaries detector is now considered:

$$\frac{d\sigma}{d\Omega} \approx \left(\frac{2r_o m}{\epsilon\theta^2}\right)^2$$

at small angles and high energies. Assuming a small cutoff angle $\theta_{min} \ll 1$, an angle so small that $\epsilon' \approx \epsilon$ and thus form factor and

magnetic scattering effects are negligible, one obtains

$$\sigma_{elastic} \approx 4\pi r_o^2 \left(\frac{m}{\epsilon\theta_{min}}\right)^2$$

$$\sigma_{elastic} \approx 10^5 \text{ microbarns} \left(\frac{m}{\epsilon\theta_{min}}\right)^2$$

for $\epsilon = 20$ BeV, $\theta_{min} = 1^\circ$, $\sigma_{elastic} \approx 1$ microbarn, which implies that this is a significant, but not major, contribution to the backgrounds in the 4π detector. Again the gain from high energy at SLAC may be seen. In addition to the above, a further suppression of the above from the form factor is present, because a 20 BeV electron scattered at 1° corresponds to $t \approx 3$ fermi^{-2} and the form factor gives another factor of 2.

B. Second-Order Processes

Consider the limitations placed on the target thickness X due to the requirement that the total effective cross section for the cascade processes be limited to several microbarns, i.e., comparable to the sum of first-order processes in a reasonable secondaries detector.

1. Electron-electron scattering, followed by Coulomb scattering

$$\sigma_{B.1,effective} \approx \iint (2\pi r_o X) \frac{m}{\epsilon'} \frac{d\epsilon'}{\epsilon'} \left(\frac{2r_o^2 m}{\epsilon'\theta^2}\right)^2 d\Omega$$

The integral extends over $\theta_{min} \to \infty$ (i.e., π) and $\epsilon' = \frac{P_T}{\theta}$; thus

$$\sigma_{B.1,effective} \approx \text{microbarns } (X)\left(\frac{m}{P_T}\right)^3$$

This result, in this approximation, is independent of θ_{min}. If $P_T \approx 50$ MeV/c, for first-order dominance it is required that

$$X \lesssim 1000 , \quad \text{for } P_T \geq 50 \text{ MeV/c}$$

The major gain seems so far to arise from the transverse momentum cutoff rather than from the thin target, as $X = 1000$ corresponds to 1 inch of liquid hydrogen.

2. Real bremsstrahlung followed by Compton scattering of the gamma ray, also producing a recoil electron

These are first-order backgrounds for real bremsstrahlung beams, so the figure of merit P_S defined above for the case of a real bremsstrahlung beam on a target will also be computed here for comparison of real photon beams with the scheme proposed in this report.

The total cross section for Compton scattering ($k < m$) is $\frac{8\pi}{3} r_o^2$. Thus the total energy radiated into 4π for a given target thickness X is proportional to

$$\frac{1}{2} \frac{X}{3} \times 10^{-5} \frac{4}{3} \int_0^m \frac{dk}{k} k \frac{8\pi}{3} r_o^2 \qquad 0 < k < m$$

or $\approx Xm$ (1.5 microbarns). Because a background cross section σ_B of 3 microbarns was shown above to give $P_S \approx 5$ hour^{-1}, one can interpret this result as giving:

$$P_S \text{ (bremss.} \rightarrow \text{Compton scattering; } k < m) \approx (10 \text{ hour}^{-1})/\tfrac{1}{2} X \text{ MeV}$$

In other words, at the data rate of 10 counts/hour from the "1 microbarn" signal, we have 0.5 X MeV radiated into 4π during the pulse in which the event occurred. To test whether any given experimental arrangement of counters and spark chambers is sensitive to this flux of low energy photons, it is easy to duplicate these fluxes with a weak photon beam and a dense target. The mean free path for Compton scattering in liquid hydrogen is $\approx$ 15 inches, which means that targets of much less than this amount must be used to test for the sensitivity in any given situation to these low energy gamma rays. A 4-inch liquid hydrogen target radiates 1 MeV/pulse into 4π at an incident electron intensity of $\approx$ 1000/pulse. Very preliminary information indicates no serious trouble in spark chambers at these gamma fluxes.[8]

Higher energy ($k > m$) gamma rays also scatter after having been produced in the target. In the limit of high incident k, the scattered energy obeys the same kinematic relation as the electron-electron scattering and is therefore mostly a function of the angle at which one observes the gamma ray.

$$\frac{d\sigma}{d\Omega} \approx \frac{r_o^2}{2}\frac{k'}{k} \qquad \text{for} \quad k \gg m$$

and the scattered photon energy is $k' \approx m/(1 - \cos\theta)$ for $\theta > \sqrt{\frac{2m}{k}}$. In performing the integral over solid angle the change in kinematics for $\theta < \sqrt{\frac{2m}{k}}$ must be taken into account. Thus the integral is evaluated

$$\int_{m/k}^{2} \frac{m}{k}\frac{d(1 - \cos\theta)}{1 - \cos\theta} + \int_{(1-\cos\theta)_{min}}^{m/k} d(1 - \cos\theta)$$

By setting $(1 - \cos\theta)_{min} \approx 0$, one obtains $\frac{m}{k}\left[\log\frac{2k}{m} + 1\right]$. Therefore, the answer sought for the effective cross section for Compton scattering of high energy gamma rays is

$$\approx \frac{1}{2}\frac{4\pi r_o^2}{3}\int_m^\infty \frac{m}{k^2}\,dk\left[\log\left(\frac{2k}{m}\right) + 1\right] \times \frac{1}{3} X \times 10^{-5}$$

By setting the quantity in brackets equal to 4, the effective cross section for gamma rays above 1/2 MeV to scatter into the detector is found to be

$\sigma_{B.2} \approx$ (0.5 microbarn) X	
high energy gammas	$k > m$

If $X \approx 1$, no difficulty with this background source should be expected. It is not presently known what the permissible tolerance for medium energy gamma fluxes in spark chamber detectors is. It is

therefore strongly recommended that an experimental determination of the exact limitations imposed by these various processes be carried out soon. Thus it can be seen that if this source of gamma rays of energy is to be reduced $\approx m/(1 - \cos\theta)$ in the detectors, relatively thin targets must be used. If $X \approx 10$, the number of these gamma rays/event is comparable to the number of inelastically scattered electrons/event. Any lead plate spark chamber for conversion of high energy gamma rays will also convert these Compton-scattered gamma rays into electron-positron pairs. The unique kinematics for the total pair energy may provide the means of rejection as well as a method for calibrating the system for momentum analysis.

Although the transverse momentum cutoff effectively removes the (electron-electron)-Coulomb scattering cascade events, it cannot remove the Compton-scattered gammas. This then limits the maximum permissible X. More cannot be said without specific experiments with specific equipment. We assign the limit $X \leq 10$ from this process.

We must now consider the associated production recoil electrons from Compton-scattered gamma rays. The maximum transverse momentum imparted by a gamma ray of energy k to a recoil electron is $k/\sqrt{1 + 2k/m}$. If $k = 20$ BeV, the maximum transverse P is 70 MeV, as for electrons from electron-electron scattering. Thus, if these latter electrons are eliminated, so will the Compton recoil electrons be eliminated. For completeness, the spectrum for the recoils is

$$\frac{d\sigma}{d\epsilon'} \approx \pi r_o^2 \frac{m}{\epsilon'} \frac{1}{k - \epsilon'} \left(\text{if } \frac{k}{2} < \epsilon' < k - \frac{m}{2}\right)$$

$$\approx 0 \quad \text{otherwise}$$

Integrating the above over the bremsstrahlung spectrum yields

$$\frac{d^2\sigma}{d\epsilon' dQ} \approx \pi r_o^2 \frac{m}{\epsilon'} \frac{d\epsilon'}{\epsilon'} \log \frac{2\epsilon'}{m}$$

This differs from the spectrum of recoils from electron-electron scattering only by the factor $\frac{1}{2} \log \frac{2\epsilon'}{m} \approx 2$, so parity between the two

effects is not reached until the target is at least 1/2 radiation length thick. Another way to state the same thing is to observe that one equivalent quantum appears to be about twice as effective as one electron in producing the $d\epsilon'/\epsilon'^2$ spectrum of low energy electrons. To make the $d\epsilon'/\epsilon'$ spectrum expected from pair production, one finds from Rossi's discussion of tridents[9] that electrons make tridents as expected with about 0.02 equivalent radiator. Hence, equivalent photons are about 50 times worse for the $d\epsilon'/\epsilon'$ part of the spectrum if the number of hydrogen atoms/cm^2 in the target is the same. If the incident beam energy is above about 10 BeV, part of the spectrum at 0° emerging from the target will be dominated by the direct pairs; this will correspond approximately to the region between $0.02\ \epsilon > \epsilon' > 200$ MeV.

3. Other contributions to background from real bremsstrahlung

The radiation length of the target in these units is $\frac{1}{3} \times 10^{-5}$ X radiation lengths, so that the 0.02 radiation length equivalent radiator means that direct electroproduction dominates completely is $X < 1000$.

C. First-Order Figure of Merit for a Real Photon Beam

Assume that a bremsstrahlung spectrum is incident on a hydrogen target. What is the figure of merit for the first-order backgrounds comparable to P_S?

Everything except Compton scattering will be neglected; the two following figures may be quoted: (1) $0 <$ incident $k < m$; (2) $k > m$. The former can probably be essentially eliminated by beam hardening, the latter substantially reduced in the same way.

(1) Low energy gammas, $0 < k < m$

$$P_S^\gamma \approx \frac{\frac{dk}{k}\,\sigma_{signal}}{\int_0^m \sigma_c\,dk} \left(\frac{\text{duty cycle}}{T_S}\right)$$

$$\boxed{P_S^\gamma \approx \frac{1}{25}\ \text{hour}^{-1}\ \text{Mev}^{-1}}$$

for $\frac{dk}{k} \approx 1\%$ and $\sigma_{signal} \approx 1$ microbarn. (This assumes that a narrow resonance is being studied.)

(2) Medium energy gammas, $k > m$.

We replace

$$\int_0^m \sigma_c dk$$

in the above by

$$\int \sigma_c \frac{dk}{k} .$$

As calculated above, the ratio

$$\frac{\int_0^m \sigma_c dk}{\int_m^\infty \sigma_c \frac{dk}{k}} \quad \text{is} \quad \approx \frac{3/2 \text{ microbarn-MeV}}{1/2 \text{ microbarn}}$$

If the cutoff is k_c rather than m, the ratio increases in the ratio k_c/m. If a liquid hydrogen beam hardener about 1 r.ℓ. thick were used, one might say $k_c \approx 10$ MeV and gain another factor of 20, yielding a best possible

$$\boxed{P_S^\gamma \approx \alpha \text{ hour}^{-1}}$$

In terms of background from the same Compton-scattered gamma ray spectrum, $P_S \approx \frac{30 \text{ hour}^{-1}}{X}$ has been deduced for $k > m$. If $X < 10$, it can be seen the electroproduction will actually have less gamma background per event in the 4π detector than will a hardened bremsstrahlung spectrum. This advantage disappears for a thicker electroproduction target.

VIII. SUMMARY AND PRELIMINARY DESIGN OBJECTIVES

From the above, "tagging" small angle electrons seems a feasible way in principle to obtain monochromatic virtual photons with 80% linear polarization.

If the total σ_B can be held to 5 to 10 microbarns,* as seems possible, then the value of

$$[\text{rate}/(\text{number of spurious tracks/event}] \approx 3 \text{ hour}^{-1}$$

can be expected for a 1/2 microbarn cross section

$$= \sigma_{sig}(q^2,k) = \tfrac{1}{2}\, \sigma_{sig}(0,k)$$

This means that for a 1% $\frac{dk}{k}$ interval and a reaction with a photoproduction cross section of 1 microbarn, one may count at 3 events/hour into 4π steradians. It would seem possible to run as high as 30 events/hour without flooding the 4π detector. Some beam intensity-target thickness combinations yielding this last rate are:

10^{12} epp and X = 1/100, corresponding to a pressure of $\approx$ 1/2 mm Hg (= 500 microns) for a 10-inch gas target

10^{9} epp and X = 10, corresponding to a pressure of 2/3 atmosphere in a 10-inch gas target

Even in the latter case, the gamma ray background will be less than that obtainable with a bremsstrahlung spectrum.

For the lowest target density, the most severe problems will result from very weak halos on the beam (the target $X \approx 1/100$ is $\approx 2 \times 10^{-8}$ radiation lengths) that strike any part of the apparatus, and from the possible need for a differentially pumped target without walls. It may

---

*σ_B was defined above as the total cross section for electrons to produce "nuclear events" in the 4π detector.

be possible to accomplish much of this by using a stainless tube cooled at both ends by liquid helium, but no thought has yet been given the problem. As for walls, 1/2 mil of mylar is roughly 10^{20} atoms of carbon/cm^2. Only one wall need be visible to the 4π detector, but even so, such a wall or its equivalent would dominate the radiation lengths in the target for $X < 15$. Such low gas pressures would probably permit the use of a much thinner wall than one would otherwise contemplate. Of course, it might suffice to use a thin low Z solid target.

The foremost problem in the electron and 4π detectors arises because the cross section for electron-electron scattering is so high that it must be impossible for any particle obeying the kinematics of this reaction to reach either detector.

For the electron detector one is therefore restricted to the observation of momentum transfers $t > t^{ee} \approx 0.5\ F^{-2}(\epsilon/20\ \text{BeV})$. It is necessary to design a spectrometer capable of detecting less than 10^{-6} of the electrons obeying $\epsilon' \approx 2m/\theta^2$, which is ≈ 3500 MeV at 1°. The design of such a system is by no means obvious, nor is it obviously impossible. Because we gain by $1/\theta^2$, it may pay to increase t/t^{ee} by increasing θ. For $\theta \approx 1/50$, $t \approx 2\ F^{-2}$ for $\epsilon = 20$ BeV, $\epsilon' = 10$ BeV. Thus the 1° to 2° detector would be about right for $k < 10$ BeV in terms of the range of momentum transfer covered.

In the 4π detector a large system is required in order to produce a cutoff in the lowest observable transverse momentum of $\approx 2m/\theta_{min}$, where θ_{min} is the minimum angle visible to the 4π detector. A $\theta_{min} \approx 1^\circ$ and minimum transverse momentum > 60 MeV/c enables one to observe the two-body decay of all known particles produced at 0° without interference from electron-electron scattering. The longitudinal B field taken for a specific point of departure in this report is obviously not essential; one could split a detector such as Frisch's at CEA in order to produce the same result. However, the longitudinal field seems better suited to measuring the Lorentz invariant transverse momenta for decay products of vector mesons produced at 0° and somewhat simplifies the electron detection problem by virtue of its axial symmetry, and it was therefore chosen for the discussion here.

Compton-scattered bremsstrahlung quanta will limit the allowed range

in X; until further experiments are done, it will not be clear whether SLAC has a clear advantage here, but it is clear throughout the body of this report how the very high energies of the linear accelerator will represent a gain, which may enable SLAC at least to be fully competitive, even in the same "photon" energy region. Lastly, it might be mentioned that a very low density target ($< 1/100$ atmosphere) might quite conceivably be polarized if a sufficient concentration of atomic hydrogen can be maintained for ≈ 2 microseconds at these (high) pressures.

A study of the extent to which these various demands on the electron spectrometer can be met should be made with the Stanford Mark III linac, where one actually would expect many of these problems to be worse than those for the 20 BeV machine. There should also be studies carried out on the permissible gamma ray intensities and to check the other background predictions above.

Another way to use the above is as a fast "bubble chamber." If relatively little selection of events is made in the 4π detector and one operates with $\frac{dk}{k} \approx 10\%$, all figures of merit could be improved by ≈ 1000. Thus several thousand interactions/hour with low background could be obtained, plus the advantages of polarization of the beam and possibly of the target as well.

The final conclusions of this report are summarized in the three tables which follow. We have assumed two different hypothetical cases:

1. In table I, it is assumed that one is interested in studying $\gamma + p \rightarrow$ 3-pronged events (mostly $\gamma + p \rightarrow p + \pi^+ + \pi^-$), with a photoproduction cross section of 40 microbarns;

2. In Table II, it is assumed that a particular isobaric state of the nucleon is produced by real photons with a cross section ≈ 1 microbarn, integrated over the width of the resonance.

TABLE I

Virtual $\gamma + p \rightarrow 3$-Prongs

$\sigma_\gamma \rightarrow 3$-prong $dk/k = 1\%$	8×10^{-4} microbarns/electron
Counting rate/hour	≈ 1000
Total reaction cross section, excluding e-e scattering	5-10 microbarns/electron
Reactions into 4π detector/pulse	5-10
Reactions from equivalent photon spectrum	3
Number of 3-prong events/pulse	1
Estimated false triggers in 4π detector (5 nsec resolving time for internal logic)	1/4-1
Singles rate in electron spectrometer/hour	4000-5000
Accidental coincidences between detected electron and real or false 3-prong event/hour	10-20
Gamma ray flux into 4π, X = 1/100, no walls (per pulse)	$\begin{cases} 10 \text{ KeV} & k < m \\ 1/200 & k > m \end{cases}$
Gamma ray flux, 1/2 mil mylar entrance window	$\begin{cases} 15 \text{ MeV} & k < m \\ 8 & k > m \end{cases}$

If mylar or an equivalent window is used, it would pay to increase X to X = 10 and decrease I_B to 10^9 epp.

TABLE II

Virtual $\gamma + p \rightarrow N^{****} \rightarrow \begin{cases} \pi^o + p \\ \eta + p \end{cases}$

σ_γ	1 microbarn
$\int \frac{dk}{k} \sigma_\gamma (N^{****})$	10^{-2} microbarn (est.)
Counting rate/hour	25
Total reactions in 4π detector, etc.	See Table I
Estimated 4π trigger rate/pulse if < 30% of nuclear interactions give $(p + 2\gamma)$ final state	1
Accidentals rate/hour from electron singles rate given in Table I, above trigger rate	20
Signal/accidentals ratio	1
Rejection by 4π trigger of false events needed for false triggers ≈ resonance decays	$1/3 \times 10^{-4}$

Gamma ray fluxes, etc., are identical with the conditions in Table I.

TABLE III

Typical Investigation of a Resonance Cross Section with Frisch's Scheme

σ_{sig}	1 microbarn
Target	10 inches of liquid hydrogen
N_γ in 1% $\frac{dk}{k}$	10^4/sec (1 gamma ray every 10^{-5} sec) in 1% dk/k
Number of events/hour	35
Total number of reactions with σ_{tot} = 200 microbarns	7×10^5/hour
Accidental coincidences if trigger is not restrictive	140 (2 nsec coincidence)
Accidental coincidences if trigger accepts 30% of nuclear reactions	50
Gamma ray flux into 4π	3 MeV/microsecond $k < m$ 2/microsecond $k > m$

These rates should be compared with those in Table II for a comparable reaction investigated using 1^o-2^o scattered electrons.

APPENDIX I

BRIEF SUMMARY OF PROPOSED PHOTON SOURCES

Positron Annihilation. Positrons annihilating in flight through a hydrogen target produce photons with an angular distribution characterized by $\sqrt{\frac{m}{e}}$ compared to that of bremsstrahlung (m/e). It is therefore possible to collimate the gamma rays in a particular direction to produce partial monochromaticity.* For 10-BeV annihilation photons, of about 300 photons/pulse entering a hydrogen bubble chamber, 83 are within 1% of 10 BeV and 184 have $k < 3$ BeV. For a total cross section of 200 microbarns, about 1 interaction every 10 bubble chamber frames comes from the annihilation peak. Assuming one expansion/second, this gives 300 interactions per hour.

Laser Photons. These are Compton-scattered by the electron beam and monochromatized by collimation. A discussion of this method appears in an internal report by R. Mozley.** About 500 photons/pulse are available in the upper 10% of the spectrum (peak energy 7.25 BeV for a 20 BeV electron beam). With a 1-inch liquid hydrogen target and the same 200 microbarn cross section, the interaction rate is $\approx$ 15,000 interactions/hour. The background is 1/30 that of a normal bremsstrahlung spectrum with the same data rate.

Coherent Bremsstrahlung from Crystals. This is another way to reduce the background over that from a bremsstrahlung spectrum. Mozley estimates a factor of 30 improvement in this case also.

Weak Bremsstrahlung Beam. The rate of 500 photons/pulse into the top 10% of the spectrum corresponds to about 5×10^{-9} radiation lengths in the direct electron beam. If a beam hardener with a lower cutoff on photon energy of $\approx$ 10 MeV is used, the same rate of 15,000 interactions per hour corresponds to 40 gamma rays Compton-scattered into a 4π detector per pulse. Most of these go forward, however, and the number decreases if a lower rate of interactions can be tolerated.

---

*Z.G.T. Guiragossián, Internal Report, Stanford Linear Accelerator Center, Stanford University, Stanford, California (December 1963).

**R. Mozley, Internal Report, Stanford Linear Accelerator Center, Stanford University, Stanford, California (June 1963).

Inelastic Muon Scattering. As with electrons, muons may produce reactions via the muon electromagnetic field.* We may assume an equivalent radiator of about 0.001 for muons. If a beam of 3×10^6 muons/sec and a 100-inch hydrogen target are available, the interaction rate for $\frac{\Delta k}{k} \approx 10\%$ is 2500 interactions/hour. The backgrounds for this process are discussed in more detail elsewhere.

Inelastic Electron Scattering. For the purpose of comparison, the proposal advanced in the body of this report would correspond to 5000 interactions/hour in a 1% dk/k interval.

---

*L. Hand and R. Wilson (see preceding section).

APPENDIX II

FRISCH'S SCHEME FOR TAGGING PHOTONS AT THE CEA

We refer the interested reader to the Proceedings of the Conference on Photon Interactions (Cambridge, Massachusetts, January 1963, p. V11.15) for a more lucid description of Professor D. H. Frisch's proposal. Briefly, a 1 mil (or less) Be wire is placed inside the equilibrium orbit of the CEA and electrons losing energy by radiation of a high energy photon are counted in a counter hodoscope placed appropriately. Again, two separate figures of merit are defined:

$$P_{tag} = \text{Rate} \times \left(\frac{\text{signal}}{\text{accidentals}}\right) \approx \left(\frac{\text{duty cycle}}{\text{resolving time of coincidence}}\right) \left(\frac{\sigma_{\text{signal}}\left(\frac{dk}{k}\right)}{\sigma_B}\right) \left(X\sigma_{sig}\right)$$

Frisch can hope to achieve a 10% duty cycle with his scheme. $\frac{dk}{k}$ is the energy interval for the desired photon energy, and X is the hydrogen target areal density. Frisch discusses the possibility of $\frac{dk}{k}$ as large as 30%, but we assume $\frac{dk}{k} = 1\%$ here to make a valid relative comparison with the scheme discussed above.

For σ_B, again take the Compton-scattered high energy ($k > 10$ MeV) gamma rays, as it is assumed that the 4π detector has lead plate spark chambers. Then $\sigma_B \approx 10^4$ microbarns; therefore (for a 10-inch liquid hydrogen target),

$$P_{tag} \approx \left(\frac{0.1}{5 \times 10^{-13} \text{ hour}}\right) \frac{10^{-2} \times 1}{10^4} \left(10^{24} \times 10^{-30}\right),$$

or $P_{tag} = 1/5 \text{ hour}^{-1}$. This figure assumes that a Compton gamma ray can trigger the 4π detector counters. If only a nuclear event can accomplish this,

$$\int \sigma_{tot} \frac{dk}{k} \rightarrow \sigma_B ,$$

which increases P_{tag} to 10 hour^{-1}. A calculation of

$$P_S \equiv \text{Rate} \times \left(\frac{\text{signal}}{\text{number of background events}} \right)$$

similar to the one in the report reveals $P_S \approx 10^6$, and the limitation on the tagging is set at 1 event/hour for a 10% signal-to-noise ratio. A good selection of the desired type of event in the 4π detector will increase P_S to $\approx$ 100 to 1000, allowing 10 to 100 events/hour for a 1 microbarn cross section. Of course, it is also true that these are not directly comparable, because they correspond to quite different physics.

Thus the scheme proposed by Frisch is roughly equal in rate to the small-angle inelastic electron scattering discussed above. It differs in being limited by accidental coincidences with the tagging counter and by presenting a much cleaner situation in the 4π secondaries detector, which is the reverse of the case for small-angle electron scattering. The difference is primarily caused by the presumed ability to make a really effective trigger in the 4π detector. If the triggering is about the same, the electroproduction is actually slightly ahead. If the requirement of 1% resolution is relaxed, P_S increases as $\Delta k/k$ for the Frisch scheme.

LIST OF REFERENCES

1. K. L. Brown, Ph.D. Thesis, Stanford University, Stanford, California (1953).
2. K. L. Brown and R. Wilson, Phys. Rev. 93, 443 (1954).
3. W. Panofsky, W. M. Woodward and G. B. Yodh, Phys. Rev. 102, 1392 (1956); and 105, 731 (1957).
4. R. H. Dalitz and D. R. Yennie, Phys. Rev. 105, 1598 (1957).
5. W.K.H. Panofsky and E. A. Allton, Phys. Rev. 110, 1155 (1958).
6. G. G. Ohlsen, Phys. Rev. 120, 584 (1960).
7. L. N. Hand, Phys. Rev. 129, 1834 (1963); and Ph.D. Thesis, Stanford University, Stanford, California (1961); unpublished.
8. M. Gourdin, Nuovo Cimento 21, 1094 (1961).
9. S. Fubini, Y. Nambu and V. Wataghin, Phys. Rev. 111, 329 (1958).
10. G. Chew, F. Low, M. Goldberger and Y. Nambu, Phys. Rev. 106, 1345 (1957).
11. P. Dennery, Phys. Rev. 124, 2000 (1961).
12. W. C. Barber, Ann. Rev. Nucl. Sci. 12, 1 (1962).
13. Dr. Joos, DESY, private communication.
14. K. Berkelman, "Electron scattering at 20 GeV," 1963 Summer Study Report, SLAC Report No. 25, Stanford Linear Accelerator Center, Stanford University, Stanford, California (Summer 1963).
15. W. N. Cottingham, Ann. Phys. 25, 424 (1963).
16. J. Walker, proposal for experiment at the Cambridge Electron Accelerator, Harvard University, Cambridge, Massachusetts.
17. N. Meisler and D. R. Yennie, Phys. Rev. 130, 1210 (1963).

LEGAL NOTICE